



TECHNISCHE  
UNIVERSITÄT  
WIEN

Vienna University of Technology

DIPLOMARBEIT

# Scattering Operators for the Spherical Harmonics Expansion of the Boltzmann Transport Equation

Ausgeführt am

Institut für Mikroelektronik  
der Technischen Universität Wien

unter der Anleitung von  
Ao.Univ.Prof. Dipl.-Ing. Dr.techn. Tibor Grasser  
und  
Dipl.-Ing. Dipl.-Ing. Karl Rupp, BSc. MSc.

durch

Peter Willibald Lagger, BSc.

Erdbergstraße 220 5/10A  
1110 Wien

Matrikelnummer 0625122  
Studienkennzahl 066 439

---

Datum

---

Unterschrift



# Kurzfassung

Diese Arbeit behandelt die Beschreibung von Streuprozessen im Rahmen der Boltzmann Transport Gleichung, welche nach Kugelflächenfunktionen (sog. Spherical Harmonics) entwickelt wird. Dabei wird auf die Arbeit von Karl Rupp [25] aufgebaut, insbesondere wird der von ihm entwickelte Simulator ViennaSHE verwendet. Der Fokus wird dabei auf einen der kompliziertesten Streumechanismen gelegt, die Elektronen-Elektronen Streuung, welche zum ersten Mal in dieser Form beschrieben wird.

Zu Beginn werden die mathematischen und physikalischen Grundlagen der Halbleiterphysik ausgearbeitet. Dabei werden die grundlegenden Halbleiter-Gleichungen, namentlich die Schrödinger Gleichung, die Boltzmann Transport Gleichung und die zugehörigen Momentengleichungen beschrieben. Letztere sollen die Vorteile der Kugelflächenfunktionsentwicklung hervorstreichen. Anschließend folgt ein Abschnitt, in dem detailliert die Entwicklung der Boltzmann Transport Gleichung nach Kugelflächenfunktionen ausgeführt wird. Des Weiteren wird der Übergang von der quantenmechanischen zur semi-klassischen Beschreibung des Elektrons beschrieben. In der semi-klassischen Beschreibung werden die Elektronen als klassische Teilchen angesehen, die Streuprozesse hingegen quantenmechanisch berücksichtigt. Basierend auf der Goldenen Regel von Fermi wird eine allgemeine Beschreibung der Streutheorie dargestellt. Die theoretischen Konzepte werden schließlich angewendet, um systematisch Ausdrücke für die Streuung an ionisierten Störstellen, die Streuung an akustischen und optischen Phononen innerhalb eines Leitungsbandes und die Elektron-Elektron Streuung zu entwickeln.

Im letzten Teil der Arbeit werden die Implementierungen für die Streuung an ionisierten Störstellen, sowie für Elektron-Elektron Streuung besprochen. Dabei wird auf die für die Elektron-Elektron Streuung vorgenommenen Vereinfachungen detailliert eingegangen. Zusätzlich werden numerische Untersuchungen des Streuoperators durchgeführt. Abschließend werden ausgewählte Simulationsergebnisse für einen Metall-Oxid-Halbleiter-Feldeffekttransistor (MOSFET) präsentiert.



# Abstract

This thesis deals with the description of scattering in the framework of the spherical harmonics expansion (SHE) of the Boltzmann Transport Equation (BTE). The focus is on one of the most complicated scattering mechanism, the electron-electron scattering, which is described for the first time in this context. It is based on the pioneering work of Karl Rupp [25], who developed the Spherical Harmonics Boltzmann Solver **ViennaSHE**. The mathematical and physical foundation, starting with the basic semiconductor equations, is presented in detail. Here, the advantages of the SHE approach are emphasized by comparison with the widely used balance equation methods (e.g. drift diffusion), which are also based on the BTE. The expansion of the BTE including the scattering operator is derived rigorously. In the following, the transition from the quantum mechanical description of the electron to the semi-classical description, where the motion of electrons is described classically and scattering is described quantum mechanically is discussed. Consequently, a general approach for describing scattering mechanisms is developed. This includes an elaboration of Fermi's Golden Rule (FGR), which is the foundation of the scattering theory.

The theoretical concepts are applied to describe ionized impurity, acoustic and optical intra-valley phonon and electron-electron scattering. Afterwards, the implementation of ionized impurity and electron-electron scattering is described. For electron-electron scattering, a simplified model for the scattering operator is presented. This is necessary in order to reduce the complexity of the implementation. Finally, the applicability of the implementation is demonstrated by numerical simulation results for a metal-oxide-semiconductor field-effect transistor (MOSFET).

# Contents

<b>1</b>	<b>Basic Semiconductor Equations</b>	<b>1</b>
1.1	The Schrödinger Equation . . . . .	1
1.1.1	De Broglie Hypothesis . . . . .	2
1.1.2	The Hamiltonian and the Correspondence Principle . . . . .	3
1.1.3	Time-independent Schrödinger Equation . . . . .	3
1.1.4	Expansion of Quantum States . . . . .	4
1.1.5	Hermitian Operators . . . . .	4
1.2	The Boltzmann Transport Equation . . . . .	5
1.2.1	Newton's Laws of Motion . . . . .	6
1.2.2	Derivation of the Boltzmann Transport Equation . . . . .	6
1.2.3	The Scattering Operator . . . . .	10
1.2.4	The Multi-Band Boltzmann-Poisson System . . . . .	14
1.3	Balance Equations . . . . .	15
1.3.1	Moments of the Distribution Function . . . . .	16
1.3.2	Balance Equations for the Boltzmann Transport Equation . . . . .	16
1.3.3	Carrier Temperature and Heat Flux . . . . .	22
1.3.4	Hydrodynamic Equations . . . . .	24
1.3.5	Drift-Diffusion Equations . . . . .	26
1.3.6	Conclusion . . . . .	27
<b>2</b>	<b>Spherical Harmonics Expansion of the Boltzmann Transport Equation</b>	<b>28</b>
2.1	Spherical Harmonics . . . . .	28
2.2	Spherical Harmonics Expansion of the Distribution Function . . . . .	32
2.3	Spherical Harmonics Expansion of the BTE . . . . .	34
2.3.1	Spherical Harmonics Expansion of the Free-Streaming Operator . . . . .	34
2.3.2	Spherical Harmonics Expansion of the Scattering Operator . . . . .	36
2.3.3	Equation System for the Spherical Harmonics Expansion Coefficients . . . . .	39
<b>3</b>	<b>Physical Modeling</b>	<b>42</b>
3.1	Semi-Classical Carrier Dynamics . . . . .	42
3.1.1	From the Wave Packet to the Particle . . . . .	43
3.1.2	Force in the Semi-Classical Approach . . . . .	43
3.1.3	Limitations of the Semi-Classical Approach . . . . .	45
3.2	Band Structure of Semiconductor Materials . . . . .	46
3.2.1	Crystals . . . . .	46
3.2.2	The Electron in a Crystal Potential and Bloch's Theorem . . . . .	48
3.2.3	Real Electronic Band-Structures . . . . .	51
3.2.4	Analytic Band Structure Models . . . . .	52
3.2.5	Model for the Valence Bands . . . . .	57

3.3	Fermi's Golden Rule . . . . .	57
3.3.1	Time-dependent Perturbation Theory . . . . .	57
3.3.2	Non-Recurring Perturbation . . . . .	59
3.3.3	Periodic Perturbation . . . . .	61
3.3.4	The Transition Rate for Scattering Events . . . . .	62
3.4	Modeling of Scattering . . . . .	64
3.4.1	Scattering Rate . . . . .	65
3.4.2	General Approach . . . . .	65
3.4.3	Example . . . . .	66
3.5	Lattice Vibrations - Phonons . . . . .	66
3.5.1	Dispersion Relation . . . . .	66
3.5.2	Phonons - Quanta Of Lattice Vibrations . . . . .	69
3.5.3	The Quantum Mechanical Phonon System . . . . .	70
3.5.4	Phonon Statistics . . . . .	71
<b>4</b>	<b>Scattering</b>	<b>72</b>
4.1	Ionized Impurity Scattering . . . . .	72
4.1.1	Potential Of a Screened Point Charge . . . . .	72
4.1.2	Transition Rate and Scattering Rate . . . . .	74
4.2	Phonon Scattering . . . . .	75
4.2.1	Scattering Potential . . . . .	75
4.2.2	Matrix Element . . . . .	75
4.2.3	Acoustic Intra-Valley Phonon Scattering . . . . .	76
4.2.4	Optical Intra-Valley Phonon Scattering . . . . .	76
4.3	Electron-Electron Scattering . . . . .	77
4.3.1	Scattering Potential And Scattering Integral . . . . .	77
4.3.2	Transition Rate . . . . .	78
4.3.3	Analysis of the Scattering Coefficient . . . . .	79
4.3.4	Scattering Operator . . . . .	80
4.3.5	SHE of the Scattering Operator . . . . .	80
<b>5</b>	<b>Implementation And Simulation</b>	<b>83</b>
5.1	Problem Setup . . . . .	83
5.1.1	The Device . . . . .	83
5.1.2	Scattering . . . . .	84
5.2	Ionized Impurity Scattering . . . . .	85
5.2.1	Implementation . . . . .	85
5.2.2	Simulation . . . . .	85
5.3	Electron-Electron Scattering . . . . .	96
5.3.1	Implementation . . . . .	97
5.3.2	Simulation . . . . .	105
<b>6</b>	<b>Conclusion and Outlook</b>	<b>110</b>

# Notation

Symbol	Meaning
$\mathbb{R}$	set of real numbers
$\mathcal{B}$	Brillouin zone
$\Re(x)$	real part of a complex number $x$
$i$	imaginary unit
$\mathbf{v}, \mathbf{w}$	vectors
$\mathbf{M}, \mathbf{N}$	matrices
$x^*$	conjugate complex of $x$
$\partial_x$	short form for partial derivative w.r.t. $x$
$\dot{x}$	short form for the time derivation $\frac{dx(t)}{dt}$
$\theta$	polar angle
$\varphi$	azimuth angle
$Y_{l,m}$	real valued spherical harmonic of major index $l$ and minor index $m$
$X_{l,m}$	projection of a quantity $X$ onto $Y_{l,m}$
$\hbar$	Planck constant divided by $2\pi$
$k_B$	Boltzmann constant
$\epsilon_0$	permittivity of free space
$\epsilon$	relative permittivity
$T$	absolute temperature
$T_L$	lattice temperature
$T_C$	carrier temperature
$q$	elementary charge
$m$	mass
$m^*$	effective mass
$\tilde{\mathbf{m}}^*$	effective mass tensor
$\nu$	index of the $\nu$ th energy band
$\eta$	index of the scattering process
$\mathcal{V}$	sample volume
$\mathcal{A}$	sample area
$\mathcal{L}$	sample length
$L$	characteristic length
$\int_{\mathcal{B}}\{\cdot\}d\mathbf{k}$	integration over the Brillouin zone
$d$	dimension
$N_d$	density of states in $\mathbf{k}$ -space for a $d$ -dimensional system
$\mathbf{Q}\{\cdot\}$	scattering operator
$\overline{\mathbf{Q}}^{\text{in}}\{\cdot\}$	in-scattering operator
$\overline{\mathbf{Q}}^{\text{out}}\{\cdot\}$	out-scattering operator
$S^{\nu,\nu'}(\mathbf{k}, \mathbf{k}')$	transition rate given by Fermi's Golden Rule, i.e. the probability per unit time for a carrier to scatter from initial state $(\nu, \mathbf{k})$ to final state $(\nu', \mathbf{k}')$



Symbol	Meaning
$\mathbf{r}$	spatial coordinate
$\mathbf{e}_r$	unit vector in radial direction
$\mathbf{k}$	wave vector
$\mathbf{p}$	momentum vector
$\mathbf{v}(\mathbf{k})$	group velocity
$\omega$	angular frequency
$\lambda$	wave length
$t$	time variable
$f^\nu(\mathbf{r}, \mathbf{k}, t)$	distribution function of the $\nu$ -th band
$g^\nu(\mathbf{r}, \varepsilon, \theta, \varphi, t)$	generalized energy distribution function of the $\nu$ -th band
$\mathbf{E}$	electric field strength
$\Phi$	electrostatic potential
$\mathbf{J}$	current density
$\mathbf{F}$	force
$n(\mathbf{r}, t)$	electron density/carrier density
$p(\mathbf{r}, t)$	hole density
$\delta_{i,j}$	Kronecker delta
$\delta(\cdot)$	Dirac distribution
$\Omega$	unit sphere
$d\Omega$	unit sphere surface element, $\sin(\theta)d\theta d\varphi$
$\mathbf{e}_\theta, \mathbf{e}_\varphi$	unit vectors, w.r.t. $\theta$ and $\varphi$
$\nabla$	Nabla operator
$(f, g)$	inner product of two (complex) functions $f$ and $g$ defined as $\int f^*(\mathbf{r})g(\mathbf{r})d^3r$
$\langle\psi $	bra-vector (Dirac notation)
$ \psi\rangle$	ket-vector (Dirac notation)
$\langle\psi_1 \psi_2\rangle$	inner product of a bra- and a ket-vector, $\langle\psi_1 \psi_2\rangle = (\psi_1, \psi_2)$
$\langle\psi_1 \hat{H} \psi_2\rangle$	matrix element defined as $\langle\psi_1 \hat{H} \psi_2\rangle = (\psi_1, H\psi_2)$
$\underline{\mathbf{A}}$	operator, regardless of its representation
$\underline{\mathbf{A}}_r$	operator in spatial representation
$\underline{\mathbf{A}}^\dagger$	the adjoint operator to $\underline{\mathbf{A}}$
$\underline{\mathbf{I}}$	identity operator $\underline{\mathbf{A}}\underline{\mathbf{I}} = \underline{\mathbf{A}}$
$\underline{\mathbf{0}}$	zero operator $\underline{\mathbf{A}} + \underline{\mathbf{0}} = \underline{\mathbf{A}}$
$\langle A \rangle$	expectation value of the operator $\underline{\mathbf{A}}$ defined as $\langle A \rangle = \langle\psi \underline{\mathbf{A}} \psi\rangle$
$\underline{\mathbf{H}}$	Hamiltonian operator
$\psi(\mathbf{r}, t)$	complex wave function
$E$	kinetic energy
$H$	total energy
$E_c(\mathbf{r}, \mathbf{k})$	total energy of an electron in the conduction band, which contains a potential energy component $E_{c0}(\mathbf{r})$ and a kinetic energy component $E(\mathbf{k})$
$E_v(\mathbf{r}, \mathbf{k})$	total energy of a hole in the valence band, which contains a potential energy component $E_{v0}(\mathbf{r})$ and a kinetic energy component $E(\mathbf{k})$
$E_{c0}(\mathbf{r})$	band edge of the conduction band
$E_{v0}(\mathbf{r})$	band edge of the valence band
$E(\mathbf{k})$	kinetic energy component of the conduction/valence band potential
$U_p(\mathbf{r})$	perturbing potential
$N_D^+$	density of ionized donors
$N_A^-$	density of ionized acceptors

# Acronyms

<b>QM</b>	quantum mechanics
<b>FGR</b>	Fermi's Golden Rule
<b>SE</b>	Schrödinger equation
<b>BTE</b>	Boltzmann Transport Equation
<b>PE</b>	Poisson Equation
<b>FDD</b>	Fermi-Dirac distribution
<b>IVP</b>	initial value problem
<b>RTA</b>	relaxation time approximation
<b>SHE</b>	spherical harmonics expansion
<b>DD</b>	drift-diffusion
<b>HD</b>	hydrodynamic
<b>LE</b>	Laplace Equation
<b>EDF</b>	generalized energy distribution function
<b>PBC</b>	periodic boundary conditions
<b>BC</b>	boundary conditions
<b>LA</b>	longitudinal acoustic
<b>TA</b>	transversal acoustic
<b>LO</b>	longitudinal optical
<b>TO</b>	transversal optical
<b>Si</b>	silicon
<b>GaAs</b>	gallium-arsenide
<b>Ge</b>	germanium

# Acknowledgement

This page is dedicated to all those who supported me during the great time of my studies at the Vienna University of Technology. In the following, some of them are listed, but I am sure that this list is not complete. Thus, my first thanks go to everybody I forget to mention.

I want to thank Prof. Grasser for offering me a great topic for this thesis and for his great lecture, which aroused my interest for device simulation.

My true thanks go to Karl Rupp, who has provided excellent guidance through out the very sophisticated topic of this thesis. He is the Mastermind behind **ViennaSHE** and without his preliminary work this all would not have been possible. I thank him for all the great discussions and for his valuable input to my work. He is a very good mentor.

I am also thankful to all my friends and colleagues at the university for the numerous inspiring discussions and for the great learning groups, which have been made some of the many exams easier to pass through. Thank you for the great time together. It was a pleasure for me.

I am much obliged to my parents. They always supported my ideas and objectives and give me the time and freedom to grow. Their contribution is essential.

Last but not least, many thanks to my brother and my sister and all the other members of my family, who are an important part of my life.

# Introduction

In 1965 Gordon E. Moore published an article with the title “Cramming more components onto integrated circuits” [22], where he predicted an exponential growth of the number of components per integrated circuit with a simultaneously exponential reduction of costs per component. Later, this became known as Moore’s law, which is still valid today. While the first integrated circuits had a minimum feature size of 10  $\mu\text{m}$ , today a minimum feature size of 22 nm and below is close to production.

High costs for the mask production, which severely limit the opportunity of prototyping, are a key driver for process- and device-simulation. While in the early stage of the technology development phenomenological models, such as the *drift-diffusion* model have been sufficient for describing the behavior of integrated devices, they are more and more losing their validity as technology evolves.

Increasing computing power allows the implementation of sophisticated physical models, like the solution technique for the BTE described in this thesis. Early models gave an insight into averaged physical quantities, such as the carrier density or the current density, while microscopic models, such as the semi-classical model based on the BTE describe the carrier distribution in the six dimensional position-momentum space and thus provide more information.

Although many solution techniques have been developed in the past, the solution of the BTE is still challenging. A direct solution is extremely difficult or even impossible due to the high dimensionality of the problem. The SHE of the BTE offers a solution method, which is already feasible. It is based on the transformation of the problem from the six dimensional location-momentum space to the four dimensional location-energy space. In contrast to the Monte-Carlo method, it offers a deterministic solution of the BTE.

This thesis deals with the SHE of the BTE with a focus on the description of scattering phenomena, especially with a focus on electron-electron scattering. Electron-electron scattering is of interest for the investigation of impact ionization, because it leads to a correction of the high energy tail of the distribution function [3, 31].

## Overview

This thesis is structured as follows:

In Chapter 1 the basic mathematical foundation of semiconductor physics is summarized, which includes the Schrödinger equation (SE), the BTE and the balance equations derived from the BTE. The SE is necessary to understand the derivation of FGR in Section 3.3. The BTE is the center of this work and thus is discussed in detail. The last part dealing with balance equations is presented in a rather general setting. It goes beyond the primary focus, but tries to point out the main advantages of the SHE-approach compared with the classical balance equations approach.

Chapter 2 comprises the mathematical background to understand the SHE of the BTE. Therefore, the complete set of orthonormal functions, which are called spherical harmonics, is introduced. It follows a detailed derivation of the SHE of the distribution function and the BTE with a focus on the scattering operator. Finally, an equation system for the coefficients of the SHE of the BTE for an

arbitrary expansion order is set up to summarize the previous results.

The basics of semi-classical modeling are presented in Chapter 3. It starts with the discussion about the quantum mechanical description of an electron as a wave packet governed by the SE and the semi-classical description as a particle governed by the BTE. A section about electronic band structures of semiconductors with a focus on the Bloch's theorem follows. Afterwards, the most important analytic band structure models are introduced. The subsequent part is dedicated to scattering. It includes a very detailed derivation of FGR, which is the basic foundation of scattering theory. This chapter is finalized with a section about the general approach to model scattering and an introduction to the concept of quantized lattice vibrations, called phonons.

In Chapter 4 a selection of scattering mechanisms, including ionized impurity scattering, acoustic and optical intra-valley phonon scattering and electron-electron scattering, is discussed. The scattering potentials are taken from the literature [12, 20, 28, 30]. The first two scattering mechanism can be treated in a straight-forward manner based on the concepts established in the previous chapters. Electron-electron scattering is described in the center-of-mass framework, thus the scattering coefficient is the same as for ionized impurity scattering. The complex terms for energy and momentum conservation make the treatment of electron-electron scattering very challenging.

The cornerstones of the implementation of ionized impurity and electron-electron scattering are discussed in Chapter 5. The derivation of the scattering operator for electron-electron scattering and the following implementation for the SHE of the BTE are described for the first time. Finally, numerical simulation results for a MOSFET are given.

In Chapter 6 final conclusions and an outlook on possible future work are drawn.



# Chapter 1

## Basic Semiconductor Equations

In this chapter the fundamental theoretical background to describe transport phenomena in semiconductors is presented. The focus is on semi-classical transport, which means that in principle the carriers are viewed as particles, but their short-range interaction is treated quantum mechanically. Therefore, at the beginning of the chapter a compact overview of quantum mechanics is given. Next, starting with Newton's laws of motion, a description of the behaviour of ideally charged carriers in a vacuum under the influence of an external force is developed. Therefore, a distribution function is introduced, leading subsequently to the Boltzmann Transport Equation (BTE). For the BTE, the focus is on the scattering operator as a foundation for Chapter 4. Then a discussion about the moments of the BTE follows, with a systematical introduction of balance equations for these moments. To get a useful description of carrier transport in terms of these balance equations, simplifications are necessary. In this context two common models are presented, the drift-diffusion (DD)-model and the hydrodynamic (HD)-model.

### 1.1 The Schrödinger Equation

At this point a short overview of the complex theory of quantum mechanics (QM) is given. A short overview of the Dirac notation is given in Appendix A. Those areas of QM relevant for this work are presented in detail. At the beginning the five fundamental axioms of QM [27] in the most general form are listed:

**Axiom 1** The state of a quantum system is described by its state vector  $|\Psi\rangle$ . The time dependency of the state vector is explicitly expressed as  $|\Psi, t\rangle$ .

**Axiom 2** The observables of the system are described by Hermitian operators  $\underline{\mathbf{A}}$ .

**Axiom 3** The expectation value of an observable with the associated operator  $\underline{\mathbf{A}}$  is given by  $\langle A \rangle := \langle \Psi | \underline{\mathbf{A}} | \Psi \rangle$ .

**Axiom 4** The temporal evolution of a quantum state  $|\Psi, t\rangle$  is described by the Schrödinger equation (SE).

$$\underline{\mathbf{H}}|\Psi, t\rangle = i\hbar \frac{\partial |\Psi, t\rangle}{\partial t}. \quad (1.1)$$

**Axiom 5** If the observable related to  $\underline{\mathbf{A}}$  in the state  $|\Psi\rangle$  is measured and  $a_n$  is obtained, then the system state collapses to  $|n\rangle$ . This is the so called reduction of quantum states ( $|\Psi\rangle \rightarrow |n\rangle$ ).

**ad Axiom 1:** The state vector  $|\Psi\rangle$  is an element of the Hilbert space  $\mathbb{H}$ , which is a complete vector space equipped with an inner product. The representation of the state vector  $|\Psi\rangle$  in the Dirac notation is independent of the basis system used. The spatial representation of the state vector reads  $\Psi(\mathbf{r})$  and is called wave function, for more information see Appendix A.

**ad Axiom 2:** The Hermitian operator  $\underline{\mathbf{A}}$  has real-valued eigenvalues and orthogonal eigenvectors, see Section 1.1.5. The eigenvalues are the possible measurements of the observables, e.g. the eigenenergies of the system are associated with the Hamilton operator  $\underline{\mathbf{H}}$ , the momentum is associated with the momentum operator  $\underline{\mathbf{P}}$ . Operators can be represented in different basis systems, analogous to state vectors  $|\Psi\rangle$ . The basis independent notation is  $\underline{\mathbf{A}}$ . An operator in a special representation is written as

$$\underline{\mathbf{A}}_{\mathbf{b}}, \quad (1.2)$$

with  $\mathbf{b}$  denoting the basis system, e.g.  $\mathbf{r}$  for the spatial representation or  $\mathbf{p}$  for the momentum representation.

**ad Axiom 3:** In the spatial representation the expectation value of an observable is defined as  $\langle A \rangle = \langle \Psi | \underline{\mathbf{A}} | \Psi \rangle := \int_{\mathbb{R}^3} \Psi^*(\mathbf{r}) \underline{\mathbf{A}}_{\mathbf{r}} \Psi(\mathbf{r}) d\mathbf{r}$  (see Appendix A).

**ad Axiom 4:** (1.1) is the most general representation of the SE. The more familiar spatial representation (see Section 1.1.2) can be obtained by projecting (1.1) onto the eigenspace of the spatial operator  $\underline{\mathbf{R}}$ . Also note that the Hamilton operator  $\underline{\mathbf{H}}$  is assumed to be time-independent.

**ad Axiom 5:** Consider the eigenvalue equation of the hermitian operator  $\underline{\mathbf{A}}$ , that is  $\underline{\mathbf{A}}|n\rangle = a_n|n\rangle$ , where  $a_n$  are the real-valued eigenvalues of this operator and  $|n\rangle$  are the corresponding orthonormal eigenstates. The eigenvalues are the possible measurements for the observable.

In the following, important concepts of QM relevant in the context of this thesis are discussed.

### 1.1.1 De Broglie Hypothesis

In the beginning of the 20th century experimental results showed that light has wave properties (e.g. double-slit experiment), as well as particle properties (photoelectric effect, Compton effect). In addition to the classical wave description of light by the Maxwell equations, the concept of light particles, so called photons, was introduced. Similar results appeared for microscopic particles, such as electrons. In classical physics, they obey Newton's laws of motion. But in double-slit experiments, these particles show properties of waves. The fact that some experiments can be described using the particle concept and others using the wave concept, is called particle-wave duality. De Broglie postulated [5, 27] that a particle with energy  $E$  and momentum  $\mathbf{p}$  can be associated with wave properties  $\omega$  and  $\mathbf{k}$ . He suggested the relations

$$\omega = \frac{E}{\hbar}, \quad (1.3)$$

$$\mathbf{k} = \frac{\mathbf{p}}{\hbar}, \quad (1.4)$$

where Planck's constant is a proportional constant. With the classical energy-momentum-relation for a free particle  $E = \mathbf{p}^2/2m$  it is concluded that

$$\omega(k) = \frac{\hbar \mathbf{k}^2}{2m}. \quad (1.5)$$



This is the dispersion relation for a free particle with mass  $m$ . The basic idea behind the de Broglie hypothesis is to describe a particle as a wave, while in classical physics the motion of particles and the spreading of waves are described by completely different concepts. It is hard to understand how to relate a particle with wave properties and vice versa. The De Broglie hypothesis offers a mathematical tool to do so.

### 1.1.2 The Hamiltonian and the Correspondence Principle

In QM the Hamiltonian (or Hamilton operator) is associated with the total energy of a quantum system. The Hamiltonian can be formulated in two steps. First the expression for the total energy of the system is formulated classically, e.g. for a particle in a potential  $U(\mathbf{r})$  we get

$$E(\mathbf{r}, \mathbf{p}) = E_{\text{kinetic}} + E_{\text{potential}} = \frac{\mathbf{p}^2}{2m} + U(\mathbf{r}). \quad (1.6)$$

Second, the correspondence principle [27] is applied to the classical energy expression to find an equation for the wave function  $\Psi(\mathbf{r}, t)$ . The correspondence principle states that

$$E \rightarrow i\hbar \frac{\partial}{\partial t}, \quad (1.7)$$

$$\mathbf{p} \rightarrow -i\hbar \nabla. \quad (1.8)$$

Application of the correspondence principle on (1.6) yields

$$i\hbar \frac{\partial \Psi(\mathbf{r}, t)}{\partial t} = \left[ -\frac{\hbar^2}{2m} \nabla^2 + U(\mathbf{r}) \right] \Psi(\mathbf{r}, t), \quad (1.9)$$

which is indeed the SE for one particle in a potential  $U(\mathbf{r})$  in the spatial representation. The Hamiltonian for this problem is found by comparing this equation with the general form (1.1), which gives

$$\mathbf{H}_{\mathbf{r}} = -\frac{\hbar^2}{2m} \nabla^2 + U(\mathbf{r}). \quad (1.10)$$

The eigenvalue equation of the Hamiltonian in the spatial representation reads

$$\mathbf{H}_{\mathbf{r}} \Psi_n(\mathbf{r}) = E_n \Psi_n(\mathbf{r}), \quad (1.11)$$

with energy eigenfunctions  $\Psi_n(\mathbf{r})$  and energy eigenvalues  $E_n$ . This is the time-independent SE in the spatial representation (see Section 1.1.3). Note that the energy eigenfunctions are orthonormal ( $\Psi_m(\mathbf{r}), \Psi_n(\mathbf{r}) = \delta_{m,n}$ ) and form a complete set in the space of square-integrable functions  $\mathbf{L}^2$ .

### 1.1.3 Time-independent Schrödinger Equation

The SE (1.1) can be simplified with the separation ansatz

$$|\Psi, t\rangle = |\Psi\rangle f(t). \quad (1.12)$$

This ansatz and a reordering (1.1) yield

$$\frac{\mathbf{H}|\Psi\rangle}{|\Psi\rangle} = i\hbar \frac{\partial_t f(t)}{f(t)} = E = \text{const.} \quad (1.13)$$

It can be argued that the equations have to be constant, because the left side is independent of the time variable  $t$ . Therefore

$$i\hbar \frac{\partial f(t)}{\partial t} = E f(t) \quad (1.14)$$

is obtained. (1.14) is solved with the ansatz  $f(t) = e^{-iEt/\hbar}$ , which yields

$$|\Psi, t\rangle = |\Psi\rangle e^{-iEt/\hbar}. \quad (1.15)$$

Finally (1.15) is substituted into (1.1). This gives the time-independent SE

$$\underline{\mathbf{H}}|n\rangle = E_n|n\rangle, \quad (1.16)$$

with the eigenenergies  $E_n$  and the corresponding eigenstates  $|n\rangle$ .

### 1.1.4 Expansion of Quantum States

Consider an orthonormal and complete set of eigenstates  $\{|n\rangle\}_n$  which forms a basis in the Hilbert space  $\mathbb{H}$ . An arbitrary state vector  $|\Psi\rangle$  can be expanded in terms of this basis

$$|\Psi\rangle = \sum_n c_n |n\rangle. \quad (1.17)$$

By multiplying (1.17) with  $\langle m|$  from the left

$$\langle m|\Psi\rangle = \sum_n c_n \langle m|n\rangle \quad (1.18)$$

and using the orthonormality property of the basis functions ( $\langle m|n\rangle = \delta_{m,n}$ ) we obtain for the expansion coefficients

$$c_n = \langle n|\Psi\rangle. \quad (1.19)$$

Eq. (1.19) can be substituted into (1.17) to yield the completeness relation

$$|\Psi\rangle = \left( \sum_n |n\rangle \langle n| \right) |\Psi\rangle. \quad (1.20)$$

From (1.20) we can identify the identity operator  $\underline{\mathbf{I}}$  as

$$\underline{\mathbf{I}} = \sum_n |n\rangle \langle n|. \quad (1.21)$$

### 1.1.5 Hermitian Operators

Hermitian operators play an important role in QM due to their advantageous properties. As a preparation for further investigations, the adjoint of an operator and hermitian operators is defined.

**Definition 1.** The adjoint of an operator  $\underline{\mathbf{A}}$  is written as  $\underline{\mathbf{A}}^\dagger$  and is defined by  $(\langle a|\underline{\mathbf{A}}|b\rangle)^* = \langle b|\underline{\mathbf{A}}^\dagger|a\rangle$  [27].

**Definition 2.** An operator is called hermitian or self-adjoint if  $\underline{\mathbf{A}} = \underline{\mathbf{A}}^\dagger$ .

**Theorem 1.** The eigenvalues of an hermitian operator are real-valued.

*Proof.* The eigenvalue equation

$$\underline{\mathbf{A}}|a\rangle = \alpha|a\rangle. \quad (1.22)$$

is multiplied by  $\langle a|$  to obtain

$$\langle a|\underline{\mathbf{A}}|a\rangle = \alpha\langle a|a\rangle. \quad (1.23)$$

Now the conjugate of (1.23) using  $\underline{\mathbf{A}} = \underline{\mathbf{A}}^\dagger$  is formed

$$(\langle a|\underline{\mathbf{A}}|a\rangle)^* = \langle a|\underline{\mathbf{A}}|a\rangle = \alpha^*\langle a|a\rangle. \quad (1.24)$$

Comparison of (1.23) and (1.24) yields that  $\alpha = \alpha^*$  and therefore  $\alpha \in \mathbb{R}$   $\square$

**Theorem 2.** *The eigenvectors to two different corresponding eigenvalues are orthogonal.*

*Proof.* Consider the eigenvalue equations for  $\underline{\mathbf{A}}$  for two different eigenvectors with different eigenvalues. The first equation is multiplied with  $\langle b|$  and the second with  $\langle a|$ :

$$\langle b|\underline{\mathbf{A}}|a\rangle = \alpha\langle b|a\rangle, \quad (1.25)$$

$$\langle a|\underline{\mathbf{A}}|b\rangle = \beta\langle a|b\rangle. \quad (1.26)$$

In the next step (1.25) is conjugated and subtracted from (1.26). With  $(\langle b|\underline{\mathbf{A}}|a\rangle)^* = \langle a|\underline{\mathbf{A}}|b\rangle$  for the hermitian operator  $\underline{\mathbf{A}}$  finally

$$\langle a|\underline{\mathbf{A}}|b\rangle - (\langle b|\underline{\mathbf{A}}|a\rangle)^* = (\beta - \alpha)\langle a|b\rangle \Rightarrow \langle a|b\rangle = 0 \quad (1.27)$$

is obtained.  $\square$

Operators in QM have to be Hermitian to yield real eigenvalues. The eigenvalues have to be real, because they determine the spectrum of the possible observables. These observables are physical quantities, which are always real-valued. To give an example, the energy spectrum is determined by the eigenvalues of the Hamiltonian operator  $\underline{\mathbf{H}}$ . The following consideration should make things clearer. The Hermitian operator  $\underline{\mathbf{A}}$  fulfills the eigenvalue equation

$$\underline{\mathbf{A}}|n\rangle = a_n|n\rangle, \quad (1.28)$$

with orthonormal eigenvectors  $|n\rangle$  and corresponding real-valued eigenvalues  $a_n$ . The eigenvectors  $|n\rangle$  form a complete set of basis vectors in the Hilbert space  $\mathbb{H}$ . According to Section 1.1.4 an arbitrary state vector  $|\Psi\rangle$  can be expanded in terms of  $\{|n\rangle\}_n$  with expansion coefficients  $c_n$

$$|\Psi\rangle = \sum_n c_n|n\rangle. \quad (1.29)$$

The expectation value of the observable  $\langle A \rangle = \langle \Psi|\underline{\mathbf{A}}|\Psi \rangle$  can now be written as

$$\langle A \rangle = \sum_n \langle n|c_n^*\underline{\mathbf{A}}c_n|n\rangle = \sum_n |c_n|^2 \langle n|\underline{\mathbf{A}}|n\rangle. \quad (1.30)$$

From (1.28) follows that  $\langle n|\underline{\mathbf{A}}|n\rangle = \langle n|a_n|n\rangle = a_n\langle n|n\rangle = a_n$ . This yields

$$\langle A \rangle = \sum_n |c_n|^2 a_n = \sum_n p_n a_n, \quad (1.31)$$

with the probability  $p_n = |c_n|^2$  to observe  $\langle A \rangle = a_n$ .

**Theorem 3.** *For an arbitrary quantum state  $|\Psi\rangle = \sum_n c_n|n\rangle$  expanded using a complete and orthonormal basis  $\{|n\rangle\}_n$  of the Hilbert space  $\mathbb{H}$  with expansion coefficients  $c_n$ , the probability to observe the eigenstate  $|n\rangle$  is given by  $|c_n|^2$ .*

## 1.2 The Boltzmann Transport Equation

The aim of this work is to describe the carrier transport in semiconductors in a semi-classical way, where the motion of carries (e.g. electrons or holes) is described by Newton's laws. In this context the term carrier denotes a charged particle. Scattering on the other hand is treated quantum mechanically using Fermi's Golden Rule (FGR) (see Section 3.3). Due to computational limitations a direct calculation of the carrier trajectories is not pursued and a distribution function is introduced instead. Subsequently a mathematical description for this distribution function is developed and adapted for carriers in semiconductor crystals. This leads to a  $M$ -particle problem first, which is approximated by a single particle approach afterwards. This makes it more appropriate for numerical simulations. In addition, long-range particle interactions are taken into account by a self consistent solution of the BTE together with the Poisson Equation (PE). Finally scattering between these carriers is considered.

### 1.2.1 Newton's Laws of Motion

The motion of a single particle in vacuum with a force  $\mathbf{F}$  is described by the initial value problem (IVP)

$$\mathbf{v} = \dot{\mathbf{r}}, \quad (1.32)$$

$$\mathbf{F} = m\dot{\mathbf{v}}, \quad (1.33)$$

where  $m \in \mathbb{R}$  is the mass,  $\mathbf{r} \in \mathbb{R}^d$  is the position and  $\mathbf{v} \in \mathbb{R}^d$  the velocity of the particle in a  $d$  dimensional space, with the initial conditions:

$$\mathbf{r}(0) = \mathbf{r}_0, \quad (1.34)$$

$$\mathbf{v}(0) = \mathbf{v}_0. \quad (1.35)$$

Generally, the particle follows a trajectory  $(\mathbf{r}(t), \mathbf{v}(t), t)$  in the  $2d$ -dimensional position-velocity-space. In practice it is not sufficient to consider a single particle (carrier) in terms of describing carrier transport phenomena in semiconductor crystals. Generalizing (1.32) and (1.33) for  $M$  identical particles yields for the  $i$ -th particle

$$\mathbf{v}_i = \dot{\mathbf{r}}_i, \quad (1.36)$$

$$\mathbf{F}_i = m\dot{\mathbf{v}}_i, \quad (1.37)$$

with initial conditions:  $\mathbf{r}_i(0) = \mathbf{r}_{i,0}, \mathbf{v}_i(0) = \mathbf{v}_{i,0}$ . The motion of all  $M$  particles is described by

$$\mathbf{v} = \dot{\mathbf{r}}, \quad (1.38)$$

$$\mathbf{F} = m\dot{\mathbf{v}}, \quad (1.39)$$

$$\mathbf{r}(0) = \mathbf{r}_0, \quad (1.40)$$

$$\mathbf{v}(0) = \mathbf{v}_0. \quad (1.41)$$

This results in a position vector  $\mathbf{r} \in \mathbb{R}^{dM}$ , with entries  $\mathbf{r} = [\mathbf{r}_1, \mathbf{r}_2, \dots, \mathbf{r}_i, \dots, \mathbf{r}_M]^T$  and analogously for  $\mathbf{v}$  and  $\mathbf{F}$ . Furthermore, carrier interactions between the particles (carriers) have to be taken into account (e.g. scattering). Simulating the trajectories for a huge number of particles is the basic idea behind so-called Monte Carlo methods (for details see e.g. [20]). Scattering events are considered by an appropriate selection of random numbers. Tracking carrier trajectories is computationally very expensive, due to the high number of simulated trajectories necessary to yield good results. By nature, Monte Carlo methods suffer from statistical fluctuations. Now, a distribution function  $f(\mathbf{r}, \mathbf{v}, t)$  is introduced, which is the probability density of the particle ensemble. It gives the probability to find a particle at location  $\mathbf{r}$ , with velocity  $\mathbf{v}$  at time  $t$ . An equation for the distribution function is derived in the next section, which offers a deterministic description of this distribution function.

### 1.2.2 Derivation of the Boltzmann Transport Equation

The distribution function  $f$  for carriers in semiconductor crystals with consideration of carrier scattering is described by the BTE. The mathematically detailed derivation of the BTE is technically very advanced and can e.g. be found in [14]. Very short and simple derivations are e.g. found in [20, 28]. These derivations ignore the transition between a  $M$ -particle problem and its single-particle approximation. In this work a compromise between these two ways is given. Therefore the cornerstones of a detailed derivation are presented, without going to deep into the technical details. A similar approach can be found in [25].

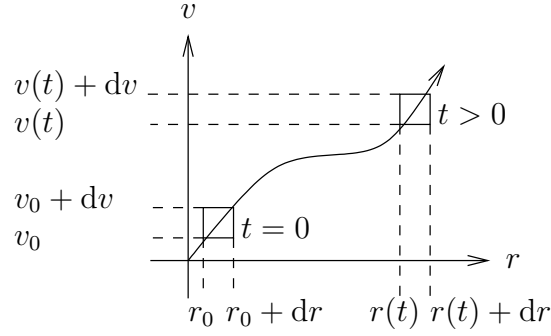


**Figure 1.1:** Trajectory in the position-velocity-space.

### Liouville Equation

In the first part of the derivation, the Liouville theorem is used to formulate the so called *classical Liouville equation*:

**Theorem 4** (Liouville Theorem). *According to [14] the distribution function (probability density)  $f(\mathbf{r}(t), \mathbf{v}(t), t)$  for a carrier ensemble is constant along the trajectories  $(\mathbf{r}(t), \mathbf{v}(t), t)$ , if and only if the following equation holds*

$$\sum_{i=1}^M \left( \frac{\partial \dot{\mathbf{r}}_i}{\partial \mathbf{r}_i} + \frac{\partial \dot{\mathbf{v}}_i}{\partial \mathbf{v}_i} \right) = 0. \quad (1.42)$$

Note that  $\mathbf{r}(t), \mathbf{v}(t) \in \mathbb{R}^{dM}$ . This equation is trivially satisfied for Newton's law ((1.36) and 1.37).

A trajectory in the position-velocity-space is illustrated in Fig. 1.1. The probability to find the carrier ensemble at time  $t = 0$  in an infinitesimal small volume does not change along the trajectories. Assuming that the initial carrier distribution at time  $t = 0$  is

$$f(\mathbf{r}(0), \mathbf{v}(0), 0) = f_0(\mathbf{r}_0, \mathbf{v}_0) = \text{const.} \quad (1.43)$$

and using Theorem 4 gives

$$f(\mathbf{r}(t), \mathbf{v}(t), t) = f_0(\mathbf{r}_0, \mathbf{v}_0) = \text{const.} \quad (1.44)$$

Derivation with respect to the time variable  $t$  leads to

$$\begin{aligned} \frac{\partial f(\mathbf{r}(t), \mathbf{v}(t), t)}{\partial t} &= \frac{\partial f}{\partial t} + \dot{\mathbf{r}} \cdot \nabla_{\mathbf{r}} f + \dot{\mathbf{v}} \cdot \nabla_{\mathbf{v}} f \\ &= \frac{\partial f}{\partial t} + \mathbf{v} \cdot \nabla_{\mathbf{r}} f + \frac{\mathbf{F}}{m} \cdot \nabla_{\mathbf{v}} f \stackrel{!}{=} 0, \end{aligned} \quad (1.45)$$

with the position vector  $\mathbf{r} \in \mathbb{R}^{dM}$ , the velocity vector  $\mathbf{v} \in \mathbb{R}^{dM}$  and the force vector  $\mathbf{F} \in \mathbb{R}^{dM}$ . This equation is called *classical Liouville equation* for a particle ensemble. This equation describes an ensemble of  $M$  particles in vacuum governed by Newton's laws ((1.36) and 1.37) and neglecting particle interactions. The distribution function  $f(\mathbf{r}, \mathbf{v}, t)$  is a mapping  $f : \mathbb{R}^{2dM+1} \mapsto \mathbb{R}$ . In general this equation system cannot be solved numerically because of its huge memory requirement. To see this, consider a mesh with  $N$  discretization points in  $d$  dimensions. Simulating  $M$  carriers would require

$$L = N^{2dM+1} b \quad (1.46)$$

bytes of memory for storing the distribution function on each grid point using  $b$  bytes. With  $b = 4$  byte,  $N = 10$ ,  $M = 10$ , one obtains for  $d = 1, 2, 3$ :

Dimension $d$	Required Memory $L$
1	$4 \times 10^{21}$ Bytes
2	$4 \times 10^{41}$ Bytes
3	$4 \times 10^{61}$ Bytes

This readily shows why a direct solution of (1.45) is not feasible. In the next section it is shown how to solve this problem with a single particle approximation. Alternatively, the *classical Liouville equation* can be formulated for a distribution function  $f(\mathbf{r}, \mathbf{p}, t)$  in the position-momentum-space. Therefore we use the relation  $\mathbf{p} = m\mathbf{v}$  to get

$$\frac{\partial f}{\partial t} + \mathbf{v} \cdot \nabla_{\mathbf{r}} f + \mathbf{F} \cdot \nabla_{\mathbf{p}} f = 0. \quad (1.47)$$

Next, the *semi-classical Liouville equation* for an ensemble of carriers in a semiconductor crystal is derived. Details on semi-classical carrier dynamics are discussed in Section 3.1. In the context of semiconductor devices it is more convenient to use the wave vector  $\mathbf{k}$  instead of the momentum  $\mathbf{p}$  as an argument for the distribution function. The distribution function now reads  $f(\mathbf{r}, \mathbf{k}, t)$ . With the relations <sup>1</sup>

$$\mathbf{v}(\mathbf{k}) = \frac{1}{\hbar} \nabla_{\mathbf{k}} E(\mathbf{k}), \quad (1.48)$$

$$\dot{\mathbf{k}} = \frac{\mathbf{F}}{\hbar}, \quad (1.49)$$

the *semi-classical Liouville equation* for an ensemble of  $M$  carriers is obtained as

$$\frac{\partial f}{\partial t} + \mathbf{v}(\mathbf{k}) \cdot \nabla_{\mathbf{r}} f + \frac{\mathbf{F}}{\hbar} \cdot \nabla_{\mathbf{k}} f = 0, \quad (1.50)$$

with  $\mathbf{r} \in \mathbb{R}^{dM}$ ,  $\mathbf{k} \in \mathcal{B}^M$  and  $\mathbf{F} = [\mathbf{F}_1, \mathbf{F}_2, \dots, \mathbf{F}_i, \dots, \mathbf{F}_M]^T \in \mathbb{R}^{dM}$ , where the wave vector is defined on the so called Brillouin zone  $\mathcal{B}$  (see Section 3.2). In the framework of the *Liouville equation* the force acting on the  $i$ -th carrier is e.g. assumed to be

$$\mathbf{F}_i = \mp q \mathbf{E}(\mathbf{x}_i(t), t), \quad (1.51)$$

where  $-q$  is for electrons and  $+q$  for holes and  $\mathbf{E}$  is the electric field strength. However, carrier interactions are still neglected.

## Vlasov Equation

The *Vlasov equation* is deduced from the *Liouville equation*. First, two-carrier long-range interactions are taken into account [14]. Therefore (1.51) is extended to

$$\mathbf{F}_i = \mp q \mathbf{E}_{\text{ext}}(\mathbf{x}_i, t) \mp q \sum_{j, j \neq i}^M \mathbf{E}_{\text{int}}(\mathbf{x}_i, \mathbf{x}_j), \quad (1.52)$$

with an external electrical field  $\mathbf{E}_{\text{ext}}$  and an internal electrical field  $\mathbf{E}_{\text{int}}$ . Commonly, Coulomb forces for the internal field are assumed:

$$\mathbf{E}_{\text{int}}(\mathbf{x}, \mathbf{y}) = \mp \frac{q}{4\pi\epsilon} \frac{\mathbf{x} - \mathbf{y}}{|\mathbf{x} - \mathbf{y}|^3}, \mathbf{x} \neq \mathbf{y}. \quad (1.53)$$

---

<sup>1</sup> $\mathbf{p} = \hbar\mathbf{k} \Rightarrow \dot{\mathbf{k}} = \dot{\mathbf{p}}/\hbar, \mathbf{F} = \dot{\mathbf{p}}$

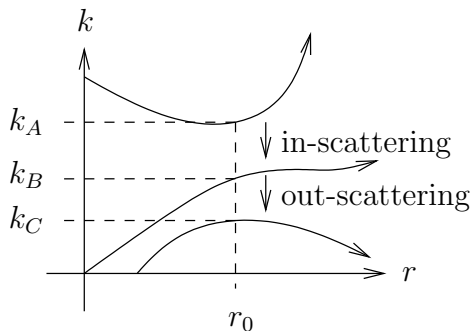


**Figure 1.2:** Scattering between different trajectories.

At this point it is referred to the literature for more details of the derivation, e.g. [14]. The *semi-classical Vlasov equation* reads

$$\frac{\partial f}{\partial t} + \mathbf{v}(\mathbf{k}) \cdot \nabla_{\mathbf{r}} f + \frac{\mathbf{F}}{\hbar} \cdot \nabla_{\mathbf{k}} f = 0, \quad (1.54)$$

with  $\mathbf{F} = [\mathbf{F}_1, \mathbf{F}_2, \dots, \mathbf{F}_i, \dots, \mathbf{F}_m]^T \in \mathbb{R}^{dM}$  and  $\mathbf{F}_i$  according to (1.52). In the limit  $M \rightarrow \infty$ , the *semi-classical Vlasov equation* can be approximated by the so called *Vlasov-Poisson system* [14]:

$$\frac{\partial f}{\partial t} + \mathbf{v}(\mathbf{k}) \cdot \nabla_{\mathbf{r}} f + \frac{\mathbf{F}}{\hbar} \cdot \nabla_{\mathbf{k}} f = 0 \quad (1.55)$$

$$\mathbf{F} = \mp \nabla_{\mathbf{r}} [E_{c0,v0}(\mathbf{r}) - q\Phi(\mathbf{r})] \quad (1.56)$$

$$\nabla^2 \Phi = -\frac{\rho}{\epsilon} \quad (1.57)$$

$$\rho = q(N_D^+ - N_A^- + p - n) \quad (1.58)$$

With the distribution function  $f(\mathbf{r}, \mathbf{k}, t) : \mathbb{R}^d \times \mathcal{B} \times \mathbb{R} \mapsto \mathbb{R}$ . Here, the problem is reduced from  $2 \times M \times d + 1$  to  $2 \times d + 1$  dimensions, which simplifies the problem substantially. Note that the force  $\mathbf{F} \in \mathbb{R}^d$  is now not defined by (1.52), but by (1.56). The minus sign in (1.56) refers to electrons and the plus sign to holes. Further details can be found in Section 3.1.2. Initial conditions and boundary conditions, as well as the equations (1.57) and (1.58) are discussed in the next section.

## Boltzmann Transport Equation

In addition to the *semi-classical Vlasov equation*, the BTE includes short-range particle interactions by introducing a scattering operator  $\underline{\mathbf{Q}}\{f\}$ . Two main assumptions lead to the BTE [14]:

- Scattering takes place instantaneously in time and changes only the wave vector (momentum) of the particle and not its location. In Fig. 1.2 an in-scattering and an out-scattering process are sketched. At location  $r = r_0$  a carrier changes its crystal momentum from  $\hbar k_A$  to  $\hbar k_B$ . From the perspective of the trajectory  $(r_B(t), k_B(t), t)$  this is an in-scattering process. Moreover, an out-scattering event from  $k_B$  to  $k_C$  is drawn.
- The rate of change due to convection and long-range carrier interaction (covered by the *semi-classical Vlasov equation*) is in balance with the rate of change due to scattering:

$$\frac{\partial f(\mathbf{r}, \mathbf{k}, t)}{\partial t} = \underline{\mathbf{Q}}\{f\}. \quad (1.59)$$

The *Vlasov-Poisson system* ((1.55) to 1.58) together with (1.59) leads to the *Boltzmann-Poisson system* for an energy band  $E_{c,v}(\mathbf{r}, \mathbf{k})$  (e.g. conduction band or valence band):

$$\frac{\partial f}{\partial t} + \mathbf{v}(\mathbf{k}) \cdot \nabla_{\mathbf{r}} f + \frac{\mathbf{F}}{\hbar} \cdot \nabla_{\mathbf{k}} f = \underline{\mathbf{Q}}\{f\} \quad (1.60)$$

$$\mathbf{F} = \mp \nabla_{\mathbf{r}} [E_{c0,v0}(\mathbf{r}) - q\Phi(\mathbf{r})] \quad (1.61)$$

$$\nabla^2 \Phi = -\frac{\rho}{\epsilon} \quad (1.62)$$

$$\rho = q(N_{\text{D}}^+ - N_{\text{A}}^- + p - n) \quad (1.63)$$

With  $\mathbf{r} \in \mathbb{R}^d$ ,  $\mathbf{k} \in \mathcal{B}$  and  $\mathbf{F} \in \mathbb{R}^d$  and the initial condition  $f(\mathbf{r}, \mathbf{k}, 0) = f_0(\mathbf{r}, \mathbf{k})$ . The boundary conditions in  $\mathbf{k}$ -space are assumed to be periodic, which reads

$$f(\mathbf{r}, -\mathbf{k}, t) = f(\mathbf{r}, \mathbf{k}, t), \quad \text{with } \mathbf{k} \in \partial\mathcal{B}. \quad (1.64)$$

This follows from the fact that  $\mathbf{k}$ -states are only unique within the first Brillouin zone  $\mathcal{B}$  and periodically repeated outside, thus (1.64) guarantees continuity at the boundaries of the first Brillouin zone. Eq. (1.60) is denoted as the BTE. It is an equation in the  $2d$ -dimensional location-momentum-space with an additional time dependency. Therefore it is a single particle approximation of an  $M$  particle problem and describes the distribution of a carrier ensemble (charged particles) in a semiconductor crystal for a band  $E_{c,v}(\mathbf{r}, \mathbf{k})$ , e.g. conduction band or valence band. In general, a distribution function for each band has to be considered [15]. More details and the calculation of  $n$  and  $p$  are discussed in Section 1.2.4. The minus sign in (1.61) refers to electrons and the plus sign to holes, cf. Section 3.1.2. Eq. (1.57) is referred to as PE. In charge-free regions, the charge density  $\rho$  vanishes and the equation reduces to the Laplace Equation (LE). The PE describes the electrostatic potential  $\Phi$  in a volume with constant permittivity  $\epsilon$ . The electrostatic potential  $\Phi$  is related to the electric field strength  $\mathbf{E}$  by

$$\mathbf{E} = -\nabla\Phi. \quad (1.65)$$

The charge density  $\rho$  has to be further specified. In semiconducting materials, there are charge contributions due to the electron density  $n$ , the hole density  $p$ , the density of ionized donors  $N_{\text{D}}^+$  and acceptors  $N_{\text{A}}^-$ . It follows that

$$\rho = q(N_{\text{D}}^+ - N_{\text{A}}^- + p - n). \quad (1.66)$$

The equation system (1.60) to (1.63) has to be solved self-consistently. Even though the distribution function  $f(\mathbf{r}, \mathbf{k}, t)$  has a statistical interpretation, it is described by a deterministic equation and therefore is not suffering from statistical fluctuations. The scattering operator is discussed in detail in the next section.

### 1.2.3 The Scattering Operator

The scattering operator  $\underline{\mathbf{Q}}\{f\}$  plays an important role in the BTE, because it introduces short-range carrier interactions. In the most general form it is written as

$$\underline{\mathbf{Q}}\{f\}(\mathbf{r}, \mathbf{k}, t) = \underbrace{\sum_{\mathbf{k}'} \underline{\mathbf{P}}^{\text{in}}\{f\}(\mathbf{r}, \mathbf{k}', \mathbf{k})}_{=:\underline{\mathbf{Q}}^{\text{in}}} - \underbrace{\sum_{\mathbf{k}'} \underline{\mathbf{P}}^{\text{out}}\{f\}(\mathbf{r}, \mathbf{k}, \mathbf{k}')}_{=:\underline{\mathbf{Q}}^{\text{out}}}, \quad (1.67)$$



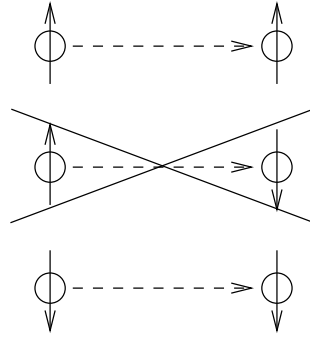


**Figure 1.3:** Scattering processes are assumed to be spin conserving.

where the operator  $\underline{\mathbf{P}}^{\text{in}}\{f\}$  gives the probability for a carrier to scatter from state  $\mathbf{k}'$  to  $\mathbf{k}$  and the operator  $\underline{\mathbf{P}}^{\text{out}}\{f\}$  gives the probability for a carrier to scatter from state  $\mathbf{k}$  to  $\mathbf{k}'$ . A summation over all  $\mathbf{k}'$ -states gives the operator  $\underline{\mathbf{Q}}^{\text{in}}\{f\}$  for the in-scattering rate and the operator  $\underline{\mathbf{Q}}^{\text{out}}\{f\}$  for the out-scattering rate. The summation reflects the discrete nature of  $\mathbf{k}$ -states. The density of states in  $\mathbf{k}$ -space is given by

$$Z(\mathbf{k}) = 2 \frac{L^d}{(2\pi)^d} = 2N_d = \text{const}, \quad (1.68)$$

where the factor 2 accounts for the spin degeneracy of electrons, this means that every state can be occupied by a spin-up and a spin-down electron. The dimension  $d$  of a conceptual sample region depends on the geometric structure of the device. The sample region is characterized by a characteristic length  $L$ . For bulk materials  $d = 3$  and the carriers are free to move in all directions. In this case a conceptual sample volume  $\mathcal{V}$  with  $|\mathcal{V}| = V_s = L^3$  is considered. In quantum wells, carriers are confined in one direction and can only move freely in a plane. Thus  $d = 2$  and a sample area  $\mathcal{A}$  with  $|\mathcal{A}| = A_s = L^2$  is considered. In quantum wires, carriers can only move freely in one direction. Here  $d = 1$  and a sample line  $\mathcal{L}$  with  $|\mathcal{L}| = L$  is considered. If the characteristic length  $L$  is large compared to the characteristic electron wavelength and small on the scale of the device, the summation over  $\mathbf{k}$ -states, according to [15, 20], can be transformed to an integral by

$$\sum_{\mathbf{k}} f(\mathbf{k}) \Leftrightarrow 2N_d \int_{\mathcal{B}} f(\mathbf{k}) d\mathbf{k}. \quad (1.69)$$

Writing (1.67) in integral form yields

$$\underline{\mathbf{Q}}\{f\}(\mathbf{r}, \mathbf{k}, t) = N_d \int_{\mathcal{B}} [\underline{\mathbf{P}}^{\text{in}}\{f\}(\mathbf{r}, \mathbf{k}', \mathbf{k}) - \underline{\mathbf{P}}^{\text{out}}\{f\}(\mathbf{r}, \mathbf{k}, \mathbf{k}')] d\mathbf{k}', \quad (1.70)$$

where the factor 2 for spin degeneracy does not have to be taken into account, because scattering processes are assumed to be spin conserving, see Fig. 1.3. Hence, the spin does not change through scattering [20]. From now on, the more convenient integral-form of the scattering operator is used. Before formulating the in-scattering operator  $\underline{\mathbf{Q}}^{\text{in}}\{f\}$  and the out-scattering operator  $\underline{\mathbf{Q}}^{\text{out}}\{f\}$  respectively, the transition rate according to [15, 20] is defined:

**Definition 3.** *The transition rate  $S(\mathbf{r}, \mathbf{k}, \mathbf{k}')$  is the probability per unit time, that a carrier in initial state  $\mathbf{k}$  scatters to the final state  $\mathbf{k}'$ . More generally, it can be written  $S_{\eta}^{\nu, \nu'}(\mathbf{r}, \mathbf{k}, \mathbf{k}')$ , where  $\nu$  and  $\nu'$  additionally defines the  $\nu$ -th and  $\nu'$ -th energy band and  $\eta$  identifies the scattering process. So the initial state is  $(\nu, \mathbf{k})$  and the final state is  $(\nu', \mathbf{k}')$ .*

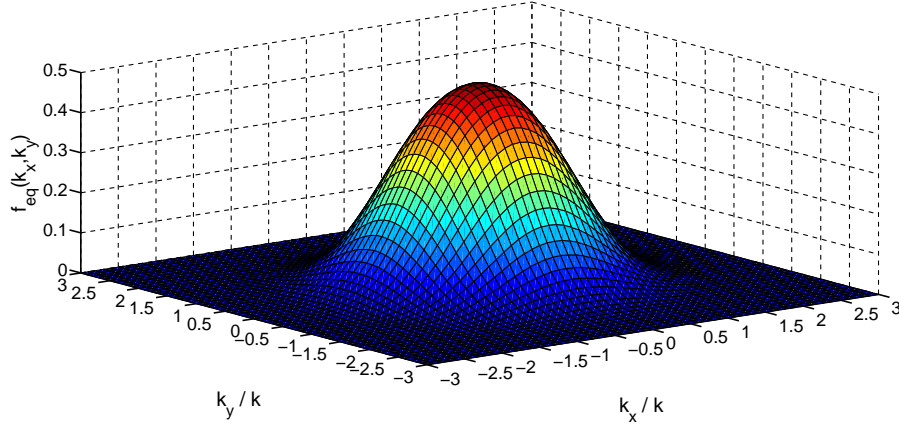


**Figure 1.4:** Distribution function in thermal equilibrium  $f_{\text{eq}}(k_x, k_y)$  as a function of the wave vector  $\mathbf{k}$ . Parabolic bands  $E(\mathbf{k}) = \hbar^2 \mathbf{k}^2 / 2m^*$  are assumed. The components of the wave vector are normalized to  $k = \sqrt{2m^* k_B T / \hbar^2}$ .

The in-scattering operator and the out-scattering operator are [14, 15]

$$\underline{\mathbf{Q}}^{\text{in}}\{f\}(\mathbf{r}, \mathbf{k}', \mathbf{k}) = N_d \int_{\mathcal{B}} S(\mathbf{r}, \mathbf{k}', \mathbf{k}) f(\mathbf{r}, \mathbf{k}', t) [1 - f(\mathbf{r}, \mathbf{k}, t)] d\mathbf{k}', \quad (1.71)$$

$$\underline{\mathbf{Q}}^{\text{out}}\{f\}(\mathbf{r}, \mathbf{k}, \mathbf{k}') = N_d \int_{\mathcal{B}} S(\mathbf{r}, \mathbf{k}, \mathbf{k}') f(\mathbf{r}, \mathbf{k}, t) [1 - f(\mathbf{r}, \mathbf{k}', t)] d\mathbf{k}'. \quad (1.72)$$

The transition rate  $S(\mathbf{r}, \mathbf{k}, \mathbf{k}')$  only gives the probability for a carrier in the initial state  $\mathbf{k}$  to scatter to the final state  $\mathbf{k}'$ , without considering the distribution of states. For this reason, an additional weighting with  $f(\mathbf{r}, \mathbf{k}', t) [1 - f(\mathbf{r}, \mathbf{k}, t)]$  for the in-scattering operator and  $f(\mathbf{r}, \mathbf{k}, t) [1 - f(\mathbf{r}, \mathbf{k}', t)]$  for the out-scattering operator is necessary, where  $f(\mathbf{r}, \mathbf{k}', t)$  is the probability that the initial state  $\mathbf{k}'$  is occupied and  $[1 - f(\mathbf{r}, \mathbf{k}, t)]$  is the probability that the final state  $\mathbf{k}$  is empty and vice versa for the out-scattering operator. For further discussions, the following abbreviations are introduced:

$$S := S(\mathbf{r}, \mathbf{k}, \mathbf{k}') \quad (1.73)$$

$$S' := S(\mathbf{r}, \mathbf{k}', \mathbf{k}) \quad (1.74)$$

$$f := f(\mathbf{r}, \mathbf{k}, t) \quad (1.75)$$

$$f' := f(\mathbf{r}, \mathbf{k}', t) \quad (1.76)$$

Using these abbreviations, the scattering operator (1.67) reads

$$\underline{\mathbf{Q}}\{f\} = N_d \int_{\mathcal{B}} S' f' (1 - f) - S f (1 - f') d\mathbf{k}'. \quad (1.77)$$

### Principle of Detailed Balance

The *principle of detailed balance* states that in thermal equilibrium the local scattering rates vanishes [14], therefore

$$\underline{\mathbf{Q}}^{\text{in}}\{f\} - \underline{\mathbf{Q}}^{\text{out}}\{f\} = 0 \quad (1.78)$$

is obtained. This is now used to derive a relation between  $S$  and  $S'$  in thermal equilibrium. To this end, the distribution function in thermal equilibrium  $f_{\text{eq}}(\mathbf{r}, \mathbf{k})$ , the so called Fermi-Dirac distribution (FDD), has to be introduced. It reads [20]

$$f_{\text{eq}}(\mathbf{r}, \mathbf{k}) = \frac{1}{1 + u(\mathbf{r}, \mathbf{k})}, \quad \text{with } u(\mathbf{r}, \mathbf{k}) = \exp\left(\frac{E_{c,v}(\mathbf{r}, \mathbf{k}) - E_F}{k_B T}\right). \quad (1.79)$$

The FDD is the solution of the BTE in thermal equilibrium, c.f. Fig. 1.4. In the following,  $E_{c,v}(\mathbf{r}, \mathbf{k})$  is abbreviated by  $E(\mathbf{k})$ . It holds that  $\underline{\mathbf{Q}}\{f\} = 0$ , because of (1.78). Together with the FDD, (1.78) gives

$$S'f'_{\text{eq}}(1 - f_{\text{eq}}) = Sf_{\text{eq}}(1 - f'_{\text{eq}}) \Rightarrow \frac{S}{S'} = \frac{f'_{\text{eq}}(1 - f_{\text{eq}})}{f_{\text{eq}}(1 - f'_{\text{eq}})}. \quad (1.80)$$

This expression can be evaluated with

$$1 - f_{\text{eq}}(\mathbf{r}, \mathbf{k}) = \frac{u(\mathbf{r}, \mathbf{k})}{1 + u(\mathbf{r}, \mathbf{k})}. \quad (1.81)$$

Finally, this yields<sup>2</sup>

$$\boxed{\frac{S(\mathbf{r}, \mathbf{k}, \mathbf{k}')}{S(\mathbf{r}, \mathbf{k}', \mathbf{k})} = \exp\left(\frac{E(\mathbf{k}) - E(\mathbf{k}')}{k_B T}\right)}. \quad (1.82)$$

It means that for  $E(\mathbf{k}) = E(\mathbf{k}')$ , in- and out-scattering are in balance:  $S(\mathbf{r}, \mathbf{k}, \mathbf{k}') = S(\mathbf{r}, \mathbf{k}', \mathbf{k})$ . In the case of  $E(\mathbf{k}) < E(\mathbf{k}')$ , the transition rate from  $\mathbf{k}$  to  $\mathbf{k}'$  is smaller than the transitions rate from  $\mathbf{k}'$  to  $\mathbf{k}$ . Thus, there is a net transition from  $\mathbf{k}'$  to  $\mathbf{k}$ , this means from the higher to the lower energy level. For  $E(\mathbf{k}) > E(\mathbf{k}')$  the situation is reversed.

### Low Density Approximation

For non-degenerated semiconductors, it is assumed that  $f(\mathbf{r}, \mathbf{k}, t) \ll 1$  and thus  $[1 - f(\mathbf{r}, \mathbf{k}, t)] \approx 1$ . So (1.77) simplifies to

$$\underline{\mathbf{Q}}_{\text{LD}}\{f\} = N_d \int_{\mathcal{B}} S(\mathbf{r}, \mathbf{k}', \mathbf{k}) f(\mathbf{r}, \mathbf{k}', t) d\mathbf{k}' - f(\mathbf{r}, \mathbf{k}, t) N_d \int_{\mathcal{B}} S(\mathbf{r}, \mathbf{k}, \mathbf{k}') d\mathbf{k}'. \quad (1.83)$$

This is the so-called low density approximation of the scattering operator. It ignores **Pauli's exclusion principle**, which states that every quantum state can be exclusively occupied by one spin-up and one spin-down electron. No two electrons can be in the same quantum state [21]. The scattering rate is defined as

$$\boxed{W(\mathbf{k}) := N_d \int_{\mathcal{B}} S(\mathbf{k}, \mathbf{k}') d\mathbf{k}'}. \quad (1.84)$$

Thus, the low-density approximation follows to

$$\boxed{\underline{\mathbf{Q}}_{\text{LD}}\{f\} = N_d \int_{\mathcal{B}} S(\mathbf{r}, \mathbf{k}', \mathbf{k}) f(\mathbf{r}, \mathbf{k}', t) d\mathbf{k}' - W(\mathbf{k}) f(\mathbf{r}, \mathbf{k}, t)}. \quad (1.85)$$

This form of the scattering operator is widely used in the following chapters.

---

<sup>2</sup>  $\frac{f'_{\text{eq}}(1 - f_{\text{eq}})}{f_{\text{eq}}(1 - f'_{\text{eq}})} = \frac{u}{(1+u')(1+u)} / \frac{u'}{(1+u)(1+u')} = \frac{u}{u'} = \frac{u(\mathbf{r}, \mathbf{k})}{u(\mathbf{r}, \mathbf{k}'')}$

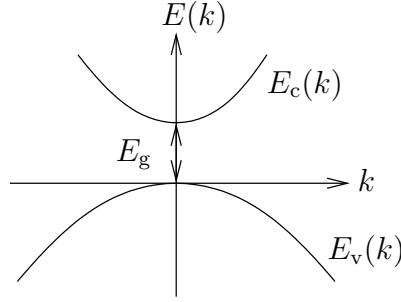


**Figure 1.5:** Simple model of the band structure of a semiconductor. The valence band is described by  $E_v(\mathbf{k})$  and the conduction band by  $E_c(\mathbf{k})$ . The band gap is  $E_g$ .

### Microscopic Relaxation Time Approximation

The relaxation time approximation (RTA) brings a further simplification of the scattering operator. It is assumed that the initial distribution is close to a Maxwell distribution [14]. In this case the following approximation can be made:

$$f(\mathbf{r}, \mathbf{k}', t) \approx n(\mathbf{r}) \exp\left(-\frac{E(\mathbf{k}')}{k_B T}\right). \quad (1.86)$$

Inserting this into (1.85) and using the *principle of detailed balance* (1.82) gives

$$\begin{aligned} \underline{\mathbf{Q}}_{\text{RTA}}\{f\} &= N_d \int_{\mathcal{B}} S(\mathbf{r}, \mathbf{k}', \mathbf{k}) n(\mathbf{r}) \exp\left(-\frac{E(\mathbf{k}')}{k_B T}\right) - S(\mathbf{r}, \mathbf{k}, \mathbf{k}') f(\mathbf{r}, \mathbf{k}, t) d\mathbf{k}' \\ &= N_d \int_{\mathcal{B}} S(\mathbf{r}, \mathbf{k}, \mathbf{k}') \left[ n(\mathbf{r}) \exp\left(-\frac{E(\mathbf{k})}{k_B T}\right) - f(\mathbf{r}, \mathbf{k}, t) \right] d\mathbf{k}' \\ &= -N_d \left[ f(\mathbf{r}, \mathbf{k}, t) - \exp\left(-\frac{E(\mathbf{k})}{k_B T}\right) n(\mathbf{r}) \right] \int_{\mathcal{B}} S(\mathbf{r}, \mathbf{k}, \mathbf{k}') d\mathbf{k}'. \end{aligned} \quad (1.87)$$

With the definition of the relaxation time

$$\tau(\mathbf{r}, \mathbf{k}) = \left( N_d \int_{\mathcal{B}} S(\mathbf{r}, \mathbf{k}, \mathbf{k}') d\mathbf{k}' \right)^{-1} \quad (1.88)$$

the scattering operator is obtained as

$$\underline{\mathbf{Q}}_{\text{RTA}}\{f\} = -\frac{1}{\tau(\mathbf{r}, \mathbf{k})} \left[ f(\mathbf{r}, \mathbf{k}, t) - \exp\left(-\frac{E(\mathbf{k})}{k_B T}\right) n(\mathbf{r}) \right]. \quad (1.89)$$

This is a very simple form of the scattering operator. On the one hand the low density approximation and the RTA simplify the numerical solution of the *Boltzmann-Poisson system* notably, on the other hand the accuracy of the solution suffers. While the low density approximation provides a linear scattering operator, the RTA additionally transforms the BTE from an integro-differential equation into a hyperbolic partial differential equation [25]. In practice always a compromise between accuracy of the solution and simplicity of the model has to be found.

#### 1.2.4 The Multi-Band Boltzmann-Poisson System

In general the band structure of semiconducting materials consists of several valence and conduction bands, which describe the behaviour of the carriers under the influence of the crystal lattice (more details in Section 3.2). A very simple model of such a semiconductor is shown in Fig. 1.5. It contains

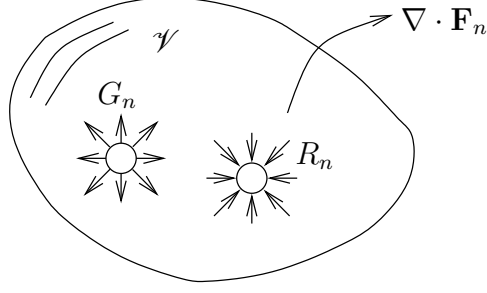


**Figure 1.6:** Visualization of a balance equation. In the sample volume  $\mathcal{V}$ , a quantity is changed due to generation  $G_n$ , destruction  $R_n$  and outflow  $\mathbf{F}_n$ .

two energy bands, the conduction band  $E_c$  and the valence band  $E_v$ . Transport is described by electrons in the conduction band and holes in the valence band. Holes are quasi-carriers, which behave like positively charged electrons. In principle a BTE has to be solved for every band. The total number of bands is  $N = N_p + N_n$ . The first  $N_p$  bands are valence bands and the last  $N_n$  bands are conduction bands. The BTE for the  $\nu$ -th band reads:

$$\frac{\partial f^\nu}{\partial t} + \mathbf{v}^\nu(\mathbf{k}) \cdot \nabla_{\mathbf{r}} f^\nu + \frac{\mathbf{F}^\nu}{\hbar} \cdot \nabla_{\mathbf{k}} f^\nu = \underline{\mathbf{Q}}^\nu \{f^\nu\} \quad (1.90)$$

$$\mathbf{F}^\nu = \mp \nabla_{\mathbf{r}} (E_{c0,v0}^\nu(\mathbf{r}) - q\Phi(\mathbf{r})) \quad (1.91)$$

The group velocity in the  $\nu$ -th band is

$$\mathbf{v}^\nu(\mathbf{k}) = \nabla_{\mathbf{k}} E_{c,v}^\nu(\mathbf{r}, \mathbf{k}). \quad (1.92)$$

Additionally, the scattering operator has to be extended. This yields

$$\underline{\mathbf{Q}}^\nu \{f^\nu\} = N_d \sum_{\nu'} \int_{\mathcal{B}} S^{\nu',\nu}(\mathbf{r}, \mathbf{k}', \mathbf{k}) f^{\nu'}(\mathbf{r}, \mathbf{k}', t) - S^{\nu,\nu'}(\mathbf{r}, \mathbf{k}, \mathbf{k}') f^\nu(\mathbf{r}, \mathbf{k}, t) d\mathbf{k}', \quad (1.93)$$

for the low density approximation. The electron and hole density are obtained as

$$p = \frac{2}{(2\pi)^d} \sum_{\nu=1}^{N_p} \int_{\mathcal{B}} f^\nu(\mathbf{r}, \mathbf{k}, t) d\mathbf{k}, \quad (1.94)$$

$$n = \frac{2}{(2\pi)^d} \sum_{\nu=N_p+1}^N \int_{\mathcal{B}} f^\nu(\mathbf{r}, \mathbf{k}, t) d\mathbf{k}, \quad (1.95)$$

$$(1.96)$$

where a summation over all valence bands for the hole density and over all conduction bands for the electron density is carried out. More details are found in Section 1.3.1. Hybrid concepts are often used in practice, where e.g. on the one hand a BTE for the conduction band is solved and on the other hand the hole density is directly calculated with a simpler model, e.g. the drift-diffusion model (see Section 1.3.5). Examples can be found in [15, 18]. Furthermore, the simpler moment-based models described by balance equations are used to compute an initial guess for the internal electrostatic field [7, 25].

### 1.3 Balance Equations

Balance equations in general describe the change of a quantity in a volume due to generation, destruction and outflow. Consider a small sample volume  $\mathcal{V}$ , which contains a quantity of amount  $N$ ,

with the related density is  $n$ . The generation rate per unit volume is  $G_n$ , the destruction rate per unit volume is  $R_n$ , and  $\mathbf{F}_n$  is the flow of  $n$  through the surface of the volume. This situation is sketched in Fig. 1.6. It holds that

$$\frac{dn}{dt} = -\nabla \cdot \mathbf{F}_n + G_n - R_n, \quad (1.97)$$

for the temporal development of  $n$  [20]. The divergence of  $\mathbf{F}_n$  describing the outflow follows from the *Gaussian theorem*. In the following a general form of balance equations for the BTE is derived.

### 1.3.1 Moments of the Distribution Function

The distribution function described by the BTE has a statistical interpretation. For an ensemble of carriers it gives the probability that a carrier at the location  $\mathbf{r}$  is in state  $\mathbf{k}$  at the time  $t$ . Device engineers are usually interested in macroscopic quantities given by the moments of this distribution function, like carrier density  $n$ , current density  $\mathbf{J}_n$ , momentum density  $\bar{\mathbf{p}}$  and energy density  $\bar{E}$ . In this section, it is discussed how these moments can be calculated from the distribution function  $f(\mathbf{r}, \mathbf{k}, t)$ . To start, a sample volume  $\mathcal{V}$  with size  $|\mathcal{V}| = V_s = L^3$  is considered. The number of carriers  $N$  is given by the distribution function  $f(\mathbf{r}, \mathbf{k}, t)$  as

$$N(\mathcal{V}, t) = \int_{\mathcal{V}} \sum_{\text{all states } \mathbf{k} \text{ at } \mathbf{r}} f(\mathbf{r}, \mathbf{k}, t) d\mathbf{r}. \quad (1.98)$$

The sum can be transformed to an integral over the Brillouin zone  $\mathcal{B}$ . According to (1.69)

$$N(\mathcal{V}, t) = \frac{2V_s}{(2\pi)^3} \int_{\mathcal{V}} \int_{\mathcal{B}} f(\mathbf{r}, \mathbf{k}, t) d\mathbf{k} d\mathbf{r}. \quad (1.99)$$

The carrier density  $n$  can be deduced by the limit  $V_s \rightarrow 0$ . This yields

$$n(\mathbf{r}, t) = \lim_{V_s \rightarrow 0} \frac{N(\mathcal{V}, t)}{V_s} = \frac{2}{(2\pi)^3} \int_{\mathcal{B}} f(\mathbf{r}, \mathbf{k}, t) d\mathbf{k}. \quad (1.100)$$

This can be easily generalized to  $d$  dimensions. Motivated by this result, a general density operator is defined:

**Definition 4.** *The density operator for a  $d$ -dimensional sample region is defined by*

$$\underline{\mathbf{N}}\{\Phi(\mathbf{k})\}(\mathbf{r}, t) = n_{\Phi} := \frac{2}{(2\pi)^d} \int_{\mathcal{B}} \Phi(\mathbf{k}) f(\mathbf{r}, \mathbf{k}, t) d\mathbf{k}, \quad (1.101)$$

for the distribution function  $f(\mathbf{r}, \mathbf{k}, t)$  together with a function of the wave vector  $\Phi(\mathbf{k})$ . It gives the density of the physical quantity specified by  $\Phi(\mathbf{k})$ . E.g. for  $\Phi(\mathbf{k}) = 1$ ,  $\mathbf{p} = \hbar\mathbf{k}$ ,  $E(\mathbf{k})$  the carrier density  $n$ , the crystal momentum density  $\bar{\mathbf{p}}$  and the energy density  $\bar{E}$  are obtained [20]. For more clarity, the short form  $n_{\Phi}$  is used in the following.

### 1.3.2 Balance Equations for the Boltzmann Transport Equation

The spherical harmonics expansion (SHE) of the BTE (1.90) is the main topic of this thesis. Another approach is to solve the balance equations for the different moments of the BTE and additionally introducing appropriate simplifications. In the following, these balance equations are first derived in a general form and then discussed for the most important moments, namely carrier density  $n$ ,

momentum density  $\bar{\mathbf{p}}$  and energy density  $\bar{E}$ . First, the density operator from (1.101) is applied to the BTE, which yields

$$\frac{2}{(2\pi)^d} \left[ \int_{\mathcal{B}} \Phi \frac{\partial f}{\partial t} d\mathbf{k} + \int_{\mathcal{B}} \Phi \mathbf{v} \cdot \nabla_{\mathbf{r}} f d\mathbf{k} + \int_{\mathcal{B}} \Phi \frac{\mathbf{F}}{\hbar} \cdot \nabla_{\mathbf{k}} f d\mathbf{k} \right] = \frac{2}{(2\pi)^d} \int_{\mathcal{B}} \Phi \underline{\mathbf{Q}} d\mathbf{k}. \quad (1.102)$$

For the first term on the left-hand side, integration with respect to  $\mathbf{k}$  and differentiation with respect to  $t$  are interchanged, to find

$$\frac{2}{(2\pi)^d} \int_{\mathcal{B}} \Phi(\mathbf{k}) \frac{\partial f}{\partial t} d\mathbf{k} = \frac{\partial}{\partial t} \left[ \frac{2}{(2\pi)^d} \int_{\mathcal{B}} \Phi(\mathbf{k}) f d\mathbf{k} \right] = \frac{\partial n_{\Phi}}{\partial t}. \quad (1.103)$$

This is the time derivative of the density operator, e.g. for  $\Phi(\mathbf{k}) = 1$  this is the time derivative of the carrier density. In the second term,  $\nabla_{\mathbf{r}}$  can be moved outside the integral, because  $\Phi(\mathbf{k})$  is independent of  $\mathbf{r}$ , to get

$$\frac{2}{(2\pi)^d} \int_{\mathcal{B}} \Phi(\mathbf{k}) \mathbf{v}(\mathbf{k}) \cdot \nabla_{\mathbf{r}} f d\mathbf{k} = \nabla_{\mathbf{r}} \cdot \left[ \frac{2}{(2\pi)^d} \int_{\mathcal{B}} \Phi(\mathbf{k}) \mathbf{v}(\mathbf{k}) f d\mathbf{k} \right] = \nabla_{\mathbf{r}} \cdot \mathbf{F}_{\Phi}, \quad (1.104)$$

where  $\mathbf{F}_{\Phi}$  defines the associated flux. The third term is reformulated to <sup>3</sup>

$$\frac{2}{(2\pi)^d} \int_{\mathcal{B}} \frac{\mathbf{F}}{\hbar} \cdot \Phi(\mathbf{k}) \nabla_{\mathbf{k}} f d\mathbf{k} = \frac{2}{(2\pi)^d} \frac{\mathbf{F}}{\hbar} \cdot \left[ \int_{\mathcal{B}} \nabla_{\mathbf{k}} [\Phi(\mathbf{k}) f] d\mathbf{k} - \int_{\mathcal{B}} f \nabla_{\mathbf{k}} \Phi(\mathbf{k}) d\mathbf{k} \right], \quad (1.105)$$

where the first term on the right-hand side is assumed to be zero [20], due to the exponential decay of  $f$  and Gauss' theorem. Thus,

$$G_{\Phi} = \frac{2}{(2\pi)^d} \frac{\mathbf{F}}{\hbar} \cdot \int_{\mathcal{B}} f \nabla_{\mathbf{k}} \Phi(\mathbf{k}) d\mathbf{k}, \quad (1.106)$$

which is denoted as field generation rate. The scattering term is divided into an intraband and an interband part, which means that all processes within an energy band ( $\nu' = \nu$ ) are considered separately from those between two different energy bands ( $\nu' \neq \nu$ ). This yields

$$\frac{2}{(2\pi)^d} \int_{\mathcal{B}} \Phi(\mathbf{k}) \underline{\mathbf{Q}}\{f\} d\mathbf{k} = \frac{2}{(2\pi)^d} \int_{\mathcal{B}} \Phi(\mathbf{k}) \left[ \underline{\mathbf{Q}}_{\text{intra}}\{f\} + \underline{\mathbf{Q}}_{\text{inter}}\{f\} \right] d\mathbf{k}, \quad (1.107)$$

with

$$\underline{\mathbf{Q}}_{\text{intra}} = N_d \int_{\mathcal{B}} S^{\nu,\nu}(\mathbf{r}, \mathbf{k}', \mathbf{k}) f^{\nu}(\mathbf{r}, \mathbf{k}', t) - S^{\nu,\nu}(\mathbf{r}, \mathbf{k}, \mathbf{k}') f^{\nu}(\mathbf{r}, \mathbf{k}, t) d\mathbf{k}', \quad (1.108)$$

$$\underline{\mathbf{Q}}_{\text{inter}} = N_d \sum_{\nu' \neq \nu} \int_{\mathcal{B}} S^{\nu',\nu}(\mathbf{r}, \mathbf{k}', \mathbf{k}) f^{\nu'}(\mathbf{r}, \mathbf{k}', t) - S^{\nu,\nu'}(\mathbf{r}, \mathbf{k}, \mathbf{k}') f^{\nu}(\mathbf{r}, \mathbf{k}, t) d\mathbf{k}'. \quad (1.109)$$

The term with the interband scattering operator is

$$S_{\Phi} = \frac{2}{(2\pi)^d} \int_{\mathcal{B}} \Phi(\mathbf{k}) \underline{\mathbf{Q}}_{\text{inter}}\{f\} d\mathbf{k}, \quad (1.110)$$

where  $S_{\Phi}$  is denoted as particle generation-recombination rate, because it describes the scattering between bands. The term with the intraband scattering operator according to [20] gives

$$R_{\Phi} = -\frac{2}{(2\pi)^d} \int_{\mathcal{B}} \Phi(\mathbf{k}) \underline{\mathbf{Q}}_{\text{intra}}\{f\} d\mathbf{k} \equiv \left\langle \frac{1}{\tau_{\Phi}} \right\rangle [n_{\Phi}(\mathbf{r}, t) - n_{\Phi}^0(\mathbf{r}, t)], \quad (1.111)$$

<sup>3</sup> $(fg)' = f'g + fg' \Rightarrow fg' = (fg)' - f'g$  and  $\mathbf{F} = \mathbf{F}(\mathbf{r})$ .

where

$$\left\langle \frac{1}{\tau_{\Phi}} \right\rangle \quad (1.112)$$

is the ensemble relaxation rate and  $n_{\Phi}^0$  the density (operator) in thermal equilibrium. The scattering recombination rate  $R_{\Phi}$  describes how an system in non-equilibrium tends back to the equilibrium. Note that (1.111) is the definition for the ensemble relaxation rate without an additional approximation. In the following the band index  $\nu$  is suppressed, because intra-band scattering is considered. Inserting (1.108) into (1.111) results in [20] <sup>4</sup>

$$\begin{aligned} \frac{2}{(2\pi)^d} \int_{\mathcal{B}} \Phi(\mathbf{k}) \underline{\mathbf{Q}}_{\text{intra}} \{f\} d\mathbf{k} &= \frac{2}{(2\pi)^d} N_d \iint_{\mathcal{B}} \Phi [S' f' - S f] d\mathbf{k}' d\mathbf{k} \\ &= \frac{2}{(2\pi)^d} N_d \left[ \iint_{\mathcal{B}} \Phi S' f' d\mathbf{k}' d\mathbf{k} - \iint_{\mathcal{B}} \Phi S f d\mathbf{k}' d\mathbf{k} \right] \\ &= \frac{2}{(2\pi)^d} N_d \left[ \iint_{\mathcal{B}} \underbrace{\Phi' S f d\mathbf{k} d\mathbf{k}'}_{\mathbf{k} \text{ and } \mathbf{k}' \text{ interchanged}} - \iint_{\mathcal{B}} \Phi S f d\mathbf{k}' d\mathbf{k} \right] \\ &= -\frac{2}{(2\pi)^d} N_d \left[ \int_{\mathcal{B}} \Phi f \int_{\mathcal{B}} S \left( 1 - \frac{\Phi'}{\Phi} \right) d\mathbf{k}' d\mathbf{k} \right] \\ &= -\frac{2}{(2\pi)^d} \int_{\mathcal{B}} \Phi f \frac{1}{\tau_{\Phi}(\mathbf{k})} d\mathbf{k}, \end{aligned} \quad (1.113)$$

with the associated relaxation rate

$$\frac{1}{\tau_{\Phi}(\mathbf{k})} = N_d \int_{\mathcal{B}} S \left( 1 - \frac{\Phi(\mathbf{k}')}{\Phi(\mathbf{k})} \right) d\mathbf{k}'. \quad (1.114)$$

For the ensemble relaxation rate

$$\left\langle \frac{1}{\tau_{\Phi}} \right\rangle \equiv \frac{\frac{2}{(2\pi)^d} \int_{\mathcal{B}} \Phi(\mathbf{k}) f(\mathbf{r}, \mathbf{k}, t) \frac{1}{\tau_{\Phi}(\mathbf{k})} d\mathbf{k}}{n_{\Phi}(\mathbf{r}, t) - n_{\Phi}^0(\mathbf{r}, t)} \quad (1.115)$$

is obtained. Finally a general form of the balance equation for a moment of the BTE defined by  $\Phi(\mathbf{k})$  follows as

$$\frac{\partial n_{\Phi}}{\partial t} = -\nabla_{\mathbf{r}} \cdot \mathbf{F}_{\Phi} + G_{\Phi} - R_{\Phi} + S_{\Phi}. \quad (1.116)$$

Any moment is given by an appropriate  $\Phi(\mathbf{k})$ . Note that  $\Phi(\mathbf{k})$  only depends on the wave vector  $\mathbf{k}$ .

### Carrier Density Balance Equation

For  $\Phi(\mathbf{k}) = 1$ , (1.101) for the density operator becomes (1.100), which defines the carrier density. Thus (1.116) with  $\Phi(\mathbf{k}) = 1$  is a balance equation for the carrier density  $n$ . In the following,  $n$  denotes the electron density, but similar results can be obtained for the hole density  $p$ . Trivially the first term becomes  $\frac{\partial n}{\partial t}$ . For  $\mathbf{F}_n$  <sup>5</sup> according to (1.104) this yields

$$\mathbf{F}_n = \frac{2}{(2\pi)^d} \int_{\mathcal{B}} \mathbf{v}(\mathbf{k}) f d\mathbf{k} = n \mathbf{v}_d, \quad (1.117)$$

<sup>4</sup> $\Phi = \Phi(\mathbf{k})$ ,  $\Phi' = \Phi(\mathbf{k}')$ ;  $S, S', f, f'$  according to the (1.73) to (1.76)

<sup>5</sup> $\mathbf{F}_{\Phi(\mathbf{k})=1} = \mathbf{F}_n$



where  $\mathbf{v}_d$  is the drift velocity. The drift velocity  $\mathbf{v}_d$  is connected to the current density  $\mathbf{J}_n$  by

$$\mathbf{J}_n = (-q)n\mathbf{v}_d. \quad (1.118)$$

Thus

$$\mathbf{F}_n = -\frac{\mathbf{J}_n}{q}. \quad (1.119)$$

The field generation rate  $G_n$  according to the approximation in (1.106) is zero, because  $\Phi = \text{const.}$  (1.110) gives

$$S_n = \frac{2}{(2\pi)^d} \int_{\mathcal{B}} \mathbf{Q}_{\text{inter}} \{f\} d\mathbf{k} \quad (1.120)$$

for the carrier generation/recombination rate. The scattering recombination rate  $R_n$  ((1.111)) is obtained as

$$R_n = 0, \quad (1.121)$$

because (1.114) is

$$\frac{1}{\tau_{\Phi}(\mathbf{k})} = N_d \int_{\mathcal{B}} S \left( 1 - \frac{\Phi(\mathbf{k}')}{\Phi(\mathbf{k})} \right) d\mathbf{k}' \Big|_{\Phi(\mathbf{k})=1} = 0. \quad (1.122)$$

It follows that the ensemble relaxation rate (1.115) is zero and therefore  $R_n = 0$ . This is expected, because scattering within an energy band does not change the number of carriers, it only changes the state of the carriers. This is a main assumption for the BTE (see Section 1.2.2). Consequently, the electron density does not relax, so the balance equation for the electron density is

$$\boxed{\frac{\partial n}{\partial t} - \nabla \cdot \mathbf{J}_n = S_n.} \quad (1.123)$$

### Momentum Balance Equation

To obtain the momentum balance equation, the same procedure as for the carrier density balance equation is followed. Set  $\Phi(\mathbf{k}) = \Phi(\mathbf{p}) = \hbar\mathbf{k} = \mathbf{p}(\mathbf{k})$ . Note that  $\Phi(\mathbf{k})$  is a vector-valued function. According to (1.103) the momentum density vector  $\bar{\mathbf{p}}$  is <sup>6</sup>

$$\bar{\mathbf{p}} = \frac{2}{(2\pi)^d} \int_{\mathcal{B}} \mathbf{p}(\mathbf{k}) f d\mathbf{k} = \frac{2}{(2\pi)^d} \int_{\mathcal{B}} \hbar\mathbf{k} f d\mathbf{k}. \quad (1.124)$$

In contrast to the carrier density  $n$ , the momentum density  $\bar{\mathbf{p}}$  is a vectorial quantity and therefore the associated flux  $\tilde{\mathbf{F}}_{\bar{\mathbf{p}}}$  is a tensor. For the  $j$ -th component of the momentum density vector  $\bar{p}_j$  and the  $i$ -th component of the velocity vector  $v_i(\mathbf{k})$ , the corresponding entry of the flux tensor  $\tilde{\mathbf{F}}_{\bar{\mathbf{p}}}$  follows from (1.104) to

$$F_{i,\bar{p}_j} = \frac{2}{(2\pi)^d} \int_{\mathcal{B}} v_i(\mathbf{k}) p_j(\mathbf{k}) f d\mathbf{k}. \quad (1.125)$$

<sup>6</sup> $\bar{\mathbf{x}}$  is the density related to the quantity  $\mathbf{x}$ , e.g.  $\mathbf{p}$  is the momentum and  $\bar{\mathbf{p}}$  the momentum density

In classical mechanics the product  $v_i p_j$  is related to the kinetic energy (see Section 1.3.3). The flux tensor for the momentum density can be written as [23]

$$\tilde{\mathbf{F}}_{\bar{\mathbf{p}}} = \sum_{i,j} F_{i,\bar{p}_j} \mathbf{e}_i \otimes \mathbf{e}_j. \quad (1.126)$$

The field generation rate (1.106) becomes

$$G_{\bar{\mathbf{p}}} = \frac{2}{(2\pi)^d} \frac{\mathbf{F}}{\hbar} \cdot \int_{\mathcal{B}} f \nabla_{\mathbf{k}} \mathbf{p}(\mathbf{k}) d\mathbf{k} = \mathbf{F} \left[ \frac{2}{(2\pi)^d} \int_{\mathcal{B}} f d\mathbf{k} \right] = n\mathbf{F}. \quad (1.127)$$

The carrier generation/recombination rate according to (1.110) is neglected. This is justified for scattering mechanisms which generate carriers with uniformly distributed momentum vectors [20]. The scattering recombination rate is

$$R_{\bar{\mathbf{p}}} = \left\langle \frac{1}{\tau_{\mathbf{p}}} \right\rangle \bar{\mathbf{p}}, \quad (1.128)$$

with  $\bar{\mathbf{p}}^0 = 0$ , because in thermal equilibrium the directions of the momentum vectors are uniformly distributed<sup>7</sup> [20]. Finally, a balance equation for the momentum density  $\bar{\mathbf{p}}$  is obtained as

$$\frac{\partial \bar{\mathbf{p}}}{\partial t} = -\nabla \cdot \tilde{\mathbf{F}}_{\bar{\mathbf{p}}} + n\mathbf{F} - \left\langle \frac{1}{\tau_{\mathbf{p}}} \right\rangle \bar{\mathbf{p}}. \quad (1.129)$$

Under the assumption of parabolic energy bands  $E(\mathbf{k}) = \frac{(\hbar\mathbf{k})^2}{2m^*}$ , it holds that

$$\mathbf{v}(\mathbf{k}) = \frac{1}{\hbar} \nabla_{\mathbf{k}} E(\mathbf{k}) = \frac{\hbar\mathbf{k}}{m^*} = \frac{\mathbf{p}}{m^*}, \quad (1.130)$$

which is equal to the classical relation. In this case the group velocity  $\mathbf{v}(\mathbf{k})$  can be identified as classical drift velocity  $\mathbf{v}_d$ . According to [20], together with<sup>8</sup>

$$\mathbf{J}_n = -qn\mathbf{v}_d = -q\bar{\mathbf{p}}/m^*, \quad (1.131)$$

(1.129) can be rewritten as

$$\frac{\partial \mathbf{J}_n}{\partial t} = \frac{q}{m^*} \nabla \cdot \tilde{\mathbf{F}}_{\bar{\mathbf{p}}} - n \frac{q}{m^*} \mathbf{F} - \left\langle \frac{1}{\tau_{\mathbf{p}}} \right\rangle \mathbf{J}_n. \quad (1.132)$$

This equation can be simplified to a DD equation (see Section 1.3.5). A similar equation can be obtained for holes.

### Energy Balance Equation

With the dispersion relation  $E(\mathbf{k})$  a balance equation for the kinetic energy density is found as

$$\bar{E} = \frac{2}{(2\pi)^d} \int_{\mathcal{B}} E(\mathbf{k}) f d\mathbf{k}. \quad (1.133)$$

<sup>7</sup> $\bar{\mathbf{p}}^0 = \frac{2}{(2\pi)^d} \int_{\mathcal{B}} \hbar\mathbf{k} f_{\text{eq}} d\mathbf{k}$ , note that  $f_{\text{eq}}$  (see (1.79) and Fig. 1.4) is an even function in  $\mathbf{k}$ , therefore the integral evaluates to zero

<sup>8</sup>From  $\mathbf{p} = m^* \mathbf{v}_d(\mathbf{r}, t) \Rightarrow \mathbf{p} = \mathbf{p}(\mathbf{r}, t) \Rightarrow \bar{\mathbf{p}} = n\mathbf{p}$ , because  $\bar{\mathbf{p}} = \frac{2}{(2\pi)^d} \int_{\mathcal{B}} \mathbf{p} f d\mathbf{k}$  (1.124)

The flux of the energy density follows directly from (1.104) to

$$\mathbf{F}_{\bar{E}} = \frac{2}{(2\pi)^d} \int_{\mathcal{B}} E(\mathbf{k}) \mathbf{v}(\mathbf{k}) f d\mathbf{k}. \quad (1.134)$$

The field generation rate ((1.106)) can be explicitly expressed as

$$G_{\bar{E}} = \frac{2}{(2\pi)^d} \frac{\mathbf{F}}{\hbar} \cdot \int_{\mathcal{B}} f \nabla_{\mathbf{k}} E(\mathbf{k}) d\mathbf{k} = \frac{2}{(2\pi)^d} \mathbf{F} \cdot \int_{\mathcal{B}} \mathbf{v}(\mathbf{k}) f d\mathbf{k} = \mathbf{F} \cdot n \mathbf{v}_d = -\frac{1}{q} \mathbf{F} \cdot \mathbf{J}_n. \quad (1.135)$$

This expression needs further explanation. First,

$$\frac{2}{(2\pi)^d} \int_{\mathcal{B}} \mathbf{v}(\mathbf{k}) f d\mathbf{k} = n \langle \mathbf{v} \rangle \quad (1.136)$$

is considered, where  $\langle \mathbf{v} \rangle$  is the mean velocity weighted by the distribution function  $f$ . The carriers velocity is divided into of two parts:

$$\mathbf{v} = \mathbf{v}_d + \mathbf{v}_{th}. \quad (1.137)$$

The drift velocity  $\mathbf{v}_d$  is due to external fields and the thermal velocity  $\mathbf{v}_{th}$  is caused by the random thermal movement of carriers. This yields

$$n \langle \mathbf{v} \rangle = n \langle \mathbf{v}_d + \mathbf{v}_{th} \rangle = n \langle \mathbf{v}_d \rangle + n \langle \mathbf{v}_{th} \rangle = n \langle \mathbf{v}_d \rangle = n \mathbf{v}_d, \quad (1.138)$$

with  $\langle \mathbf{v}_{th} \rangle = 0$ , because the direction of the thermal velocity vector is uniformly distributed [20]. It can be said that the thermal velocity  $\mathbf{v}_{th}$  take place in a random manner and thus does not contribute to the macroscopically observable current density. Thus (1.135) is not an approximation. The particle generation/recombination rate can be calculated according to (1.110):

$$S_{\bar{E}} = \frac{2}{(2\pi)^d} \int_{\mathcal{B}} \Phi(\mathbf{k}) \underline{\mathbf{Q}}_{inter} \{f\} d\mathbf{k}. \quad (1.139)$$

For the scattering recombination rate (1.111)

$$R_{\bar{E}} = \left\langle \frac{1}{\tau_E} \right\rangle [\bar{E}(\mathbf{r}, t) - \bar{E}^0(\mathbf{r}, t)] \quad (1.140)$$

is found. Finally, the balance equation for the energy density is formulated as

$$\frac{\partial \bar{E}}{\partial t} = -\nabla \cdot \mathbf{F}_{\bar{E}} - \frac{1}{q} \mathbf{F} \cdot \mathbf{J}_n - \left\langle \frac{1}{\tau_E} \right\rangle [\bar{E}(\mathbf{r}, t) - \bar{E}^0(\mathbf{r}, t)] + S_{\bar{E}}. \quad (1.141)$$

## Summary

An arbitrary number of such balance equations can be formulated. In principle, this technique can be used to solve the BTE with an arbitrary accuracy. The more balance equations are included, the better is the accuracy of the model. In practice only a few moments ( $n, \bar{\mathbf{p}}, \bar{E}$ ) are considered and *closure conditions*, which are additional simplifications and assumptions, are necessary to eliminate all unknowns. The main problem is that the interpretation of balance equations for moments of higher order is very difficult or even impossible and therefore also the formulation of closure conditions. Here, a short summary for a better overview is given:

balance equation for	equ.	unknowns	unknowns, related to $f$
carrier density $n$	1.123	$n, \mathbf{J}_n$	$S_n\{f\}$
momentum density $\bar{\mathbf{p}}$	1.129	$\bar{\mathbf{p}}$	$\tilde{\mathbf{F}}_{\bar{\mathbf{p}}}\{f\}, \left\langle \frac{1}{\tau_{\bar{\mathbf{p}}}} \right\rangle \{f\}$
current density $\mathbf{J}_n$	1.132	$\mathbf{J}_n$	$\tilde{\mathbf{F}}_{\bar{\mathbf{p}}}\{f\}, \left\langle \frac{1}{\tau_{\bar{\mathbf{p}}}} \right\rangle \{f\}$
kinetic energy density $\bar{E}$	1.141	$\bar{E}, \mathbf{J}_n$	$\mathbf{F}_{\bar{E}}\{f\}, \left\langle \frac{1}{\tau_{\bar{E}}} \right\rangle \{f\}, S_{\bar{E}}\{f\}$

In principle, all unknowns, which depend on the distribution function  $f$ , have to be expressed as a function of the other unknowns, because the distribution function  $f$  cannot be calculated with the method of balance equations. A transport model which includes the carrier density balance equation (1.123), the momentum balance equation (1.129) and the energy balance equation (1.141) is now considered. There are three equations for four unknowns. So this equation system is not solvable without additional assumptions. Using the current density balance equation (1.132) instead of the momentum balance equation (1.129), three equations and three unknowns are obtained. Mind that the current density balance equation is a special case for the momentum balance equation under the assumption of parabolic bands, hence an additional assumption is made. In general, there is always one unknown (which does not depend on  $f$ ) more than the number of balance equation. Detailed discussions are e.g. found in [20]. Furthermore, all models have to be solved self-consistently including the PE (1.62), because the force  $\mathbf{F}$  according to (1.61) depends on the electrostatic potential  $\Phi$ .

### 1.3.3 Carrier Temperature and Heat Flux

In order to simplify the momentum and energy balance equations (see (1.129) and (1.141)), the momentum density flux  $\tilde{\mathbf{F}}_{\bar{\mathbf{p}}}$  and the energy density flux  $\mathbf{F}_{\bar{E}}$  are expressed in terms of the carrier temperature and the heat flux. These two quantities are defined in this section. In the following, simple parabolic energy bands are assumed. According to (1.130),  $\mathbf{p} = m^*\mathbf{v}$  and therefore

$$E = \frac{\mathbf{p}^2}{2m^*} = \frac{m^*\mathbf{v}^2}{2} = \frac{\mathbf{p} \cdot \mathbf{v}}{2}, \quad (1.142)$$

which is equivalent to the expressions in classical mechanics. The kinetic energy tensor is defined as

$$\tilde{\mathbf{E}} = \sum_{i,j} \bar{E}_{i,j} \mathbf{e}_i \otimes \mathbf{e}_j, \quad (1.143)$$

with

$$\bar{E}_{i,j} = \frac{2}{(2\pi)^d} \int_{\mathcal{B}} \frac{p_i v_j}{2} f d\mathbf{k}. \quad (1.144)$$

A comparison with (1.125) yields

$$\tilde{\mathbf{F}}_{\bar{\mathbf{p}}} = 2\tilde{\mathbf{E}}. \quad (1.145)$$

Assuming a parabolic, spherical energy band,  $\bar{E}_{i,i}$  can be rewritten as

$$\begin{aligned} \bar{E}_{i,i} &= \frac{2}{(2\pi)^d} \int_{\mathcal{B}} \frac{p_i v_i}{2} f d\mathbf{k} \\ &= \frac{2}{(2\pi)^d} \int_{\mathcal{B}} \frac{m^* v_i^2}{2} f d\mathbf{k} \\ &= \frac{nm^*}{2} \langle v_i^2 \rangle. \end{aligned} \quad (1.146)$$

Using the definition

$$n \langle \mathbf{v}^2 \rangle = \frac{2}{(2\pi)^d} \int_{\mathcal{B}} \mathbf{v}^2 f d\mathbf{k}, \quad (1.147)$$

the weighted mean of the squared velocity evaluates to

$$\langle \mathbf{v}^2 \rangle = \langle (\mathbf{v}_d + \mathbf{v}_{th})^2 \rangle = \mathbf{v}_d^2 + \langle \mathbf{v}_{th}^2 \rangle, \quad (1.148)$$

where it is assumed that  $\mathbf{v}_d$  and  $\mathbf{v}_{th}$  are uncorrelated. The total kinetic energy density is the trace of the energy density tensor

$$\bar{E} = \text{tr}(\tilde{\mathbf{E}}) = \sum_i \bar{E}_{i,i} = \frac{nm^*}{2} \langle \mathbf{v}^2 \rangle = \frac{nm^*}{2} \mathbf{v}_d^2 + \frac{nm^*}{2} \langle \mathbf{v}_{th}^2 \rangle. \quad (1.149)$$

The kinetic energy density due to the thermal movement of the carriers in thermal equilibrium for parabolic bands according to [20] is

$$\bar{E}_{th} = 3 \frac{1}{2} nk_B T_L, \quad (1.150)$$

with lattice temperature  $T_L$ . The factor 3 appears because every spatial direction has a contribution of  $\frac{1}{2} nk_B T_L$ . Thermal equilibrium yields that  $T_L = T_C$ , where  $T_C$  is the carrier temperature. The carrier temperature  $T_C$  is implicitly determined by

$$3 \frac{1}{2} nk_B T_C \equiv \frac{nm^*}{2} \langle \mathbf{v}_{th}^2 \rangle. \quad (1.151)$$

The mean of the squared thermal velocity  $\langle \mathbf{v}_{th}^2 \rangle$  is directly connected to the carrier temperature  $T_C$ . This equation is generalized to

$$\frac{1}{2} nk_B T_{i,j} \equiv \frac{nm^*}{2} \langle v_{th,i} v_{th,j} \rangle, \quad (1.152)$$

where  $T_{i,j}$  describes the elements of the temperature tensor  $\tilde{\mathbf{T}}$ . The momentum density flux ((1.126)) using (1.145) becomes

$$\tilde{\mathbf{F}}_{\bar{\mathbf{p}}} = 2\tilde{\mathbf{E}}_d + nk_B \tilde{\mathbf{T}}, \quad (1.153)$$

where

$$\tilde{\mathbf{E}}_d = \sum_{i,j} \frac{nm^*}{2} v_{d,i} v_{d,j} \mathbf{e}_i \otimes \mathbf{e}_j \quad (1.154)$$

is the part of the energy density tensor due to the drift velocity. In the next step, the expression for the energy flux  $\mathbf{F}_{\bar{E}}$  is simplified according to (1.134). This yields

$$\mathbf{F}_{\bar{E}} = \frac{2}{(2\pi)^d} \int_{\mathcal{B}} \frac{m^* \mathbf{v}^2}{2} \mathbf{v} f d\mathbf{k} = \frac{nm^*}{2} \langle \mathbf{v}^2 \mathbf{v} \rangle. \quad (1.155)$$

From (1.137) follows

$$\begin{aligned} \mathbf{F}_{\bar{E}} &= \frac{nm^*}{2} \langle \mathbf{v}^2 \mathbf{v} \rangle \\ &= \frac{nm^*}{2} \langle \mathbf{v}^2 (\mathbf{v}_d + \mathbf{v}_{th}) \rangle \\ &= \frac{nm^*}{2} \langle \mathbf{v}^2 \mathbf{v}_d \rangle + \frac{nm^*}{2} \langle \mathbf{v}^2 \mathbf{v}_{th} \rangle \\ &= \frac{nm^*}{2} \langle \mathbf{v}^2 \rangle \mathbf{v}_d + \frac{nm^*}{2} \langle \mathbf{v}^2 \mathbf{v}_{th} \rangle. \end{aligned} \quad (1.156)$$

With (1.149) this yields

$$\mathbf{F}_{\bar{E}} = \bar{E}\mathbf{v}_d + \frac{nm^*}{2} \langle \mathbf{v}^2 \mathbf{v}_{th} \rangle. \quad (1.157)$$

The second term on the right-hand side needs a further analysis:

$$\frac{nm^*}{2} \langle \mathbf{v}^2 \mathbf{v}_{th} \rangle = \frac{nm^*}{2} \langle (\mathbf{v}_d^2 + 2\mathbf{v}_d \cdot \mathbf{v}_{th} + \mathbf{v}_{th}^2) \mathbf{v}_{th} \rangle. \quad (1.158)$$

The first term on the right-hand side vanishes, because

$$\frac{nm^*}{2} \langle \mathbf{v}_d^2 \mathbf{v}_{th} \rangle = \frac{nm^*}{2} \mathbf{v}_d^2 \langle \mathbf{v}_{th} \rangle \quad (1.159)$$

and  $\langle \mathbf{v}_{th} \rangle = 0$ . For the second term the  $i$ -th component of the inner product is considered. A projection onto  $\mathbf{e}_j$ , together with (1.152) yields

$$\begin{aligned} \frac{nm^*}{2} 2 \langle (v_{d,i} v_{th,i}) \mathbf{v}_{th} \rangle \cdot \mathbf{e}_j &= \\ \frac{nm^*}{2} 2 \langle (v_{d,i} v_{th,i}) v_{th,j} \rangle &= \\ \frac{nm^*}{2} 2 v_{d,i} \langle v_{th,i} v_{th,j} \rangle &= v_{d,i} n k_B T_{i,j}. \end{aligned} \quad (1.160)$$

Thus the second term is

$$\mathbf{v}_d \cdot n k_B \tilde{\mathbf{T}}. \quad (1.161)$$

The third term is very similar to the first one. Instead of the drift velocity  $\mathbf{v}_d$ , the energy flux caused by the thermal velocity  $\mathbf{v}_{th}$  (heat flux) is described:

$$\mathbf{Q} = \frac{nm^*}{2} \langle \mathbf{v}_{th}^2 \mathbf{v}_{th} \rangle. \quad (1.162)$$

Finally, (1.157) is written as

$$\mathbf{F}_{\bar{E}} = \bar{E}\mathbf{v}_d + \mathbf{v}_d \cdot n k_B \tilde{\mathbf{T}} + \mathbf{Q}. \quad (1.163)$$

Now consider a small volume element. The first term on the right-hand side is the energy density within this small volume element times the velocity at which it moves. The second term is the velocity of the volume element times the pressure of the electron gas. The third term describes the loss of energy through the outflow of heat [20].

### 1.3.4 Hydrodynamic Equations

In the following the carrier density balance equation (1.123), the momentum balance equation (1.129) and the energy balance equation (1.141) are simplified to obtain the so-called hydrodynamic equations. The aim is to derive an equation system for the carrier density  $n$ , the drift velocity  $\mathbf{v}_d$  and the carrier temperature  $T_C$  as unknowns. As discussed before, further assumptions are necessary. The heat flux according to (1.162) is approximated by

$$\mathbf{Q} = -\kappa \nabla T_C, \quad (1.164)$$

with the thermal conductivity  $\kappa$ . It is assumed that the temperature tensor is diagonal, with entries

$$T_{i,j} = T_C \delta_{i,j}. \quad (1.165)$$

Therefore, the divergence of the temperature tensor is simplified to <sup>9</sup>

$$\nabla \cdot \tilde{\mathbf{T}} = \nabla T_C. \quad (1.166)$$

With these simplifications the divergence of the momentum density flow  $\tilde{\mathbf{F}}_{\bar{\mathbf{p}}}$  (1.153) is obtained as

$$\begin{aligned} \nabla \cdot \tilde{\mathbf{F}}_{\bar{\mathbf{p}}} &= 2\nabla \cdot \tilde{\mathbf{E}}_d + nk_B \nabla \cdot \tilde{\mathbf{T}} \\ &= \nabla \cdot \sum_{i,j} [nm^* v_{d,i} v_{d,j} \mathbf{e}_i \otimes \mathbf{e}_j] + nk_B \nabla T_C, \end{aligned} \quad (1.167)$$

with the drift part of the energy density tensor  $\tilde{\mathbf{E}}_d$  according to (1.154). The divergence of the energy density flow  $\mathbf{F}_{\bar{E}}$  (1.163) reads

$$\begin{aligned} \nabla \cdot \mathbf{F}_{\bar{E}} &= \bar{E} \nabla \cdot \mathbf{v}_d + \nabla \cdot (\mathbf{v}_d \cdot nk_B \tilde{\mathbf{T}}) + \nabla \cdot \mathbf{Q} \\ &= \bar{E} \nabla \cdot \mathbf{v}_d + k_B \nabla \cdot \left( n \mathbf{v}_d \cdot \sum_i T_C \mathbf{e}_i \otimes \mathbf{e}_i \right) - \nabla \cdot (\kappa \nabla T_C) \\ &= \bar{E} \nabla \cdot \mathbf{v}_d + k_B \nabla \cdot (n T_C \mathbf{v}_d) - \nabla \cdot (\kappa \nabla T_C) \\ &= [\bar{E} + k_B n T_C] \nabla \cdot \mathbf{v}_d + k_B T_C \mathbf{v}_d \cdot \nabla n + [k_B n \mathbf{v}_d - \nabla \kappa] \cdot \nabla T_C - \kappa \nabla^2 T_C. \end{aligned} \quad (1.168)$$

Finally, the equation system for the three unknowns  $n$ ,  $\mathbf{v}_d$  and  $T_C$  is:

$$\frac{\partial n}{\partial t} = \nabla \cdot \mathbf{J}_n + S_n, \quad (1.169)$$

$$\frac{\partial \bar{\mathbf{p}}}{\partial t} = -\nabla \cdot \tilde{\mathbf{F}}_{\bar{\mathbf{p}}} + n \mathbf{F} - \left\langle \frac{1}{\tau_{\bar{\mathbf{p}}}} \right\rangle \bar{\mathbf{p}}, \quad (1.170)$$

$$\frac{\partial \bar{E}}{\partial t} = -\nabla \cdot \mathbf{F}_{\bar{E}} - \frac{1}{q} \mathbf{F} \cdot \mathbf{J}_n - \left\langle \frac{1}{\tau_E} \right\rangle [\bar{E}(\mathbf{r}, t) - \bar{E}^0(\mathbf{r}, t)] + S_{\bar{E}}. \quad (1.171)$$

The constitutive relations are

$$\mathbf{J}_n = qn \mathbf{v}_d, \quad (1.172)$$

$$\bar{\mathbf{p}} = nm^* \mathbf{v}_d, \quad (1.173)$$

$$\bar{E} = \frac{nm^* \mathbf{v}_d^2}{2} + \frac{3}{2} nk_B T_C. \quad (1.174)$$

The ensemble relation rates ( $\langle 1/\tau_{\bar{\mathbf{p}}} \rangle$ ,  $\langle 1/\tau_E \rangle$ ) and the generation/recombination rates ( $S_n$ ,  $S_{\bar{E}}$ ) has to be expressed by the three unknowns. The force  $\mathbf{F}$  is given by (1.61). In addition the PE have to be considered. These equations are known as *hydrodynamic equations*, because of their similarity to the equations used to analyze fluid flows [20]. For further details it is referred to the literature, e.g. [20] or [14] for the more mathematically interested reader.

<sup>9</sup> $\nabla \cdot \tilde{\mathbf{T}} = \sum_i (\mathbf{e}_i \partial_i) \cdot T_C \mathbf{e}_i \otimes \mathbf{e}_i = \sum_i \partial_i T_C \otimes \mathbf{e}_i = \sum_i \partial_i T_C \mathbf{e}_i = \nabla T_C.$

### 1.3.5 Drift-Diffusion Equations

The DD equations are one of the simplest descriptions of carrier transport in semiconductors. In this section they are directly derived from the current density balance equation, cf. (1.132), which describes a moment of the BTE. The current density  $\mathbf{J}_n$  is related to the momentum density  $\tilde{\mathbf{p}}$  in the case of simple parabolic bands, see Section 1.3.2. Therefore the DD equations follow from the BTE. The current density balance equation (1.132) is rearranged as follows:

$$\mathbf{J}_n + \frac{1}{\langle 1/\tau_{\mathbf{p}} \rangle} \frac{\partial \mathbf{J}_n}{\partial t} = \frac{q}{\langle 1/\tau_{\mathbf{p}} \rangle m^*} \nabla \cdot \tilde{\mathbf{F}}_{\tilde{\mathbf{p}}} + \frac{q^2 n}{\langle 1/\tau_{\mathbf{p}} \rangle m^*} \mathbf{E}. \quad (1.175)$$

Note that the force term is assumed to be  $\mathbf{F} = -q\mathbf{E}$ . The mobility is defined as

$$\mu_n = \frac{q}{\langle 1/\tau_{\mathbf{p}} \rangle m^*}. \quad (1.176)$$

Neglecting the change of the current density  $\mathbf{J}_n$  over  $\frac{1}{\langle 1/\tau_{\mathbf{p}} \rangle}$  gives

$$\mathbf{J}_n = nq\mu_n \mathbf{E} + \mu_n \nabla \cdot \tilde{\mathbf{F}}_{\tilde{\mathbf{p}}}. \quad (1.177)$$

Further, it is assumed that the momentum flux tensor according to (1.153) reduces to

$$\tilde{\mathbf{F}}_{\tilde{\mathbf{p}}} \approx nk_B \tilde{\mathbf{T}}. \quad (1.178)$$

This means, that the part due to drift is neglected. Furthermore, the temperature tensor  $\tilde{\mathbf{T}}$  is supposed to be diagonal, with entries

$$T_{i,j} = T_C \delta_{i,j}. \quad (1.179)$$

Substitution into (1.177) yields

$$\begin{aligned} \mathbf{J}_n &= nq\mu_n \mathbf{E} + \mu_n \nabla \cdot [nk_B \tilde{\mathbf{T}}] \\ &= nq\mu_n \mathbf{E} + \mu_n k_B \tilde{\mathbf{T}} \cdot \nabla n + \mu_n nk_B \nabla \cdot \tilde{\mathbf{T}} \\ &= nq\mu_n \mathbf{E} + \mu_n k_B \tilde{\mathbf{T}} \cdot \nabla n + \mu_n nk_B \nabla \mathbf{T}_C \\ &= nq\mu_n \mathbf{E} + \mu_n k_B \left[ \sum_i T_C \mathbf{e}_i \otimes \mathbf{e}_i \cdot (\mathbf{e}_i \partial_i) \right] n + \mu_n nk_B \nabla \mathbf{T}_C \\ &\approx nq\mu_n \mathbf{E} + qD_n \cdot \nabla n. \end{aligned} \quad (1.180)$$

It is presumed that the temperature in the considered region is approximately constant and therefore  $\nabla \mathbf{T}_C = 0$ . Furthermore we introduced the diffusion coefficient

$$D_n = \frac{\mu_n k_B T_C}{q}. \quad (1.181)$$

Finally, the DD equations are written in the form

$$\frac{\partial n}{\partial t} = \nabla \cdot \mathbf{J}_n + S_n, \quad (1.182)$$

$$\mathbf{J}_n = nq\mu_n \mathbf{E} + qD_n \cdot \nabla n, \quad (1.183)$$

with the carrier density balance equation 1.123 [20].



### 1.3.6 Conclusion

In the previous sections a method for solving the BTE via balance equations for its moments was presented. This method has two main disadvantages. First, the approach is not scalable. Due to the nature of the balance equations, assumptions have to be made and the number of equations is limited. As an example, the balance equations for the first two moments can be simplified to the so called DD-model or for the first three moments to the so called HD-model. These two models have a simple interpretation, but it is not possible to scale this approach for an arbitrary number of balance equations, because the system is getting too complex and the interpretation is not possible anymore. The second disadvantage is that less information than what is provided by the distribution function  $f(\mathbf{r}, \mathbf{k}, t)$  is obtained. In Chapter 2, the so called SHE of the BTE is discussed. This approach overcomes the disadvantages of the balance equation method.

## Chapter 2

# Spherical Harmonics Expansion of the Boltzmann Transport Equation

In the first part of this chapter, the so-called spherical harmonics  $Y_{l,m}(\theta, \varphi)$  are introduced, which are the angular part of the solution of the Laplace Equation (LE) in spherical coordinates. They form a complete orthonormal set with respect to the inner product of  $\mathbf{L}^2(\Omega)$ , which is the space of square-integrable functions on the unit sphere  $\Omega$ . This property is used to expand the distribution function  $f(\mathbf{r}, \mathbf{k}, t)$  in terms of spherical harmonics  $Y_{l,m}(\theta, \varphi)$  in the second part of this chapter. The state-vector  $\mathbf{k}$  is transformed to spherical coordinates in the energy space, which are  $(E, \theta, \varphi)$ . This leads to the generalized energy distribution function (EDF)  $\mathbf{g}(\mathbf{r}, E, \theta, \varphi, t)$ , which describes the distribution of carriers in energy space. Then, this projection is applied to the Boltzmann Transport Equation (BTE) term-wise, in order to derive an equation system for the expansion coefficients of the EDF  $\mathbf{g}_{l,m}(\mathbf{r}, E, t)$ . For an infinitely large number of equations, this equation system provides an exact solution of the BTE, similar to the equation system of *balance equations* in Section 1.3. The big advantage of the spherical harmonics expansion (SHE) approach is that the expansion order can in principle be chosen arbitrarily, without bothering about *closure conditions*. For details on *closure conditions* consult Section 1.3.2. An adaptive control of the expansion order is also possible [13, 25].

### 2.1 Spherical Harmonics

The aim of this section is to derive the solution of the LE in spherical coordinates by a separation ansatz. The focus is on the angular part of the solution, from which the spherical harmonics  $Y_{l,m}(\theta, \varphi)$  are then obtained. A discussion about the LE can be found e.g. in [10, 23]. Readers with interest in mathematical details are referred to [25], where some additional proofs are given. The LE describes the electrostatic potential  $\Phi$  in a charge-free space. In spherical coordinates  $(r, \theta, \varphi)$  it reads

$$\nabla^2 \Phi = \frac{1}{r^2} \frac{\partial}{\partial r} \left( r^2 \frac{\partial \Phi}{\partial r} \right) + \frac{1}{r^2 \sin(\theta)} \frac{\partial}{\partial \theta} \left( \sin(\theta) \frac{\partial \Phi}{\partial \theta} \right) + \frac{1}{r^2 \sin^2(\theta)} \frac{\partial^2 \Phi}{\partial \varphi^2} = 0. \quad (2.1)$$

With the separation ansatz

$$\Phi(r, \theta, \varphi) = R(r)P(\theta)Q(\varphi), \quad (2.2)$$

(2.1) is rewritten to

$$\frac{PQ}{r^2} \frac{d}{dr} \left( r^2 \frac{dR}{dr} \right) + \frac{RQ}{r^2 \sin(\theta)} \frac{d}{d\theta} \left( \sin(\theta) \frac{dP}{d\theta} \right) + \frac{RP}{r^2 \sin^2(\theta)} \frac{d^2 Q}{d\varphi^2} = 0. \quad (2.3)$$

A multiplication with  $r^2 \sin^2(\theta)/(RPQ)$  yields

$$\frac{\sin^2(\theta)}{R} \frac{d}{dr} \left( r^2 \frac{dR}{dr} \right) + \frac{\sin(\theta)}{P} \frac{d}{d\theta} \left( \sin(\theta) \frac{dP}{d\theta} \right) + \underbrace{\frac{1}{Q} \frac{d^2 Q}{d\varphi^2}}_{=-m^2} = 0, \quad (2.4)$$

where the first two terms depend on  $r$  and  $\varphi$  and the third one only on  $\theta$ . Therefore, the first two terms are equal to a constant, say  $m^2$ , and the third one is equal to  $-m^2$ . In the next step, the last term is substituted by  $-m^2$  and the equation is divided by  $\sin^2(\theta)$ , thus

$$\underbrace{\frac{1}{R} \frac{d}{dr} \left( r^2 \frac{dR}{dr} \right)}_{l(l+1)} + \underbrace{\frac{1}{P \sin(\theta)} \frac{d}{d\theta} \left( \sin(\theta) \frac{dP}{d\theta} \right)}_{-l(l+1)} - \frac{m^2}{\sin^2(\theta)} = 0. \quad (2.5)$$

This is an equation where the first term only depends on  $r$  and the second and the third one only on  $\theta$ . Again it can be concluded that the first term is equal to an constant, which is cleverly chosen as  $l(l+1)$ . Consequently, the second and third terms are equal to  $-l(l+1)$ . Finally, three separated equations for each of the factors  $R, P, Q$  are obtained:

$$\frac{d}{dr} \left( r^2 \frac{dR}{dr} \right) - l(l+1)R = 0 \quad (2.6)$$

$$\frac{1}{\sin(\theta)} \frac{d}{d\theta} \left( \sin(\theta) \frac{dP}{d\theta} \right) + \left[ l(l+1) - \frac{m^2}{\sin^2(\theta)} \right] P = 0 \quad (2.7)$$

$$\frac{d^2 Q}{d\varphi^2} + m^2 Q = 0 \quad (2.8)$$

Eq. (2.6) describes the radial component and is not of interest with regard to the *spherical harmonics* and therefore not discussed further, because the *spherical harmonics* describe only the angular part of the solution given by (2.7) and (2.8). The general solution of (2.8) for  $m^2 \neq 0$  with arbitrary constants  $A$  and  $B$  is

$$Q_m(\varphi) = A \cos(m\varphi) + B \sin(m\varphi). \quad (2.9)$$

With the substitution  $\cos(\theta) \mapsto \xi$ , (2.7) takes the form

$$\frac{d}{d\theta} \left[ (1 - \xi^2) \frac{dP}{d\xi} \right] + \left[ l(l+1) - \frac{m^2}{1 - \xi^2} \right] P = 0 \quad (2.10)$$

and is named the *associated Legendre differential equation* and for  $m^2 = 0$  the *Legendre differential equation*, which is

$$\frac{d}{d\theta} \left[ (1 - \xi^2) \frac{dP}{d\xi} \right] + l(l+1)P = 0. \quad (2.11)$$

This equation is solved by the so called *Legendre polynomials*, which are given by

$$P_l(\xi) = \frac{1}{2^l l!} \frac{d^l}{d\xi^l} (\xi^2 - 1)^l, \quad (2.12)$$

with  $l = 0, 1, 2, \dots$  and  $\xi \in [-1, 1]$ . A discussion about (2.11) is found in [10, 25, 29]. The *Legendre polynomials* form a complete set of orthogonal functions with respect to the inner product on  $\mathbf{L}^2([-1, 1])$ ,

which is the space of square-integrable functions on the interval  $[-1, 1]$ . The corresponding orthogonality relation is given by

$$\int_{-1}^1 P_{l'}(\xi)P_l(\xi)d\xi = \frac{2}{2l+1}\delta_{l',l}. \tag{2.13}$$

The *associated Legendre differential equation* (2.10) has solutions of the form

$$P_l^m(\xi) = (-1)^m(1-\xi^2)^{m/2}\frac{d^m}{d\xi^m}P_l(\xi), \tag{2.14}$$

for  $m = 0, 1, 2, \dots, l$ . They are called *associated Legendre functions*. With

$$P_l^{-m}(\xi) = (-1)^m\frac{(l-m)!}{(l+m)!}P_l^m(\xi), \tag{2.15}$$

the solutions for  $m < 0$  are related to those for  $m > 0$ . For a fixed  $m \geq 0$ , the *associated Legendre functions* form a complete set of orthogonal functions with respect to the inner product on  $\mathbf{L}^2([-1, 1])$ , with the orthogonality relation

$$\int_{-1}^1 P_{l'}^m(\xi)P_l^m(\xi)d\xi = \frac{2}{2l+1}\frac{(l+m)!}{(l-m)!}\delta_{l',l}. \tag{2.16}$$

Finally, (2.9), (2.14) and (2.15) are used to define a set of orthonormal functions called *spherical harmonics* [10, 25]. The normalization factors are found due to (2.16) and  $\int_0^{2\pi} \sin^2(m\varphi)d\varphi = \int_0^{2\pi} \cos^2(m\varphi)d\varphi = \pi$ , as well as  $\int_0^{2\pi} d\varphi = 2\pi$ .

**Definition 5** (Real-Valued Spherical Harmonics). *The real-valued spherical harmonics according to [25] are defined by*

$$Y_{l,m}(\theta, \varphi) := \begin{cases} \sqrt{\frac{1}{\pi}\frac{(l-m)!}{(l+m)!}\frac{2l+1}{2}}P_l^m(\cos(\theta))\cos(m\varphi), & m > 0 \\ \sqrt{\frac{1}{2\pi}\frac{2l+1}{2}}P_l(\cos(\theta)), & m = 0 \\ \sqrt{\frac{1}{\pi}\frac{(l+m)!}{(l-m)!}\frac{2l+1}{2}}P_l^{-m}(\cos(\theta))\sin(m\varphi), & m < 0. \end{cases} \tag{2.17}$$

The *spherical harmonics* form a complete orthonormal set with respect to the inner product on  $\mathbf{L}^2(\Omega)$ . The orthogonality relation reads

$$\int_{\Omega} Y_{l',m'}Y_{l,m}d\Omega = \delta_{l',l}\delta_{m',m}, \tag{2.18}$$

where  $\int_{\Omega}\{\cdot\}d\Omega$  denotes integration over the unit sphere  $\Omega$  and is a short-hand notation for

$$\int_0^{2\pi} \int_0^{\pi} \{\cdot\} \sin(\theta)d\theta d\varphi \Leftrightarrow \int_{\Omega} \{\cdot\}d\Omega. \tag{2.19}$$

In Fig. 2.1 and Fig. 2.2 the first sixteen spherical harmonics are illustrated. There also exists a complex-valued form of the *spherical harmonics*, which is given by

$$Y_{l,m}(\theta, \varphi) = \sqrt{\frac{1}{2\pi}\frac{(l-m)!}{(l+m)!}\frac{2l+1}{2}}P_l^m(\cos(\theta))e^{im\varphi}. \tag{2.20}$$

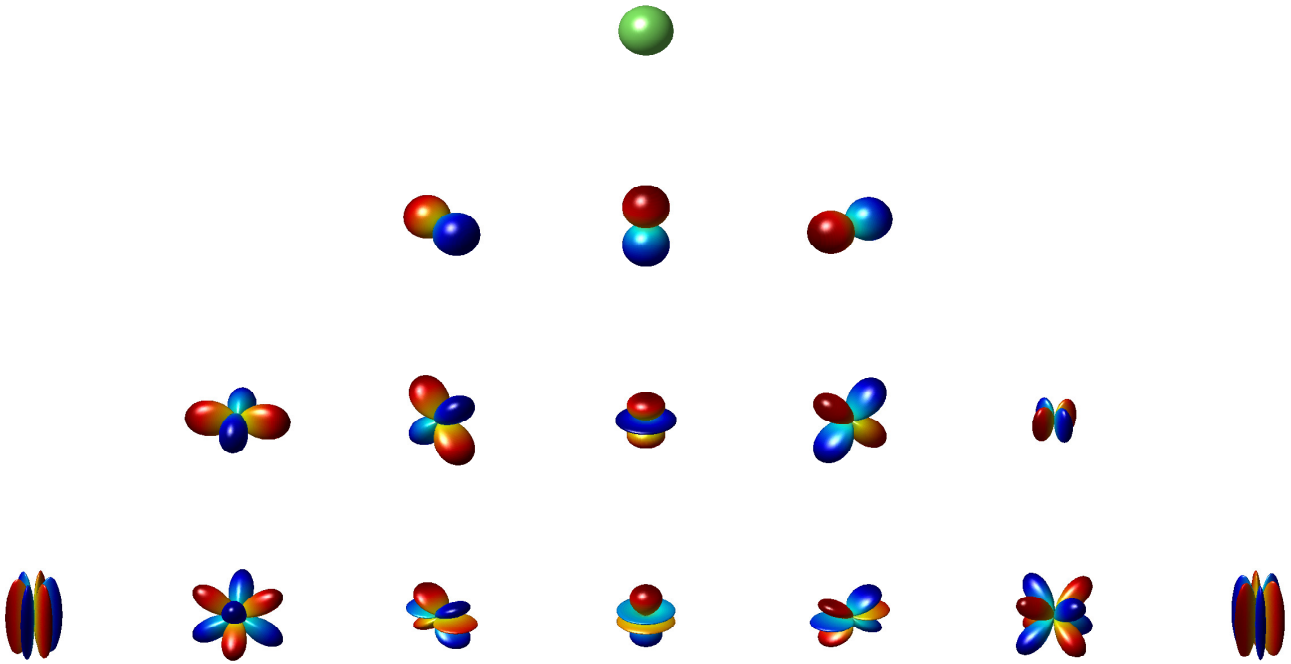


**Figure 2.1:** Plot of the first sixteen spherical harmonics  $Y_{l,m}(\theta, \varphi)$  in spherical coordinates  $(r, \theta, \varphi)$ , with  $r = |Y_{l,m}(\theta, \varphi)|$ . The transition from blue to red is according to the transition from negative to positive values of  $Y_{l,m}$ . The number of the row corresponds to the value of  $l$ , starting with  $l = 0$ . In each row,  $m$  ranges from  $-l$  to  $l$  in steps of 1.

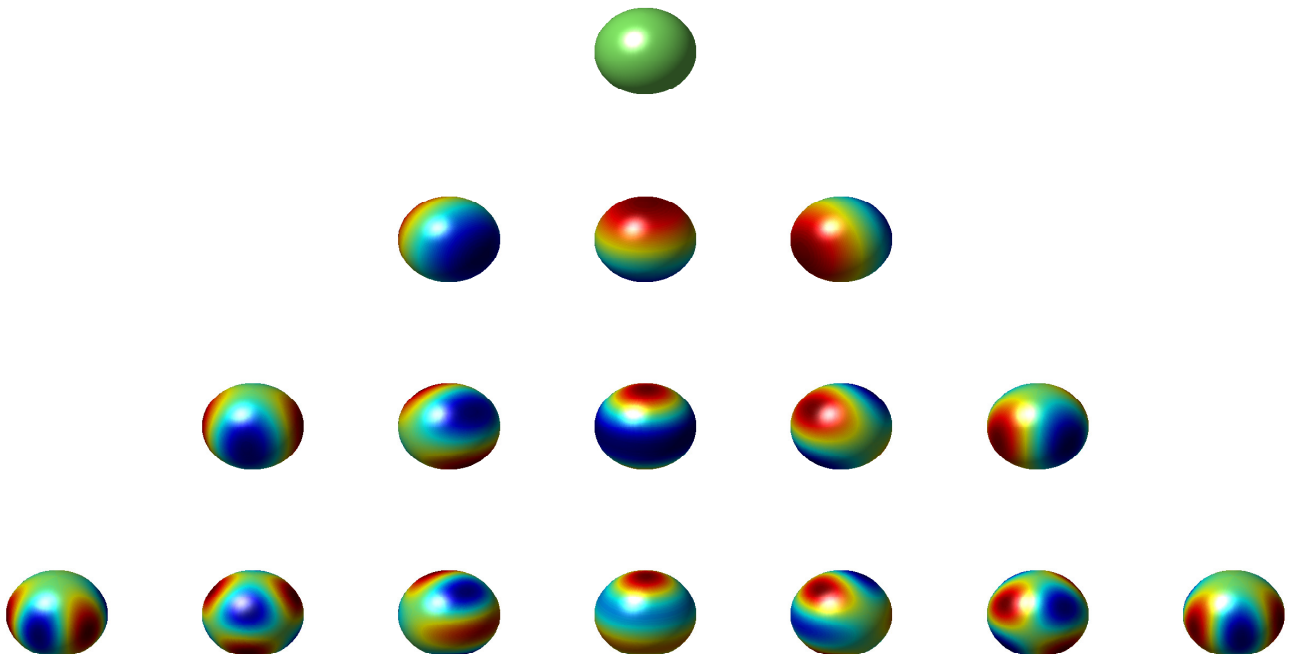


**Figure 2.2:** Plot of the first sixteen spherical harmonics  $Y_{l,m}(\theta, \varphi)$  over the unit sphere. The transition from blue to red is according to the transition from negative to positive values of  $Y_{l,m}$ . The number of the row corresponds to the value of  $l$ , starting with  $l = 0$ . In each row,  $m$  ranges from  $-l$  to  $l$  in steps of 1.

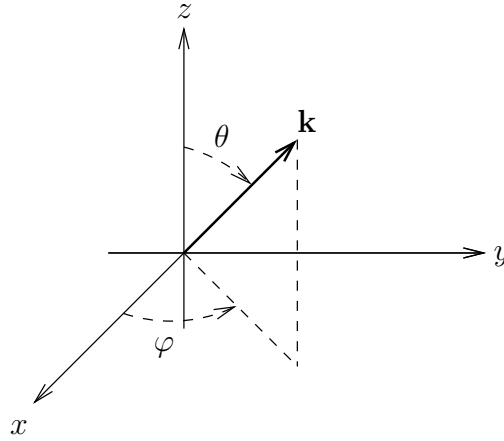


**Figure 2.3:** The wave vector  $\mathbf{k}$  in spherical coordinates.

## 2.2 Spherical Harmonics Expansion of the Distribution Function

In the last section, the so called *spherical harmonics*  $Y_{l,m}(\theta, \varphi)$  were introduced. In the following, a formalism to expand the distribution function  $f(\mathbf{r}, \mathbf{k}, t)$  with *spherical harmonics* is developed. Therefore, the expansion coefficients are obtained by projecting the distribution function onto *spherical harmonics* on equi-energy surfaces. For this purpose, the  $\mathbf{k}$ -vector is transformed to spherical coordinates in the energy space, given by  $(E, \theta, \varphi)$ . In general, the relation between the wave vector  $\mathbf{k}$  and the energy  $E$  in the  $\nu$ -th energy band is given by

$$E_{c,v}^\nu = E_{c,v}^\nu(\mathbf{k}), \quad (2.21)$$

where “c” denotes a conduction band and “v” a valence band respectively. This is a mapping  $E : \mathbb{R}^3 \rightarrow \mathbb{R}$ . Note that in the following these indices are omitted. The  $\mathbf{k}$ -vector is now written with respect to spherical coordinates, which yields

$$\mathbf{k} = k \mathbf{e}_k, \quad (2.22)$$

where  $k = |\mathbf{k}|$  and  $\mathbf{e}_k = \mathbf{e}_k(\theta, \varphi)$  is the unit vector in radial direction. According to Fig. 2.3, the unit vector  $\mathbf{e}_k$  depends on the polar angle  $\theta$  and the azimuth angle  $\varphi$ . Thus

$$E = E^\nu(k, \varphi, \theta), \quad (2.23)$$

and for a bijective mapping between  $E$  and  $k$ , the magnitude of the wave vector is

$$k = k^\nu(E, \theta, \varphi), \quad (2.24)$$

which is a mapping  $k : \mathbb{R}^3 \rightarrow \mathbb{R}$ . Therefore the wave vector itself follows as

$$\mathbf{k} = \mathbf{k}(E, \theta, \varphi) = k^\nu(E, \theta, \varphi) \mathbf{e}_k(\theta, \varphi). \quad (2.25)$$

Next, an expression for the SHE-coefficients is developed. Therefore, a projection of the distribution function  $f$  onto spherical harmonics on equi-energy surfaces is carried out by

$$f_{l,m}(\mathbf{r}, E, t) = \frac{2}{(2\pi)^3} \int_B \delta(E - E(\mathbf{k})) Y_{l,m}(\theta, \varphi) f(\mathbf{r}, \mathbf{k}, t) d\mathbf{k}. \quad (2.26)$$

The  $\mathbf{k}$ -volume-element is transformed to spherical coordinates, with

$$d\mathbf{k} = dk_x dk_y dk_z \rightarrow k^2 \sin(\theta) dk d\theta d\varphi. \quad (2.27)$$

The integral in (2.26) is simplified with (2.19) to yield

$$\begin{aligned}
f_{l,m}(\mathbf{r}, E, t) &= \frac{2}{(2\pi)^3} \int_{\Omega} \int \delta(E - E(\mathbf{k})) Y_{l,m}(\theta, \varphi) f(\mathbf{r}, \mathbf{k}(E, \theta, \varphi), t) k^2 dk \sin(\theta) d\theta d\varphi \\
&= \frac{2}{(2\pi)^3} \int_{\Omega} \int_{\mathbb{R}_0^+} \delta(E - E') Y_{l,m}(\theta, \varphi) f(\mathbf{r}, \mathbf{k}(E', \theta, \varphi), t) k^2 \frac{dk(E', \theta, \varphi)}{dE'} dE' d\Omega \\
&= 2 \int_{\Omega} Y_{l,m}(\theta, \varphi) f(\mathbf{r}, \mathbf{k}(E, \theta, \varphi), t) Z(E, \theta, \varphi) d\Omega,
\end{aligned} \tag{2.28}$$

with the *generalized density of states* for one spin direction:

**Definition 6** (Generalized Density Of States). *The generalized density of states is defined as:*

$$Z(E, \theta, \varphi) := \frac{k^2}{(2\pi)^3} \frac{\partial k(E, \theta, \varphi)}{\partial E}. \tag{2.29}$$

The following definition is used, to keep the expressions short and clear:

**Definition 7** (Generalized Energy Distribution Function). *The generalized energy distribution function (EDF) is defined as*

$$\mathbf{g}(\mathbf{r}, E, \theta, \varphi, t) = 2Z(E, \theta, \varphi) f(\mathbf{r}, \mathbf{k}(E, \theta, \varphi), t). \tag{2.30}$$

The projection of the EDF  $\mathbf{g}(\mathbf{r}, E, \theta, \varphi, t)$  onto spherical harmonics  $Y_{l,m}(\theta, \varphi)$  on equi-energy surfaces reads:

$$\mathbf{g}_{l,m}(\mathbf{r}, E, t) = \int_{\Omega} Y_{l,m}(\theta, \varphi) \mathbf{g}(\mathbf{r}, E, \theta, \varphi, t) d\Omega. \tag{2.31}$$

Furthermore, the projection can be carried out in energy space, without bothering about the transformation from  $\mathbf{k}$ -space to energy space, thus the projection integral is simplified. The expansion of the EDF  $\mathbf{g}$  into real-valued orthonormal spherical harmonics  $Y_{l,m}(\theta, \varphi)$  is given by

$$\mathbf{g}(\mathbf{r}, E, \theta, \varphi, t) = \sum_{l=0}^{\infty} \sum_{m=-l}^l \mathbf{g}_{l,m}(\mathbf{r}, E, t) Y_{l,m}(\theta, \varphi). \tag{2.32}$$

The carrier density can be obtained directly from the zeroth order term of the expansion of the EDF, according to

$$n(\mathbf{r}, t) = \frac{1}{Y_{0,0}} \int_{\mathbb{R}_0^+} g_{0,0}(\mathbf{r}, E, t) dE, \text{ with } Y_{0,0} = \frac{1}{\sqrt{4\pi}}. \tag{2.33}$$

In the following, an equation system for the expansion coefficients of the EDF is developed [15, 25].

## 2.3 Spherical Harmonics Expansion of the BTE

The expansion coefficients  $\mathbf{g}_{l,m}(\mathbf{r}, E, t)$  according to (2.31) are now used to solve the BTE. The aim is to develop an equation system for the expansion coefficients. Therefore, the BTE according to (1.60) is projected onto spherical harmonics  $Y_{l,m}(\theta, \varphi)$  in the same way as the distribution function  $f(\mathbf{r}, \mathbf{k}, t)$  in (2.28):

$$2 \int_{\Omega} Y_{l,m}(\theta, \varphi) \{\text{BTE}\} Z(E, \theta, \varphi) d\Omega \quad (2.34)$$

The same approach is e.g. followed in [15, 25]. An alternative approach can be found in [7], where the distribution function is also expanded in spherical harmonics and an equation system for the unknown expansion coefficients is obtained by substituting the expansion ansatz directly into the BTE and balancing the harmonic components of the same order. This entails a lot of bookkeeping. Moreover, a flexible control of the expansion order is not possible and the approach is limited to low expansion orders.

### 2.3.1 Spherical Harmonics Expansion of the Free-Streaming Operator

The projection of the BTE is done term-by-term. For the first term on the left-hand side,

$$\frac{\partial f}{\partial t} \rightarrow 2 \int_{\Omega} Y_{l,m}(\theta, \varphi) \frac{\partial f}{\partial t} Z(E, \theta, \varphi) d\Omega = \frac{\partial \mathbf{g}_{l,m}}{\partial t} \quad (2.35)$$

is obtained. Before examining the second term, the *generalized current density* is introduced:

**Definition 8** (Generalized Current Density). *The generalized current density is defined by*

$$\begin{aligned} \mathbf{j}_{l,m}(\mathbf{r}, E, t) &= 2 \int_{\Omega} Y_{l,m}(\theta, \varphi) \mathbf{v}(\mathbf{k}(E, \theta, \varphi)) f(\mathbf{r}, \mathbf{k}(E, \theta, \varphi), t) Z(E, \theta, \varphi) d\Omega \\ &= \int_{\Omega} Y_{l,m}(\theta, \varphi) \mathbf{v}(\mathbf{k}(E, \theta, \varphi)) \mathbf{g}(\mathbf{r}, E, \theta, \varphi, t) d\Omega. \end{aligned} \quad (2.36)$$

The group velocity does not depend on the spatial coordinate  $\mathbf{r}$ , so  $\mathbf{v}(\mathbf{k}) \nabla_{\mathbf{r}} f = \nabla_{\mathbf{r}} (\mathbf{v}(\mathbf{k}) f)$ , thus the second term, also called *diffusion term*, is

$$\begin{aligned} \mathbf{v}(\mathbf{k}) \cdot \nabla_{\mathbf{r}} f &\rightarrow 2 \int_{\Omega} Y_{l,m}(\theta, \varphi) \mathbf{v}(\mathbf{k}(E, \theta, \varphi)) \cdot \nabla_{\mathbf{r}} f Z(E, \theta, \varphi) d\Omega \\ &= \nabla_{\mathbf{r}} \cdot 2 \int_{\Omega} Y_{l,m}(\theta, \varphi) \mathbf{v}(\mathbf{k}(E, \theta, \varphi)) f Z(E, \theta, \varphi) d\Omega \\ &= \nabla_{\mathbf{r}} \cdot \mathbf{j}_{l,m}. \end{aligned} \quad (2.37)$$

The current density  $\mathbf{J}$  is directly obtained by

$$\mathbf{J}(\mathbf{r}, t) = \frac{1}{Y_{0,0}} \int_{\mathbb{R}_0^+} \mathbf{j}_{0,0}(\mathbf{r}, E, t) dE, \quad (2.38)$$

with  $Y_{0,0} = 1/\sqrt{4\pi}$ . The projection of the third term is obtained using integration by parts and periodic boundary conditions in  $\mathbf{k}$  according to (1.64). First, the projection integral is set up. This gives

$$\begin{aligned} \frac{\mathbf{F}}{\hbar} \cdot \nabla_{\mathbf{k}} f &\rightarrow \frac{2}{(2\pi)^3} \int_{\mathcal{B}} \delta(E - E(\mathbf{k})) Y_{l,m}(\theta, \varphi) \frac{\mathbf{F}}{\hbar} \cdot \nabla_{\mathbf{k}} f d\mathbf{k} \\ &= \frac{2}{(2\pi)^3} \frac{\mathbf{F}}{\hbar} \cdot \int_{\mathcal{B}} \delta(E - E(\mathbf{k})) Y_{l,m}(\theta, \varphi) \nabla_{\mathbf{k}} f d\mathbf{k}. \end{aligned} \quad (2.39)$$



An appropriate test function  $\gamma(E)$  is used to avoid formal difficulties with the Dirac distribution  $\delta$  and an integration over the energy space is made. With integration by parts, the integral (2.39) is rearranged to

$$\begin{aligned}
& \frac{2}{(2\pi)^3} \frac{\mathbf{F}}{\hbar} \cdot \int_{\mathbb{R}_0^+} \gamma(E) \int_{\mathcal{B}} \delta(E - E(\mathbf{k})) Y_{l,m}(\theta, \varphi) \nabla_{\mathbf{k}} f d\mathbf{k} dE \\
&= \frac{2}{(2\pi)^3} \frac{\mathbf{F}}{\hbar} \cdot \int_{\mathcal{B}} \gamma(E(\mathbf{k})) Y_{l,m}(\theta, \varphi) \nabla_{\mathbf{k}} f d\mathbf{k} \\
&= \frac{2}{(2\pi)^3} \frac{\mathbf{F}}{\hbar} \cdot \left[ \underbrace{\gamma(E(\mathbf{k})) Y_{l,m}(\theta, \varphi) f \Big|_{\partial\mathcal{B}}}_{=0; \text{ BC according to (1.64)}} - \int_{\mathcal{B}} \nabla_{\mathbf{k}} [\gamma(E(\mathbf{k})) Y_{l,m}(\theta, \varphi)] f d\mathbf{k} \right] \\
&= -\frac{2}{(2\pi)^3} \frac{\mathbf{F}}{\hbar} \cdot \int_{\mathcal{B}} \left[ \frac{\partial\gamma}{\partial E} \underbrace{\nabla_{\mathbf{k}}(E(\mathbf{k}))}_{=\hbar\mathbf{v}(\mathbf{k})} Y_{l,m}(\theta, \varphi) + \gamma \nabla_{\mathbf{k}} Y_{l,m}(\theta, \varphi) \right] f d\mathbf{k}. \tag{2.40}
\end{aligned}$$

The gradient of the spherical harmonics  $Y_{l,m}(\theta, \varphi)$  in spherical coordinates  $(k, \theta, \varphi)$  reads

$$\nabla_{\mathbf{k}} Y_{l,m}(\theta, \varphi) = \underbrace{\frac{\partial Y_{l,m}}{\partial k}}_{=0} \mathbf{e}_k + \frac{1}{k} \frac{\partial Y_{l,m}}{\partial \theta} \mathbf{e}_\theta + \frac{1}{k \sin(\theta)} \frac{\partial Y_{l,m}}{\partial \varphi} \mathbf{e}_\varphi. \tag{2.41}$$

Now (2.40) is transformed to spherical coordinates, using the abbreviation  $\mathbf{k} = \mathbf{k}(E, \theta, \varphi)$ :

$$\begin{aligned}
& -\mathbf{F} \cdot \left[ \int_{\mathbb{R}_0^+} \frac{\partial\gamma}{\partial E} \underbrace{2 \int_{\Omega} Y_{l,m} \mathbf{v} f Z d\Omega}_{=\mathbf{j}_{l,m}} dE + \int_{\mathbb{R}_0^+} \gamma \underbrace{\frac{2}{\hbar} \int_{\Omega} \nabla_{\mathbf{k}} Y_{l,m}(\theta, \varphi) f Z d\Omega}_{=\mathbf{\Gamma}_{l,m}} dE \right] \\
&= -\mathbf{F} \cdot \left[ \int_{\mathbb{R}_0^+} \frac{\partial\gamma}{\partial E} \mathbf{j}_{l,m} dE + \int_{\mathbb{R}_0^+} \gamma \mathbf{\Gamma}_{l,m} dE \right] \\
&= -\mathbf{F} \cdot \left[ \gamma \mathbf{j}_{l,m} \Big|_{-\infty}^{+\infty} - \int_{\mathbb{R}_0^+} \gamma \frac{\partial \mathbf{j}_{l,m}}{\partial E} dE + \int_{\mathbb{R}_0^+} \gamma \mathbf{\Gamma}_{l,m} dE \right] \\
&= \mathbf{F} \cdot \int_{\mathbb{R}_0^+} \gamma \left[ \frac{\partial \mathbf{j}_{l,m}}{\partial E} - \mathbf{\Gamma}_{l,m} \right] dE. \tag{2.42}
\end{aligned}$$

Since  $\gamma$  is arbitrary, it is concluded, that the integral can be evaluated to

$$\mathbf{F} \cdot \left[ \frac{\partial \mathbf{j}_{l,m}}{\partial E} - \mathbf{\Gamma}_{l,m} \right], \tag{2.43}$$

with the angular force coupling term

$$\mathbf{\Gamma}_{l,m}(\mathbf{r}, E, t) = \int_{\Omega} \frac{1}{\hbar |\mathbf{k}(E, \theta, \varphi)|} \left[ \frac{\partial Y_{l,m}}{\partial \theta} \mathbf{e}_\theta + \frac{1}{\sin(\theta)} \frac{\partial Y_{l,m}}{\partial \varphi} \mathbf{e}_\varphi \right] \mathbf{g}(\mathbf{r}, E, \theta, \varphi, t) d\Omega. \tag{2.44}$$

Therefore, the projection of the *drift term* is

$$\frac{\mathbf{F}}{\hbar} \cdot \nabla_{\mathbf{k}} f \rightarrow \mathbf{F} \cdot \left[ \frac{\partial \mathbf{j}_{l,m}}{\partial E} - \mathbf{\Gamma}_{l,m} \right]. \tag{2.45}$$

The right-hand side of the BTE is treated in the next section [15, 25].

### 2.3.2 Spherical Harmonics Expansion of the Scattering Operator

The projection of the scattering operator  $\underline{\mathbf{Q}}\{f\}$  onto spherical harmonics  $Y_{l,m}(\theta, \varphi)$  is discussed in a very rigorous way, based on the results of [15, 25]. Thereby, the most general form is used. The transition rate  $S^{\nu, \nu'}(\mathbf{r}, \mathbf{k}, \mathbf{k}')$  is calculated using FGR, see Section 3.3. Here, it is adopted for multi-band structures. The total transition rate between an initial state  $(\nu, \mathbf{k})$  and a final state  $(\nu', \mathbf{k}')$  according to (3.129) is

$$\begin{aligned} S^{\nu, \nu'}(\mathbf{r}, \mathbf{k}, \mathbf{k}') &= \frac{1}{V_s} \sum_{\eta} c_{\eta, +}^{\nu, \nu'}(\mathbf{r}, \mathbf{k}, \mathbf{k}') \delta[E^{\nu'}(\mathbf{k}') - E^{\nu}(\mathbf{k}) - \hbar\omega_{\eta}] \\ &\quad + c_{\eta, -}^{\nu, \nu'}(\mathbf{r}, \mathbf{k}, \mathbf{k}') \delta[E^{\nu'}(\mathbf{k}') - E^{\nu}(\mathbf{k}) + \hbar\omega_{\eta}] \\ &= \frac{1}{V_s} \sum_{\eta} c_{\eta, \pm}^{\nu, \nu'}(\mathbf{r}, \mathbf{k}, \mathbf{k}') \delta[E^{\nu'}(\mathbf{k}') - E^{\nu}(\mathbf{k}) \mp \hbar\omega_{\eta}], \end{aligned} \quad (2.46)$$

where  $\eta$  denotes the scattering process and  $E^{\nu} = E_{c,v}^{\nu}(\mathbf{r}, \mathbf{k})$  is the dispersion relation of the  $\nu$ -th energy band. The first term describes absorption and the second emission. In the following the two terms are written in the combined form. The indices c and v denoting conduction band and valence band respectively are omitted.

#### Projection of the In-Scattering Operator

The in-scattering operator according to (1.71) is generalized for a multi-band system. For the  $\nu$ -th band it reads

$$\underline{\mathbf{Q}}^{\nu, \text{in}}\{f\} = \frac{V_s}{(2\pi)^3} \sum_{\nu'} \int_{\mathcal{B}} S^{\nu', \nu}(\mathbf{r}, \mathbf{k}', \mathbf{k}) f^{\nu'}(\mathbf{r}, \mathbf{k}', t) d\mathbf{k}', \quad (2.47)$$

where a summation over all bands  $\nu'$  and an integration within every band over all states  $\mathbf{k}'$  is carried out. Projection onto spherical harmonics  $Y_{l,m}$  on equi-energy surfaces according to (2.34) reads

$$\underline{\mathbf{Q}}_{l,m}^{\nu, \text{in}}\{f\} = 2 \int_{\Omega} Y_{l,m}(\theta, \varphi) \underline{\mathbf{Q}}^{\nu, \text{in}}\{f\} Z^{\nu}(E, \theta, \varphi) d\Omega. \quad (2.48)$$

Now (2.46) is substituted into (2.47). Therefore,

$$\underline{\mathbf{Q}}^{\nu, \text{in}}\{f\} = \frac{1}{(2\pi)^3} \sum_{\nu'} \sum_{\eta} \int_{\mathcal{B}} c_{\eta, \pm}^{\nu', \nu}(\mathbf{r}, \mathbf{k}', \mathbf{k}) \delta[E^{\nu}(\mathbf{k}) - E^{\nu'}(\mathbf{k}') \mp \hbar\omega_{\eta}] f^{\nu'}(\mathbf{r}, \mathbf{k}', t) d\mathbf{k}' \quad (2.49)$$

is obtained. A transformation to spherical coordinates with the relations

$$\begin{aligned} \mathbf{k} &= \mathbf{k}^{\nu} = \mathbf{k}^{\nu}(E, \theta, \varphi), \\ \mathbf{k}' &= \mathbf{k}^{\nu'} = \mathbf{k}^{\nu'}(E', \theta', \varphi'), \\ E &= E^{\nu}(\mathbf{k}), \\ E' &= E^{\nu'}(\mathbf{k}'), \\ Z' &= Z^{\nu'}(E', \theta', \varphi') \end{aligned} \quad (2.50)$$

is performed. Eq. (2.49) now reads

$$\begin{aligned} \underline{\mathbf{Q}}^{\nu, \text{in}}\{f\} &= \sum_{\nu'} \sum_{\eta} \int_{\mathbb{R}_0^+} \int_{\Omega'} c_{\eta, \pm}^{\nu', \nu}(\mathbf{r}, \mathbf{k}', \mathbf{k}) \delta[E - E' \mp \hbar\omega_{\eta}] f^{\nu'}(\mathbf{r}, \mathbf{k}', t) Z' d\Omega' dE' \\ &= \frac{1}{2} \sum_{\nu'} \sum_{\eta} \int_{\Omega'} c_{\eta, \pm}^{\nu', \nu}(\mathbf{r}, \tilde{\mathbf{k}}', \mathbf{k}) \underbrace{2f^{\nu'}(\mathbf{r}, \tilde{\mathbf{k}}', t) Z^{\nu'}(E \mp \hbar\omega_{\eta}, \theta', \varphi')}_{=g^{\nu'}(\mathbf{r}, E \mp \hbar\omega_{\eta}, \theta', \varphi')} d\Omega', \end{aligned} \quad (2.51)$$

with the abbreviation

$$\tilde{\mathbf{k}}' = \mathbf{k}' (E \mp \hbar\omega, \theta', \varphi'). \quad (2.52)$$

Finally, the EDF is expanded according to

$$\mathbf{g}'(\mathbf{r}, E \mp \hbar\omega_\eta, \theta', \varphi', t) = \sum_{l'=0}^{\infty} \sum_{m'=-l'}^{l'} \mathbf{g}'_{l',m'}(\mathbf{r}, E \mp \hbar\omega_\eta, t) Y_{l',m'}(\theta', \varphi') \quad (2.53)$$

and (2.51) is plugged into (2.48) to get

$$\underline{\mathbf{Q}}_{l,m}^{\nu,\text{in}}\{g\}(\mathbf{r}, E, t) = \sum_{\nu'} \sum_{\eta} \sum_{l'=0}^{\infty} \sum_{m'=-l'}^{l'} \underline{\mathbf{Q}}_{\eta,l,m,l',m'}^{\nu',\nu,\text{in}}(\mathbf{r}, E) \mathbf{g}'_{l',m'}(\mathbf{r}, E \mp \hbar\omega_\eta, t), \quad (2.54)$$

with

$$\begin{aligned} \underline{\mathbf{Q}}_{\eta,l,m,l',m'}^{\nu',\nu,\text{in}}(\mathbf{r}, E) &= \int_{\Omega} Y_{l,m}(\theta, \varphi) Z^\nu(E, \theta, \varphi) \\ &\times \int_{\Omega'} c_{\eta,\pm}^{\nu',\nu}(\mathbf{r}, E \mp \hbar\omega_\eta, \theta', \varphi', E, \theta, \varphi) Y_{l',m'}(\theta', \varphi') d\Omega' d\Omega. \end{aligned} \quad (2.55)$$

### Projection of the Out-Scattering Operator

The out-scattering operator according to (1.72) is generalized for a multi-band system. For the  $\nu$ -th band

$$\underline{\mathbf{Q}}^{\nu,\text{out}}\{f\} = \left[ \frac{V_s}{(2\pi)^3} \sum_{\nu'} \int_B S^{\nu,\nu'}(\mathbf{r}, \mathbf{k}, \mathbf{k}') d\mathbf{k}' \right] f^\nu(\mathbf{r}, \mathbf{k}, t) \quad (2.56)$$

is obtained. The projection onto spherical harmonics  $Y_{l,m}$  on equi-energy surfaces according to (2.34) is written as

$$\underline{\mathbf{Q}}_{l,m}^{\nu,\text{out}}\{f\} = 2 \int_{\Omega} Y_{l,m}(\theta, \varphi) \underline{\mathbf{Q}}^{\nu,\text{out}}\{f\} Z^\nu(E, \theta, \varphi) d\Omega. \quad (2.57)$$

Eq. (2.46) is substituted into (2.56), which gives

$$\underline{\mathbf{Q}}^{\nu,\text{out}}\{f\} = \left[ \frac{1}{(2\pi)^3} \sum_{\nu'} \sum_{\eta} \int_B c_{\eta,\pm}^{\nu,\nu'}(\mathbf{r}, \mathbf{k}, \mathbf{k}') \delta[E^{\nu'}(\mathbf{k}') - E^\nu(\mathbf{k}) \mp \hbar\omega_\eta] d\mathbf{k}' \right] f^\nu(\mathbf{r}, \mathbf{k}, t). \quad (2.58)$$

A transformation to spherical coordinates with the abbreviations according to (2.50) yields

$$\begin{aligned} \underline{\mathbf{Q}}^{\nu,\text{out}}\{f\} &= \left[ \sum_{\nu'} \sum_{\eta} \int_{\mathbb{R}_0^+} \int_{\Omega'} c_{\eta,\pm}^{\nu,\nu'}(\mathbf{r}, \mathbf{k}, \mathbf{k}') \delta[E' - E \mp \hbar\omega_\eta] Z' d\Omega' dE' \right] f^\nu(\mathbf{r}, \mathbf{k}, t) \\ &= \left[ \sum_{\nu'} \sum_{\eta} \int_{\Omega'} c_{\eta,\pm}^{\nu,\nu'}(\mathbf{r}, \mathbf{k}, \tilde{\mathbf{k}}') Z^{\nu'}(E \pm \hbar\omega_\eta, \theta', \varphi') d\Omega' \right] f^\nu(\mathbf{r}, \mathbf{k}, t). \end{aligned} \quad (2.59)$$

Finally, the EDF is expanded into spherical harmonics according to (2.53) and the projection of the outscattering term onto spherical harmonics is written as

$$\underline{\mathbf{Q}}_{l,m}^{\nu,\text{out}}\{g\}(\mathbf{r}, E, t) = \sum_{\nu'} \sum_{\eta} \sum_{l'=0}^{\infty} \sum_{m'=-l'}^{l'} \underline{\mathbf{Q}}_{\eta,l,m,l',m'}^{\nu',\nu,\text{out}}(\mathbf{r}, E) \mathbf{g}'_{l',m'}(\mathbf{r}, E, t), \quad (2.60)$$

with

$$\begin{aligned} \underline{\mathbf{Q}}_{\eta,l,m,l',m'}^{\nu,\nu',\text{out}}(\mathbf{r}, E) &= \int_{\Omega} Y_{l,m}(\theta, \varphi) Y_{l',m'}(\theta, \varphi) \\ &\times \int_{\Omega'} c_{\eta,\pm}^{\nu,\nu'}(\mathbf{r}, E, \theta, \varphi, E \pm \hbar\omega_{\eta}, \theta', \varphi') Z^{\nu'}(E \pm \hbar\omega_{\eta}, \theta', \varphi') d\Omega' d\Omega. \end{aligned} \quad (2.61)$$

### Velocity Randomization

The transition rate is often approximated as *velocity randomizing* [15]. This means, that the scattering rate  $S^{\nu,\nu'}(\mathbf{r}, \mathbf{k}, \mathbf{k}')$  from (2.46) is independent of the angles  $\theta$  and  $\varphi$  and therefore is expressed as

$$S^{\nu,\nu'}(\mathbf{r}, E, E') = \frac{1}{V_s} \sum_{\eta} c_{\eta,\pm}^{\nu,\nu'}(\mathbf{r}, E, E') \delta[E' - E \mp \hbar\omega_{\eta}], \quad (2.62)$$

with the abbreviations from (2.50). This simplifies the expressions for in- and out-scattering considerably. The projection of the *generalized density of states* onto spherical harmonics, given by

$$Z_{l,m}^{\nu}(E) = \int_{\Omega} Y_{l,m}(\theta, \varphi) Z^{\nu}(E, \theta, \varphi) d\Omega, \quad (2.63)$$

is used in the following. Together with the orthonormality property of the spherical harmonics according to (2.18), this yields for the in-scattering operator

$$\begin{aligned} \underline{\mathbf{Q}}_{\eta,l,m,l',m'}^{\nu',\nu,\text{in}}(\mathbf{r}, E) &= c_{\eta,\pm}^{\nu',\nu}(\mathbf{r}, E \mp \hbar\omega_{\eta}, E) \underbrace{\int_{\Omega} Y_{l,m}(\theta, \varphi) Z^{\nu}(E, \theta, \varphi) d\Omega}_{=Z_{l,m}^{\nu}(E)} \int_{\Omega'} Y_{l',m'}(\theta', \varphi') d\Omega' \\ &= c_{\eta,\pm}^{\nu',\nu}(\mathbf{r}, E \mp \hbar\omega_{\eta}, E) Z_{l,m}^{\nu}(E) \int_{\Omega'} Y_{l',m'}(\theta', \varphi') d\Omega' \\ &= \frac{1}{Y_{0,0}} c_{\eta,\pm}^{\nu',\nu}(\mathbf{r}, E \mp \hbar\omega_{\eta}, E) Z_{l,m}^{\nu}(E) \underbrace{\int_{\Omega} Y_{0,0} Y_{l',m'}(\theta', \varphi') d\Omega'}_{=\delta_{0,l'}\delta_{0,m'}} \\ &= \frac{1}{Y_{0,0}} c_{\eta,\pm}^{\nu',\nu}(\mathbf{r}, E \mp \hbar\omega_{\eta}, E) Z_{l,m}^{\nu}(E) \delta_{0,l'} \delta_{0,m'}. \end{aligned} \quad (2.64)$$

With the assumption of velocity randomization and the orthonormality property according to (2.18), the out-scattering operator simplifies to

$$\begin{aligned} \underline{\mathbf{Q}}_{\eta,l,m,l',m'}^{\nu,\nu',\text{out}}(\mathbf{r}, E) &= c_{\eta,\pm}^{\nu,\nu'}(\mathbf{r}, E, E \pm \hbar\omega_{\eta}) \underbrace{\int_{\Omega} Y_{l,m}(\theta, \varphi) Y_{l',m'}(\theta, \varphi) d\Omega}_{=\delta_{l,l'}\delta_{m,m'}} \\ &\times \int_{\Omega'} Z^{\nu'}(E \pm \hbar\omega_{\eta}, \theta', \varphi') d\Omega' \\ &= c_{\eta,\pm}^{\nu,\nu'}(\mathbf{r}, E, E \pm \hbar\omega_{\eta}) \int_{\Omega'} Z^{\nu'}(E \pm \hbar\omega_{\eta}, \theta', \varphi') d\Omega' \delta_{l,l'} \delta_{m,m'} \\ &= \frac{1}{Y_{0,0}} c_{\eta,\pm}^{\nu,\nu'}(\mathbf{r}, E, E \pm \hbar\omega_{\eta}) \underbrace{\int_{\Omega'} Y_{0,0} Z^{\nu'}(E \pm \hbar\omega_{\eta}, \theta', \varphi') d\Omega'}_{=Z_{0,0}^{\nu'}(E \pm \hbar\omega_{\eta})} \delta_{l,l'} \delta_{m,m'} \\ &= \frac{1}{Y_{0,0}} c_{\eta,\pm}^{\nu,\nu'}(\mathbf{r}, E, E \pm \hbar\omega_{\eta}) Z_{0,0}^{\nu'}(E \pm \hbar\omega_{\eta}) \delta_{l,l'} \delta_{m,m'}. \end{aligned} \quad (2.65)$$

Finally, the result is summarized to

$$\underline{\mathbf{Q}}_{\eta,l,m,l',m'}^{\nu,\nu,\text{in}}(\mathbf{r}, E) = \frac{1}{Y_{0,0}} c_{\eta,\pm}^{\nu,\nu}(\mathbf{r}, E \mp \hbar\omega_\eta, E) Z_{l,m}^\nu(E) \delta_{0,l'} \delta_{0,m'}, \quad (2.66)$$

$$\underline{\mathbf{Q}}_{\eta,l,m,l',m'}^{\nu,\nu,\text{out}}(\mathbf{r}, E) = \frac{1}{Y_{0,0}} c_{\eta,\pm}^{\nu,\nu}(\mathbf{r}, E, E \pm \hbar\omega_\eta) Z_{0,0}^{\nu'}(E \pm \hbar\omega_\eta) \delta_{l,l'} \delta_{m,m'}. \quad (2.67)$$

### 2.3.3 Equation System for the Spherical Harmonics Expansion Coefficients

With the results from Section 2.3.1 and Section 2.3.2 an equation system for the spherical harmonics expansion coefficients  $\mathbf{g}_{l,m}(\mathbf{r}, E, t)$  of the EDF is formulated. In the following, the *Einstein convention of implicitly summing over pairs of identical indices* for the indices of the spherical harmonics is used. This means that

$$\sum_{l'=0} \sum_{m'=-l'}^{l'} a_{l,m}^{l',m'} b_{l',m'} \stackrel{\text{Einstein summation convention}}{\iff} a_{l,m}^{l',m'} b_{l',m'}. \quad (2.68)$$

At this point the projection of the BTE onto spherical harmonics is generalized for a multi-band system. For the  $\nu$ -th energy band  $E_{c,\nu}^\nu(\mathbf{r}, \mathbf{k})$  this gives

$$\frac{\partial f^\nu}{\partial t} \rightarrow \frac{\partial \mathbf{g}_{l,m}^\nu}{\partial t}, \quad (2.69)$$

$$\mathbf{v}^\nu(\mathbf{k}) \cdot \nabla_{\mathbf{r}} f^\nu \rightarrow \nabla_{\mathbf{r}} \cdot \mathbf{j}_{l,m}^{\nu'}, \quad (2.70)$$

$$\frac{\mathbf{F}^\nu}{\hbar} \cdot \nabla_{\mathbf{k}} f^\nu \rightarrow \mathbf{F}^\nu \cdot \left[ \frac{\partial \mathbf{j}_{l,m}^{\nu'}}{\partial E} - \mathbf{\Gamma}_{l,m}^\nu \right], \quad (2.71)$$

$$\underline{\mathbf{Q}}^{\nu,\text{in}}\{f\} \rightarrow \sum_{\nu'} \sum_{\eta} \underline{\mathbf{Q}}_{\eta,l,m,l',m'}^{\nu',\nu,\text{in}}(\mathbf{r}, E) \mathbf{g}_{l',m'}^{\nu'}(\mathbf{r}, E \mp \hbar\omega_\eta, t), \quad (2.72)$$

$$\underline{\mathbf{Q}}^{\nu,\text{out}}\{f\} \rightarrow \sum_{\nu'} \sum_{\eta} \underline{\mathbf{Q}}_{\eta,l,m,l',m'}^{\nu,\nu',\text{out}}(\mathbf{r}, E) \mathbf{g}_{l',m'}^{\nu'}(\mathbf{r}, E, t), \quad (2.73)$$

with

$$\mathbf{j}_{l,m}^{\nu'}(\mathbf{r}, E, t) = \int_{\Omega} Y_{l,m}(\theta, \varphi) \mathbf{v}^\nu(\mathbf{k}^\nu(E, \theta, \varphi)) \mathbf{g}^\nu(\mathbf{r}, E, \theta, \varphi, t) d\Omega. \quad (2.74)$$

$$\mathbf{\Gamma}_{l,m}^\nu(\mathbf{r}, E, t) = \int_{\Omega} \frac{1}{\hbar |\mathbf{k}^\nu(E, \theta, \varphi)|} \left[ \frac{\partial Y_{l,m}}{\partial \theta} \mathbf{e}_\theta + \frac{1}{\sin(\theta)} \frac{\partial Y_{l,m}}{\partial \varphi} \mathbf{e}_\varphi \right] \mathbf{g}^\nu(\mathbf{r}, E, \theta, \varphi, t) d\Omega. \quad (2.75)$$

This equations can be rewritten with an expansion of the EDF  $\mathbf{g}(\mathbf{r}, E, \theta, \varphi, t)$  with spherical harmonics  $Y_{l,m}(\theta, \varphi)$ . This yields

$$\mathbf{j}_{l,m}^{\nu'}(\mathbf{r}, E, t) = \mathbf{g}_{l',m'}^{\nu'}(\mathbf{r}, E, t) \underbrace{\int_{\Omega} Y_{l,m}(\theta, \varphi) Y_{l',m'}(\theta, \varphi) \mathbf{v}^\nu(\mathbf{k}^\nu(E, \theta, \varphi)) d\Omega}_{=:\mathbf{v}_{l,m}^{\nu',l',m'}(E)}, \quad (2.76)$$

$$\mathbf{\Gamma}_{l,m}^\nu(\mathbf{r}, E, t) = \mathbf{g}_{l',m'}^{\nu'}(\mathbf{r}, E, t) \underbrace{\int_{\Omega} \frac{1}{\hbar |\mathbf{k}^\nu(E, \theta, \varphi)|} \left[ \frac{\partial Y_{l,m}}{\partial \theta} \mathbf{e}_\theta + \frac{1}{\sin(\theta)} \frac{\partial Y_{l,m}}{\partial \varphi} \mathbf{e}_\varphi \right] Y_{l',m'}(\theta, \varphi) d\Omega}_{=:\mathbf{\Gamma}_{l,m}^{\nu',l',m'}(E)}. \quad (2.77)$$

Now the full system of partial differential equations is written as

$$\begin{aligned}
 & \frac{\partial \mathbf{g}_{l,m}^{\nu'}}{\partial t} + \mathbf{v}_{l,m}^{\nu',l',m'} \cdot \nabla_{\mathbf{r}} \mathbf{g}_{l',m'}^{\nu'} + \mathbf{F}^{\nu'} \cdot \left[ \frac{\partial \mathbf{v}_{l,m}^{\nu',l',m'} \mathbf{g}_{l,m}^{\nu'}}{\partial E} - \mathbf{\Gamma}_{l,m}^{\nu',l',m'} \mathbf{g}_{l,m}^{\nu'} \right] \\
 & = \sum_{\nu'} \sum_{\eta} \mathbf{Q}_{\eta,l,m,l',m'}^{\nu',\nu',\text{in}} \mathbf{g}_{l',m'}^{\nu'}(\mathbf{r}, E \mp \hbar\omega_{\eta}, t) - \mathbf{Q}_{\eta,l,m,l',m'}^{\nu',\nu',\text{out}} \mathbf{g}_{l',m'}^{\nu'}(\mathbf{r}, E, t),
 \end{aligned} \tag{2.78}$$

with  $l = 0, 1, 2, \dots$  and  $m = -l, \dots, l$ . For numerical simulations the expansion order is limited to a finite value  $L$ , thus  $l = 0, 1, 2, \dots, L$ . This is an expansion with  $(L + 1)^2$  terms. The primed indices are given by  $l' = 0, 1, 2, \dots, L$  and  $m' = -l', \dots, l'$ . The operators  $\mathbf{Q}_{\eta,l,m,l',m'}^{\nu',\nu',\text{in}}$  and  $\mathbf{Q}_{\eta,l,m,l',m'}^{\nu',\nu',\text{out}}$  on the right-hand side are given by (2.55), respectively (2.61). They can be simplified to (2.66), respectively (2.67) [15, 25, 26].

### H-Transformation

The discretization of the system of equations described by (2.78) can be simplified by applying the  $H$ -transformation, as described in [9], which is a transformation defined by

$$E \mapsto H, \tag{2.79}$$

where  $E$  is the kinetic energy and  $H$  is the total energy of the system. The total energy is discussed in Section 3.1.2. The theorem of energy conservation states, that the systems total energy is constant in time and only changes by the exchange of energy with another system, e.g. the phonon system, where the energy of a phonon is emitted or absorbed. This is the so-called phonon scattering, which is described in Section 4.2. The situation is sketched in Fig. 2.4. The total energy  $H$  does not change along the trajectory in the  $H$ - $\mathbf{r}$ -space (solid arrow), except for inelastic scattering (curled arrows), where the carrier scatters to another trajectory. Thus, an alignment of the grid to the total energy  $H$  instead of the kinetic energy  $E$  is numerically attractive. The system of equations (2.78) using the  $H$ -transform is simplified to

$$\begin{aligned}
 & \frac{\partial \mathbf{g}_{l,m}^{\nu'}}{\partial t} + \mathbf{v}_{l,m}^{\nu',l',m'} \cdot \nabla_{\mathbf{r}} \mathbf{g}_{l',m'}^{\nu'} - \mathbf{F}^{\nu'} \cdot \mathbf{\Gamma}_{l,m}^{\nu',l',m'} \mathbf{g}_{l,m}^{\nu'} \\
 & = \sum_{\nu'} \sum_{\eta} \mathbf{Q}_{\eta,l,m,l',m'}^{\nu',\nu',\text{in}} \mathbf{g}_{l',m'}^{\nu'}(\mathbf{r}, H \mp \hbar\omega_{\eta}, t) - \mathbf{Q}_{\eta,l,m,l',m'}^{\nu',\nu',\text{out}} \mathbf{g}_{l',m'}^{\nu'}(\mathbf{r}, H, t).
 \end{aligned} \tag{2.80}$$

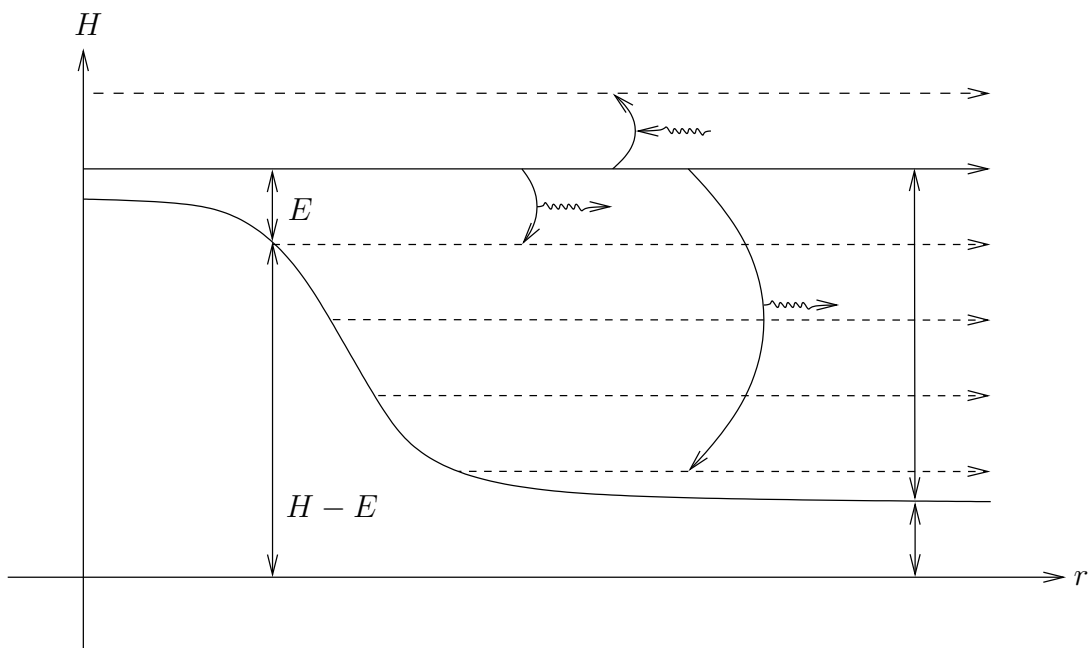


**Figure 2.4:** A sample carrier trajectory in the  $H$ - $r$ -space (solid arrow).  $E$  is the kinetic energy and  $H$  the total energy. The carrier can scatter to other trajectories (dashed arrows) by emission or absorption of a energy quantum, e.g. a phonon (curled arrows).

## Chapter 3

# Physical Modeling

In Chapter 1, the fundamental semiconductor equations are introduced, where the quantum-mechanical picture and the semi-classical description are discussed. In the first part of this chapter, a connection between the classical particle and the quantum mechanical picture is drawn. Therefore, an electron is described as wave packet and the properties of the wave packet are linked with classical particle properties. Subsequently it is assumed that under certain conditions an electron in a semiconducting material can be described as a particle. A discussion of the limits of this approach is given. Then, the basic concepts used to describe crystalline structures are presented. These concepts are necessary to understand the behavior of electrons in a crystal, which is influenced by the potential of the atomic nuclei. This potential is assumed to be periodic with the periodicity of the lattice, leading to the well-known Bloch theorem, which is derived in detail and forms the basis for the calculation of electronic band structures. In this work, only general properties of real electronic band structures are discussed. Then, the most important analytical approximations for electronic band structures are introduced. In the following, the fundamental theorem of scattering theory, i.e. Fermi's Golden Rule (FGR), is derived. For this purpose, a first-order perturbation method, which only accounts for the correlation of the initial and the final state of the electron and neglects correlations with other electron states, is used. With FGR the transition rate  $S(\mathbf{k}, \mathbf{k}')$  from an initial state  $\mathbf{k}$  to a final state  $\mathbf{k}'$  is calculated. The transition rate is due to perturbing potentials on the atomic scale and thus has to be calculated quantum mechanically. In Section 3.4 the most important results for the modeling of scattering in the semi-classical framework are summarized. The chapter is finalized with the discussion of lattice vibrations and their quanta, so-called phonons.

### 3.1 Semi-Classical Carrier Dynamics

A rigorous treatment of carrier transport requires a full quantum mechanical approach, where electrons are described as quantum states governed by the Schrödinger equation (SE). More precisely, electrons in semiconductor crystals are so-called Bloch states. In the so-called semi-classical approach, electrons are treated as particles governed by Newton's laws, while scattering is modeled quantum mechanically using FGR, see Section 3.3. The velocity is assumed to be the group velocity  $\mathbf{v}(\mathbf{k})$ . The fundamental equation in the semi-classical transport regime is the Boltzmann Transport Equation (BTE). In the following, a discussion about the connection between quantum mechanical wave packets, localized in the  $\mathbf{k}$ -space, and semi-classical particles is established. This particles have a well-defined position  $\mathbf{r}$  and momentum  $\mathbf{p}$ . Furthermore, the force on a semi-classical particle is derived and the limits of the semi-classical approach are discussed.



### 3.1.1 From the Wave Packet to the Particle

A wave packet is a solution of the SE, where an electron is described by states, which are well-defined both in position and momentum space. A wave packet centered around  $\mathbf{r} = \mathbf{r}_0$  and  $\mathbf{k} = \mathbf{k}_0$  is given by

$$\Psi(\mathbf{r}, t) = \int_{\mathbb{R}^3} a(\mathbf{k} - \mathbf{k}_0) e^{i(\mathbf{k} \cdot (\mathbf{r} - \mathbf{r}_0) - \omega(\mathbf{k})t)} d\mathbf{k}, \quad (3.1)$$

with an arbitrary weighting-function  $a(\mathbf{k})$ . The weighting function  $a(\mathbf{k})$  is chosen in a such way, that at  $\mathbf{k} = \mathbf{k}_0$  it possesses a maximum and drops to zero as  $|\mathbf{k}| \rightarrow \infty$ , as sketched in Fig. 3.1 for one dimension. The  $i$ -th component of the phase velocity  $\mathbf{v}_{\text{ph}}$  in Cartesian coordinates is obtained by setting the argument of the exponential to a constant and taking the time derivative as

$$\frac{\partial}{\partial t} [k_i r_i - \omega(k_i)t] = \frac{\partial}{\partial t} \text{const.} = 0 \Rightarrow v_{\text{ph},i} = \dot{r}_i = \frac{\omega(k_i)}{k_i}. \quad (3.2)$$

Due to the dispersion relation  $\omega(\mathbf{k})$ , every component of the continuous superposition in (3.1) has a different phase velocity  $\mathbf{v}_{\text{ph}}(\mathbf{k})$  in general. Therefore, the center of the wave packet and its shape change with time. This effect is called dispersion. The center moves with the group velocity  $\mathbf{v}(\mathbf{k})$ , which is according to [20, 27] given by

$$\mathbf{v}(\mathbf{k}) = \frac{1}{\hbar} \nabla_{\mathbf{k}} E(\mathbf{k}). \quad (3.3)$$

In semi-classical transport theory for the velocity of a particle, the group velocity according to (3.3) is used and it is assumed that for every time  $t$  the momentum and location of the particle is well-defined. This is in contradiction to Heisenberg's uncertainty principle, which states that [27]

$$\Delta r_i \Delta p_j \geq \frac{\hbar}{2} \delta_{i,j}, \quad (3.4)$$

for every combination of  $(i, j) \in \{x, y, z\}^2$ . This is denoted as position-momentum uncertainty relation. It states that the position of a carrier and its momentum cannot be exactly determined at the same time. Another relation for energy and time states that

$$\Delta E \Delta t \geq \hbar, \quad (3.5)$$

expressing that the exact energy of a carrier cannot be determined in a finite time. To summarize, a wave-packet in the semi-classical approach is treated as a classical particle, as sketched in Fig. 3.2. The velocity of this particle is equal to the group velocity  $\mathbf{v}(\mathbf{k})$  of the wave-packet. The momentum  $\mathbf{p}$  of the carrier and the wave-vector  $\mathbf{k}$  of the wave-packet are related via  $\hbar$ . The following relations are used:

$$\dot{\mathbf{r}} = \mathbf{v}(\mathbf{k}), \quad (3.6)$$

$$\mathbf{p} = \hbar \mathbf{k}, \quad (3.7)$$

$$\mathbf{F} = \hbar \dot{\mathbf{k}}. \quad (3.8)$$

### 3.1.2 Force in the Semi-Classical Approach

In the following, a force equation for an electron in an energy potential is derived. It is then generalized for holes. The total energy of an electron in the conduction band is given by

$$H = E_c(\mathbf{r}, \mathbf{k}, t) = E_{c0}(\mathbf{r}) - q\Phi(\mathbf{r}, t) + E(\mathbf{k}), \quad (3.9)$$

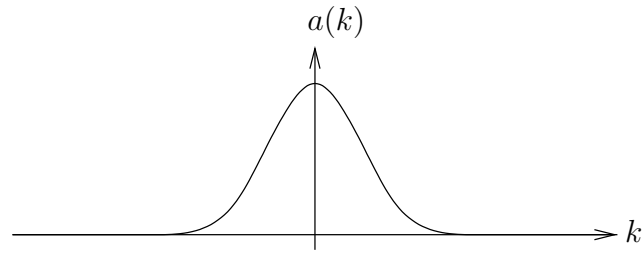


**Figure 3.1:** Example for a weighting function  $a(k)$  used to define a wave packet.

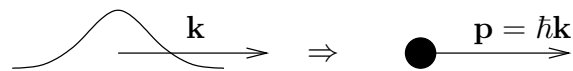


**Figure 3.2:** The wave packet on the left-hand side is a solution of the SE. Position and wave vector (momentum) cannot be both exactly determined simultaneously due to *Heisenberg's uncertainty principle*. In the semi-classical transport theory it is treated as a particle, as shown on the right side. Here, both position and momentum are exactly determined.

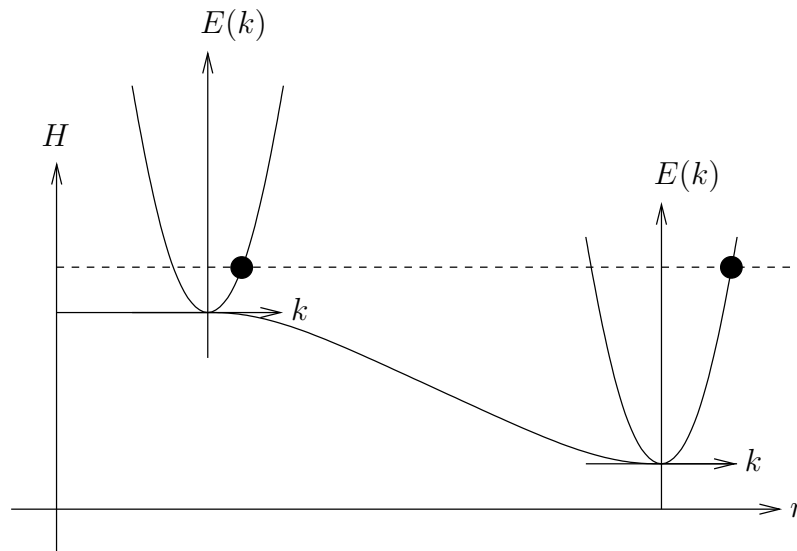


**Figure 3.3:** An electron in a slowly varying conduction energy band potential  $E_{c0}(r)$ , with kinetic energy  $E(k)$ . The force on the particle is given by  $F = q\nabla_{\mathbf{r}}\Phi(r)$ . A similar illustration can be found in [20].

where  $E_{c0}(\mathbf{r})$  is the potential energy due to material variations, representing the bottom of the conduction band. For bulk materials this is a constant, but for heterostructures it varies with position depending on the material composition [19].  $\Phi(\mathbf{r}, t)$  is the electrostatic potential due to built-in and applied electric fields and  $E(\mathbf{k})$  is the kinetic energy component. The total derivative with respect to time  $t$  of the energy  $E_c(\mathbf{r}, \mathbf{k})$  is obtained as

$$\frac{dE_c(\mathbf{r}, \mathbf{k}, t)}{dt} = \underbrace{\frac{\partial E_c(\mathbf{r}, \mathbf{k}, t)}{\partial t}}_{-q\dot{\Phi}(\mathbf{r}, t)} + \underbrace{\dot{\mathbf{r}}}_{\mathbf{v}(\mathbf{k})} \cdot \nabla_{\mathbf{r}} E_c(\mathbf{r}, \mathbf{k}, t) + \underbrace{\dot{\mathbf{k}}}_{\mathbf{F}/\hbar} \cdot \nabla_{\mathbf{k}} E_c(\mathbf{r}, \mathbf{k}, t). \quad (3.10)$$

The time derivative of  $\mathbf{r}$  is identified as the group velocity  $\mathbf{v}(\mathbf{k})$ , according to the semi-classical picture of an electron. The time derivative of  $\mathbf{k}$  multiplied by  $\hbar$  gives the force  $\mathbf{F}$  acting on this electron. It is assumed, that the total energy  $E_c(\mathbf{r}, \mathbf{k}, t)$  changes only due to the changes of the electrostatic field  $\Phi(\mathbf{r}, t)$ , so

$$\frac{dE_c(\mathbf{r}, \mathbf{k}, t)}{dt} = -q\dot{\Phi}(\mathbf{r}, t). \quad (3.11)$$

From (3.10) and (3.11) follows that:

$$\mathbf{v}(\mathbf{k}) \cdot \nabla_{\mathbf{r}} [E_{c0}(\mathbf{r}) - q\Phi(\mathbf{r})] + \frac{\mathbf{F}}{\hbar} \cdot \underbrace{\nabla_{\mathbf{k}} E(\mathbf{k})}_{\hbar\mathbf{v}(\mathbf{k})} \stackrel{!}{=} 0. \quad (3.12)$$

This finally yields

$$\mathbf{F} = \frac{\partial(\hbar\mathbf{k})}{\partial t} = -\nabla_{\mathbf{r}} [E_{c0}(\mathbf{r}) - q\Phi(\mathbf{r}, t)]. \quad (3.13)$$

This is very similar to the classical force term  $\mathbf{F} = \dot{\mathbf{p}}$ . Here  $\hbar\mathbf{k}$  is the crystal momentum. In Fig. 3.3, an electron in a slowly varying potential is sketched for the illustration of (3.13). It can be seen that the electron gathers kinetic energy in the region where the potential declines.

The total energy for holes is given by

$$E_v(\mathbf{r}, \mathbf{k}, t) = E_{v0}(\mathbf{r}) - q\Phi(\mathbf{r}, t) - E(\mathbf{k}), \quad (3.14)$$

and thus the force term becomes

$$\mathbf{F} = \frac{\partial(\hbar\mathbf{k})}{\partial t} = \nabla_{\mathbf{r}} [E_{v0}(\mathbf{r}) - q\Phi(\mathbf{r}, t)]. \quad (3.15)$$

In bulk materials, where  $E_{c0}(\mathbf{r})$  and  $E_{v0}(\mathbf{r})$  are constants, the force vector for electrons (3.13) and the force vector for holes (3.15) are exactly opposing each other [9, 15, 20].

### 3.1.3 Limitations of the Semi-Classical Approach

The BTE is a single-particle approximation of a many-particle problem, where the correlations between carriers are neglected. Carrier correlations are considered in the framework of the so called *Boltzmann-Poisson system*, where additionally the Poisson Equation (PE) is included self-consistently. Furthermore, scattering is assumed to be instantaneously in time and localized in space, cf. Section 1.2. Carriers are treated as semi-classical particles obeying Newton's laws. Therefore, the position  $\mathbf{r}$  and momentum  $\mathbf{p}$  of a particle are exactly specified at the same time. Scattering on the other hand is treated quantum mechanically using first-order perturbation theory. In the following, some qualitative estimates based on the considerations in [20] are given using *Heisenberg's uncertainty principle*. A

spread in energy in the order of  $\Delta E \simeq k_B T$  and a parabolic dispersion relation are assumed, hence  $\Delta k \simeq \sqrt{2m^*k_B T}/\hbar$ . From the *position-momentum uncertainty relation* (3.4) and  $\Delta p = \hbar\Delta k$  follows that

$$\Delta r \geq \frac{1}{2\Delta k} = \frac{\hbar}{2\sqrt{2m^*k_B T}}. \quad (3.16)$$

Therefore it is claimed that

$$\Delta r \gg \lambda_B, \quad (3.17)$$

where  $\lambda_B = h/\sqrt{2m^*k_B T}$  is the wavelength of a thermal average carrier. For  $m^* = m_e$  and  $T = 300$  K,  $\lambda_B$  is approximately 8 nm. In [20], a value of  $\lambda_B \simeq 10 - 20$  nm is given. The condition in (3.17) should be satisfied, when the potential varies slowly on the scale of  $\lambda_B$ . If  $\Delta t$  in the *energy-time uncertainty relation* (3.5) is taken to be the mean time  $\tau$  between scattering events (collisions), it shows that

$$\tau \gg \frac{\hbar}{k_B T}. \quad (3.18)$$

Together with the thermal velocity  $v_{th} = \sqrt{2k_B T/m^*}$ , an estimate for the mean free path  $l_{mfp} = v_{th}\tau$  is given by

$$l_{mfp} \gg \lambda_B, \quad (3.19)$$

where some factors are omitted. The mean free path is the mean distance between collisions. A condition for the maximum operation frequency  $f$  is obtained from (3.18) as

$$f \ll \frac{k_B T}{h}, \quad (3.20)$$

for  $T = 300$  K this yields  $f \ll 6$  THz, which is easily fulfilled for modern devices. Note that  $h$  is used here instead of  $\hbar$  to be in compliance with [20]. Thus in practice the main limitation comes from condition (3.17).

## 3.2 Band Structure of Semiconductor Materials

The electronic band structure is the relation between the energy  $E$  of an electron and its wave vector  $\mathbf{k}$ . This section deals with the fundamentals of electronic band structures and starts with a discussion about crystals and basic concepts to describe them. This is necessary to understand the formation of energy bands in crystals, which describe the behavior of electrons in such materials. Finally, the most important analytical models for the approximation of real electronic band structures are presented.

### 3.2.1 Crystals

Crystals are spatially periodic arrangements of atoms, which form a solid in this configuration. Crystals show a short-range order, as well as a long-range order of atoms, distinguishing them from amorphous materials and liquids, where only a short-range order is observed [6]. In this work, the focus is on crystalline semiconductors, like silicon (Si), gallium-arsenide (GaAs) or germanium (Ge). In the following, the usual mathematical concepts for the description of crystalline structures are presented.

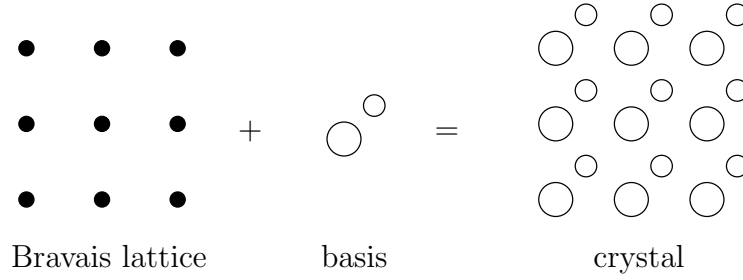


**Figure 3.4:** Every crystal is specified by a Bravais lattice and a basis.

### The Bravais Lattice and the Basis

An ideal crystal is built up of an identical group of atoms, called a **basis**, which is repeated periodically. The mathematical set of points, where this basis is fixed, is called **Bravais lattice** [16]. Therefore, each crystal is fully described by a **Bravais lattice** and a **basis**, which is sketched in Fig. 3.4. A Bravais lattice in three dimensions is again described by a set of **translation vectors**  $\{\mathbf{a}_1, \mathbf{a}_2, \mathbf{a}_3\}$  as the set of points  $\mathcal{P}$  given by

$$\mathcal{P} = \{\mathbf{p}_{u,v,w} = \mathbf{p}_{\mathbf{u}} = u\mathbf{a}_1 + v\mathbf{a}_2 + w\mathbf{a}_3 \mid u, v, w \in \mathbb{Z}\}. \quad (3.21)$$

The translation vectors span the so-called **primitive unit cell**. Since the choice of the translation vectors is not unique, a unique cell, called **Wigner-Seitz cell**, is defined as the **Voronoi box**  $\mathcal{V}_{\mathbf{u}}$  around a lattice point  $\mathbf{p}_{\mathbf{u}}$ , see Fig. 3.5 [16, 21]. A Voronoi box  $\mathcal{V}_{\mathbf{u}}$  around a lattice point  $\mathbf{p}_{\mathbf{u}} \in \mathcal{P}$ , is the set of points closer to  $\mathbf{p}_{\mathbf{u}}$  than to any other point  $\mathbf{p}_{\mathbf{v}} \in \mathcal{P}$  with  $\mathbf{u} \neq \mathbf{v}$  [25]:

$$\mathcal{V}_{\mathbf{u}} = \{\mathbf{r} \in \mathbb{R}^3 \mid |\mathbf{r} - \mathbf{p}_{\mathbf{u}}| \leq |\mathbf{r} - \mathbf{p}_{\mathbf{v}}| \quad \forall \mathbf{v} \neq \mathbf{u}\} \quad (3.22)$$

It is constructed as follows: First, vectors from  $\mathbf{p}_{\mathbf{u}}$  to  $\mathbf{p}_{\mathbf{n}} \in \mathcal{P}$ , where  $\mathbf{n}$  is the index of nearest neighbors of  $\mathbf{u}$  are drawn. Next, the perpendicular bisecting planes of this vectors are constructed. The smallest enclosed volume is found to be the Voronoi box around  $\mathbf{p}_{\mathbf{u}}$  [16].

### The Brillouin Zone

From now on, a finite crystal is considered. It is composed out of  $N = N_1 \times N_2 \times N_3$  unit cells, where  $N_1$ ,  $N_2$  and  $N_3$  are the number of unit cells along  $\mathbf{a}_1$ ,  $\mathbf{a}_2$  and  $\mathbf{a}_3$  respectively. The volume of one unit cell is given by  $V_{\text{cell}}$ , thus the volume of the crystal is  $V_{\text{crystal}} = NV_{\text{cell}}$ . The Brillouin zone  $\mathcal{B}$  is now further specified. For this purpose, a translation vector

$$\mathbf{T}_{u,v,w} := u\mathbf{a}_1 + v\mathbf{a}_2 + w\mathbf{a}_3, \quad (3.23)$$

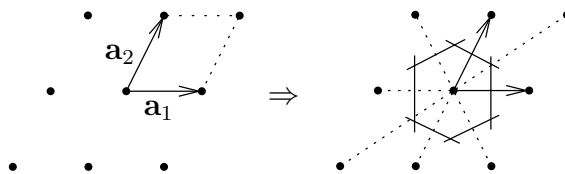


**Figure 3.5:** Two dimensional Bravais lattice. *Left:* The primitive translation vectors  $\mathbf{a}_i$  span a primitive lattice cell. The choice of lattice vectors is not unique. *Right:* The Wigner-Seitz cell is a unique lattice cell, which is the Voronoi box around a lattice point.

with  $u \in [0, N_1]$ ,  $v \in [0, N_2]$ ,  $w \in [0, N_3]$  is defined. In the following, the indices are omitted to keep the expressions compact. An arbitrary, but periodic function

$$U(\mathbf{r}) = U(\mathbf{r} + \mathbf{T}), \quad (3.24)$$

with the periodicity of the lattice is considered. The *Fourier transform* of this function normalized to the volume of the crystal  $V_{\text{crystal}}$  reads

$$V(\mathbf{q}) = \frac{1}{V_{\text{crystal}}} \int_{\text{crystal}} U(\mathbf{r}) e^{-i\mathbf{q}\cdot\mathbf{r}} d\mathbf{r}. \quad (3.25)$$

Because of the periodicity of  $U(\mathbf{r})$ , the integral over the crystal can be decomposed into  $N$  integrals over each of the identical unit cells, which is

$$\begin{aligned} V(\mathbf{q}) &= \frac{1}{V_{\text{crystal}}} \sum_{u,v,w} \int_{\text{cell}} U(\mathbf{r} + \mathbf{T}) e^{-i\mathbf{q}\cdot(\mathbf{r}+\mathbf{T})} d\mathbf{r} \\ &= \frac{1}{N} \sum_{u,v,w} e^{i\mathbf{q}\cdot\mathbf{T}} \frac{1}{V_{\text{cell}}} \int_{\text{cell}} U(\mathbf{r}) e^{-i\mathbf{q}\cdot\mathbf{r}} d\mathbf{r}. \end{aligned} \quad (3.26)$$

The summation over complex exponentials for a large number of unit cells is negligible because of destructive interference. Expectations are at  $\mathbf{q} \cdot \mathbf{T} = 2\pi n$ , with  $n \in \mathbb{Z}$ , where they interfere constructively. This must hold for each component of  $\mathbf{T}$ , hence  $\mathbf{q} \cdot \mathbf{a}_i = 2\pi n$ . Consequently, a set of vectors  $\{\mathbf{b}_1, \mathbf{b}_2, \mathbf{b}_3\}$  is defined by

$$\mathbf{b}_i \cdot \mathbf{a}_j = 2\pi \delta_{i,j}, \quad (3.27)$$

with  $i, j = 1, 2, 3$ . The vectors  $\mathbf{b}_i$  are the primitive translation vectors of the so-called **reciprocal lattice**, with the translation vector

$$\mathbf{G} = \mathbf{G}_{u,v,w} = u\mathbf{b}_1 + v\mathbf{b}_2 + w\mathbf{b}_3. \quad (3.28)$$

The **Brillouin zone** is now introduced as the Wigner-Seitz cell of the reciprocal lattice. The periodic function  $U(\mathbf{r})$  has only non-zero Fourier components at the points of the reciprocal lattice. In the next section, the well known **Bloch theorem** is derived, using the results above [21].

### 3.2.2 The Electron in a Crystal Potential and Bloch's Theorem

The result of F. Bloch is derived in the following, because it provides important information about the behavior of electrons in crystalline structures and forms the basis behind electronic band structure calculations [1]. An electron in a crystal experiences a background potential, the so-called crystal potential  $U_{\text{crystal}}(\mathbf{r})$ , which is periodic due to the periodicity of the lattice. Since the motion of the electrons is governed by the Schrödinger equation (SE), the problem is set up in an one-electron approximation as

$$\underbrace{\left[ -\frac{\hbar}{2m_e} \nabla^2 + U_{\text{crystal}}(\mathbf{r}) + U_s(\mathbf{r}, t) \right]}_{\mathbf{H}(\mathbf{r}, t)} \Psi(\mathbf{r}, t) = -i\hbar \frac{\partial \Psi(\mathbf{r}, t)}{\partial t}. \quad (3.29)$$

The different parts of the Hamiltonian operator  $\mathbf{H}(\mathbf{r}, t)$  are now further described:

**Kinetic Energy.**  $-\frac{\hbar}{2m_e} \nabla^2$  refers to the kinetic energy of the electron due to the *correspondence principle* discussed in Section 1.1.2.

**Crystal Potential.**  $U_{\text{crystal}}(\mathbf{r})$  is the cell-periodic potential of the nuclei, neglecting their vibrations. These are treated as **phonons** and included in the scattering potential  $U_s(\mathbf{r}, t)$ . Phonon scattering is described in Section 4.2.

**Scattering Potential.**  $U_s(\mathbf{r}, t)$  denotes the potential due to imperfections of the crystal. It is distinguished between dynamic potentials, e.g. lattice vibrations (phonons) and static potentials, e.g. impurities. Scattering is treated via first-order perturbation theory, which in this context is named Fermi's Golden Rule (FGR), see Section 3.3.

In the following, the influence of the time-independent and periodic crystal potential  $U_{\text{crystal}}(\mathbf{r})$  is investigated. Thus (3.29) reduces to an eigenvalue problem:

$$\underbrace{\left[ -\frac{\hbar}{2m_e} \nabla^2 + U_{\text{crystal}}(\mathbf{r}) \right]}_{\mathbf{H}_{\text{crystal}}(\mathbf{r})} \Psi(\mathbf{r}) = E\Psi(\mathbf{r}). \quad (3.30)$$

For reason of symmetry, it holds that

$$U_{\text{crystal}}(\mathbf{r}) = U_{\text{crystal}}(\mathbf{r} + \mathbf{T}), \quad (3.31)$$

which implies that all information about  $U_{\text{crystal}}(\mathbf{r})$  is included in one unit cell. This simplifies the solution of (3.30). In the following the operator  $\mathbf{H}_{\text{crystal}}$  is written as  $\mathbf{H}$  and the translation operator

$$\mathbf{T}_{u,v,w} \{ \Psi(\mathbf{r}) \} = \mathbf{T}_{\mathbf{u}} := \Psi(\mathbf{r} + \mathbf{T}_{u,v,w}) \quad (3.32)$$

is used. There holds

$$\mathbf{T}_{\mathbf{u}} \mathbf{H} = \mathbf{H}, \quad (3.33)$$

because the crystal potential  $U(\mathbf{r})$  is periodic with the periodicity of the lattice and the  $\nabla^2$ -operator is translation invariant. Moreover, the two operators commute:

$$\mathbf{T}_{\mathbf{u}} \mathbf{H} = \mathbf{H} \mathbf{T}_{\mathbf{u}}. \quad (3.34)$$

Using these relations, the translation operator  $\mathbf{T}_{\mathbf{u}}$  applied to (3.30) yields

$$\mathbf{H} \Psi(\mathbf{r}) = \mathbf{T}_{\mathbf{u}} \mathbf{H} \Psi(\mathbf{r}) = \mathbf{H} \underbrace{\mathbf{T}_{\mathbf{u}} \Psi(\mathbf{r})}_{\Psi(\mathbf{r} + \mathbf{T}_{\mathbf{u}})} = E \Psi(\mathbf{r}). \quad (3.35)$$

This means that the energy eigenvalue of the state  $\Psi(\mathbf{r})$  is the same in each unit cell. It follows immediately that the eigenstates of  $\mathbf{T}_{\mathbf{u}}$  are linked with the eigenstates of  $\mathbf{H}$  in the form

$$\mathbf{H} t_{\mathbf{u}} \Psi(\mathbf{r}) = E \Psi(\mathbf{r}), \quad (3.36)$$

with  $t_{\mathbf{u}}$  defined by the eigenvalue equation

$$\mathbf{T}_{\mathbf{u}} \Psi(\mathbf{r}) = t_{\mathbf{u}} \Psi(\mathbf{r}). \quad (3.37)$$

Obviously, it holds that

$$\mathbf{T}_{\mathbf{u}_1 + \mathbf{u}_2} = \mathbf{T}_{\mathbf{u}_1} \mathbf{T}_{\mathbf{u}_2}. \quad (3.38)$$

Therefore the translation operator can be decomposed into elementary translations

$$\mathbf{T}_{\mathbf{u}} = (\mathbf{T}_{1,0,0})^u (\mathbf{T}_{0,1,0})^v (\mathbf{T}_{0,0,1})^w. \quad (3.39)$$

The same decomposition is possible for the eigenvalues <sup>1</sup>:

$$t_{\mathbf{u}} = (t_{1,0,0})^u (t_{0,1,0})^v (t_{0,0,1})^w \quad (3.40)$$

This allows to rewrite (3.37) in the form

$$\Psi(\mathbf{r} + \mathbf{T}_{u,v,w}) = (t_{1,0,0})^u (t_{0,1,0})^v (t_{0,0,1})^w \Psi(\mathbf{r}). \quad (3.41)$$

It is argued that the law of *energy conservation* requires that a translation operator does not attenuate or amplify a state, thus it is claimed that  $|t_{\mathbf{u}}| = 1$ . Therefore,  $t_{\mathbf{u}}$  is a phase factor, which is chosen as

$$t_{\mathbf{u}} = t_{u,v,w} = (e^{i2\pi c_1})^u (e^{i2\pi c_2})^v (e^{i2\pi c_3})^w = e^{i2\pi(c_1 u + c_2 v + c_3 w)}, \quad (3.42)$$

with constants  $c_1$ ,  $c_2$  and  $c_3$ . Assuming periodic boundary conditions, there holds

$$t_{0,0,0} = t_{N_1, N_2, N_3}, \quad (3.43)$$

and therefore

$$c_i = \frac{1}{N_i}, \text{ with } i = 1, 2, 3. \quad (3.44)$$

Using (3.27), (3.42) is expressed as

$$t_{\mathbf{u}} = e^{\mathbf{k} \cdot \mathbf{T}_{\mathbf{u}}}, \quad (3.45)$$

where

$$\mathbf{k} = \frac{u}{N_1} \mathbf{b}_1 + \frac{v}{N_2} \mathbf{b}_2 + \frac{w}{N_3} \mathbf{b}_3, \quad (3.46)$$

is a vector of the **reciprocal space**, with  $u \in [0, N_1]$ ,  $v \in [0, N_2]$ ,  $w \in [0, N_3]$ . The  $\mathbf{k}$ -vector can be restricted to one primitive unit cell of the reciprocal lattice, usually to the first **Brillouin zone**  $\mathcal{B}$ , because

$$e^{(\mathbf{k} + \mathbf{G}_{\mathbf{u}}) \cdot \mathbf{T}_{\mathbf{u}}} = e^{\mathbf{k} \cdot \mathbf{T}_{\mathbf{u}}}. \quad (3.47)$$

Finally (3.45) is inserted into (3.41), which gives

$$\Psi(\mathbf{r} + \mathbf{T}_{\mathbf{u}}) = e^{\mathbf{k} \cdot \mathbf{T}_{\mathbf{u}}} \Psi(\mathbf{r}). \quad (3.48)$$

This is the so-called **Bloch theorem**. It shows, that the state from cell to cell differs only by a phase factor  $e^{\mathbf{k} \cdot \mathbf{T}_{\mathbf{u}}}$ . Thus, the eigenvalue-problem in (3.30) is now formulated as

$$\mathbf{H} \Psi_{\mathbf{k}}^{\nu}(\mathbf{r}) = E_{\mathbf{k}}^{\nu} \Psi_{\mathbf{k}}^{\nu}(\mathbf{r}), \quad (3.49)$$

with band index  $\nu$ . The states  $\Psi_{\mathbf{k}}^{\nu}(\mathbf{r})$  are called **Bloch states** or **Bloch waves**. These are given in the form

$$\Psi_{\mathbf{k}}^{\nu}(\mathbf{r}) = u_{\mathbf{k}}^{\nu}(\mathbf{r}) e^{i\mathbf{k} \cdot \mathbf{r}}, \quad (3.50)$$

thus electrons in a crystal potential  $U_{\text{crystal}}(\mathbf{r})$  are plane waves modulated by the cell-periodic function

$$u_{\mathbf{k}}^{\nu}(\mathbf{r}) = u_{\mathbf{k}}^{\nu}(\mathbf{r} + \mathbf{T}_{\mathbf{u}}). \quad (3.51)$$

It can be easily seen, that (3.50) fulfills (3.48). To complement this very abstract derivation, a physical interpretation of the result is given:

<sup>1</sup>Example:  $\mathbf{T}_{2,0,0} \Psi(\mathbf{r}) = t_{2,0,0} \Psi(\mathbf{r}) \Leftrightarrow \mathbf{T}_{1,0,0} \underbrace{\mathbf{T}_{1,0,0}}_{t_{1,0,0} \Psi(\mathbf{r})} \Psi(\mathbf{r}) = (t_{1,0,0})^2 \Psi(\mathbf{r})$



**The Bandstructure.** The  $\mathbf{k}$ -vector according to (3.46) takes only discrete values. Since crystals consist of a huge number of unit cells, the  $\mathbf{k}$ -vector is assumed to be continuous. This is not true for quantum structures like quantum wells or quantum wires, but holds for bulk materials. The number of different  $\mathbf{k}$ -values is equal to the number of unit cells. Each  $\mathbf{k}$  characterizes a Bloch state. The energy eigenvalue  $E_{\mathbf{k}}^{\nu}$  in (3.49) thus takes the form  $E^{\nu}(\mathbf{k})$ , which is called an energy band. There exist an infinite number of bands [20] labeled by  $\nu$ . These bands are separated by band gaps, i.e. zones on the energy axis, where no state exists. In semiconductors at zero temperature the last occupied band is named **valence band** and the first unoccupied band is named **conduction band**. In metals, the last band is only partially occupied, which is the reason for their good conductivity. In general, bands can be degenerated, i.e. for one  $\mathbf{k}$ -value more than one  $E$ -value can be found, see Section 3.2.3.

**The Crystal Momentum.** As stated in Section 3.1.1, the momentum of an electron is given by  $\hbar\mathbf{k}$ , which is also called the crystal momentum. The momentum is, as well as the energy, a conserved quantity. For the crystal momentum, the conservation law differs from the classical conservation law. According to (3.47),  $\mathbf{k}$  and  $\mathbf{k} + \mathbf{G}_{\mathbf{u}}$  describe the same state, hence

$$\mathbf{k} \equiv \mathbf{k} + \mathbf{G}_{\mathbf{u}}. \quad (3.52)$$

It follows directly, that

$$E^{\nu}(\mathbf{k}) = E^{\nu}(\mathbf{k} + \mathbf{G}_{\mathbf{u}}), \quad (3.53)$$

which means, that the energy bandstructure is periodic with the periodicity of the reciprocal lattice. Therefore it is sufficient to know the bandstructure in the first Brillouin zone  $\mathcal{B}$ . The conservation law for the crystal momentum is thus given by

$$(\mathbf{k}_1 + \mathbf{k}_2) \bmod \mathbf{G}_{\mathbf{u}}, \quad (3.54)$$

with the modulo-operation mod. In the next section, the band structure for cubic semiconductors, like Si, GaAs or Ge, is discussed [21].

### 3.2.3 Real Electronic Band-Structures

The calculation of real electronic band structures is a very sophisticated task. In general, the band structure of a material is a set  $\{E^{\nu}(\mathbf{k})\}_{\nu}$ , which is the solution of (3.49). According to (3.53),  $E^{\nu}(\mathbf{k})$  is periodic in  $\mathbf{k}$ . The whole information about the band-structure is contained within the first Brillouin zone. Fig. 3.6 shows the first Brillouin zone of the face-centered-cubic-lattice. The plotted high symmetry points according to [28] are given by:

$$\begin{aligned} \Gamma &= (0, 0, 0) \\ \text{X} &= \frac{2\pi}{a} (1, 0, 0) \\ \text{L} &= \frac{2\pi}{a} \left( \frac{1}{2}, \frac{1}{2}, \frac{1}{2} \right) \\ \text{K} &= \frac{2\pi}{a} \left( \frac{3}{4}, \frac{3}{4}, 0 \right) \\ \text{W} &= \frac{2\pi}{a} \left( 1, \frac{1}{2}, 0 \right) \end{aligned}$$

In Fig. 3.7 the **many-valley model** of the band structure for cubic semiconductors like Si, GaAs or Ge is shown. It reflects the main properties of real electronic band structures. The term **valley**

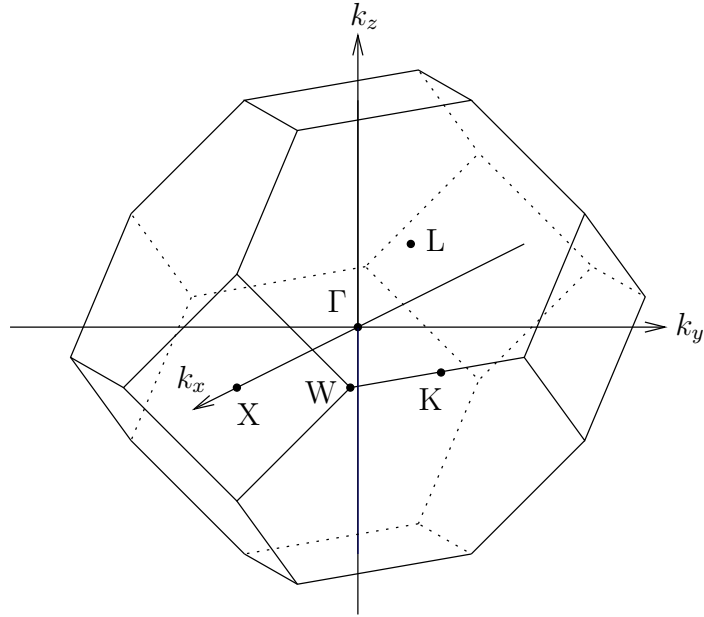


**Figure 3.6:** First Brillouin zone of diamond and zinc-blende structures with high symmetry points.

Material	$E_{\Gamma}$ [eV]	$E_L$ [eV]	$E_{\Delta}$ [eV]	$E_{so}$ [eV]	$m_l^*$ [ $m_e$ ]	$m^*$ [ $m_e$ ]	$m_t^*$ [ $m_e$ ]	$\alpha$ [eV $^{-1}$ ]	A	B	C
Si	4.08	1.87	1.13	0.044	0.98		0.19	0.5	4.22	0.78	4.80
Ge	0.89	0.76	0.96	0.29	1.64		0.083	0.65	13.35	8.50	13.11
GaAs	1.42	1.71	1.90	0.34		0.067		0.64	7.65	4.82	7.71

**Table 3.1:** Parameters of the many valley model [30].

denotes the local minima of the conduction band. The parameters for chosen materials are given in Table 3.1. Electrons exist in either of the three valleys of the conduction band, but are not able to move between these valleys in a continuous manner. They can only scatter from one valley to another by so-called inter-valley scattering. The maxima of the valence bands are located at  $\Gamma$ . The *light-hole*- and *heavy-hole*-band are degenerated at this point. The maximum of the so-called *split-off*-band is shifted by  $E_{so}$  due to spin-orbit interaction [12]. A very good discussion about the basics of band structure calculations is found in [8]. In [28] an overview of some important band structure calculation techniques can be found. In [4], a thorough description of the so-called tight-binding method with instructive examples is given. A very detailed book on band structure calculations is [21]. In the next section, expressions for the approximation of the band structure for the valleys of the conduction band and for the valence bands are given.

### 3.2.4 Analytic Band Structure Models

The most important analytic band structure models, which are widely used in electronic device simulation, are presented. The starting point is the band structure described by the dispersion relation  $E^{\nu}(\mathbf{k})$ , for the  $\nu$ -th band. The analytic models discussed in the following give approximations to the valleys of the conduction band and for the valence bands respectively.

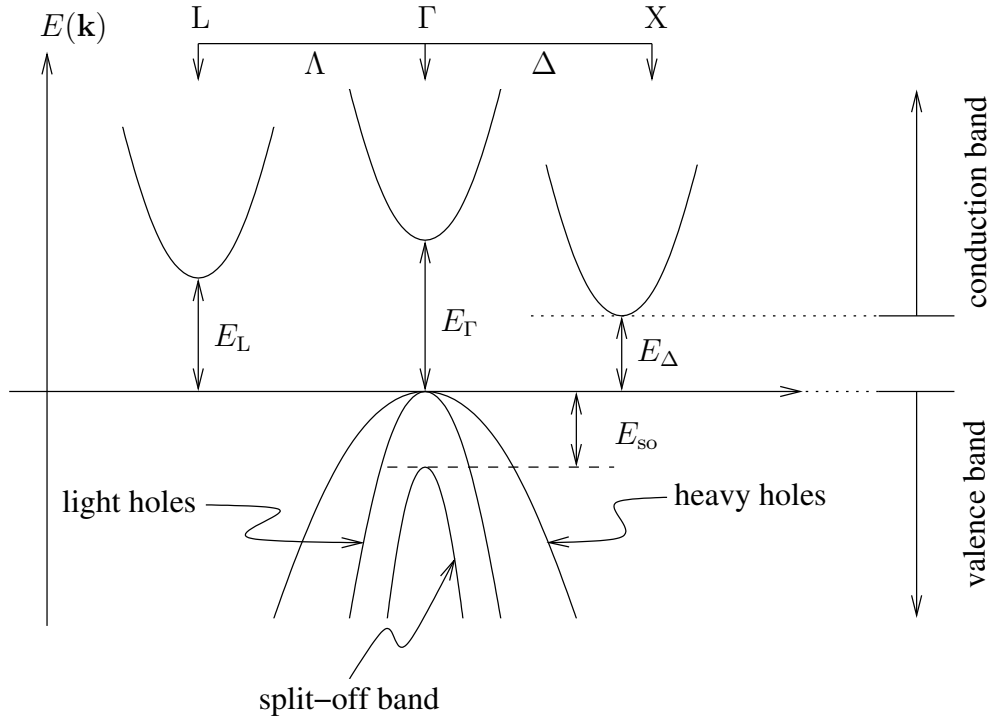


**Figure 3.7:** Many valley model of the band structure for cubic semiconductors, like Si, GaAs, and Ge [12, 30].

### Effective Mass Approximation

The band structure  $E(\mathbf{k})$  is expanded in a Taylor series around the minimum at  $\mathbf{k}_0$ . The expansion up to the second order is

$$E(\mathbf{k}) \approx E(\mathbf{k}_0) + \frac{1}{2} \sum_i \sum_j (k_i - k_{i,0}) \left. \frac{\partial^2 E}{\partial k_i \partial k_j} \right|_{\mathbf{k}=\mathbf{k}_0} (k_j - k_{j,0}), \quad (3.55)$$

with  $i, j = x, y, z$ . In analogy to the dispersion relation of the free electron, which is  $E(k) = \hbar^2 k^2 / 2m_e$ , it is appropriate to define the effective mass tensor

$$\tilde{\mathbf{m}}^* = \hbar^2 \begin{bmatrix} \frac{\partial^2 E}{\partial k_x \partial k_x} & \frac{\partial^2 E}{\partial k_x \partial k_y} & \frac{\partial^2 E}{\partial k_x \partial k_z} \\ \frac{\partial^2 E}{\partial k_y \partial k_x} & \frac{\partial^2 E}{\partial k_y \partial k_y} & \frac{\partial^2 E}{\partial k_y \partial k_z} \\ \frac{\partial^2 E}{\partial k_z \partial k_x} & \frac{\partial^2 E}{\partial k_z \partial k_y} & \frac{\partial^2 E}{\partial k_z \partial k_z} \end{bmatrix}^{-1}. \quad (3.56)$$

By choosing an appropriate coordinate system, the effective mass tensor takes a diagonal form:

$$\tilde{\mathbf{m}}^* = \begin{bmatrix} m_x^* & 0 & 0 \\ 0 & m_y^* & 0 \\ 0 & 0 & m_z^* \end{bmatrix}. \quad (3.57)$$

A coordinate transformation of the form  $\mathbf{k}' = \mathbf{k} - \mathbf{k}_0$ , where  $\mathbf{k}_0$  is the coordinate vector of the concerned minimum, is performed. In the following,  $\mathbf{k}'$  is simply written as  $\mathbf{k}$ , because the energy band relation is always given in the transformed coordinate system. Therefore the band-structure for the conduction band near the minimum  $\mathbf{k}_0$  is approximated as

$$E(\mathbf{k}) \cong E_{c0} + \frac{\hbar^2 k_x^2}{2m_x} + \frac{\hbar^2 k_y^2}{2m_y} + \frac{\hbar^2 k_z^2}{2m_z}, \quad (3.58)$$

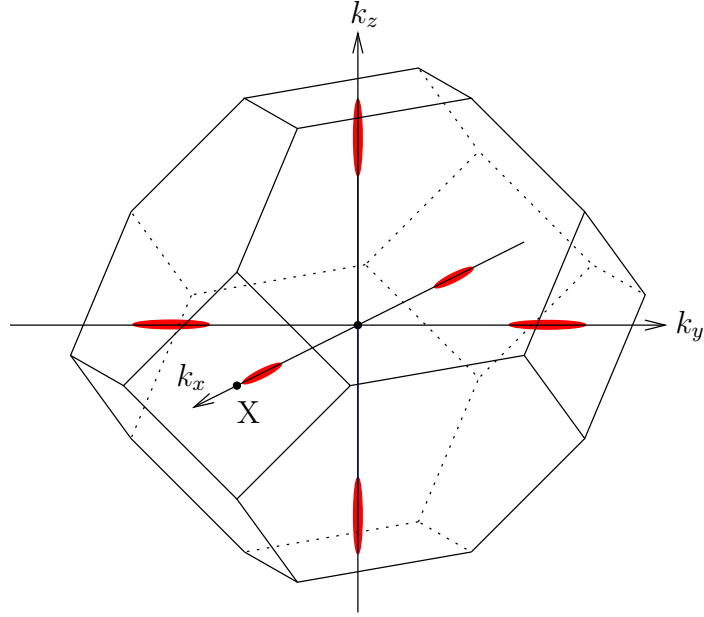


**Figure 3.8:** The six deepest minima of the conduction band of Si are the so-called  $\Delta$ -valleys. The red ellipsoids are equi-energy surfaces of the conduction band.

with  $m_x$ ,  $m_y$  and  $m_z$ , depending on  $\mathbf{k}_0$ . For Si, the six deepest minimas lie on the lines between the  $\Gamma$ -point and the six X-points at 85% of distance, see Fig. 3.8 [17]. For the  $\Delta$ -valley pairs on each axis, an effective mass tensor in the diagonal form is found. For the  $x$ -axis it reads

$$\tilde{\mathbf{m}}^* = \begin{bmatrix} m_1^* & 0 & 0 \\ 0 & m_t^* & 0 \\ 0 & 0 & m_t^* \end{bmatrix}, \quad (3.59)$$

with the longitudinal effective mass  $m_1^*$  and the transversal effective mass  $m_t^*$ . For the  $y$ -axis pair,  $m_y^* = m_1^*$  and  $m_x^* = m_z^* = m_t^*$  and for the  $z$ -axis pair,  $m_z^* = m_1^*$  and  $m_x^* = m_y^* = m_t^*$ . Values for the effective masses are found in Table 3.1. The simplest band structure approximation with a scalar effective mass  $m^*$  is parabolic and given by

$$E(\mathbf{k}) = \frac{\hbar^2 \mathbf{k}^2}{2m^*}. \quad (3.60)$$

The group velocity follows as

$$\mathbf{v}(\mathbf{k}) = \frac{\hbar \mathbf{k}}{m^*} \quad (3.61)$$

and the wave vector  $\mathbf{k}(E, \theta, \varphi)$  is given by

$$\mathbf{k}(E, \theta, \varphi) = \frac{\sqrt{2m^*E}}{\hbar} \mathbf{e}_{\mathbf{k}}. \quad (3.62)$$

The generalized density of states defined in (2.29) reads

$$\begin{aligned} Z(E, \theta, \varphi) = Z(E) &= \frac{k^2}{(2\pi)^3} \frac{\partial k(E, \theta, \varphi)}{\partial E} \\ &= \frac{(m^*)^{3/2} \sqrt{2}}{(2\pi \hbar)^3} \sqrt{E}. \end{aligned} \quad (3.63)$$

This explicit expressions of  $\mathbf{v}(\mathbf{k})$ ,  $\mathbf{k}(E, \theta, \varphi)$  and  $Z(E, \theta, \varphi)$  are of particular importance for SHE-simulations [12, 17, 20].

### Herring-Vogt Transformation

In general, the *effective mass approximation* is anisotropic, therefore the equi-energy surfaces are ellipsoids described by (3.58). A transformation of the form

$$\mathbf{k}' = \mathbf{T}\mathbf{k}, \quad (3.64)$$

with the transformation matrix  $\mathbf{T}$ , maps the elliptical dispersion relation to a spherical one. In the original space, the energy relation reads

$$E(\mathbf{k}) = E(\mathbf{k}_0) + \frac{\hbar^2}{2} \sum_i k_i \left( \frac{1}{m^*} \right)_{i,i} k_i, \quad (3.65)$$

with  $(1/m^*)_{i,i}$  are the diagonal elements of the inverse effective mass tensor (3.57) and  $i = x, y, z$ . For the transformation matrix, the ansatz

$$k'_i = T_{i,i} k_i = \sqrt{\frac{m_{i,i}^*}{m_{\text{DOS}}^*}} k_i, \quad (3.66)$$

with the *density of state effective mass*  $m_{\text{DOS}}^*$ , which will be defined later, and  $E(\mathbf{k}_0) = 0$  leads to

$$E(\mathbf{k}) = \frac{\hbar^2}{2m_{\text{DOS}}^*} \sum_i k_i T_{i,i}^2 k_i = \frac{\hbar^2 \mathbf{T}^2 |\mathbf{k}|^2}{2m_{\text{DOS}}^*} = \frac{\hbar^2 |\mathbf{k}'|^2}{2m_{\text{DOS}}^*}, \quad (3.67)$$

therefore the equi-energy surfaces in the transformed space are spheres. To determine the *density of state effective mass*  $m_{\text{DOS}}^*$ , it is assumed, that the volume elements are equal in the original space and in the transformed space, which reads

$$\prod_i dk'_i = \prod_i T_{i,i} dk_i = \prod_i \sqrt{\frac{m_{i,i}^*}{m_{\text{DOS}}^*}} dk_i = \sqrt{\frac{\prod_i m_{i,i}^*}{(m_{\text{DOS}}^*)^i}} \prod_i dk_i. \quad (3.68)$$

This gives a definition for the *density of state effective mass*  $m_{\text{DOS}}^*$ :

**Definition 9** (Density Of State Effective Mass). *The density of state effective mass  $m_{\text{DOS}}^*$  is defined as:*

$$m_{\text{DOS}}^* := \left( \prod_i m_{i,i}^* \right)^{1/i} = \begin{cases} \sqrt[3]{m_x m_y m_z}, & \text{for 3 dimensions} \\ \sqrt{m_x m_y}, & \text{for 2 dimensions} \end{cases} \quad (3.69)$$

The Herring-Vogt transformation can also be used in connection with non-parabolic energy bands, which are described in the next section [12, 17].

### Non-Parabolic Energy Band Approximation

The *effective mass approximation* is only valid for  $\mathbf{k}$ -vectors close to the concerned band minimum  $\mathbf{k}_0$ . A better approximation of the real band structure is obtained by

$$E(1 + \alpha E) = \gamma(E) = \frac{\hbar^2 \mathbf{k}^2}{2m^*}, \quad (3.70)$$

where  $\alpha$  is the *non-parabolicity factor* and  $\gamma(E)$  an implicit function in  $E$ . The right-hand side of (3.70) can be replaced by the right-hand side of (3.58) or (3.67). A description as in (3.70) enables the

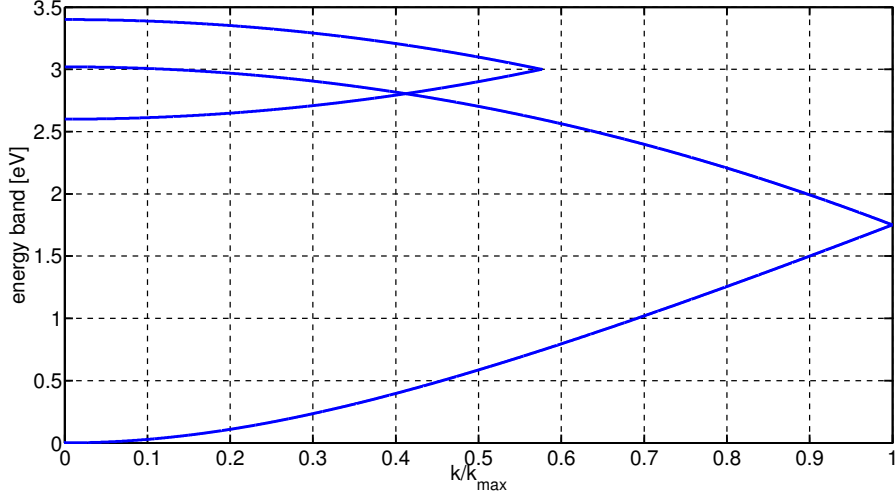


**Figure 3.9:** Plot of the four analytic bands of the Modena model.

separation between the non-parabolicity correction and the Herring-Vogt transformed effective mass approximation. The derivative of  $\gamma(E)$  with respect to  $E$  is given by

$$\gamma'(E) = \frac{\partial \gamma}{\partial E} = 1 + 2\alpha E. \quad (3.71)$$

The group velocity  $\mathbf{v}(\mathbf{k})$  for a non-parabolic band according to (3.70) is obtained as

$$\mathbf{v}(\mathbf{k}) = \frac{\hbar \mathbf{k}}{m_c^*}, \quad (3.72)$$

with the *conductivity mass*  $m_c^* = m^*(1 + 2\alpha E)$ . This expression is very similar to (3.61) [12,17].

### The Modena Model

The *Modena model* [2], is an analytical band-structure model, which includes an approximation of the real band structure in the six equivalent  $\Delta$ -valleys and in the 12 equivalent L-point-valleys. The parameters were found by fitting the resulting density of states against a full-band density of states calculation and are given in Table 3.2. The four analytic model bands are:

$$E(1 + \alpha E) = \frac{\hbar^2 k^2}{2m_1^*}, \quad \text{electron-like band in the } \Delta\text{-valley} \quad (3.73)$$

$$E = E_{2,\max} - \frac{\hbar^2 k^2}{2m_2^*}, \quad \text{hole-like band in the } \Delta\text{-valley} \quad (3.74)$$

$$E = E_{3,\min} + \frac{\hbar^2 k^2}{2m_3^*}, \quad \text{electron-like band in the L-point-valley} \quad (3.75)$$

$$E = E_{4,\max} - \frac{\hbar^2 k^2}{2m_4^*}, \quad \text{hole-like band in the L-point-valley} \quad (3.76)$$

In Fig. 3.9 these bands are plotted. The first band is non-parabolic, with  $\alpha = 0.35 \text{ eV}^{-1}$ . The first and second band, as well as the third and fourth band can be combined to one band respectively. For each band, a BTE has to be solved and inter-band transitions have to be taken into account [2, 25].

Index $i$	Type	$m_i^*/m_e$	$E_{i,\min}$ [eV]	$E_{i,\max}$ [eV]	Valley, Number
1	electron	0.320	0	1.75	$\Delta$ -valley, 6
2	hole	0.712	1.75	3.02	$\Delta$ -valley, 6
3	electron	0.750	2.60	3.00	L-point-valley, 12
4	hole	0.750	3.00	3.40	L-point-valley, 12

**Table 3.2:** Parameters of the *Modena model*.

### 3.2.5 Model for the Valence Bands

In [12], a non-spherical approximation for valence bands is given as

$$E(\mathbf{k}) = E(k, \theta, \varphi) = ak^2 [1 \mp g(\theta, \varphi)], \quad (3.77)$$

where  $-$  and  $+$  refer to heavy and light holes, respectively. The parameters of the angular function

$$g(\theta, \varphi) = [b^2 + c^2 (\sin^4 \theta \cos^2 \varphi \sin^2 \varphi + \sin^2 \theta \cos^2 \theta)]^{1/2}, \quad (3.78)$$

are given by

$$a = \frac{\hbar^2 |A|}{2m_e}, b = \frac{|B|}{|A|}, c = \frac{|C|}{|A|}, \quad (3.79)$$

where  $|A|$ ,  $|B|$  and  $|C|$  are found in Table 3.1.

## 3.3 Fermi's Golden Rule

In Section 3.1, a general description of semi-classical treatment of carrier dynamics is given. For carrier scattering a quantum mechanical approach is used. Therefore, the SE needs to be solved. In Section 1.1 the Hamiltonian is assumed to be constant in time. To model scattering it is necessary to add a time-dependent perturbation to the Hamiltonian. The solution of the SE with such a perturbed Hamiltonian is discussed in this section. Then, the so-called Fermi's Golden Rule (FGR) specialised for electrons in a crystal potential (see Section 3.2) is presented. In the context of this work, FGR provides a tool for calculating the transition rate of a specific scattering mechanism, which is described by its scattering potential  $U_s(\mathbf{r}, t)$ . The transition rate  $S(\mathbf{k}, \mathbf{k}', t)$  is the probability per unit time for a carrier to scatter from initial state  $\mathbf{k}$  to final state  $\mathbf{k}'$ , when interacting with the scattering potential  $U_s(\mathbf{r}, t)$  (see Fig. 3.10).

### 3.3.1 Time-dependent Perturbation Theory

In the time-dependent perturbation theory, the time-independent Hamiltonian  $\underline{\mathbf{H}}_0$  describes the unperturbed problem. The perturbation  $\underline{\mathbf{U}}_p(t)$  is added with a weighting parameter  $\lambda \in [0, 1]$ . This gives the SE

$$[\underline{\mathbf{H}}_0 + \lambda \underline{\mathbf{H}}'(t)] |\psi, t\rangle = i\hbar \frac{\partial |\psi, t\rangle}{\partial t}, \quad (3.80)$$

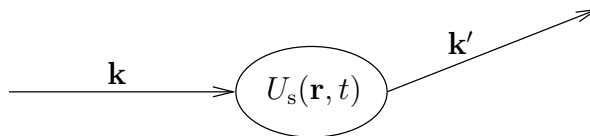


**Figure 3.10:** Illustration of a generic scattering event. A carrier with initial state  $\mathbf{k}$  interacts with a scattering potential  $U_s(\mathbf{r}, t)$  and changes its state to  $\mathbf{k}'$ .

with the time-dependent state vector  $|\psi, t\rangle$ . The unperturbed problem

$$\underline{\mathbf{H}}_0|n\rangle = E_n|n\rangle \quad (3.81)$$

is assumed to be solved for orthonormal eigenfunctions  $|n\rangle$  and corresponding eigenvalues  $E_n$ . The state vector  $|\Psi, t\rangle$  in (3.80) is expanded using these eigenfunctions to

$$|\Psi, t\rangle = \sum_n c_n(t)|n\rangle, \quad (3.82)$$

with time dependent expansion coefficients  $c_n(t)$ . This ansatz is substituted into (3.80) to obtain

$$[\underline{\mathbf{H}}_0 + \lambda \underline{\mathbf{H}}'(t)] \sum_n c_n(t)|n\rangle = i\hbar \frac{\partial}{\partial t} \sum_n c_n(t)|n\rangle. \quad (3.83)$$

Multiplying (3.83) with  $\langle m|$  from the left and using the orthonormality property  $\langle m|n\rangle = \delta_{m,n}$  yields

$$E_m c_m(t) + \lambda \sum_n \langle m|\underline{\mathbf{H}}'(t)|n\rangle c_n(t) = i\hbar \frac{dc_m(t)}{dt}. \quad (3.84)$$

By making the ansatz  $c_m(t) = a_m(t)e^{-i\omega_m t}$  with  $\omega_m = E_m/\hbar$ , (3.84) simplifies to

$$\lambda \sum_n \langle m|\underline{\mathbf{H}}'|n\rangle a_n(t) e^{i(\omega_m - \omega_n)t} = i\hbar \frac{da_m(t)}{dt}. \quad (3.85)$$

This equation is equivalent to the SE (3.80), because the eigenfunctions  $|n\rangle$  form a complete basis. In the next step the coefficients  $a_m(t)$  are expanded in powers of lambda in the form

$$a_m(t) = a_m^{(0)}(t) + \lambda a_m^{(1)}(t) + \lambda^2 a_m^{(2)}(t) + \dots \quad (3.86)$$

This series inserted into (3.85) yields

$$i\hbar \frac{da_m^{(0)}(t)}{dt} + i\hbar \lambda \frac{da_m^{(1)}(t)}{dt} + \mathcal{O}(\lambda^2) = \lambda \sum_n \langle m|\underline{\mathbf{H}}'|n\rangle a_n^{(0)}(t) e^{i(\omega_m - \omega_n)t} + \mathcal{O}(\lambda^2). \quad (3.87)$$

The two series are compared for zeroth and first order in  $\lambda$  to get

$$\lambda^0: i\hbar \frac{da_m^{(0)}(t)}{dt} = 0 \Rightarrow a_m^{(0)} = \text{const.} \quad (3.88)$$

$$\lambda^1: i\hbar \frac{da_m^{(1)}(t)}{dt} = \sum_n \langle m|\underline{\mathbf{H}}'|n\rangle a_n^{(0)} e^{i(\omega_m - \omega_n)t}. \quad (3.89)$$

Assuming that the system is in the eigenstate  $|n\rangle$  at  $t = 0$ , the expansion coefficients are

$$a_m^{(0)} = \delta_{m,n}, \quad (3.90)$$

$$a_m^{(l)}(t = 0) = 0, \text{ with } l \geq 1. \quad (3.91)$$

With (3.89), (3.90) and (3.91) the temporal evolution of  $a_m^{(1)}(t)$  is expressed as

$$a_m^{(1)}(t) = -\frac{i}{\hbar} \int_0^t \langle m|\underline{\mathbf{H}}'|n\rangle e^{i(\omega_m - \omega_n)t'} dt'. \quad (3.92)$$



The probability to find the system with initial state  $|n\rangle$  in final state  $|m\rangle$  with  $m \neq n$  for  $t > 0$  (transition probability) is according to Section 1.1.5 given by

$$\begin{aligned} p_{n,m}(t) &= |c_m(t)|^2 = |a_m(t)|^2 = |a_m^{(0)} + \lambda a_m^{(1)}(t) + \lambda^2 a_m^{(2)}(t) + \dots|^2 \\ &= \left| \sum_k \lambda^k a_m^{(k)} \right|^2. \end{aligned} \quad (3.93)$$

The Born approximation is used [27]: It claims that  $|\lambda| \ll 1$ , so  $|\lambda|^2 \ll |\lambda|$ . Including expansion coefficients up to the first order,

$$p_{n,m}(t) \approx |a_m^{(1)}(t)|^2 = \left| \frac{1}{\hbar} \int_0^t \langle m | \underline{\mathbf{H}}' | n \rangle e^{i(\omega_m - \omega_n)t'} dt' \right|^2 \quad (3.94)$$

is obtained. Note that only the correlation of the initial state  $|n\rangle$  and the final state  $|m\rangle$  via the perturbing potential  $\underline{\mathbf{H}}'$  is considered. The correlations to all other states are neglected. The transitions rate  $S_{n,m}$  from initial state  $|n\rangle$  to final state  $|m\rangle$  is defined by the transition probability per time unit as

$$S_{n,m} = \frac{p_{n,m}}{t} \quad (3.95)$$

### 3.3.2 Non-Recurring Perturbation

Here, perturbations constant in time for  $t \geq 0$  and zero for  $t < 0$  are considered. In the following, they are denoted as *non-recurring*. Starting with the transition probability (3.94), the transition rate  $S_{n,m}$  for the non-recurring perturbation

$$\underline{\mathbf{H}}'(t) = \underline{\mathbf{H}}'\sigma(t) \quad (3.96)$$

is calculated. The step function  $\sigma(t)$  is defined by

$$\sigma(t) = \begin{cases} 0, & t < 0 \\ 1, & t \geq 0 \end{cases}. \quad (3.97)$$

The correct interpretation of (3.96) is that  $\underline{\mathbf{H}}'(t)$  describes a perturbation, which occurs only for times  $t \geq 0$ . Evaluating (3.94) with the potential from (3.96) and substituting  $(\omega_m - \omega_n) \mapsto \Omega$  yields

$$\begin{aligned} p_{n,m}(t) &= \left| \frac{1}{\hbar} \langle m | \underline{\mathbf{H}}' | n \rangle \int_0^t e^{i\Omega t'} dt' \right|^2 \\ &= \frac{1}{\hbar^2} |\langle m | \underline{\mathbf{H}}' | n \rangle|^2 \left| \frac{e^{i\Omega t} - 1}{i\Omega} \right|^2 \\ &= \frac{1}{\hbar^2} |\langle m | \underline{\mathbf{H}}' | n \rangle|^2 \frac{\sin^2(\Omega t/2)}{(\Omega/2)^2}. \end{aligned} \quad (3.98)$$

For a further analysis, the function sequence

$$\Sigma_t(\alpha) = \frac{\sin^2(\alpha t)}{\alpha^2 t} \quad (3.99)$$

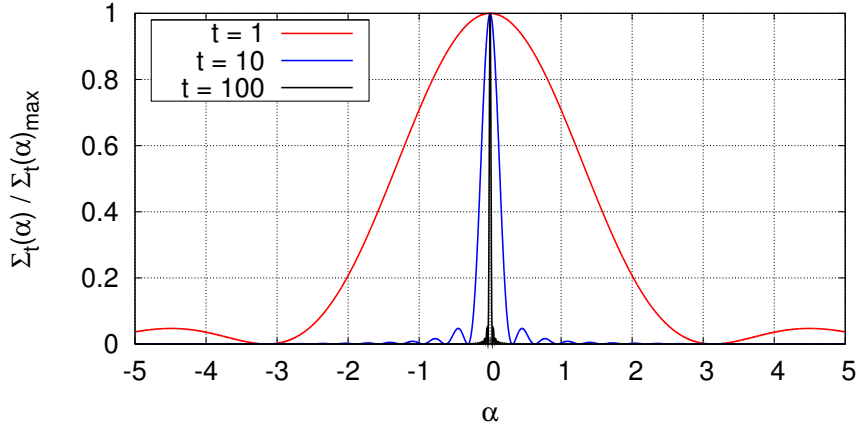


**Figure 3.11:** The  $\Sigma_t(\alpha)$ -function (3.99) normalized to its maximum. For sufficiently large  $t$ , this function is more and more like a Dirac distribution  $\delta(\alpha)$ .

is defined and (3.98) is rewritten to

$$p_{n,m}(t) = \frac{t}{\hbar^2} |\langle m | \mathbf{H}' | n \rangle|^2 \Sigma_t(\Omega/2). \quad (3.100)$$

It is claimed that  $\lim_{t \rightarrow \infty} \Sigma_t(\alpha) = \pi \delta(\alpha)$ . To proof this, the function sequence  $\Sigma_t(\alpha)$  is multiplied by a test function  $F(\alpha)$  and integrated over  $\alpha$ . The integral

$$\int_{-\infty}^{+\infty} \Sigma_t(\alpha) F(\alpha) d\alpha \quad (3.101)$$

can be rewritten with the substitution  $\alpha \mapsto x/t$  and  $d\alpha \mapsto dx/t$ . The limit  $t \rightarrow \infty$  gives

$$\lim_{t \rightarrow \infty} \int_{-\infty}^{+\infty} \Sigma_t(\alpha) F(\alpha) d\alpha = \lim_{t \rightarrow \infty} \int_{-\infty}^{+\infty} \frac{\sin^2(x)}{x^2} F(x/t) dx = F(0)\pi, \quad (3.102)$$

with

$$\int_{-\infty}^{+\infty} \frac{\sin^2(x^2)}{x^2} dx = \pi. \quad (3.103)$$

Comparing (3.102) with  $\int_{-\infty}^{+\infty} \delta(x) F(x) dx = F(0)$  yields

$$\lim_{t \rightarrow \infty} \Sigma_t(\alpha) = \pi \delta(\alpha). \quad (3.104)$$

This result is also confirmed by a plot of  $\Sigma_t(\alpha)$  for different values of the transition time  $t$  (see Fig. 3.11). For a sufficiently large time  $t$ , it is concluded that

$$\Sigma_t(\alpha) \cong \pi \delta(\alpha). \quad (3.105)$$

Therefore, (3.100) is written as

$$p_{n,m}(t) \cong \frac{\pi t}{\hbar^2} |\langle m | \mathbf{H}' | n \rangle|^2 \delta(\Omega/2) = \frac{2\pi t}{\hbar^2} |\langle m | \mathbf{H}' | n \rangle|^2 \delta(\Omega), \quad (3.106)$$

using  $\delta(\Omega/2) = 2\delta(\Omega)$ <sup>2</sup>. From that, the transition rate (3.95) for the non-recurring potential (3.96) follows as<sup>3</sup>

$$S_{n,m} = \frac{2\pi}{\hbar} |\langle m | \mathbf{H}' | n \rangle|^2 \delta(E_m - E_n). \quad (3.107)$$

<sup>2</sup>  $\int_{-\infty}^{+\infty} \delta(x) dx \stackrel{x \mapsto y/a}{=} \int_{-\infty}^{+\infty} \delta(y/a) dy/a = 1 \Rightarrow \int_{-\infty}^{+\infty} \delta(y/a) dy = a \Rightarrow \delta(y/a) = a\delta(y)$

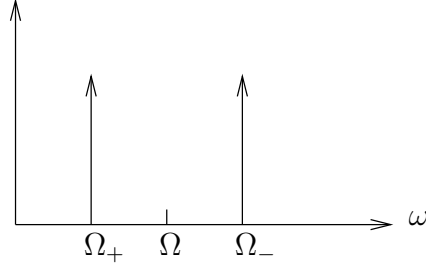


**Figure 3.12:** A periodic perturbation potential (3.109) leads to two possible transition frequencies at  $\Omega_+ = \Omega - \hbar\omega$  and  $\Omega_- = \Omega + \hbar\omega$ , with  $\Omega = \omega_m - \omega_n$ .

The Dirac distribution  $\delta(E_m - E_n)$  is an expression of energy conservation and reflects the fact that the energy of the final state  $|m\rangle$  is equal to the energy of the initial state  $|n\rangle$  ( $E_m = E_n$ ). The Dirac distribution  $\pi\delta(\Omega/2)$  in (3.106) is an approximation for  $\Sigma_t(\Omega/2)$  in (3.100). The larger the transition time  $t$  becomes, the better is the approximation. Moreover, only for an infinite time  $t$  the approximation is precise. Therefore, this is a good approximation for infrequent transitions, when the time between two transition events is relatively large. For short transition times, energy conservation is not strictly satisfied. This is a consequence of Heisenberg's uncertainty principle, which states that  $\Delta E \Delta t \gtrsim \hbar$  [20, 27]. The energy difference  $\Delta E$  occurs between the initial and the final state, due to finite transition times  $t$ . This means that the final state is not well-defined for finite transition times  $t$ . The matrix element  $\langle m | \underline{\mathbf{H}}' | n \rangle$  is evaluated according to Appendix A by

$$\langle m | \underline{\mathbf{H}}' | n \rangle = \int_{\mathbb{R}^3} \Psi_m^*(\mathbf{r}) H'(\mathbf{r}) \Psi_n(\mathbf{r}) d\mathbf{r}. \quad (3.108)$$

For a discussion about the matrix element, see Section 3.3.4.

### 3.3.3 Periodic Perturbation

In this section, the perturbation scattering operator is assumed to be periodic in time:

$$\underline{\mathbf{H}}'(t) = \underline{\mathbf{H}}' e^{-i\omega t} + \underline{\mathbf{H}}'^{\dagger} e^{i\omega t}, \quad (3.109)$$

where  $\underline{\mathbf{H}}'$  is a time-independent operator. Equation (3.109) has to be interpreted as a harmonic perturbation. It is important to note that the operator is not applied to the exponentials.  $\underline{\mathbf{H}}'(t)$  is Hermitian by construction and therefore has real-valued eigenvalues. The transition probability (3.94) now reads

$$p_{n,m}(t) = \left| \frac{1}{\hbar} \int_0^t \langle m | \underline{\mathbf{H}}' | n \rangle e^{i(\omega_m - \omega_n - \omega)t'} + \langle m | \underline{\mathbf{H}}'^{\dagger} | n \rangle e^{i(\omega_m - \omega_n + \omega)t'} dt' \right|^2. \quad (3.110)$$

Simplifying the expression with  $\Omega_+ = \omega_m - \omega_n - \omega$  and  $\Omega_- = \omega_m - \omega_n + \omega$  and integrating yields

$$\begin{aligned} p_{n,m}(t) &= \left| \frac{1}{\hbar} \int_0^t \left[ \langle m | \underline{\mathbf{H}}' | n \rangle e^{i\Omega_+ t'} + \langle m | \underline{\mathbf{H}}'^{\dagger} | n \rangle e^{i\Omega_- t'} \right] dt' \right|^2 \\ &= \frac{1}{\hbar^2} \left| \langle m | \underline{\mathbf{H}}' | n \rangle \frac{e^{i\Omega_+ t} - 1}{i\Omega_+} + \langle m | \underline{\mathbf{H}}'^{\dagger} | n \rangle \frac{e^{i\Omega_- t} - 1}{i\Omega_-} \right|^2 \\ &= |z_1 + z_2|^2 \\ &= |z_1|^2 + |z_2|^2 + 2\Re(z_1^* z_2). \end{aligned} \quad (3.111)$$

<sup>3</sup> $\delta(\Omega) = \delta(\omega_m - \omega_n) = \delta((E_m - E_n)/\hbar) = \hbar\delta(E_m - E_n)$

For  $t \rightarrow \infty$ , the correlation term  $2\Re(z_1^* z_2)$  vanishes, because two Dirac distributions  $\delta(\Omega)$  at  $\Omega = \Omega_+, \Omega_-$  are obtained in the limit (see Fig. 3.12). The transition probability for a periodic perturbation potential (3.109) therefore is

$$\begin{aligned} p_{n,m}(t) &= \frac{1}{\hbar^2} \left[ \left| \langle m | \underline{\mathbf{H}}' | n \rangle \right|^2 \frac{\sin^2(\Omega_+ t/2)}{(\Omega_+/2)^2} + \left| \langle m | \underline{\mathbf{H}}'^{\dagger} | n \rangle \right|^2 \frac{\sin^2(\Omega_- t/2)}{(\Omega_-/2)^2} \right] \\ &= \frac{t}{\hbar^2} \left[ \left| \langle m | \underline{\mathbf{H}}' | n \rangle \right|^2 \Sigma_t(\Omega_+/2) + \left| \langle m | \underline{\mathbf{H}}'^{\dagger} | n \rangle \right|^2 \Sigma_t(\Omega_-/2) \right] \\ &\simeq \frac{\pi t}{\hbar^2} \left[ \left| \langle m | \underline{\mathbf{H}}' | n \rangle \right|^2 \delta(\Omega_+/2) + \left| \langle m | \underline{\mathbf{H}}'^{\dagger} | n \rangle \right|^2 \delta(\Omega_-/2) \right]. \end{aligned} \quad (3.112)$$

Finally, the transition rate for a periodic perturbation potential follows to be <sup>4</sup>

$$\begin{aligned} S_{n,m} &= \frac{2\pi}{\hbar} \left[ \left| \langle m | \underline{\mathbf{H}}' | n \rangle \right|^2 \delta(E_m - E_n - \hbar\omega) \right. \\ &\quad \left. + \left| \langle m | \underline{\mathbf{H}}'^{\dagger} | n \rangle \right|^2 \delta(E_m - E_n + \hbar\omega) \right]. \end{aligned} \quad (3.113)$$

Here, two types of transitions occur. The first Dirac distribution requires  $E_m = E_n + \hbar\omega$ . This means an absorption of an energy quantum  $\hbar\omega$ . The second Dirac distribution requires  $E_m = E_n - \hbar\omega$ , which refers to an emission of an energy quantum  $\hbar\omega$  originating from e.g. a photon or a phonon.

### 3.3.4 The Transition Rate for Scattering Events

The transition rates in (3.107) and (3.113) are now specialized for carriers in a periodic crystal potential  $U_{\text{crystal}}(\mathbf{r})$ . The influence of a crystal potential is discussed in Section 3.2.2. Therefore the initial state  $|n\rangle$  and the final state  $|m\rangle$  are specialized to  $|\nu, \mathbf{k}\rangle$  and  $|\nu', \mathbf{k}'\rangle$ , where  $\nu$  is the band index and  $\mathbf{k}$  the wave vector of the carrier. The perturbing potential  $\underline{\mathbf{H}}'$  is now identified as the *scattering potential*. The matrix element for carriers in a periodic crystal potential with scattering potential  $H'(\mathbf{r})$  is given as

$$\langle \nu', \mathbf{k}' | \underline{\mathbf{H}}' | \nu, \mathbf{k} \rangle = \int_{\mathbb{R}^3} [\Psi_{\mathbf{k}'}^{\nu'}(\mathbf{r})]^* H'(\mathbf{r}) \Psi_{\mathbf{k}}^{\nu}(\mathbf{r}) d\mathbf{r} \quad (3.114)$$

with *Bloch waves* according to (3.50), which are given by

$$\Psi_{\mathbf{k}}^{\nu}(\mathbf{r}) = u_{\mathbf{k}}^{\nu}(\mathbf{r}) e^{i\mathbf{k}\cdot\mathbf{r}}, \quad (3.115)$$

where  $u_{\mathbf{k}}^{\nu}(\mathbf{r})$  is a cell-periodic function. For the following consideration, the matrix element is normalized to a sample volume  $\mathcal{V}$ , which gives

$$\langle \nu', \mathbf{k}' | \underline{\mathbf{H}}' | \nu, \mathbf{k} \rangle = \frac{1}{V_s} \int_{\mathcal{V}} [u_{\mathbf{k}'}^{\nu'}(\mathbf{r})]^* H'(\mathbf{r}) u_{\mathbf{k}}^{\nu}(\mathbf{r}) e^{i(\mathbf{k}-\mathbf{k}')\cdot\mathbf{r}} d\mathbf{r}. \quad (3.116)$$

In the following, it is shown how this integral can be written as two separate integrals [11, 20, 30]. The scattering potential is expanded in a Fourier series. This is possible with the assumption of periodic boundary conditions (PBC), which is reasonable considering that the crystal consists out of  $N$  unit cells. The same result is obtained by a Fourier transformation. The Fourier series for the scattering potential reads

$$H'(\mathbf{r}, t) = \sum_{\beta} U_{\beta} e^{i\beta\cdot\mathbf{r}}. \quad (3.117)$$

<sup>4</sup> $\delta(\Omega_+/2) = 2\delta(\Omega_+) = 2\delta(\omega_m - \omega_n - \omega) = 2\hbar\delta(E_m - E_n - \hbar\omega)$ , analogous for  $\delta(\Omega_-)$ .

This is plugged into (3.116) to get

$$\langle \nu', \mathbf{k}' | \underline{\mathbf{H}}' | \nu, \mathbf{k} \rangle = \sum_{\beta} U_{\beta} \frac{1}{V_s} \int_{\mathcal{V}} \left[ u_{\mathbf{k}'}^{\nu'}(\mathbf{r}) \right]^* u_{\mathbf{k}}^{\nu}(\mathbf{r}) e^{i(\mathbf{k}-\mathbf{k}'+\beta)\cdot\mathbf{r}} d\mathbf{r}. \quad (3.118)$$

The crucial step is to transform the spatial coordinate with  $\mathbf{r} \mapsto \mathbf{r}' + \mathbf{T}$ , where  $\mathbf{r}'$  is the coordinate vector within a unit cell and  $\mathbf{T}$  is the translation vector defined by (3.23). Therefore, instead of one integral over the whole sample volume  $\mathcal{V}$ ,  $N$  integrals over each unit cell are performed:

$$\langle \nu', \mathbf{k}' | \underline{\mathbf{H}}' | \nu, \mathbf{k} \rangle = \sum_{\beta} U_{\beta} \underbrace{\sum_{u,v,w} e^{i(\mathbf{k}-\mathbf{k}'+\beta)\cdot\mathbf{T}}}_{\neq 0, \text{ for } \mathbf{k}-\mathbf{k}'+\beta=\mathbf{G}} \frac{1}{NV_{\text{cell}}} \int_{\text{cell}} \left[ u_{\mathbf{k}'}^{\nu'}(\mathbf{r}') \right]^* u_{\mathbf{k}}^{\nu}(\mathbf{r}') e^{i(\mathbf{k}-\mathbf{k}'+\beta)\cdot\mathbf{r}'} d\mathbf{r}'$$

Constructive interference of the complex exponentials is only achieved for  $\mathbf{k} - \mathbf{k}' + \beta = \mathbf{G}$ , where  $\mathbf{G}$  is the translation vector of the reciprocal lattice according to (3.28). For a fixed  $\mathbf{G}$ , the summation evaluates to

$$\sum_{u,v,w} e^{i\mathbf{G}\cdot\mathbf{T}_u} = \sum_{u,v,w} e^{i2\pi n} \Big|_{n \in \mathbb{Z}} = N. \quad (3.119)$$

Now, the matrix element can be simplified to

$$\begin{aligned} \langle \nu', \mathbf{k}' | \underline{\mathbf{H}}' | \nu, \mathbf{k} \rangle &= \sum_{\beta} U_{\beta} \left[ \frac{1}{V_{\text{cell}}} \int_{\text{cell}} \left[ u_{\mathbf{k}'}^{\nu'}(\mathbf{r}') \right]^* u_{\mathbf{k}}^{\nu}(\mathbf{r}') e^{i(\mathbf{k}-\mathbf{k}'+\beta)\cdot\mathbf{r}'} d\mathbf{r}' \right] \\ &\times \delta(\mathbf{k} - \mathbf{k}' + \beta - \mathbf{G}). \end{aligned} \quad (3.120)$$

Defining the overlap integral as

$$I(\nu, \mathbf{k}; \nu', \mathbf{k}') := \frac{1}{V_{\text{cell}}} \int_{\text{cell}} \left[ u_{\mathbf{k}'}^{\nu'}(\mathbf{r}) \right]^* u_{\mathbf{k}}^{\nu}(\mathbf{r}) e^{i\mathbf{G}\cdot\mathbf{r}} d\mathbf{r}, \quad (3.121)$$

and explicitly writing the expansion coefficient of the Fourier series as

$$U_{\beta} = \frac{1}{V_s} \int_{\mathcal{V}} H'(\mathbf{r}) e^{-i\beta\cdot\mathbf{r}} d\mathbf{r} \quad (3.122)$$

finally yields <sup>5</sup>

$$\begin{aligned} \langle \nu', \mathbf{k}' | \underline{\mathbf{H}}' | \nu, \mathbf{k} \rangle &= \sum_{\mathbf{G}} \left[ \frac{1}{V_s} \int_{\mathcal{V}} e^{-i\mathbf{k}'\cdot\mathbf{r}} H'(\mathbf{r}) e^{i\mathbf{k}\cdot\mathbf{r}} e^{-i\mathbf{G}\cdot\mathbf{r}} d\mathbf{r} \right] I(\nu, \mathbf{k}; \nu', \mathbf{k}') \\ &\times \delta(\mathbf{k} - \mathbf{k}' + \beta - \mathbf{G}). \end{aligned} \quad (3.123)$$

Here, scattering within a unit cell of the reciprocal lattice ( $\mathbf{G} = 0$ ) and between unit cells ( $\mathbf{G} \neq 0$ ) is distinguished. The first kind are a so-called N-processes and the second are so-called U-processes, where N stands for normal and U for the German word Umklapp. The word Umklapp refers to the fact that according to (3.52), a wave vector  $\mathbf{k}' = \mathbf{k} + \mathbf{G}$  is "umgeklappt" to  $\mathbf{k}$ . The following considerations are refined to N-processes, for which a scattering integral is defined by

$$I_s(\mathbf{k}, \mathbf{k}') := I_s(\mathbf{k}' - \mathbf{k}) := \frac{1}{V_s} \int_{\mathcal{V}} H'(\mathbf{r}) e^{-i(\mathbf{k}'-\mathbf{k})\cdot\mathbf{r}} d\mathbf{r}, \quad (3.124)$$

<sup>5</sup>The sum over  $\beta$  can be written as the sum over  $\mathbf{G} + \mathbf{k}' - \mathbf{k}$ , which is simply the sum over  $\mathbf{G}$ .

which is the Fourier transform of the scattering potential  $H'(\mathbf{r})$ . For scattering within a parabolic band ( $\nu = \nu'$ ), it is assumed that the overlap integral  $I(\mathbf{k}, \mathbf{k}') \simeq 1$  [20]. This assumption is made for all considerations to follow. For details on the overlap integral, it is referred to the literature [11, 30]. To summarize, the matrix element is written as the product of the overlap integral and the scattering integral as:

$$\langle \mathbf{k}' | \underline{\mathbf{H}}' | \mathbf{k} \rangle = I(\mathbf{k}, \mathbf{k}') I_s(\mathbf{k}, \mathbf{k}') \delta(\mathbf{k}' - \mathbf{k} - \boldsymbol{\beta}) \quad (3.125)$$

This form is approachable for analytical calculations of the transition rate. The matrix element for  $\underline{\mathbf{H}}'^{\dagger}$  is obtained as

$$\langle \mathbf{k}' | \underline{\mathbf{H}}'^{\dagger} | \mathbf{k} \rangle = I(\mathbf{k}, \mathbf{k}') I_s(\mathbf{k}, \mathbf{k}') \delta(\mathbf{k}' - \mathbf{k} + \boldsymbol{\beta}). \quad (3.126)$$

The dirac-distribution is an expression of momentum conservation. Finally, the transition rate derived from (3.113) is obtained as

$$S(\mathbf{r}, \mathbf{k}, \mathbf{k}') = \frac{2\pi}{\hbar} [I(\mathbf{k}, \mathbf{k}') I_s(\mathbf{k}, \mathbf{k}')]^2 \delta(\mathbf{k}' - \mathbf{k} \mp \boldsymbol{\beta}) \times \delta(E(\mathbf{k}') - E(\mathbf{k}) \mp \hbar\omega). \quad (3.127)$$

This is the general case for inelastic scattering. The energy quantum  $\hbar\omega$  describes the exchanged energy, e.g. the energy of the absorbed or emitted phonon or photon. In general, the angular frequency  $\omega$  is a function of the wave vector  $\boldsymbol{\beta}$ , e.g. a phonon. To be compatible with the statements in Section 2.3.2, the transition rate for a scattering process denoted by  $\eta$  can be written in the form

$$S_{\eta}(\mathbf{r}, \mathbf{k}, \mathbf{k}') = \frac{1}{V_s} c_{\eta, \pm}(\mathbf{r}, \mathbf{k}, \mathbf{k}') \delta(E(\mathbf{k}') - E(\mathbf{k}) \mp \hbar\omega_{\eta}), \quad (3.128)$$

where the scattering coefficient for absorption is  $c_{\eta, +}(\mathbf{r}, \mathbf{k}, \mathbf{k}')$  and for emission  $c_{\eta, -}(\mathbf{r}, \mathbf{k}, \mathbf{k}')$ . For elastic scattering,  $\omega_{\eta}$  vanishes and the scattering coefficients for absorption and emission are equal, so  $c_{\eta, +}(\mathbf{r}, \mathbf{k}, \mathbf{k}') = c_{\eta, -}(\mathbf{r}, \mathbf{k}, \mathbf{k}') = c_{\eta}(\mathbf{r}, \mathbf{k}, \mathbf{k}')$ . The expression  $\omega_{\eta}$  accounts for the different treatment of the angular frequency depending on the scattering process. In general it is a function of the wave vector  $\boldsymbol{\beta}$ , but in some cases it is approximated to be constant. The total transition rate is according to [15] calculated by

$$S(\mathbf{r}, \mathbf{k}, \mathbf{k}') = \sum_{\eta} S_{\eta}(\mathbf{r}, \mathbf{k}, \mathbf{k}') = \frac{1}{V_s} \sum_{\eta} c_{\eta, \pm}(\mathbf{r}, \mathbf{k}, \mathbf{k}') \delta(E(\mathbf{k}') - E(\mathbf{k}) \mp \hbar\omega_{\eta}) \quad (3.129)$$

This expression can be easily generalized for scattering between different energy bands.

### 3.4 Modeling of Scattering

As a preparation for the discussion of selected scattering mechanism in Chapter 4, the general approach of modeling scattering within the framework of the semi-classical BTE is summarized in this section. Furthermore, a simple example is given.

### 3.4.1 Scattering Rate

The low-density approximation (1.85) of the scattering operator includes the scattering rate according to (1.84). It is convenient to transform the integral in (1.84) to spherical coordinates, which reads

$$\begin{aligned} W(\mathbf{k}) &= N_d \int_{\mathcal{B}} S(\mathbf{k}, \mathbf{k}') d\mathbf{k}' \\ &= V_s \int_{\mathbb{R}_0^+} \int_{\Omega'} S(\mathbf{k}(E, \theta, \varphi), \mathbf{k}'(E', \theta', \varphi')) Z(E', \theta', \varphi') d\Omega' dE'. \end{aligned} \quad (3.130)$$

Because of the  $\delta$ -distribution for the energy conservation in (3.127), this form can be evaluated very easily.

### 3.4.2 General Approach

The procedure for describing a scattering process is summarized in the following. It is sufficient to derive the scattering potential  $H'(\mathbf{r})$ , afterwards the approach is straight-forward.

**Identification of the scattering potential  $H'(\mathbf{r})$ .** Here it has to be distinguished between non-recurring potentials described in Section 3.3.2 and periodic ones described in Section 3.3.3:

- **Non-Recurring** (elastic scattering process)  
The energy of the final state is equal to the energy of the initial state.
- **Periodic** (inelastic scattering process)  
E.g. phonon scattering, where a phonon is absorbed or emitted.

**Evaluation of the scattering integral  $I_s(\mathbf{k}, \mathbf{k}')$ .** The scattering integral is defined in (3.124). It is the Fourier transformed scattering potential. For simplicity, the overlap integral  $I(\mathbf{k}, \mathbf{k}')$  is assumed to be of order 1.

**Evaluation of the transition rate  $S(\mathbf{k}, \mathbf{k}')$ .** Again, it has to be distinguished between non-recurring and periodic potentials. In the case of **non-recurring** potentials, the momentum conservation is ensured by the scattering source, therefore the transition rate reads

$$S(\mathbf{k}, \mathbf{k}') = \frac{2\pi}{\hbar} [I_s(\mathbf{k}, \mathbf{k}')]^2 \delta(E(\mathbf{k}') - E(\mathbf{k})) \quad (3.131)$$

In the case of **periodic** potentials, a phonon with energy  $\hbar\omega_\eta$  and momentum  $\hbar\mathbf{q}$  is absorbed or emitted, and the transition rate is obtained by

$$S(\mathbf{k}, \mathbf{k}') = \frac{2\pi}{\hbar} [I_s(\mathbf{k}, \mathbf{k}')]^2 \delta(\mathbf{k}' - \mathbf{k} \mp \mathbf{q}) \times \delta(E(\mathbf{k}') - E(\mathbf{k}) \mp \hbar\omega_\eta) \quad (3.132)$$

**Evaluation of the scattering rate  $W(E)$  according to (3.130):**

$$W(E) = V_s \int_{\mathbb{R}_0^+} \int_{\Omega'} S(\mathbf{k}(E, \theta, \varphi), \mathbf{k}'(E', \theta', \varphi')) Z(E', \theta', \varphi') d\Omega' dE' \quad (3.133)$$

This general approach is widely used in Chapter 4.

### 3.4.3 Example

Consider a simple non-recurring potential switched on at  $t = 0$  given by

$$H'(\mathbf{r}) = A\delta(\mathbf{r}), \quad (3.134)$$

with a-priori free parameter  $A$ . The scattering integral according to (3.124) can immediately be written as

$$I_s(\mathbf{k}, \mathbf{k}') = \frac{1}{V_s} \int_{\mathcal{V}} H'(\mathbf{r}) e^{-i(\mathbf{k}' - \mathbf{k}) \cdot \mathbf{r}} d\mathbf{r} = \frac{A}{V_s}. \quad (3.135)$$

The transition rate given by (3.131) follows as

$$\begin{aligned} S(\mathbf{k}, \mathbf{k}') &= \frac{2\pi}{\hbar} \frac{A^2}{V_s^2} \delta(E(\mathbf{k}') - E(\mathbf{k})) \\ &= \frac{C}{V_s} \delta(E(\mathbf{k}') - E(\mathbf{k})), \end{aligned} \quad (3.136)$$

where  $C$  is a constant. Note that this is of the form (3.128). (3.136) is an approximation for strongly screened impurity scattering, which is discussed in Section 4.1. The scattering rate is

$$\begin{aligned} W(\mathbf{k}) &= V_s \int_{\mathbb{R}_0^+} \int_{\Omega'} S(\mathbf{k}(E, \theta, \varphi), \mathbf{k}'(E', \theta', \varphi')) Z(E', \theta', \varphi') d\Omega' dE' \\ &= C \int_{\mathbb{R}_0^+} \int_{\Omega'} \delta(E' - E) Z(E', \theta', \varphi') d\Omega' dE' \\ &= C \int_{\Omega'} Z(E, \theta', \varphi') d\Omega'. \end{aligned} \quad (3.137)$$

For the case that the *generalized density of states*  $Z$  depends only on the energy  $E$ , it is found that

$$W(E) \propto Z(E). \quad (3.138)$$

Thus the scattering rate is proportional to the final density of states.

## 3.5 Lattice Vibrations - Phonons

In Section 3.2.1 and Section 3.2.2 the problem of calculating the behavior of electrons in a perfect crystalline structure with a periodic crystal potential is covered. The solution of the SE for such a periodic potential are the so-called Bloch states, which are eigenstates of a perfect crystal potential. In this model it is assumed that the atoms are placed on a rigid lattice, the so-called Bravais lattice, but atoms in real crystals vibrate around their lattice positions. These vibrations are an important scattering mechanism. In the following, a simple model for such lattice vibrations is developed.

### 3.5.1 Dispersion Relation

Atoms are arranged in crystalline structures due to the minimization of the total energy of the system. In a crystal, atoms tend to their equilibrium positions in the presence of repulsive and attractive potentials. The overall potential profile, the so-called binding potential or binding energy  $U(r)$ , where  $r$  is the inter-atomic distance, is schematically drawn in Fig. 3.13. At  $T = 0\text{K}$ , the nuclei rest at their



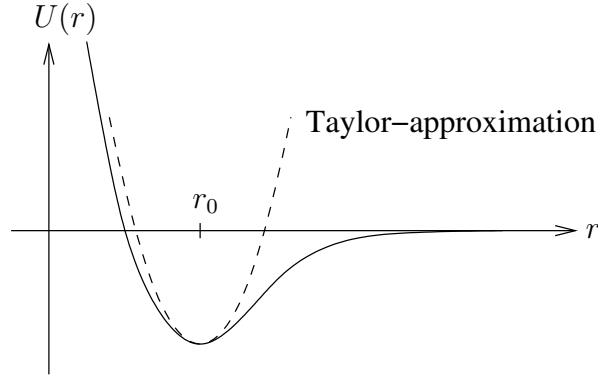


**Figure 3.13:** Simple schematic drawing of the binding energy  $U(r)$  versus the inter-atomic distance  $r$  between two atoms of a crystal.

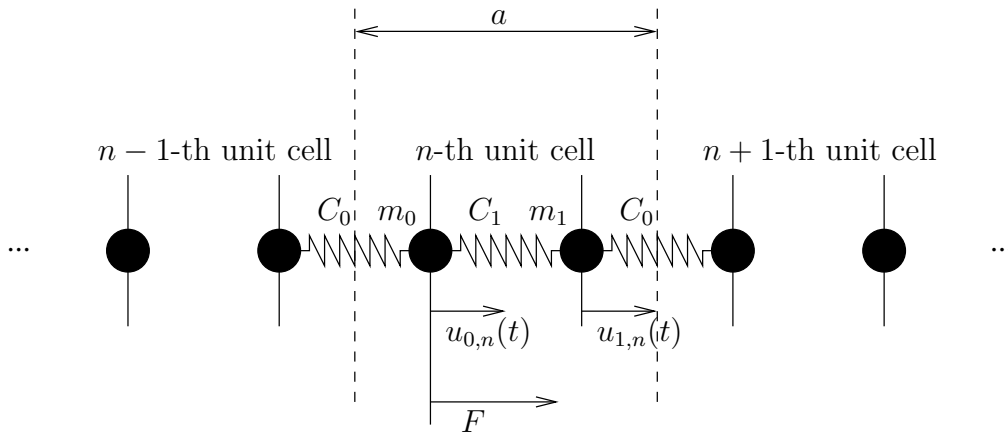


**Figure 3.14:** Cut-out of a simple one dimensional model crystal with two different sorts of atoms per unit cell.

equilibrium positions, which are given by the lattice points. For  $T > 0$  K, the nuclei vibrate around these points. A Taylor-series expansion of the binding energy at the equilibrium position  $r = r_0$  yields

$$U(r) = U(r_0) + \underbrace{\frac{dU(r)}{dr} \Big|_{r_0}}_{=0} (r - r_0) + \frac{1}{2} \underbrace{\frac{d^2U(r)}{dr^2} \Big|_{r_0}}_{=:C} (r - r_0)^2 + \dots \quad (3.139)$$

The linear term is zero, because the binding energy  $U(r)$  has a local minimum at  $r = r_0$ . The expansion is truncated after the second term. The second spatial derivative of the binding energy is identified as a force constant:

$$C := \frac{d^2U(r)}{dr^2} \Big|_{r_0}. \quad (3.140)$$

The restoring force is thus given by

$$F = -C(r - r_0). \quad (3.141)$$

The vibrations of the crystal are described by a simple mass-spring approximation for a two atoms basis, considering only the interaction between nearest neighbors. Cubic semiconductors in the diamond and zinc-blende structure such as Si, Ge, or GaAs have a two atoms basis. A potential of the

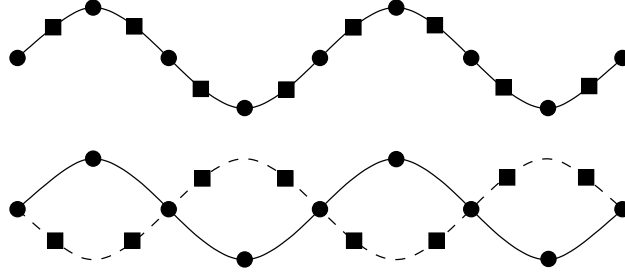


**Figure 3.15:** Illustration of acoustic and optical modes of the same wavelength. The upper curve shows an acoustic mode, where the displacement of the two atoms of the basis are in the same direction. The lower curve shows an optical mode, where the displacement is in opposite direction.

form (3.139) is called harmonic oscillator potential. Momentum conservation using the notation from Fig. 3.14 for the atom with index 0 of the  $n$ -th unit cell reads

$$m_0 \frac{d^2 u_{0,n}(t)}{dt^2} = F_{1,n-1;0,n} + F_{0,n;1,n}, \quad (3.142)$$

where  $m_0$  is the mass of the vibrating atom with index 0 in the unit cell and  $u_{0,n}(t)$  is displacement relative to the lattice position. The force between the atom with index 1 of the  $(n-1)$ -th unit cell and the atom with index 0 of the  $n$ -th unit cell according to (3.141) is given by

$$F_{1,n-1;0,n} = -C_0(u_{0,n} - u_{1,n-1}). \quad (3.143)$$

In the same way, the force between the atom with index 0 and the atom with index 1 of the  $n$ -th unit cell is obtained as

$$F_{0,n;1,n} = -C_1(u_{0,n} - u_{1,n}). \quad (3.144)$$

Collecting the results, (3.142) is written as

$$m_0 \frac{d^2 u_{0,n}(t)}{dt^2} = C_0(u_{1,n-1} - u_{0,n}) + C_1(u_{1,n} - u_{0,n}). \quad (3.145)$$

The displacement of the atom with index 1 of the  $n$ -th unit cell  $u_{1,n}(t)$  is obtained in a similar way:

$$m_1 \frac{d^2 u_{1,n}(t)}{dt^2} = C_1(u_{0,n} - u_{1,n}) + C_0(u_{0,n+1} - u_{1,n}) \quad (3.146)$$

(3.145) and (3.146) are solved by the ansatz:

$$u_{0,n} = u_0 \exp(iqna) \exp(-i\omega t), \quad (3.147)$$

$$u_{1,n} = u_1 \exp(iqna) \exp(-i\omega t). \quad (3.148)$$

This leads to the algebraic linear system of equations given by

$$-m_0 \omega^2 u_0 = C_0(u_1 e^{-iqa} - u_0) + C_1(u_1 - u_0), \quad (3.149)$$

$$-m_1 \omega^2 u_1 = C_1(u_0 - u_1) + C_0(u_0 e^{iqa} - u_1). \quad (3.150)$$

which is written as matrix equation in the following way:

$$\begin{bmatrix} m_0 \omega^2 - C_0 - C_1 & C_0 e^{-iqa} + C_1 \\ C_0 e^{iqa} + C_1 & m_1 \omega^2 - C_0 - C_1 \end{bmatrix} \begin{bmatrix} u_0 \\ u_1 \end{bmatrix} = \begin{bmatrix} 0 \\ 0 \end{bmatrix} \quad (3.151)$$

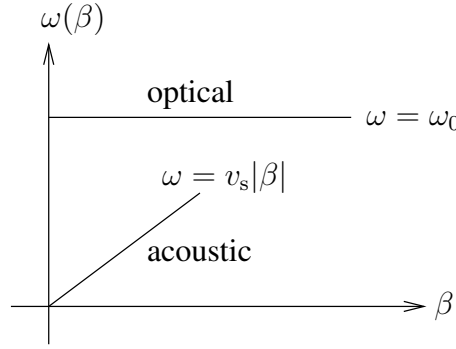


**Figure 3.16:** Simple approximation for the dispersion relation of phonons.

This equation can easily be solved by hand. In general, this equation system describes the propagation of waves along symmetry directions, where the wavefronts (surfaces of constant phase) include only one of the two basis atoms. Modes where the displacement of the two basis atoms is in the same direction are called **acoustic**, those where the displacement is in opposite direction are called **optical**, see Fig. 3.15. For a two atoms basis, there are six branches of the dispersion relation, including one longitudinal acoustic (LA) mode, two transversal acoustic (TA) modes, one longitudinal optical (LO) mode, and two transversal optical (TO) modes. This is equal to the degree of freedom for each of the two atoms. Fig. 3.16 shows a simple approximation of the result, which is used in the following to model the effects of scattering in Chapter 4, with one acoustic and one optical branch. In this approximation, the dispersion relation for acoustic phonons is written as

$$\omega(\beta) \simeq v_s|\beta|, \quad (3.152)$$

where  $v_s$  is the sound velocity and  $\beta$  the magnitude of the phonon wave vector. For optical phonons it is assumed that

$$\omega \simeq \omega_0, \quad (3.153)$$

with a constant angular frequency  $\omega_0$  [16, 20, 28].

### 3.5.2 Phonons - Quanta Of Lattice Vibrations

The energy of lattice vibrations is quantized. The energy quantum is called **phonon**, in analogy to the energy quanta of electromagnetic waves, which are called photons. In Section 3.5.1, lattice vibrations are described as elastic waves by a undamped mass-spring approximation. In classical mechanics the ideal mass-spring system is called **harmonic oscillator**. Its Hamiltonian, i.e. the total energy of the system, is given by

$$H = \frac{p^2}{2m} + \frac{m\omega^2}{2}x^2, \quad (3.154)$$

where  $p$  is the momentum,  $m$  the mass,  $\omega$  the angular frequency and  $x$  the displacement from equilibrium. In quantum mechanics (QM) it is advantageous to write the Hamiltonian operator in terms of a creation operator  $\underline{\mathbf{a}}^\dagger$  and an annihilation operator  $\underline{\mathbf{a}}$ , as

$$\underline{\mathbf{H}} = \hbar\omega \left( \underline{\mathbf{a}}^\dagger \underline{\mathbf{a}} + \frac{1}{2} \right). \quad (3.155)$$

The denotation of the two operators is clarified in the following. The *occupation number operator*  $\underline{\mathbf{N}}$  is defined as

$$\underline{\mathbf{N}} := \underline{\mathbf{a}}^\dagger \underline{\mathbf{a}}. \quad (3.156)$$

The eigenvalues  $n$  of the occupation number operator are described by

$$\underline{\mathbf{N}}|n\rangle = n|n\rangle. \quad (3.157)$$

The eigenvalue  $n$  is called **occupation number**, it gives the number of phonons in the oscillating mode. The creation operator  $\underline{\mathbf{a}}^\dagger$  increases the occupation number  $n$  by 1. It “creates” a phonon:

$$\underline{\mathbf{a}}^\dagger|n\rangle = \sqrt{n+1}|n+1\rangle. \quad (3.158)$$

In analogy to the creation operator  $\underline{\mathbf{a}}^\dagger$ , the annihilation operator  $\underline{\mathbf{a}}$  decreases the occupation number  $n$  by 1, which is described by

$$\underline{\mathbf{a}}|n\rangle = \sqrt{n}|n-1\rangle. \quad (3.159)$$

Thus it can be said, that the annihilation operator “annihilates” a phonon. The eigenvalues of the Hamiltonian operator  $\underline{\mathbf{H}}$  are directly obtained from (3.157) as

$$E_n = \hbar\omega\left(n + \frac{1}{2}\right). \quad (3.160)$$

It can be seen, that the energy of a phonon is  $\hbar\omega$ . The so-called *zero point energy*, given by  $E_0 = (\hbar\omega)/2$ , is a consequence of *Heisenberg’s uncertainty relation*. More details can be found in [16, 27].

### 3.5.3 The Quantum Mechanical Phonon System

The Hamiltonian operator for the phonon system is written as the superposition of single quantum mechanical harmonic oscillators, given by

$$\underline{\mathbf{H}} = \sum_{\beta} \hbar\omega_{\beta} \left( \underline{\mathbf{a}}_{\beta}^{\dagger} \underline{\mathbf{a}}_{\beta} + \frac{1}{2} \right), \quad (3.161)$$

with the occupation number operator  $\underline{\mathbf{N}}_{\beta} = \underline{\mathbf{a}}_{\beta}^{\dagger} \underline{\mathbf{a}}_{\beta}$ . This is motivated by the binding potential  $U(r)$  according to (3.139), which is approximately the potential of a harmonic oscillator. The eigenvalue equation from (3.157) is now generalized to

$$\underline{\mathbf{N}}_{\beta}|n_{\beta}\rangle = n_{\beta}|n_{\beta}\rangle. \quad (3.162)$$

For the treatment of phonon scattering, the following matrix elements are relevant:

$$\langle n_{\beta} - 1 | \underline{\mathbf{a}}_{\beta} | n_{\beta} \rangle = \sqrt{n_{\beta}} \quad (3.163)$$

$$\langle n_{\beta} + 1 | \underline{\mathbf{a}}_{\beta}^{\dagger} | n_{\beta} \rangle = \sqrt{n_{\beta} + 1} \quad (3.164)$$

They are used in Section 4.2 to evaluate the transition rates for phonon scattering. Kittel [12, 30] proposed to write the displacement of an ion at lattice site  $\mathbf{T}$  in terms of the creation operator  $\underline{\mathbf{a}}^\dagger$  and annihilation operator  $\underline{\mathbf{a}}$  as

$$\mathbf{u}(\mathbf{T}, t) = \sum_{\beta} \left( \frac{\hbar}{2\rho_m V_s \omega_{\beta}} \right)^{1/2} \left[ \underline{\mathbf{a}}_{\beta} \exp(i\beta \cdot \mathbf{T}) + \underline{\mathbf{a}}_{\beta}^{\dagger} \exp(-i\beta \cdot \mathbf{T}) \right] \mathbf{e}_{\beta}, \quad (3.165)$$

where  $\mathbf{T}$  is the translation vector according to (3.23),  $\rho_m$  is the mass density of the crystal and  $\mathbf{e}_{\beta}$  is the polarization vector. This is similar to the displacement operator of a single quantum mechanical oscillator given by

$$\underline{\mathbf{X}} = \left[ \frac{\hbar}{2m\omega} \right]^{1/2} (\underline{\mathbf{a}}^{\dagger} + \underline{\mathbf{a}}), \quad (3.166)$$

where  $m$  is the mass of the oscillator and  $\omega$  its angular frequency [12, 16, 27, 30].

### 3.5.4 Phonon Statistics

In contrast to electrons, which are **Fermions** obeying the Pauli exclusion principle, phonons are **Bosons**. The number of phonons in thermal equilibrium in mode  $\beta$  is given by Bose-Einstein-statistics as

$$\langle n_{\beta} \rangle = \frac{1}{\exp\left(\frac{\hbar\omega_{\beta}}{k_{\text{B}}T}\right) - 1}. \quad (3.167)$$

With the assumption of  $\hbar\omega_{\beta} \ll k_{\text{B}}T$ , the exponential can be expanded into a Taylor series around  $x_0 = 0$ <sup>6</sup>, therefore the Bose-Einstein-statistic is simplified to

$$\langle n_{\beta} \rangle \simeq \frac{k_{\text{B}}T}{\hbar\omega_{\beta}}. \quad (3.168)$$

Except for low temperatures, this approximation holds for acoustic phonons and is known as *equipartition*. It can be interpreted very easily. The thermal energy is  $k_{\text{B}}T$  and the energy of a phonon is  $\hbar\omega_{\beta}$  and therefore (3.168) is the number of phonons needed to account for the thermal energy [12, 20, 30].

---

<sup>6</sup> $\exp(x) = \sum_{k=0}^{\infty} \frac{x^k}{k!}$

# Chapter 4

## Scattering

The methods developed in the previous chapter are applied in this chapter to examine a number of selected scattering mechanisms, including ionized impurity scattering, phonon scattering, and electron-electron scattering. The procedure is according to the general approach described in Section 3.4.2, with a focus on the specific properties of each scattering process.

### 4.1 Ionized Impurity Scattering

In this section, the Herring-Brooks model for ionized impurity scattering is presented. First, the potential of a point charge surrounded by mobile carriers is derived. Afterwards, the transition rate and the scattering coefficient are examined.

#### 4.1.1 Potential Of a Screened Point Charge

The potential of a fixed point charge surrounded by free carriers is investigated. This is a simple model of a charged impurity in a semiconductor. A point charge attracts free carriers, which in turn change the potential. Such a potential is called a *screened potential*. This problem cannot be solved analytically, therefore the aim is to find an approximate solution. The following assumptions are imposed:

- The problem is solved for a bulk material, with the doping density  $N_D^+$ .
- The electron concentration without the perturbing point charge is equal to the doping density:  $n = n_0 = N_D^+$ . This is a good approximation in the so-called saturation range, where all dopants are ionized [28] and expresses space charge neutrality of the bulk material. The electrostatic potential  $\Phi(\mathbf{r})$  in this case is governed by the Laplace Equation (LE). The boundary conditions (BC) for the electrostatic potential  $\Phi$  are chosen to be constant, therefore the potential is also constant. In the following it is set to zero.
- In the vicinity of the perturbing point charge, the electron density differs from the unperturbed density by  $\Delta n(\mathbf{r})$ . Thus, the electron density is given by  $n(\mathbf{r}) = n_0 + \Delta n(\mathbf{r})$ .
- The space charge density  $\rho(\mathbf{r})$  for the perturbed case is given by  $\rho(\mathbf{r}) = q\delta(\mathbf{r}) - q\Delta n(\mathbf{r})$ .

The electrostatic potential  $\Phi(\mathbf{r})$  is described by the Poisson Equation (PE):

$$\nabla^2 \Phi(\mathbf{r}) = -\frac{\rho(\mathbf{r})}{\epsilon}. \quad (4.1)$$

To solve this equation, the electrostatic potential  $\Phi(\mathbf{r})$  and the electron density  $n(\mathbf{r})$  are connected via the *Boltzmann statistics* given by

$$n(\mathbf{r}) = N_c \exp\left(-\frac{E_c(\mathbf{r}) - E_F}{k_B T}\right) = N_c \exp\left(-\frac{E_{c0} - q\Phi(\mathbf{r}) - E_F}{k_B T}\right), \quad (4.2)$$

where  $N_c$  is the *effective density of states*,  $E_F$  is the Fermi-level and  $E_{c0}$  is the constant conduction band edge. Note that this is an approximation for non-degenerated semiconductors in thermal equilibrium.

The electron density  $n$  is expanded into a Taylor series at  $\Phi = 0$  and the series is truncated after the linear term:

$$\begin{aligned} n &\simeq n_0 + \left. \frac{\partial n}{\partial \Phi} \right|_{\Phi=0} \Phi \\ &= n_0 + \frac{qn_0}{k_B T} \Phi. \end{aligned} \quad (4.3)$$

It follows immediately, that

$$\Delta n \simeq \frac{qn_0}{k_B T} \Phi. \quad (4.4)$$

By collecting the results and assumptions above, the problem is formulated as

$$\nabla^2 \Phi(\mathbf{r}) = -\frac{q}{\epsilon} \left( \delta(\mathbf{r}) - \frac{qn_0}{k_B T} \Phi \right). \quad (4.5)$$

The solution of this equation can be found in the Fourier domain. The Fourier transformed of the potential is written as

$$\tilde{\Phi}(\boldsymbol{\beta}) = \mathcal{F}\{\Phi(\mathbf{r})\}. \quad (4.6)$$

Fourier transformation of (4.5) yields

$$\begin{aligned} \nabla^2 \Phi(\mathbf{r}) - \underbrace{\frac{q^2 n_0}{\epsilon k_B T}}_{=: 1/\lambda_D^2} \Phi(\mathbf{r}) &= -\frac{q}{\epsilon} \delta(\mathbf{r}) \quad \Big| \quad \mathcal{F}\{\cdot\} \\ \Leftrightarrow (i\boldsymbol{\beta})^2 \tilde{\Phi} - \frac{1}{\lambda_D^2} \tilde{\Phi} &= -\frac{q}{\epsilon} \\ \Leftrightarrow -\boldsymbol{\beta}^2 \tilde{\Phi} - \frac{1}{\lambda_D^2} \tilde{\Phi} &= -\frac{q}{\epsilon}, \end{aligned} \quad (4.7)$$

where the *Debye length*  $\lambda_D$  is defined as

$$\lambda_D^2 := \frac{\epsilon k_B T}{q^2 n_0}. \quad (4.8)$$

Finally, the Fourier transformed electro-static potential reads

$$\tilde{\Phi}(\boldsymbol{\beta}) = \frac{q}{\epsilon (\boldsymbol{\beta}^2 + 1/\lambda_D^2)}. \quad (4.9)$$

The potential in real-space is found, e.g. by back-transforming  $\tilde{\Phi}(\boldsymbol{\beta})$  or solving (4.5) in spherical coordinates, as [20, 28, 30]

$$\Phi(\mathbf{r}) = \Phi(r) = \frac{q}{4\pi\epsilon r} e^{-r/\lambda_D}, \quad (4.10)$$

which is the potential of a point source in free space (Coulomb potential) multiplied by a screening factor  $e^{-r/\lambda_D}$ . The Debye length  $\lambda_D$  is interpreted as a screening length. For  $\lambda_D \rightarrow \infty$ , a pure Coulomb potential is obtained. For  $\lambda_D \rightarrow 0$ , the potential is strongly screened, in which case it can be approximated by an Dirac-distribution, see Section 3.4.3.

### 4.1.2 Transition Rate and Scattering Rate

Following the general approach described in Section 3.4.2 and using the result from (4.10), the scattering potential is identified as

$$H'(r) = \frac{Zq^2}{4\pi\epsilon r} e^{-r/\lambda_D}, \quad (4.11)$$

where  $Z$  gives the number of charge units of the impurity center. The scattering integral  $I_s(\mathbf{k}, \mathbf{k}')$  according to (3.124) is evaluated using (4.9), which yields

$$I_s(\boldsymbol{\beta}) = \frac{Zq^2}{V_s\epsilon} \frac{1}{\boldsymbol{\beta}^2 + 1/\lambda_D^2}, \quad (4.12)$$

with  $\boldsymbol{\beta} = \mathbf{k}' - \mathbf{k}$ . The transition rate for this non-recurring potential according to (3.131) directly follows as

$$S_1(\mathbf{k}, \mathbf{k}') = \frac{2\pi}{\hbar} \left( \frac{Zq^2}{V_s\epsilon} \right)^2 \frac{1}{(\boldsymbol{\beta}^2 + 1/\lambda_D^2)^2} \delta(E(\mathbf{k}') - E(\mathbf{k})). \quad (4.13)$$

This equation gives the scattering rate for a *single* ionized impurity. It is now generalized by multiplication with the number of impurities in the conceptual sample volume  $V_s$  given by  $N_I V_s$ , with impurity density  $N_I$ . This finally gives

$$S(\mathbf{k}, \mathbf{k}') = \frac{2\pi}{\hbar} \frac{N_I Z^2 q^4}{V_s \epsilon^2} \frac{1}{(\boldsymbol{\beta}^2 + 1/\lambda_D^2)^2} \delta(E(\mathbf{k}') - E(\mathbf{k})). \quad (4.14)$$

For further considerations,  $\boldsymbol{\beta}^2$  is expressed explicitly as

$$\boldsymbol{\beta}^2 = (\mathbf{k}' - \mathbf{k})^2 = \mathbf{k}'^2 + \mathbf{k}^2 - 2k'k \cos \alpha, \quad (4.15)$$

where  $\alpha$  is the scattering angle, i.e. the angle between  $\mathbf{k}'$  and  $\mathbf{k}$ . Assuming simple spherical, parabolic energy bands, there holds  $|\mathbf{k}'| = |\mathbf{k}|$ . In this case (4.15) reads

$$\boldsymbol{\beta}^2 = 2k^2(1 - \cos \alpha). \quad (4.16)$$

Eq. (3.62) gives an explicit expression for the magnitude of the wave vector  $k$  as a function of the energy  $E$ , thus

$$\begin{aligned} S(\mathbf{k}, \mathbf{k}') &= \frac{2\pi}{\hbar} \frac{N_I Z^2 q^4}{V_s \epsilon^2} \frac{1}{\left(2[k(E)]^2(1 - \cos \alpha) + 1/\lambda_D^2\right)^2} \delta(E' - E) \\ &= \frac{2\pi}{\hbar} \frac{N_I Z^2 q^4}{V_s \epsilon^2} \frac{1}{\left(4m^* E \hbar^{-2}(1 - \cos \alpha) + 1/\lambda_D^2\right)^2} \delta(E' - E). \end{aligned} \quad (4.17)$$

The scattering coefficient defined by (3.128) is obtained as

$$c_{ii}(E, \theta, \varphi, \theta', \varphi') = \frac{2\pi N_I Z^2 q^4}{\hbar \epsilon^2} \frac{1}{\left[4m^* E \hbar^{-2}(1 - \cos \alpha) + 1/\lambda_D^2\right]^2}, \quad (4.18)$$



where “ii” stands for *ionized impurity*. The scattering angle  $\alpha$  can be explicitly written in spherical coordinates  $(k, \theta, \varphi)$  as

$$\begin{aligned}\cos(\alpha(\theta, \varphi, \theta', \varphi')) &= \frac{\mathbf{k}' \cdot \mathbf{k}}{k^2} \\ &= \sin \theta \sin \theta' (\cos \varphi \cos \varphi' + \sin \varphi \sin \varphi') + \cos \theta \cos \theta' \\ &= \sin \theta \sin \theta' \cos(\varphi - \varphi') + \cos \theta \cos \theta'.\end{aligned}\quad (4.19)$$

## 4.2 Phonon Scattering

Phonon scattering accounts for lattice vibrations, which are always present at a temperature  $T > 0$  K. Electrons interact with the lattice by absorbing and emitting phonons, thus phonon scattering is in general inelastic. Here two selected phonon scattering mechanism are presented, further details and discussions can be found in the literature [12, 20, 28, 30].

### 4.2.1 Scattering Potential

Lattice vibrations cause a dynamic change of the lattice constant, i.e. the distance between neighboring atoms, which in turn directly change the crystal potential  $U_{\text{crystal}}(\mathbf{r})$ . The *deformation potential method* is a phenomenological description, where the scattering potential is expressed as

$$H' = \tilde{\mathbf{D}} \frac{\partial \mathbf{u}}{\partial \mathbf{r}}, \quad (4.20)$$

with the deformation of the crystal due to phonons  $\partial \mathbf{u} / \partial \mathbf{r}$  and the *deformation potential tensor*  $\tilde{\mathbf{D}}$ . Similar to (3.165), the atomic displacement is written as

$$\begin{aligned}\mathbf{u}(\mathbf{r}) &= \sum_{\beta} \left( \frac{\hbar}{2\rho_m V_s \omega_{\beta}} \right)^{1/2} \left( \mathbf{a}_{\beta} \exp(i\boldsymbol{\beta} \cdot \mathbf{r}) + \mathbf{a}_{\beta}^{\dagger} \exp(-i\boldsymbol{\beta} \cdot \mathbf{r}) \right) \mathbf{e}_{\beta} \\ &= \sum_{\beta} \left( \frac{\hbar}{2\rho_m V_s \omega_{\beta}} \right)^{1/2} \left( \mathbf{a}_{\beta} + \mathbf{a}_{-\beta}^{\dagger} \right) e^{i\boldsymbol{\beta} \cdot \mathbf{r}} \mathbf{e}_{\beta},\end{aligned}\quad (4.21)$$

where  $\rho_m$  is the mass density of the crystal and  $\mathbf{e}_{\beta}$  is the polarization vector [12, 30].

### 4.2.2 Matrix Element

The matrix elements according to (3.125) and (3.126) have to be extended to take the phonon system into account. The matrix element used to describe the absorption of a phonon is given by

$$\langle \mathbf{k}', n_{\beta} + 1 | \underline{\mathbf{H}}' \mathbf{a}_{\beta}^{\dagger} | \mathbf{k}, n_{\beta} \rangle = \langle \mathbf{k}' | \underline{\mathbf{H}}' | \mathbf{k} \rangle \langle n_{\beta} + 1 | \mathbf{a}_{\beta}^{\dagger} | n_{\beta} \rangle, \quad (4.22)$$

where it is assumed that the phonon and electron system can be separated, because they are two different quantum systems. Between these two quantum systems, energy is exchanged via scattering. In the case of the emission of a phonon, the matrix element reads

$$\langle \mathbf{k}', n_{\beta} - 1 | \underline{\mathbf{H}}'^{\dagger} \mathbf{a}_{\beta} | \mathbf{k}, n_{\beta} \rangle = \langle \mathbf{k}' | \underline{\mathbf{H}}'^{\dagger} | \mathbf{k} \rangle \langle n_{\beta} - 1 | \mathbf{a}_{\beta} | n_{\beta} \rangle. \quad (4.23)$$

Therefore, the usual expressions according to (3.125) and (3.126) for the electron and (3.163) and (3.164) for the phonon are used [12].

### 4.2.3 Acoustic Intra-Valley Phonon Scattering

In the following, a simple spherical band is assumed. The scattering potential according to (4.20) for acoustic phonon scattering simplifies to [12, 30]

$$H' = D_A \nabla \cdot \mathbf{u}(\mathbf{r}, t), \quad (4.24)$$

where  $D_A$  is the *deformation potential* and  $\mathbf{u}(\mathbf{r}, t)$  is the atomic displacement. Inserting (4.21) yields

$$H' = \sum_{\beta} i\beta D_A \left( \frac{\hbar}{2\rho_m V_s \omega_{\beta}} \right)^{1/2} (\mathbf{a}_{\beta} + \mathbf{a}_{-\beta}^{\dagger}) e^{i\beta \cdot \mathbf{r}}, \quad (4.25)$$

with  $\beta = \mathbf{e}_{\beta} \cdot \boldsymbol{\beta}$ . This is a Fourier series and therefore can directly be used as matrix element for the electronic system. It can be shown that due to the dirac-distribution for the momentum conservation in (3.132), only one term of the sum remains [12]. Thus, the transition rate is

$$S(\mathbf{k}, \mathbf{k}') = \frac{\pi \beta^2 D_A^2}{\rho_m V_s \omega_{\beta}} \left[ n_{\beta} + \frac{1}{2} \mp \frac{1}{2} \right] \delta(E(\mathbf{k}') - E(\mathbf{k}) \mp \hbar \omega_{\beta}) \quad (4.26)$$

Using the expression for the phonon dispersion relation near  $\beta = 0$  according to (3.152), which is given by

$$\omega(\beta) \simeq v_s |\beta|, \quad (4.27)$$

together with the equipartition from (3.168) for  $n_{\beta}$  and assuming that  $E \gg \hbar \omega_{\beta}$  and  $n_{\beta} \gg 1$  (elastic approximation), one obtains

$$\begin{aligned} S(\mathbf{k}, \mathbf{k}') &= \frac{\pi k_B T \beta^2 D_A^2}{\rho_m V_s \hbar \omega_{\beta}^2} \delta(E(\mathbf{k}') - E(\mathbf{k})) \\ &= \frac{\pi k_B T D_A^2}{\rho_m V_s \hbar v_s^2} \delta(E(\mathbf{k}') - E(\mathbf{k})). \end{aligned} \quad (4.28)$$

Finally, the scattering coefficient defined by (3.128) is

$$c_{ac} = \frac{\pi k_B T D_A^2}{\rho_m \hbar v_s^2}, \quad (4.29)$$

where “ac” stands for *acoustic intra-valley phonon scattering*. Here, a linear temperature dependence of the scattering rate is found. The scattering rate defined by (3.130) is

$$\begin{aligned} W(E) &= 4\pi c_{ac, \text{intra}} Z(E) \\ &= 4\pi c_{ac, \text{intra}} \frac{(m^*)^{3/2} \sqrt{2}}{(2\pi \hbar)^3} \sqrt{E}. \end{aligned} \quad (4.30)$$

### 4.2.4 Optical Intra-Valley Phonon Scattering

For optical intra-valley phonon scattering a very similar result as for acoustic intra-valley phonon scattering is obtained. The scattering potential for optical intra-valley phonon scattering is assumed to be proportional to the atomic displacement and not to its derivative as in the case of acoustic

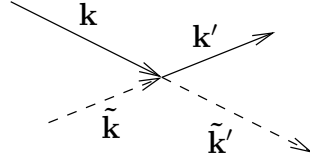


**Figure 4.1:** An incident electron with state  $\mathbf{k}$  and a hole with state  $\tilde{\mathbf{k}}$  interact and scatter to the states  $\mathbf{k}'$  and  $\tilde{\mathbf{k}}'$  respectively. In this depiction, energy and momentum is transferred from the electron in state  $\mathbf{k}$  to the hole in state  $\tilde{\mathbf{k}}$ .

vibrations. Starting from (4.26), replacing  $\beta^2 D_A^2$  with the squared optical coupling constant  $(D_t K)^2$ , the following expression is obtained:

$$S(\mathbf{k}, \mathbf{k}') = \frac{\pi(D_t K)^2}{\rho_m V_s \omega_\beta} \left[ n_\beta + \frac{1}{2} \mp \frac{1}{2} \right] \delta(E(\mathbf{k}') - E(\mathbf{k}) \mp \hbar \omega_\beta). \quad (4.31)$$

For the dispersion relation  $\omega_\beta$  the simple model from (3.153), where  $\omega_\beta = \omega_{\text{op}} = \text{const}$ , is used. Thus, the number of phonons  $n_\beta = n_{\text{op}}$  is also independent of the phonon wave vector  $\beta$ . Finally, the transition rate reads

$$S(\mathbf{k}, \mathbf{k}') = \frac{\pi(D_t K)^2}{\rho_m V_s \omega_{\text{op}}} \left[ n_{\text{op}} + \frac{1}{2} \mp \frac{1}{2} \right] \delta(E(\mathbf{k}') - E(\mathbf{k}) \mp \hbar \omega_{\text{op}}), \quad (4.32)$$

where the scattering coefficient according to (3.128) is identified as

$$c_{\text{op};\pm} = \frac{\pi(D_t K)^2}{\rho_m \omega_{\text{op}}} \left[ n_{\text{op}} + \frac{1}{2} \mp \frac{1}{2} \right], \quad (4.33)$$

where “op” stands for *optical intra-valley phonon scattering*. The scattering rate defined in (3.130) is given by

$$\begin{aligned} W(E) &= 4\pi c_{\text{op},\text{intra};\pm} Z(E \pm \hbar \omega_{\text{op}}) \\ &= 4\pi c_{\text{ac},\text{intra};\pm} \frac{(m^*)^{3/2} \sqrt{2}}{(2\pi \hbar)^3} \sqrt{E \pm \hbar \omega_{\text{op}}}. \end{aligned} \quad (4.34)$$

Thus, the scattering rate  $W(E)$  is proportional to the generalized density of states  $Z$  at the final energy  $E \pm \hbar \omega_{\text{op}}$  [12].

## 4.3 Electron-Electron Scattering

First, electron-hole scattering is examined, where the setting is sketched in Fig. 4.1. An electron in initial state  $\mathbf{k}$  interacts with a hole in initial state  $\tilde{\mathbf{k}}$ . The carriers scatter to  $\mathbf{k}'$  and  $\tilde{\mathbf{k}}'$ , respectively. Afterwards, the result is generalized for electron-electron scattering.

### 4.3.1 Scattering Potential And Scattering Integral

The hole in the state  $\tilde{\mathbf{k}}$  is the source for the scattering process. The potential of a hole is written as

$$H'(r) = \frac{q^2}{4\pi\epsilon r} e^{-r/\lambda_D}, \quad (4.35)$$

which is equal to the potential of an ionized impurity, cf. Section 4.1 [30]. In contrast to ionized impurity scattering, the scattering source is moving. The scattering integral is extended to

$$I_s(\mathbf{k}, \mathbf{k}') = \frac{1}{V_s^2} \frac{q^2}{4\pi\epsilon} \int_{\mathcal{V}} \int_{\mathcal{V}} e^{-i(\mathbf{k}' \cdot \mathbf{r} + \tilde{\mathbf{k}}' \cdot \tilde{\mathbf{r}})} \frac{e^{-|\mathbf{r} - \tilde{\mathbf{r}}|/\lambda_D}}{|\mathbf{r} - \tilde{\mathbf{r}}|} e^{i(\mathbf{k} \cdot \mathbf{r} + \tilde{\mathbf{k}} \cdot \tilde{\mathbf{r}})} \mathbf{r} d\mathbf{r} d\tilde{\mathbf{r}}, \quad (4.36)$$

where  $\mathbf{r}$  and  $\tilde{\mathbf{r}}$  are the spatial coordinates of the electron and the hole respectively. In the following, the spatial coordinates  $\mathbf{r}$  and  $\tilde{\mathbf{r}}$  as well as the state vectors  $\mathbf{k}$  and  $\tilde{\mathbf{k}}$  are transformed to the so-called center-of-mass (cm) coordinate system:

$$\mathbf{k}_{\text{cm}} = \frac{\mathbf{k} + \tilde{\mathbf{k}}}{2}, \quad (4.37)$$

$$\mathbf{K} = \frac{\mathbf{k} - \tilde{\mathbf{k}}}{2}, \quad (4.38)$$

$$\mathbf{r}_{\text{cm}} = \frac{m^* \mathbf{r} + \tilde{m}^* \tilde{\mathbf{r}}}{m^* + \tilde{m}^*}, \quad (4.39)$$

$$\mathbf{R} = \mathbf{r} - \tilde{\mathbf{r}}. \quad (4.40)$$

Here, the effective mass of the electron  $m^*$  and of the hole  $\tilde{m}^*$  are used. Hence, the scattering integral simplifies to [28, 30]

$$\begin{aligned} I_s(\mathbf{K}, \mathbf{K}') &= \frac{1}{V_s} \frac{q^2}{4\pi\epsilon} \int_{\mathcal{V}} e^{-i\mathbf{K}' \cdot \mathbf{R}} \frac{e^{-|\mathbf{R}|/\lambda_D}}{|\mathbf{R}|} e^{i\mathbf{K} \cdot \mathbf{R}} d\mathbf{R} \\ &= \frac{q^2}{V_s \epsilon} \frac{1}{\beta^2 + 1/\lambda_D^2}, \end{aligned} \quad (4.41)$$

with  $\boldsymbol{\beta} = \mathbf{K}' - \mathbf{K}$ . In the center-of-mass coordinate system, the result is the same as for ionized impurity scattering.

### 4.3.2 Transition Rate

The transition rate for dynamic processes according to (3.132) has to be used, because the source of the scattering event is a hole, which is described by a quantum mechanic wave function. This yields

$$S_1(\mathbf{k}, \tilde{\mathbf{k}}; \mathbf{k}', \tilde{\mathbf{k}}') = \frac{2\pi}{\hbar} \frac{q^4}{V_s^2 \epsilon^2} \frac{1}{[\beta^2 + 1/\lambda_D^2]^2} \delta(\mathbf{k} + \tilde{\mathbf{k}} - \mathbf{k}' - \tilde{\mathbf{k}}') \delta(E + \tilde{E} - E' - \tilde{E}'), \quad (4.42)$$

with  $\boldsymbol{\beta} = \mathbf{K}' - \mathbf{K}$  [20, 28, 31]. This result is very similar to ionized impurity scattering, except for the expression for energy and momentum conservation. Eq. (4.42) only accounts for a single hole in the sample volume  $\mathcal{V}$ . Thus, a multiplication with the number of holes  $V_s p(\mathbf{r})$  in the sample volume is required:

$$\begin{aligned} S(\mathbf{r}, \mathbf{k}, \tilde{\mathbf{k}}; \mathbf{k}', \tilde{\mathbf{k}}') &= \frac{2\pi}{\hbar} \frac{q^4 p(\mathbf{r})}{V_s \epsilon^2} \frac{1}{[\beta^2 + 1/\lambda_D^2]^2} \\ &\quad \times \delta(\mathbf{k} + \tilde{\mathbf{k}} - \mathbf{k}' - \tilde{\mathbf{k}}') \delta(E + \tilde{E} - E' - \tilde{E}'). \end{aligned} \quad (4.43)$$

According to [24, 28, 30], electron-electron scattering can be treated similarly. The main difference is that two colliding electrons cannot be distinguished from each other. The matrix element

$$\langle \mathbf{k}', \tilde{\mathbf{k}}' | \underline{\mathbf{H}}' | \mathbf{k}, \tilde{\mathbf{k}} \rangle = \langle \mathbf{K}' | \underline{\mathbf{H}}' | \mathbf{K} \rangle, \quad (4.44)$$

which has been derived for electron-hole scattering has to be substituted by

$$|\langle \mathbf{K}' | \mathbf{H}' | \mathbf{K} \rangle|^2 \mapsto |\langle \mathbf{K}' | \mathbf{H}' | \mathbf{K} \rangle|^2 + |\langle \tilde{\mathbf{K}}' | \mathbf{H}' | \mathbf{K} \rangle|^2 - \langle \mathbf{K}' | \mathbf{H}' | \mathbf{K} \rangle \langle \tilde{\mathbf{K}}' | \mathbf{H}' | \mathbf{K} \rangle, \quad (4.45)$$

with  $\tilde{\mathbf{K}}' = (\tilde{\mathbf{k}} - \mathbf{k})/2$ . Furthermore, the hole density  $p(\mathbf{r})$  is replaced by the electron density  $n(\mathbf{r})$ . In the following, the suggestion of [20] is followed, where the transition rate for electron-electron scattering is approximated by that of electron-hole scattering and  $n(\mathbf{r})$  is used instead of  $p(\mathbf{r})$ . This simplifies the further derivations.

### 4.3.3 Analysis of the Scattering Coefficient

The transition rate (4.43) for electron-electron scattering is now rewritten to

$$S(\mathbf{r}, \mathbf{k}, \tilde{\mathbf{k}}, \mathbf{k}', \tilde{\mathbf{k}}') = \frac{1}{V_s} c_{ee}(\mathbf{r}, \mathbf{k}, \tilde{\mathbf{k}}, \mathbf{k}', \tilde{\mathbf{k}}') \delta(\mathbf{k} + \tilde{\mathbf{k}} - \mathbf{k}' - \tilde{\mathbf{k}}') \delta(E + \tilde{E} - E' - \tilde{E}'), \quad (4.46)$$

with the scattering coefficient

$$c_{ee} = \frac{2\pi q^4 n(\mathbf{r})}{\hbar \epsilon^2} \frac{1}{[\beta^2 + 1/\lambda_D^2]^2}, \quad (4.47)$$

where

$$\beta = \mathbf{K}' - \mathbf{K}. \quad (4.48)$$

Using the definitions

$$\mathbf{K}' = \frac{\mathbf{k}' - \tilde{\mathbf{k}}'}{2}, \quad (4.49)$$

$$\mathbf{K} = \frac{\mathbf{k} - \tilde{\mathbf{k}}}{2}, \quad (4.50)$$

and taking momentum conservation, expressed by

$$\begin{aligned} \mathbf{k} + \tilde{\mathbf{k}} &= \mathbf{k}' + \tilde{\mathbf{k}}' \\ \Rightarrow \tilde{\mathbf{k}} &= \mathbf{k}' + \tilde{\mathbf{k}}' - \mathbf{k} \end{aligned} \quad (4.51)$$

into account, it is found that

$$\beta = \frac{1}{2} (\mathbf{k}' - \tilde{\mathbf{k}}' - \mathbf{k} + \tilde{\mathbf{k}}) = \mathbf{k}' - \mathbf{k}. \quad (4.52)$$

Thus  $\beta$  only depends on the state vectors of the in-scattered electron. Alternatively,  $\beta$  can be expressed by the wave vectors of the second electron as

$$\beta = \tilde{\mathbf{k}} - \tilde{\mathbf{k}}'. \quad (4.53)$$

Finally, the scattering coefficient is rewritten as

$$c_{ee}(\mathbf{r}, \mathbf{k}, \mathbf{k}') \Rightarrow c_{ee}(\mathbf{r}, E, \theta, \varphi, E', \theta', \varphi'), \quad (4.54)$$

or equivalently

$$c_{ee}(\mathbf{r}, \tilde{\mathbf{k}}, \tilde{\mathbf{k}}') \Rightarrow c_{ee}(\mathbf{r}, \tilde{E}, \tilde{\theta}, \tilde{\varphi}, \tilde{E}', \tilde{\theta}', \tilde{\varphi}'). \quad (4.55)$$

To simplify the further treatment of electron-electron scattering, one of these two equivalent forms can be used. For the following the first form is chosen.

#### 4.3.4 Scattering Operator

In the following, the scattering operator for electron-electron scattering is considered. It is assumed that the two electrons populate the same conduction band valley. Thus, the same distribution function  $f(\mathbf{r}, \mathbf{k}, t)$  is used for each of them. The in-scattering operator is given by

$$\underline{\mathbf{Q}}^{\text{in}}\{f\}(\mathbf{r}, \mathbf{k}, t) = N_d \int_{\mathcal{B}} \int_{\mathcal{B}} \int_{\mathcal{B}} S(\mathbf{k}', \tilde{\mathbf{k}}'; \mathbf{k}, \tilde{\mathbf{k}}) f(\mathbf{k}') f(\tilde{\mathbf{k}}') d\tilde{\mathbf{k}} d\mathbf{k}' d\tilde{\mathbf{k}}'. \quad (4.56)$$

The out-scattering operator is obtained as

$$\underline{\mathbf{Q}}^{\text{out}}\{f\}(\mathbf{r}, \mathbf{k}, t) = f(\mathbf{k}) N_d \int_{\mathcal{B}} \int_{\mathcal{B}} \int_{\mathcal{B}} S(\mathbf{k}, \tilde{\mathbf{k}}; \mathbf{k}', \tilde{\mathbf{k}}') f(\tilde{\mathbf{k}}) d\tilde{\mathbf{k}} d\mathbf{k}' d\tilde{\mathbf{k}}'. \quad (4.57)$$

The transition rate is a symmetric function in  $\mathbf{k}, \tilde{\mathbf{k}}; \mathbf{k}', \tilde{\mathbf{k}}'$ :

$$S(\mathbf{k}, \tilde{\mathbf{k}}; \mathbf{k}', \tilde{\mathbf{k}}') = S(\mathbf{k}', \tilde{\mathbf{k}}'; \mathbf{k}, \tilde{\mathbf{k}}) \quad (4.58)$$

Thus, the total scattering operator can be written in the form

$$\underline{\mathbf{Q}}\{f\} = N_d \int_{\mathcal{B}} \int_{\mathcal{B}} \int_{\mathcal{B}} S(\mathbf{k}, \tilde{\mathbf{k}}; \mathbf{k}', \tilde{\mathbf{k}}') \left[ f(\mathbf{k}') f(\tilde{\mathbf{k}}') - f(\mathbf{k}) f(\tilde{\mathbf{k}}) \right] d\tilde{\mathbf{k}} d\mathbf{k}' d\tilde{\mathbf{k}}'. \quad (4.59)$$

The term  $f(\mathbf{k}') f(\tilde{\mathbf{k}}') - f(\mathbf{k}) f(\tilde{\mathbf{k}})$  is of particular interest. Assuming detailed balance between in- and out-scattering yields

$$f(\mathbf{k}') f(\tilde{\mathbf{k}}') = f(\mathbf{k}) f(\tilde{\mathbf{k}}). \quad (4.60)$$

This equation can be solved by the following ansatz:

$$f(\mathbf{k}) = e^{C\mathbf{k}^2}, \quad (4.61)$$

with a constant  $C$ . Thus

$$e^{C(\mathbf{k}'^2 + \tilde{\mathbf{k}}'^2)} = e^{C(\mathbf{k}^2 + \tilde{\mathbf{k}}^2)}. \quad (4.62)$$

This is true for spherical, parabolic bands, because it reflects the conservation of energy. Therefore, it is concluded, that

$$f(E(\mathbf{k})) \propto e^{-E(\mathbf{k})/(k_B T_C)}, \quad (4.63)$$

which is a classical Maxwell distribution with the carrier temperature  $T_C$  instead of the lattice temperature  $T_L$ . Consequently, electron-electron scattering distorts the distribution function towards a heated Maxwellian distribution. This effect is also observed in simulation results presented in Chapter 5 and in literature [20, 31].

#### 4.3.5 SHE of the Scattering Operator

Insertion of the transition rate (4.46) into the scattering operator (4.59) yields

$$\underline{\mathbf{Q}}\{f\}(\mathbf{r}, \mathbf{k}, t) = \frac{1}{(2\pi)^3} \int_{\mathcal{B}} \int_{\mathcal{B}} \int_{\mathcal{B}} c_{ee}(\mathbf{r}, \mathbf{k}, \mathbf{k}') \left[ f(\mathbf{k}') f(\tilde{\mathbf{k}}') - f(\mathbf{k}) f(\tilde{\mathbf{k}}) \right] \times \delta(\mathbf{k} + \tilde{\mathbf{k}} - \mathbf{k}' - \tilde{\mathbf{k}}') \delta(E + \tilde{E} - E' - \tilde{E}') d\tilde{\mathbf{k}} d\mathbf{k}' d\tilde{\mathbf{k}}'. \quad (4.64)$$

These abbreviations are used in the following:

$$\begin{aligned}
\mathbf{k} &= \mathbf{k}(E, \theta, \varphi), & Z &= Z(E, \theta, \varphi), \\
\tilde{\mathbf{k}} &= \mathbf{k}(\tilde{E}, \tilde{\theta}, \tilde{\varphi}), & \tilde{Z} &= Z(\tilde{E}, \tilde{\theta}, \tilde{\varphi}), \\
\mathbf{k}' &= \mathbf{k}(E', \theta', \varphi'), & Z' &= Z(E', \theta', \varphi'), \\
\tilde{\mathbf{k}}' &= \mathbf{k}(\tilde{E}', \tilde{\theta}', \tilde{\varphi}'), & \tilde{Z}' &= Z(\tilde{E}', \tilde{\theta}', \tilde{\varphi}').
\end{aligned} \tag{4.65}$$

Before performing the projection onto spherical harmonics, a transformation to spherical coordinates is necessary. This is done separately for the in- and the out-scattering operator, respectively.

### Projection of the In-Scattering Operator

Starting with the in-scattering operator according to (4.64), the integration with respect to  $\tilde{\mathbf{k}}$  is performed:

$$\begin{aligned}
\underline{\mathbf{Q}}^{\text{in}}\{f\}(\mathbf{r}, \mathbf{k}, t) &= \frac{1}{(2\pi)^3} \int_{\mathcal{B}} \int_{\mathcal{B}} c_{\text{ee}}(\mathbf{r}, \mathbf{k}, \mathbf{k}') f(\mathbf{k}') f(\tilde{\mathbf{k}}') \\
&\quad \times \delta(E + E(\mathbf{k}' + \tilde{\mathbf{k}}' - \mathbf{k}) - E' - \tilde{E}') d\mathbf{k}' d\tilde{\mathbf{k}}'.
\end{aligned} \tag{4.66}$$

To keep the expression clear, the abbreviation  $E^* = E(\mathbf{k}' + \tilde{\mathbf{k}}' - \mathbf{k})$  is introduced. A transformation to spherical coordinates gives

$$\begin{aligned}
\underline{\mathbf{Q}}^{\text{in}}\{f\}(\mathbf{r}, \mathbf{k}, t) &= (2\pi)^3 \int_{\mathbb{R}_0^+} \int_{\mathbb{R}_0^+} \int_{\Omega'} \int_{\tilde{\Omega}'} c_{\text{ee}}(\mathbf{r}, \mathbf{k}, \mathbf{k}') f(\mathbf{k}') f(\tilde{\mathbf{k}}') Z' \tilde{Z}' \\
&\quad \times \delta(E + E^* - E' - \tilde{E}') dE' d\tilde{E}' d\Omega' d\tilde{\Omega}'.
\end{aligned} \tag{4.67}$$

A spherical harmonics expansion of the form

$$f(\mathbf{r}, \mathbf{k}, t) = f(\mathbf{r}, E, \theta, \varphi, t) = \sum_{l=0}^{\infty} \sum_{m=-l}^l f_{l,m}(\mathbf{r}, t) Y_{l,m}(\theta, \varphi) \tag{4.68}$$

yields

$$\begin{aligned}
\underline{\mathbf{Q}}^{\text{in}}\{f\} &= (2\pi)^3 \sum_{l'=0}^{\infty} \sum_{m'=-l'}^{l'} \sum_{l''=0}^{\infty} \sum_{m''=-l''}^{l''} \\
&\quad \times \int_{\mathbb{R}_0^+} \int_{\mathbb{R}_0^+} f_{l',m'}(E') f_{l'',m''}(\tilde{E}') \\
&\quad \times \left[ \int_{\Omega'} \int_{\tilde{\Omega}'} c_{\text{ee}}(\mathbf{r}, \mathbf{k}, \mathbf{k}') Z' \tilde{Z}' \delta(E + E^* - E' - \tilde{E}') \right. \\
&\quad \left. \times Y_{l',m'}(\theta', \varphi') Y_{l'',m''}(\tilde{\theta}', \tilde{\varphi}') d\Omega' d\tilde{\Omega}' \right] dE' d\tilde{E}'.
\end{aligned} \tag{4.69}$$

Finally, the expansion coefficients of the in-scattering operator are obtained using the projection of the form (2.34) as

$$\begin{aligned}
\underline{\mathbf{Q}}_{l,m}^{\text{in}}\{f\}(\mathbf{r}, E, t) &= 2(2\pi)^3 \sum_{l'=0}^{\infty} \sum_{m'=-l'}^{l'} \sum_{l''=0}^{\infty} \sum_{m''=-l''}^{l''} \\
&\times \int_{\mathbb{R}_0^+} \int_{\mathbb{R}_0^+} f_{l',m'}(E') f_{l'',m''}(\tilde{E}') \\
&\times \left[ \int_{\Omega} \int_{\Omega'} \int_{\tilde{\Omega}'} c_{ee}(\mathbf{r}, \mathbf{k}, \mathbf{k}') \delta(E + E^* - E' - \tilde{E}') Z Z' \tilde{Z}' \right. \\
&\times \left. Y_{l,m}(\theta, \varphi) Y_{l',m'}(\theta', \varphi') Y_{l'',m''}(\tilde{\theta}', \tilde{\varphi}') d\Omega d\Omega' d\tilde{\Omega}' \right] dE' d\tilde{E}'. \quad (4.70)
\end{aligned}$$

### Projection of the Out-Scattering Operator

Here, the out-scattering operator defined by (4.64) is examined. Integration over  $\tilde{\mathbf{k}}$  is performed as for the in-scattering operator, to get

$$\begin{aligned}
\underline{\mathbf{Q}}^{\text{out}}\{f\}(\mathbf{r}, \mathbf{k}, t) &= \frac{1}{(2\pi)^3} f(\mathbf{k}) \int_{\mathcal{B}} \int_{\mathcal{B}} c_{ee}(\mathbf{r}, \mathbf{k}, \mathbf{k}') f(\mathbf{k}' + \tilde{\mathbf{k}}' - \mathbf{k}) \\
&\times \delta(E + E^* - E' - \tilde{E}') d\mathbf{k}' d\tilde{\mathbf{k}}'. \quad (4.71)
\end{aligned}$$

A transformation to spherical coordinates yields

$$\begin{aligned}
\underline{\mathbf{Q}}^{\text{out}}\{f\}(\mathbf{r}, \mathbf{k}, t) &= (2\pi)^3 f(\mathbf{k}) \int_{\mathbb{R}_0^+} \int_{\mathbb{R}_0^+} \int_{\Omega'} \int_{\tilde{\Omega}'} c_{ee}(\mathbf{r}, \mathbf{k}, \mathbf{k}') f(\mathbf{k}' + \tilde{\mathbf{k}}' - \mathbf{k}) Z' \tilde{Z}' \\
&\times \delta(E + E^* - E' - \tilde{E}') dE' d\tilde{E}' d\Omega' d\tilde{\Omega}'. \quad (4.72)
\end{aligned}$$

A spherical harmonics expansion of the form (4.68) gives

$$\begin{aligned}
\underline{\mathbf{Q}}^{\text{out}}\{f\} &= (2\pi)^3 \sum_{l'=0}^{\infty} \sum_{m'=-l'}^{l'} \sum_{l''=0}^{\infty} \sum_{m''=-l''}^{l''} f_{l',m'}(E) \\
&\times \int_{\mathbb{R}_0^+} \int_{\mathbb{R}_0^+} \int_{\Omega'} \int_{\tilde{\Omega}'} c_{ee}(\mathbf{r}, \mathbf{k}, \mathbf{k}') f_{l'',m''}(E^*) Z' \tilde{Z}' \\
&\times \delta(E + E^* - E' - \tilde{E}') Y_{l,m}(\theta, \varphi) Y_{l',m'}(\theta', \varphi') Y_{l'',m''}(\theta^*, \varphi^*) d\Omega' d\tilde{\Omega}' dE' d\tilde{E}'. \quad (4.73)
\end{aligned}$$

The expansion coefficients of the out-scattering operator are obtained using the projection of the form (2.34) as

$$\begin{aligned}
\underline{\mathbf{Q}}_{l,m}^{\text{out}}\{f\}(\mathbf{r}, E, t) &= 2(2\pi)^3 \sum_{l'=0}^{\infty} \sum_{m'=-l'}^{l'} \sum_{l''=0}^{\infty} \sum_{m''=-l''}^{l''} f_{l',m'}(E) \\
&\times \int_{\mathbb{R}_0^+} \int_{\mathbb{R}_0^+} \int_{\Omega} \int_{\Omega'} \int_{\tilde{\Omega}'} c_{ee}(\mathbf{r}, \mathbf{k}, \mathbf{k}') \\
&\times \delta(E + E^* - E' - \tilde{E}') f_{l'',m''}(E^*) Z Z' \tilde{Z}' \\
&\times Y_{l,m}(\theta, \varphi) Y_{l',m'}(\theta', \varphi') Y_{l'',m''}(\theta^*, \varphi^*) d\Omega d\Omega' d\tilde{\Omega}' dE' d\tilde{E}'. \quad (4.74)
\end{aligned}$$

Details on the implementation of these expressions are found in the next chapter.



# Chapter 5

## Implementation And Simulation

This chapter deals with the implementation and simulation of ionized impurity and electron-electron scattering in **ViennaSHE**, a Spherical Harmonics Boltzmann solver developed by Karl Rupp *et al.* at the Institute for Microelectronics at the Vienna University of Technology.

### 5.1 Problem Setup

Here, the device structure and the parameters for the scattering operators used for the simulations are presented.

#### 5.1.1 The Device

The simulations are done for a 2D MOS transistor with gate length  $l_g$  shown in Fig. 5.1. The contact regions of lengths  $l_s$  and  $l_d$  are such that  $l_s = l_g$ ,  $l_d = l_g$  and  $l_c = l_g/2$ . The oxide thickness is given by  $t_{ox} = l_g/2$  and the height of the device is  $l_b = 5l_g$ . There is also an overlap given by  $l_o = l_g/5$  between the source region and the gate region, and the drain region and the gate region respectively. Dirichlet boundary conditions for the electrostatic potential  $\Phi(x, y)$  and for the expansion coefficients  $g_{l,m}$  of the EDF are used at the drain- and source-contacts [25]. Everywhere else, Neumann boundary conditions (no out-flux) are assumed. The device is structured in the following way:

**Gate:** The material of the gate-oxide is Hafnium-oxide with a relative permittivity of  $\epsilon_r = 25$ . The electrostatic potential at the gate electrode is  $\Phi(x, y) = V_g$ , with  $x \in [l_g, 2l_g]$  and  $y = -l_g/2$ .

**Drain:** The doping of the drain region is  $N_D = 1 \times 10^{20} \text{ cm}^{-3}$  and  $N_A = 1 \times 10^2 \text{ cm}^{-3}$ . The electrostatic potential at the drain electrode is  $\Phi(x, y) = V_d$ , the expansion coefficients of the EDF are chosen to match a contact electron density  $n_{\text{contact}}$  as

$$g_{l,m}(x, y, E) = \begin{cases} 2Z(E)n_{\text{contact}}k_B T \exp[-E/(k_B T)] & , l = 0, m = 0 \\ 0 & , l \neq 0, m \neq 0 \end{cases} , \quad (5.1)$$

with  $x \in [2.5l_g, 3l_g]$  and  $y = 0$ , which is the Maxwellian distribution function [25].

**Source:** The doping of the source region is  $N_D = 1 \times 10^{20} \text{ cm}^{-3}$  and  $N_A = 1 \times 10^2 \text{ cm}^{-3}$ . The electrostatic potential at the source electrode is  $\Phi(x, y) = V_s$ , the expansion coefficients of the EDF are chosen according to (5.1), but with  $x \in [0, l_g/2]$  and  $y = 0$ .

**Bulk:** The doping of the bulk region is  $N_D = 1 \times 10^{16} \text{ cm}^{-3}$  and  $N_A = 1 \times 10^4 \text{ cm}^{-3}$ . The electrostatic potential at the bulk-contact is  $\Phi(x, y) = V_b$ , with  $x \in [0, 3l_g]$  and  $y = l_b$ .

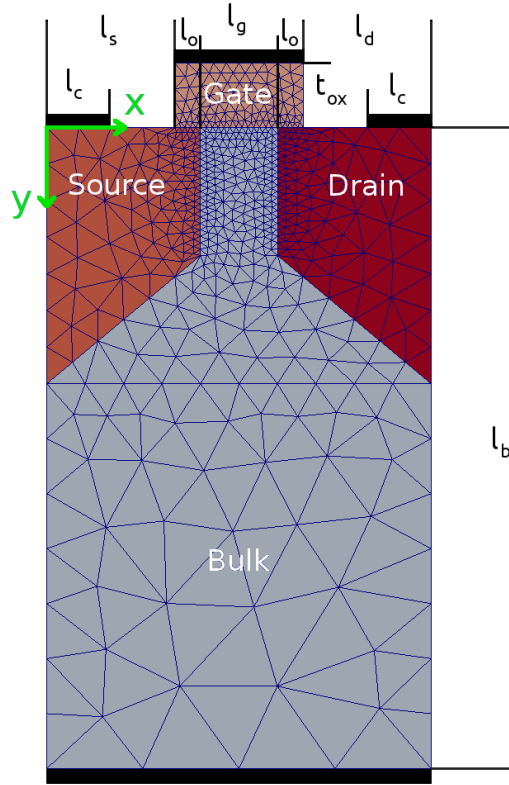


**Figure 5.1:** Generic MOS transistor used for the simulations showing the simulation mesh. The contacts are drawn as black rectangles.

In the following, results for the generic device in Fig. 5.1 for various gate lengths  $l_g$  are presented. The conduction band edge is marked by crosses. All simulation are carried out for each of the three bias points:

**Bias point A:**  $V_{ds} = 1.0 \text{ V}$ ,  $V_g = 0.8 \text{ V}$ , logic operation - on state

**Bias point B:**  $V_{ds} = 1.0 \text{ V}$ ,  $V_g = 0.0 \text{ V}$ , logic operation - off state

**Bias point C:**  $V_{ds} = 0.3 \text{ V}$ ,  $V_g = 0.8 \text{ V}$ , low resistance

### 5.1.2 Scattering

The mesh for the  $x$ - $y$ -plane is depicted in Fig. 5.1. The energy mesh is uniform with a mesh spacing of  $q/80\text{V}$ . A simple, parabolic energy band with  $m^* = 1.08 \times 9.11 \times 10^{-31} \text{ kg}$  is used. For all simulation the temperature is  $T = 300 \text{ K}$ . The scattering coefficients derived in Chapter 4 are used for the implementation. In the following, values for the constants and unknown quantities are given.

quantity	symbol	value	reference
impurity density	$N_I$	$N_D + N_A$	
number of charge units	$Z$	1	
effective electron mass	$m^*$	$1.08 \times 9.11 \times 10^{-31}$ kg	
deformation potential	$D_A$	$9q$	
mass density of Si	$\rho_m$	$2330$ kg/m <sup>3</sup>	
sound velocity in Si	$v_s$	$9000$ m/s	
optical coupling constant	$D_t K$	$5q \times 10^{10}$ m <sup>-1</sup>	
optical phonon energy	$\hbar\omega_{op}$	$q/20V$	

**Table 5.1:** Constants used for the implementation of the scattering operators.

For the Debye length  $\lambda_D$  (4.8), the following values are used:

quantity	symbol	value
permittivity	$\epsilon$	$\epsilon_0\epsilon_{Si}$
relative permittivity of Si	$\epsilon_{Si}$	11.9
electron concentration	$n_0$	$N_D$

All constants used for the implementation of the scattering operators are listed in Table 5.1. All values for the constants are chosen as in the implementation of **ViennaSHE**.

## 5.2 Ionized Impurity Scattering

In this section, the implementation of ionized impurity scattering for **ViennaSHE** is described, followed by a presentation of the simulation results. Boundary effects are discussed in detail. Moreover, a comparison of the resulting distribution function with and without the inclusion of ionized impurity scattering is given.

### 5.2.1 Implementation

Starting with the scattering coefficient  $c_{ii}(E, \theta, \varphi, \theta', \varphi')$  according to (4.18), a simplified version for a first estimation neglecting the angular dependency, given by

$$c_{ii} \simeq c_{ii}(E) = \frac{2\pi N_I Z^2 q^4}{\hbar\epsilon^2} \frac{1}{[4m^* E \hbar^{-2} + 1/\lambda_D^2]^2}. \quad (5.2)$$

is used. Thus, the scattering operators according to (2.66) for in- and (2.67) for out-scattering respectively are obtained. The implementation requires only the definition of the scattering coefficient. Everything else is provided by **ViennaSHE**.

### 5.2.2 Simulation

In Fig. 5.2 the distribution function  $f$  for a device with  $l_g = 100$  nm plotted along the  $x$ -axis and over the total energy  $H$  is shown. The gate potential is  $V_g = 0.8$  V and the drain-source potential  $V_{ds} = 1$  V. At the boundaries the distribution function takes a Maxwellian shape. The ripples of  $f$  are due to intra-valley optical phonon scattering with a constant phonon energy  $\hbar\omega_{op}$ . The distribution function only exists for  $H \geq E_{c0} - q\Phi(x, t)$ . The forbidden region contains all  $H < E_{c0} - q\Phi(x, t)$ . At

$H = E_{c0} - q\Phi(x, t)$ , the conduction band edge is located, where the kinetic energy of the electrons is zero. Note that at the contact regions the mesh is very coarse, cf. Fig. 5.1. Thus, the conduction band edge in Fig. 5.2 is also very coarse and will be examined in more detail later.

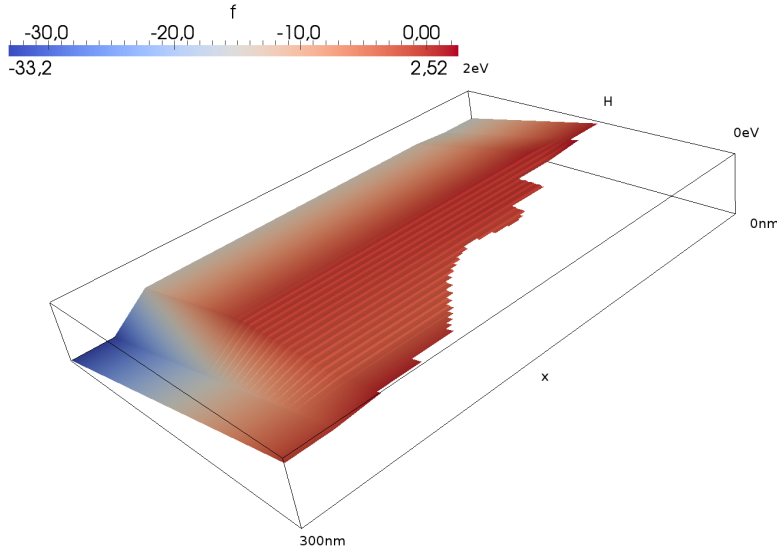


**Figure 5.2:** Distribution function  $f$  over the  $H$ - $x$ -plane for a device with  $l_g = 100$  nm for  $V_g = 0.8$  V and  $V_{ds} = 1$  V.

## 20 nm-Device

In this section, a 20 nm-device is investigated using a two-dimensional plot of the distribution function  $f$  over the total energy  $H$  for selected values of  $x$ . At the beginning some general considerations about such plots by means of Fig. 5.3 are made, where the device operates at **bias point A**. These considerations are valid for all the following discussions.

The distribution function at the boundaries is plotted in dashed lines, where the upper line is at the source-contact at  $x = 0$  and the lower one at the drain-contact at  $x = 3l_g$ . The distance between these two lines at the  $H$ -axis is equal to  $qV_{ds}$ . Electrons are injected at the source-contact and at the drain-contact respectively. Starting at the source contact, electrons are affected by a falling energy potential, thus they are able to gain kinetic energy, which again is partially absorbed by optical intra-valley phonon scattering. The ripples of the distribution function are caused by the constant energy of the optical phonons given by  $\hbar\omega_{op}$ . Acoustic intra-valley phonon scattering and ionized impurity scattering are energy conserving and thus do not dissipate energy, but they have an indirect impact on the dissipation process, as will be seen later.

To better understand boundary effects, the distribution function for the region at the source contact is now examined in depth. In Fig. 5.4 the distribution function  $f$  is plotted starting at  $x = l_g/4$ , this is in the middle of the source contact region. Using a refined mesh in the considered region, the distribution function changes noticeable, which is documented in Fig. 5.5. Both meshes are directly compared in Fig. 5.6. The reason for this effect is the very coarse mesh used for the first simulation. Thus, Fig. 5.4 shows only a rough interpolation of the result.

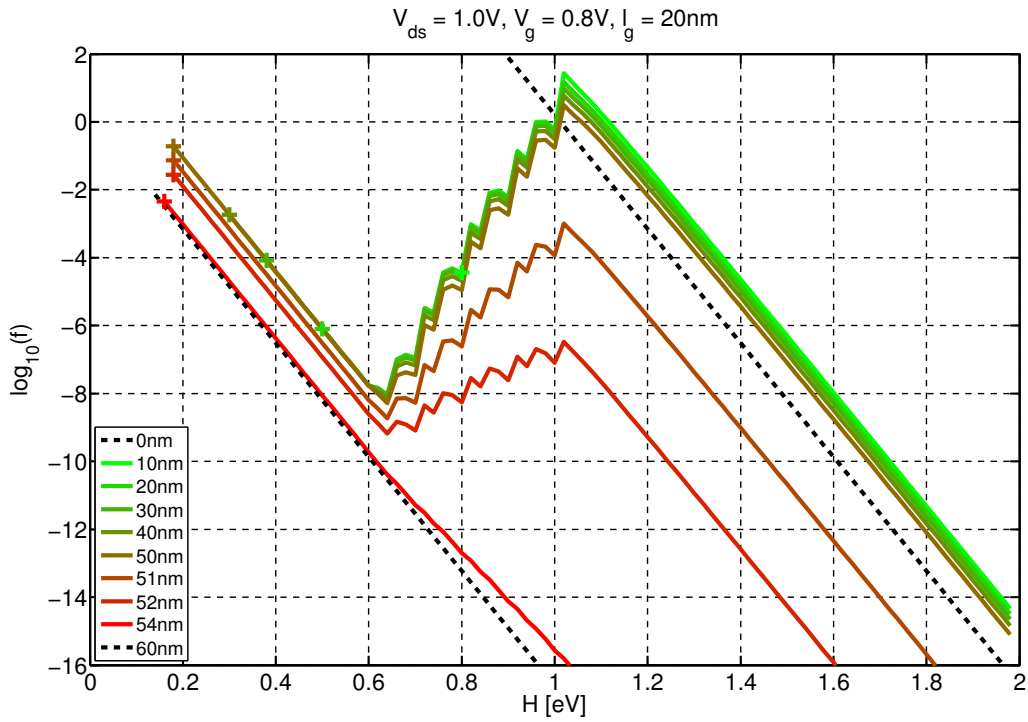


**Figure 5.3:** Distribution function  $f$  over total energy  $H$  for selected values of  $x$ .

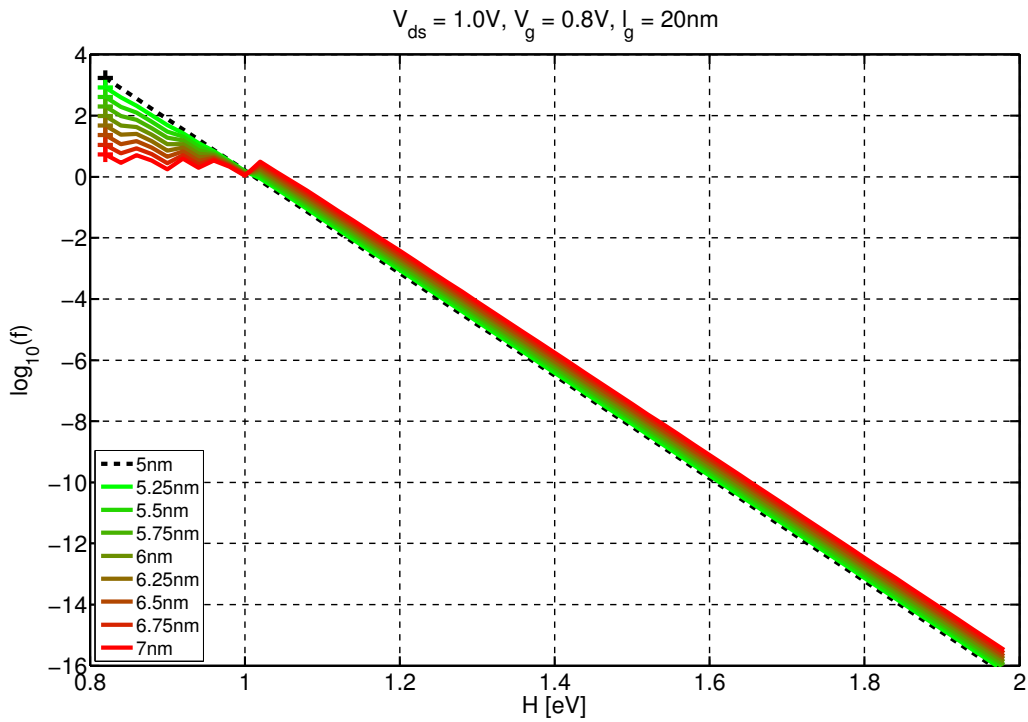


**Figure 5.4:** Distribution function  $f$  for the 20nm-device at the source contact at  $x \gtrsim 5$  nm.

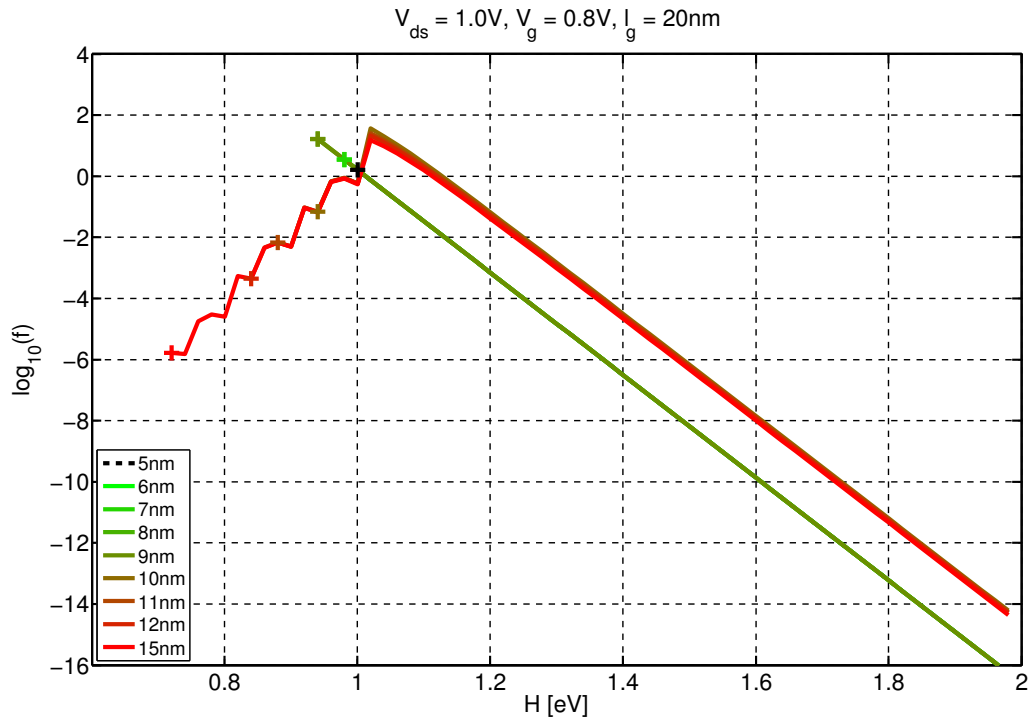


**Figure 5.5:** Distribution function  $f$  for the 20 nm-device at the source contact at  $x \gtrsim 5$  nm using a refined mesh.

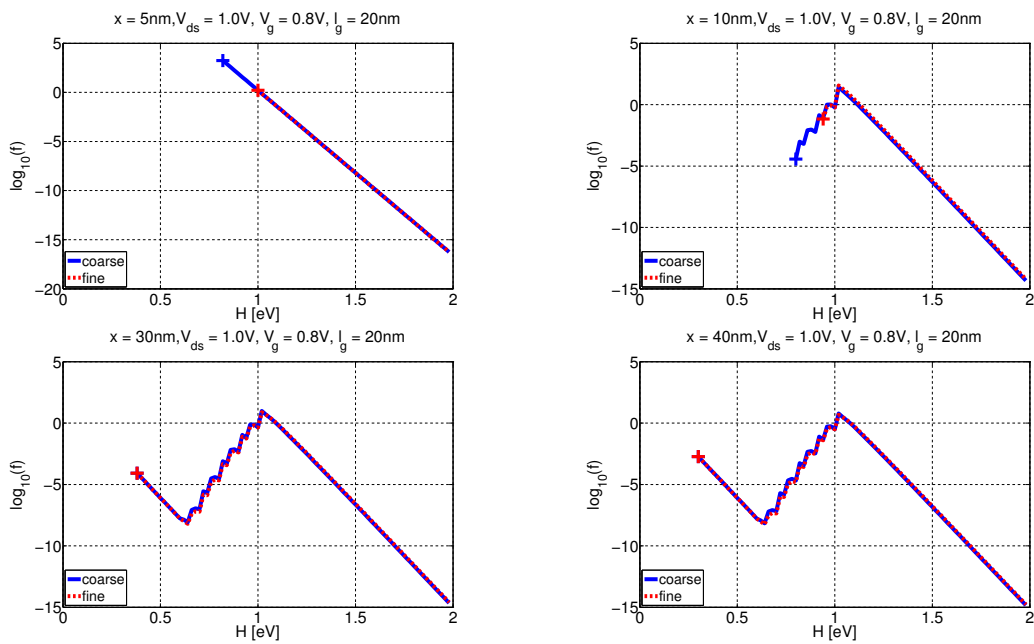


**Figure 5.6:** Comparison of the coarse mesh depicted in Fig. 5.1 and the one, which is refined at the source contact.

The situation near the source contact is now discussed for the more accurate result depicted in Fig. 5.5. There, it can be seen, that near the contact,  $f$  is extended to the bottom of the conduction band, c.f. Fig. 5.7. This behavior can be explained by a simple Maxwell distribution

$$f \propto \exp\left(-\frac{E - q\Phi(x)}{k_B T}\right). \quad (5.3)$$

For fixed values of the kinetic energy  $E$ ,  $f$  increases exponentially, because  $\Phi(x)$  increases, and thus the band edge is decreasing, c.f. Fig. 5.7. This effect is not observed for the coarse mesh used for the simulations, c.f. Fig. 5.4. It occurs for a mesh, which is refined in the source region, c.f. Fig. 5.5. This model holds, until scattering becomes dominant. Fig. 5.6 shows that if one is only interested in the distribution function  $f$  in the region of the channel, the coarse mesh is sufficient for an estimate. More accurate results also demand a fine mesh in the contact regions.

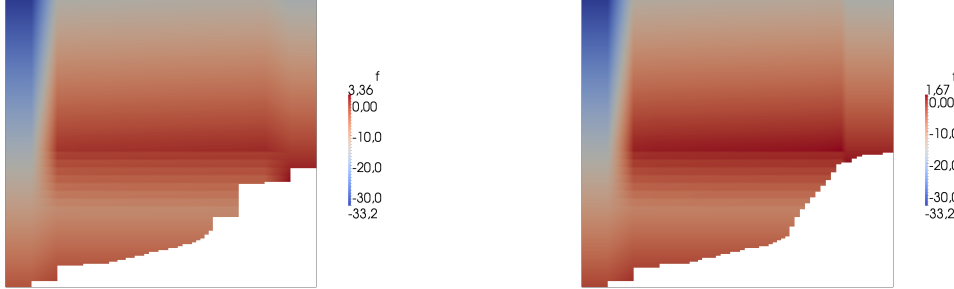


**Figure 5.7:** Comparison of the resulting distribution function  $f$  for the the coarse mesh depicted in Fig. 5.1 (left) and the one, which is refined at the source contact (right).

The shift of the distribution function  $f$  to higher values in Fig. 5.5 starting between  $x = 9$  nm and  $x = 10$  nm is now discussed. To investigate the influence of discretization errors, the simulation is repeated for a refined energy mesh, with a energy spacing of  $q/240$  V. A comparison between the coarse and fine energy grid is given in Fig. 5.8. This does not provide an explanation of the shift. Subsequently, the influence of the constant phonon energy  $\hbar\omega_{\text{op}}$  is investigated. In Fig. 5.9, the distribution function  $f$  for  $\hbar\omega_{\text{op}} = q/40$  V and still using the fine energy grid is shown. The comparison with the result from above in Fig. 5.10 suggests, that the shift is independent of the phonon energy  $\hbar\omega_{\text{op}}$ . From this it follows that the shift is likely to be a numerical effect, which stems from the choice of Dirichlet boundary conditions for the EDF at the contacts.

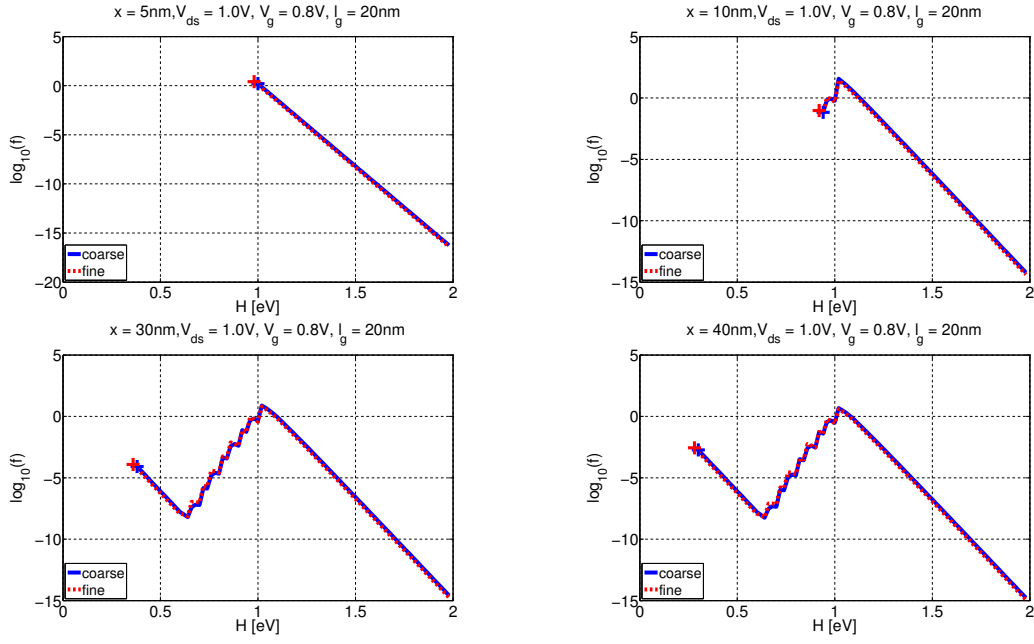


**Figure 5.8:** Comparison of the distribution for a coarse energy mesh (energy spacing  $q/80V$ ) and a fine one (energy spacing  $q/240V$ ).

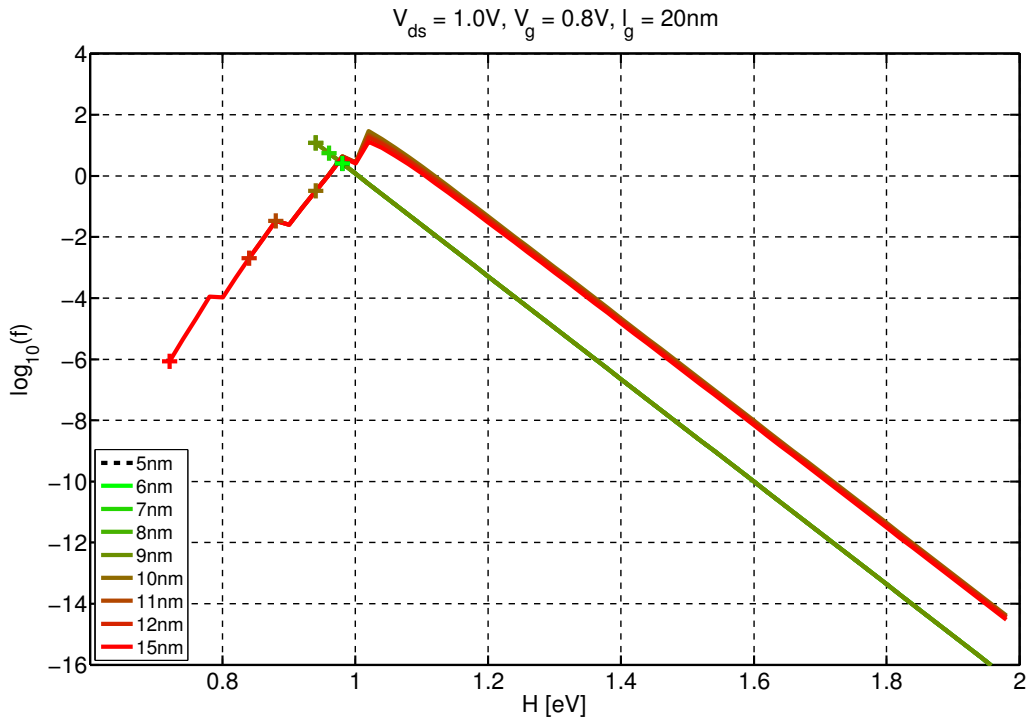


**Figure 5.9:** Distribution function  $f$  for the 20nm-device at the source contact at  $x > 5nm$  for a phonon energy of  $\hbar\omega_{op} = q/40V$ .



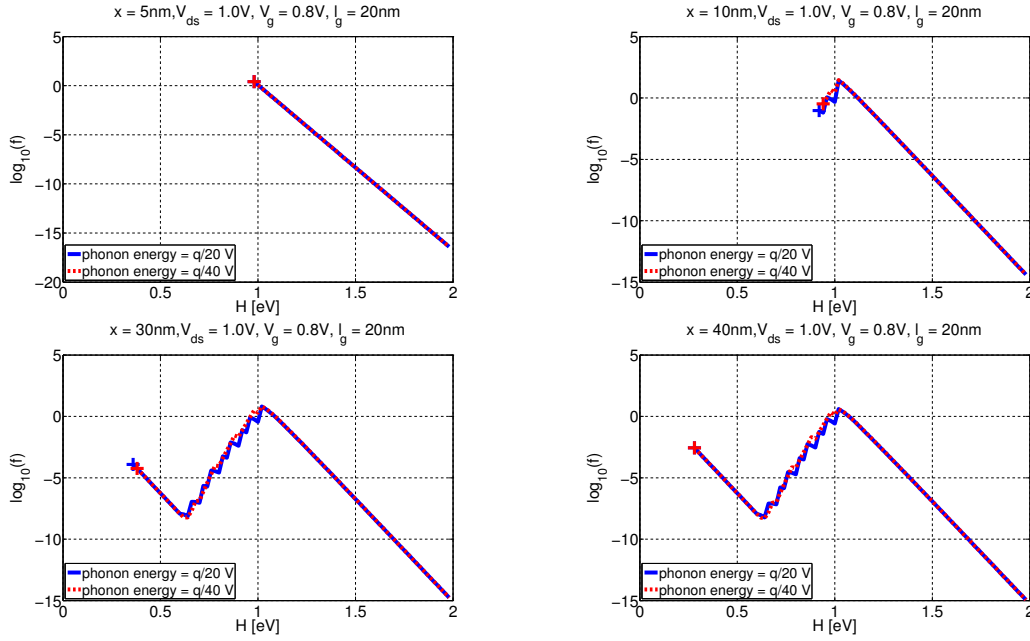


**Figure 5.10:** Comparison of the results for two different phonon energies.

At the end of the source contact between  $x = 9$  nm and  $x = 10$  nm, the effects of phonon scattering become visible, cf. Fig. 5.5. The distribution function  $f$  takes a triangular shape. The shorter the device, the sharper is this triangular shape. Between  $x = 10$  nm and  $x = 20$  nm, the influence of the drain contact becomes apparent and the distribution function  $f$  in the device is more and more drawn up to the distribution function at the drain contact, cf. Fig. 5.3.

In Fig. 5.11 the distribution function is plotted for **bias point B**. At first sight, it looks much like Fig. 5.3, but the crosses marking the conduction band edge are shifted to higher values of the total energy  $H$ . This is a result of the changed gate potential.

Fig. 5.12 shows the distribution function for **bias point C**. Due to the lower  $V_{ds} = 0.3$  V, the electrons are not able to gain as much kinetic energy as for  $V_{ds} = 1.0$  V.

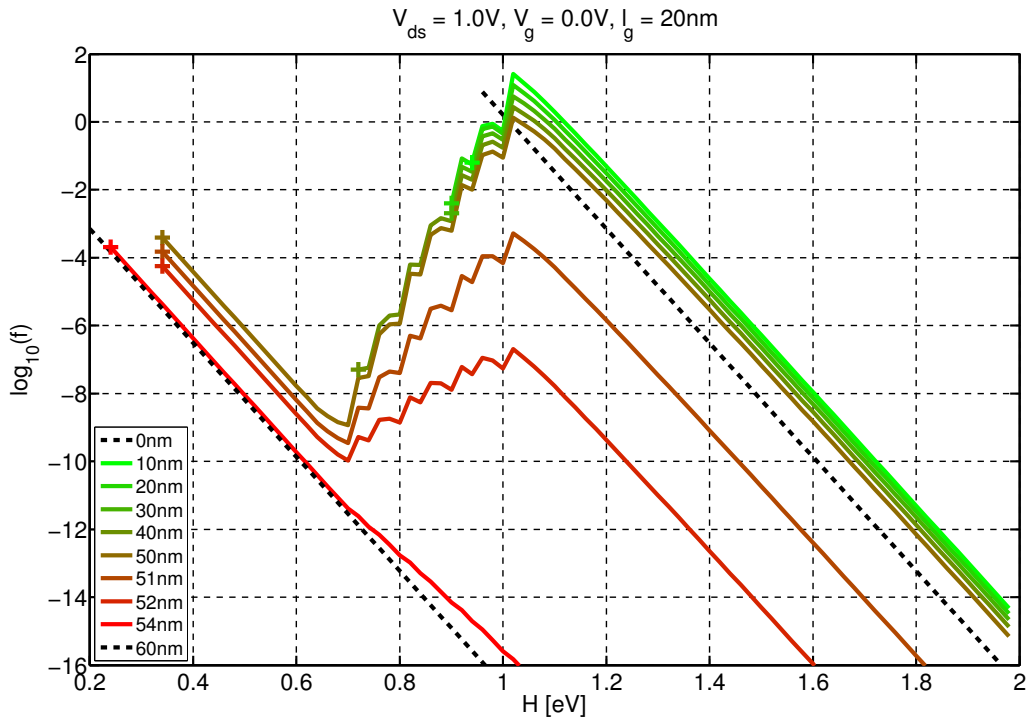


Figure 5.11: Distribution function for a 20 nm-device.

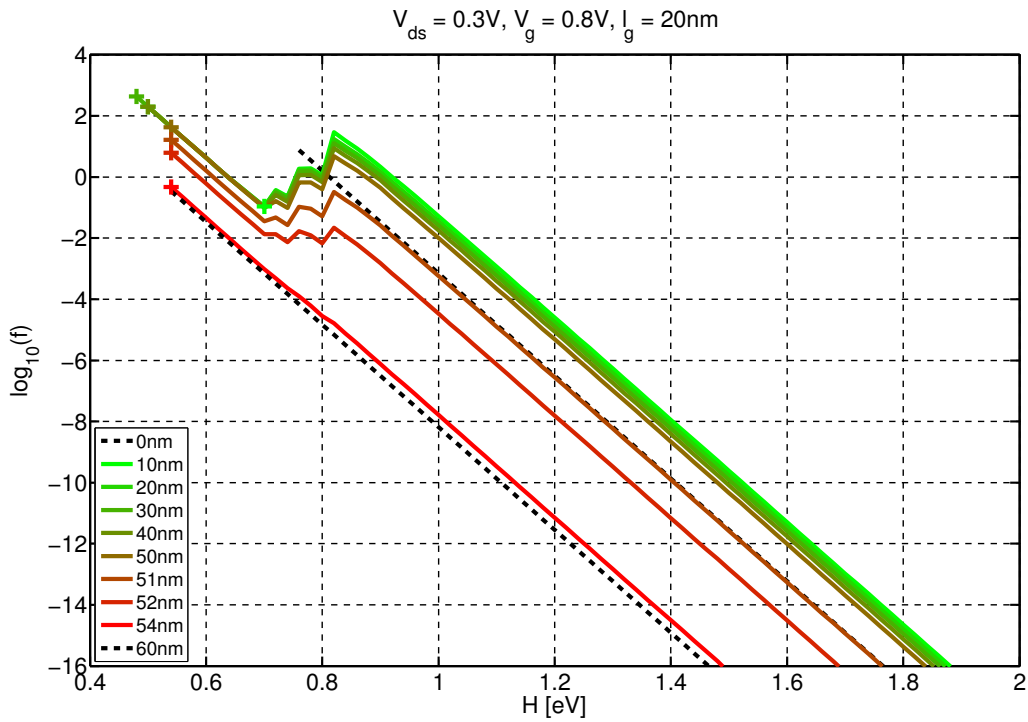
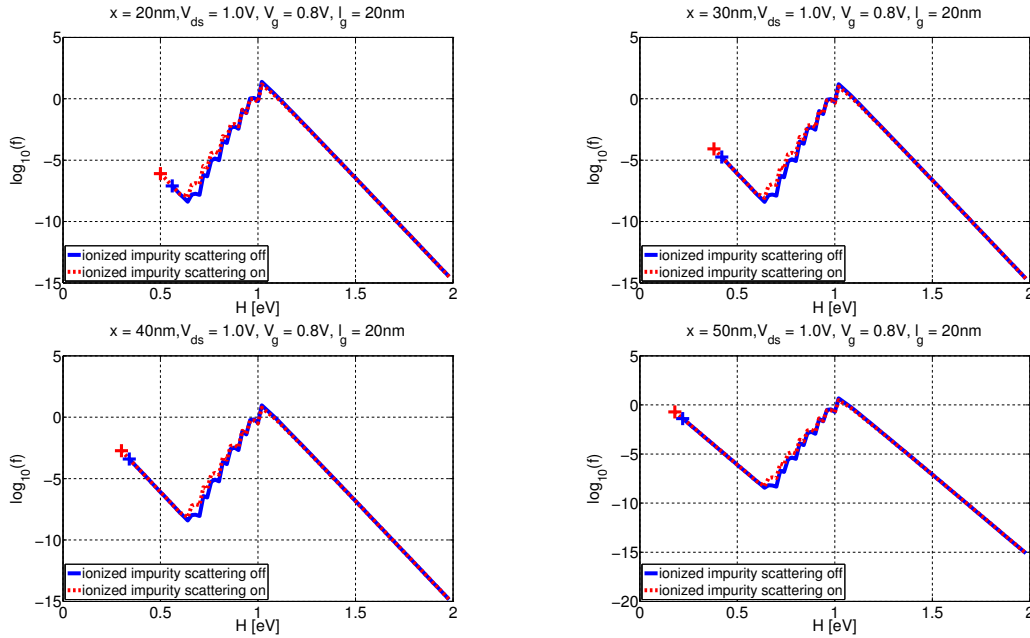
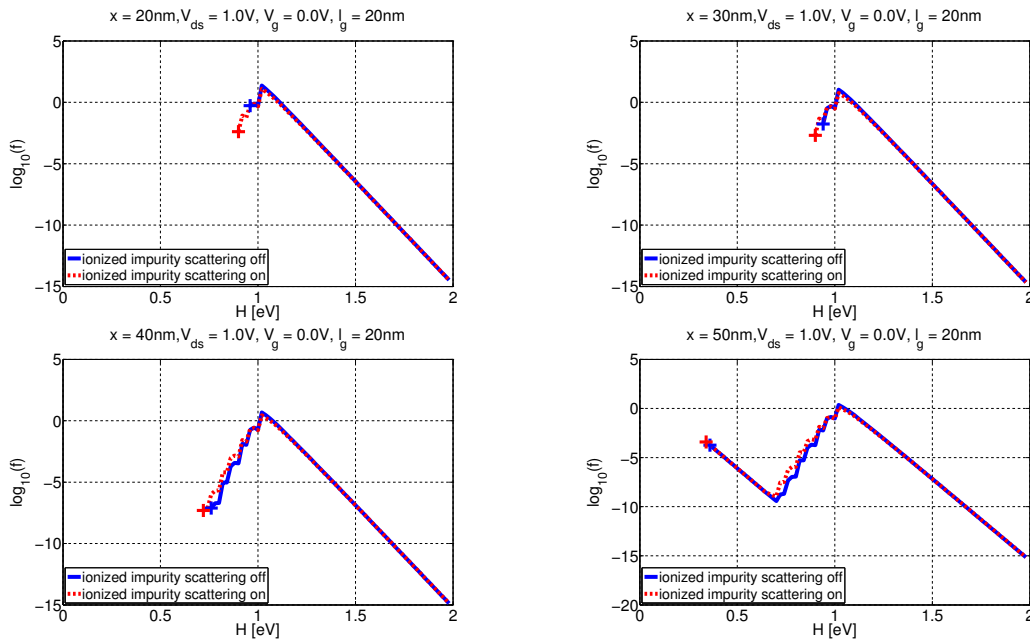


Figure 5.12: Distribution function for a 20 nm-device.

Finally, the influence of ionized impurity scattering is discussed. Therefore, the simulations for **bias point A** and **bias point B** are repeated without ionized impurity scattering. In Fig. 5.13 and Fig. 5.14 a comparison is given. As expected from (5.2), ionized impurity scattering influences the shape of the distribution function especially for low values of the kinetic energy  $E$ . It tends to smooth the distribution function and influences the band edge.



**Figure 5.13:** Comparison of the distribution function with and without ionized impurity scattering in bias point A.



**Figure 5.14:** Comparison of the distribution function with and without ionized impurity scattering in bias point B.

## 100 nm-Device

The discussion for the 100 nm-device is limited to the **bias point A**, because the qualitative behavior of the distribution function is the same as before. The main difference to the 20 nm-device is that the effects of optical phonon scattering becomes more important. In Fig. 5.15 the distribution function is depicted. The sharp triangular shape of the distribution function seen before is smoothed out. This is a consequence of the increased energy dissipation due to optical phonon scattering, which is caused by the increased gate length  $l_g$ . A longer gate length results in a rise of the transition time of the electrons through the channel, which in turn increases the probability of scattering. Especially the impact of ionized impurity scattering as a catalyst for optical phonon scattering is confirmed, as shown in Fig. 5.16, where it can be seen clearly that ionized impurity scattering amplifies the effects of smoothing the distribution function.

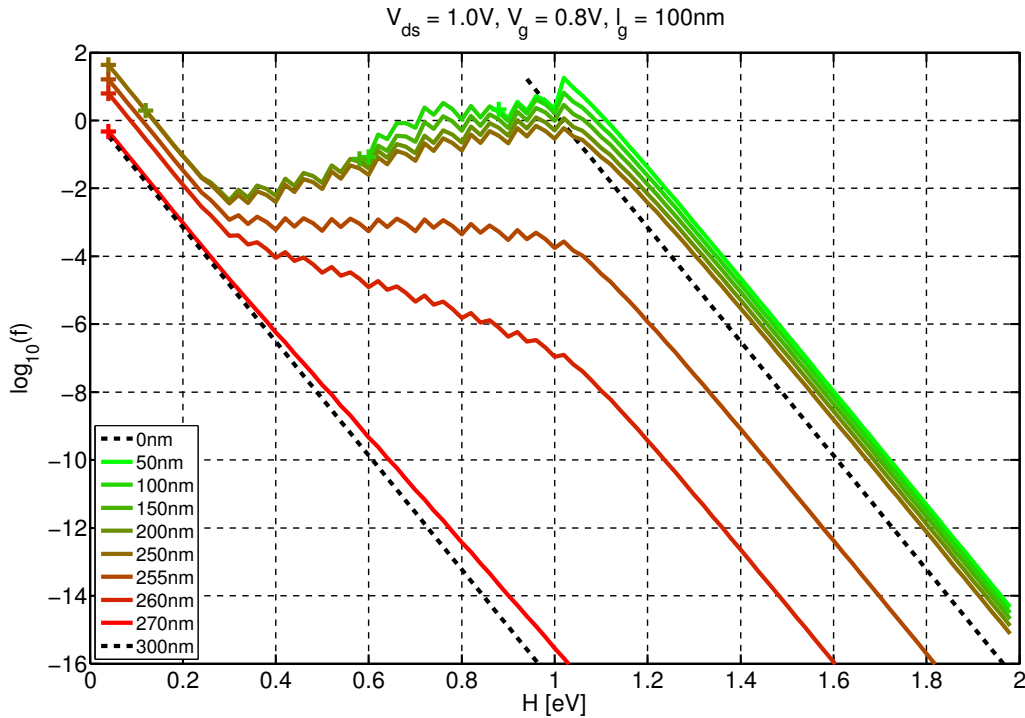


**Figure 5.15:** Distribution function for **bias point A** for a 100 nm-device.

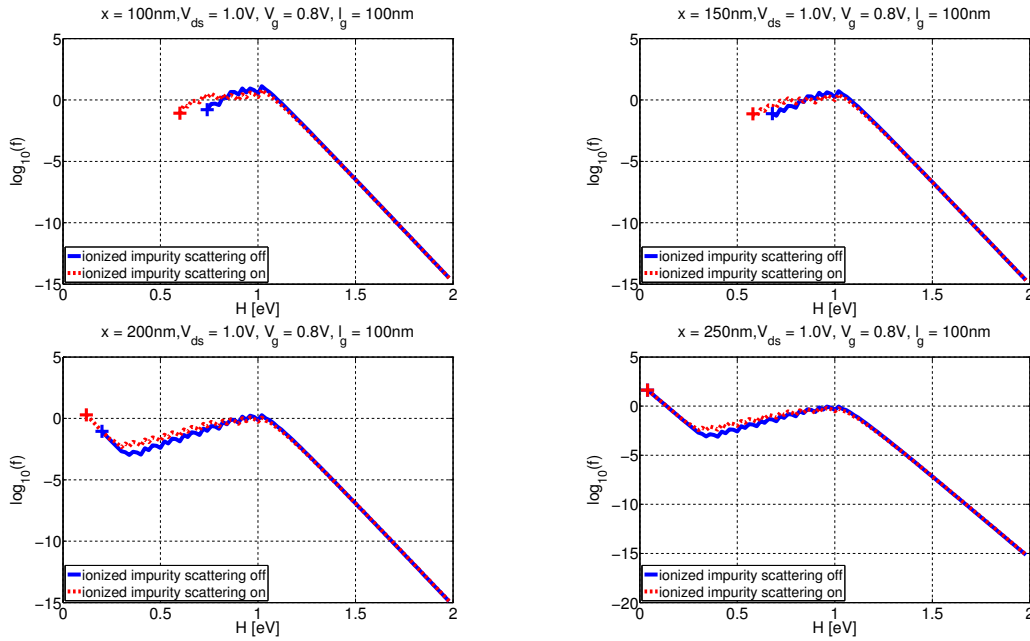


**Figure 5.16:** Comparison of the distribution function with and without ionized impurity scattering in bias point A.

### 300 nm-Device

The resulting distribution function for **bias point C** presented in Fig. 5.17 shows the strong impact of energy dissipation due to optical phonon scattering. The sharp triangular shape is completely smoothed out and barely recognizable. In Fig. 5.18, the influence of ionized impurity scattering for the **bias point A** is depicted. Here, it can be seen again that ionized impurity scattering tends to flatten the distribution function  $f$  by amplifying the effects of optical phonon scattering.

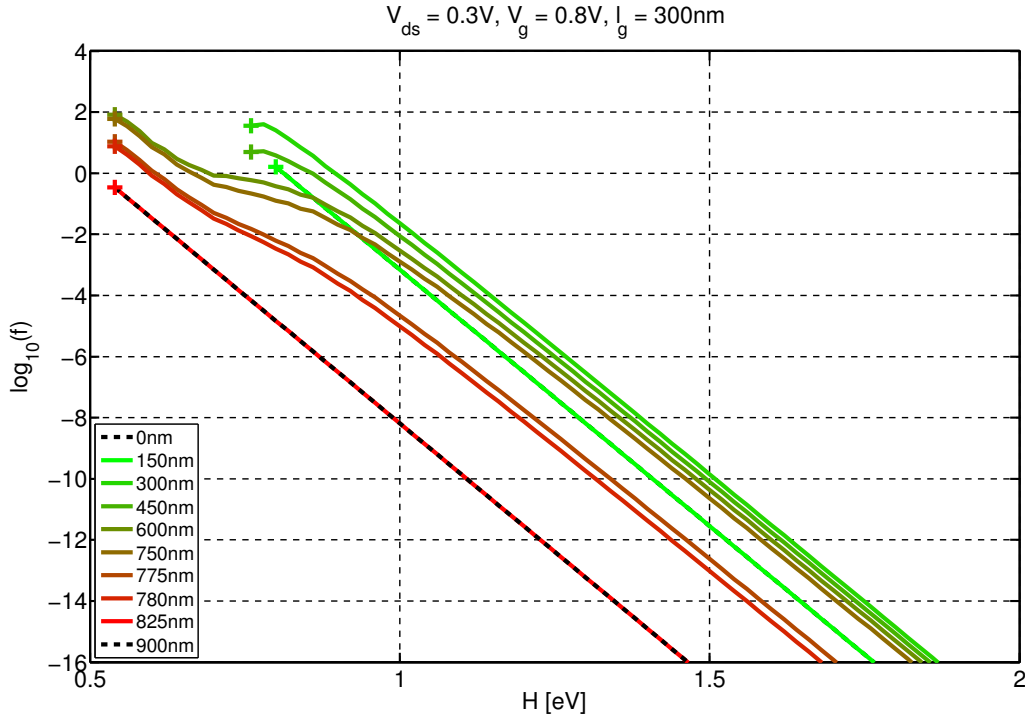


Figure 5.17: Distribution function for a 300 nm-device for **bias point C**.

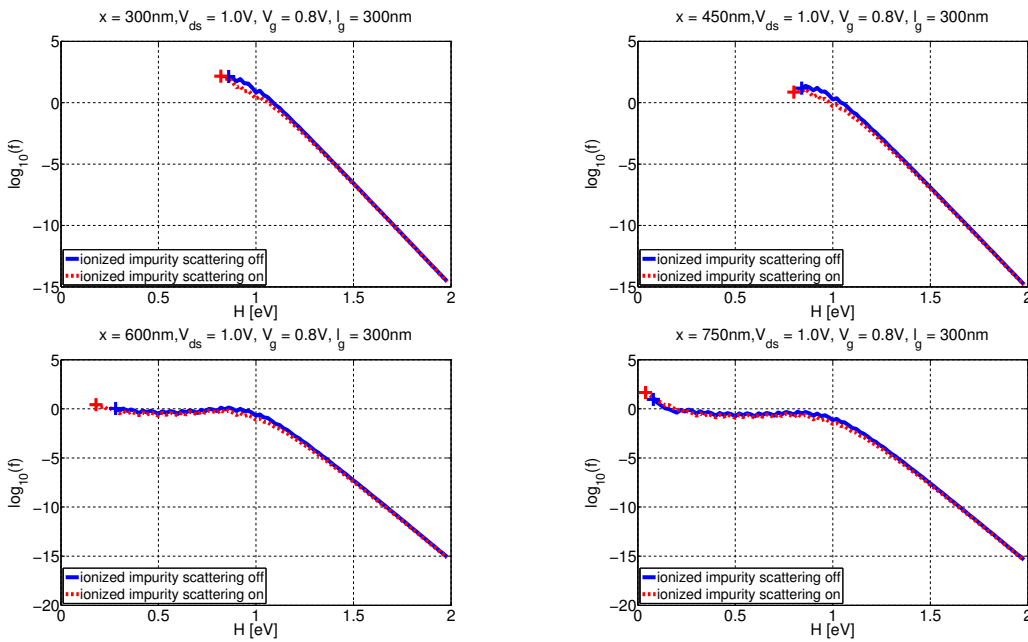


Figure 5.18: Influence of ionized impurity scattering on the resulting distribution function  $f$  for **bias point A**.

### 5.3 Electron-Electron Scattering

In this section, the implementation of electron-electron-scattering for ViennaSHE is described. Afterwards, simulation results are presented.

### 5.3.1 Implementation

The implementation of electron-electron scattering is more difficult than the implementation of ionized impurity scattering described before, because the scattering operator is much more complex. In the following some numerical studies of the in-scattering operator  $\mathbf{Q}^{\text{in}}$  including all angular dependencies are presented. It is found that a simplification of the scattering operator is necessary in order to allow for an implementation.

#### Numerical Study of the In-Scattering Operator

The in-scattering operator in spherical coordinates is given by (4.69). It contains an integral over the unit spheres  $\Omega'$  and  $\tilde{\Omega}'$  respectively, which is now examined. It reads

$$I_{l',m',l'',m''}(E, E', \tilde{E}') = \int_{\Omega'} \int_{\tilde{\Omega}'} c_{ee} \delta(E + E^* - E' - \tilde{E}') Y_{l',m'}(\theta', \varphi') Y_{l'',m''}(\tilde{\theta}', \tilde{\varphi}') d\Omega' d\tilde{\Omega}', \quad (5.4)$$

with

$$E^* = E(\mathbf{k}' + \tilde{\mathbf{k}}' - \mathbf{k}). \quad (5.5)$$

Assuming that  $\theta = 0$  and  $\varphi = 0$ , all variables in (5.4) are determined. This four-fold integral is now evaluated numerically using `Maple`, for which the dirac-distribution has to be approximated appropriately. A number of different implementations are tested, with the result, that

$$\delta(x) \approx d_\varepsilon(x) = \frac{1}{\pi} \frac{\varepsilon}{x^2 + \varepsilon^2} \quad (5.6)$$

performs best. The parameter  $\varepsilon$  is a “small” number, where the term “small” depends on the problem. In this context  $\varepsilon$  has to be small compared to the energies  $E, E^*, E'$  and  $\tilde{E}'$ . The integration is performed for a fixed value of  $E$  over a non-uniform energy-grid in the  $E' - \tilde{E}'$ -space. An adaptive algorithm is used to find the “best”  $\varepsilon$  for a limited computation time  $t_{\text{max}}$ . For the following, the reciprocal of  $\varepsilon$  is defined as

$$\eta := \frac{1}{\varepsilon}. \quad (5.7)$$

Thus, the higher  $\eta$ , the higher is the accuracy of the result. In conclusion, the main challenge is to find an appropriate approximation of the dirac-distribution in order to optimize the computation time of the four-fold-integral, without sacrificing too much accuracy. For an implementation of electron-electron-scattering for `ViennaSHE`, such an approach is not feasible due to excessive computational time. Thus, a similar study for the out-scattering operator is not made. Some selected results of (5.4) are found in Fig. 5.19, Fig. 5.20 and Fig. 5.21.

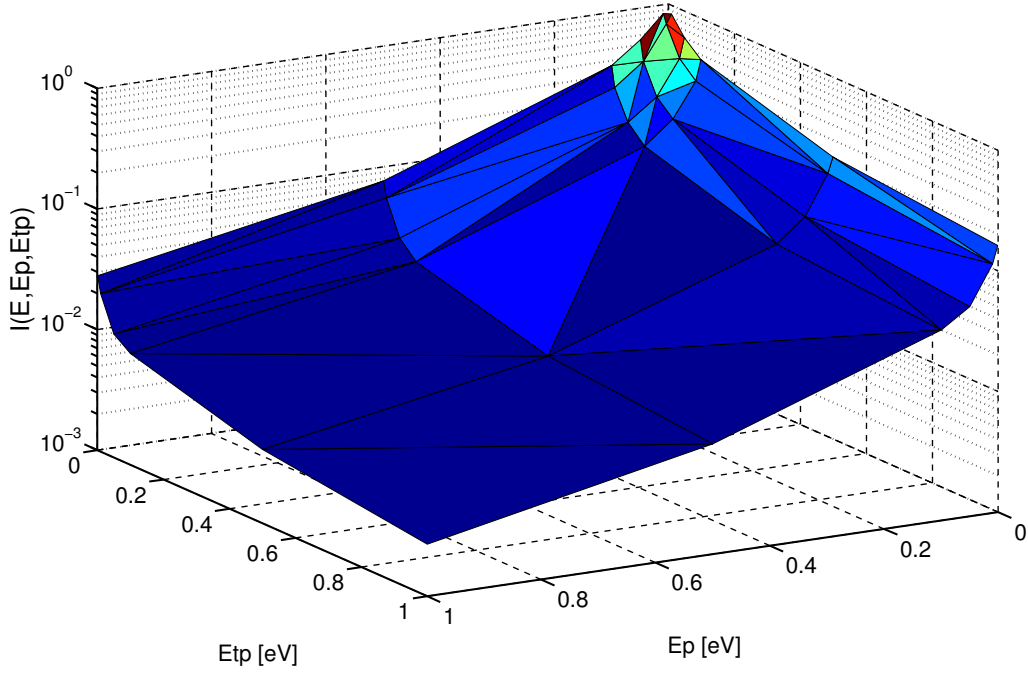


**Figure 5.19:** Plot of the integral  $I$  according to (5.4) scaled by  $1 \times 10^{11}$  for  $E = 10$  meV as a function of  $E_p \equiv E'$  and  $E_{tp} \equiv \tilde{E}'$ , for  $t_{\max} = 10$  s.

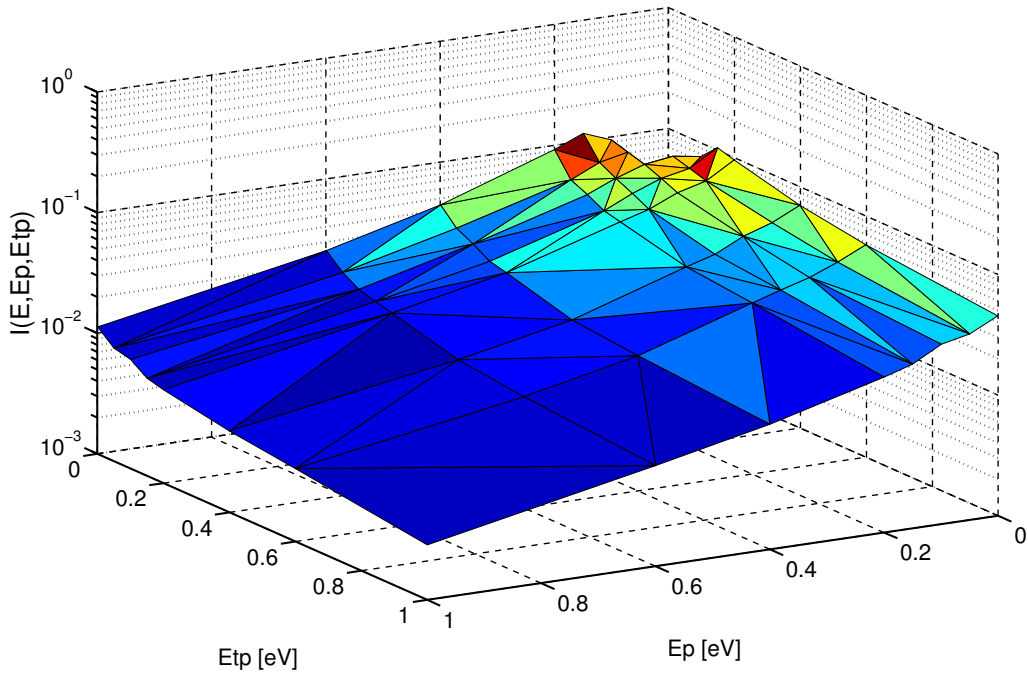


**Figure 5.20:** Plot of the integral  $I$  according to (5.4) scaled by  $1 \times 10^{11}$  for  $E = 100$  meV as a function of  $E_p \equiv E'$  and  $E_{tp} \equiv \tilde{E}'$ , for  $t_{\max} = 10$  s.



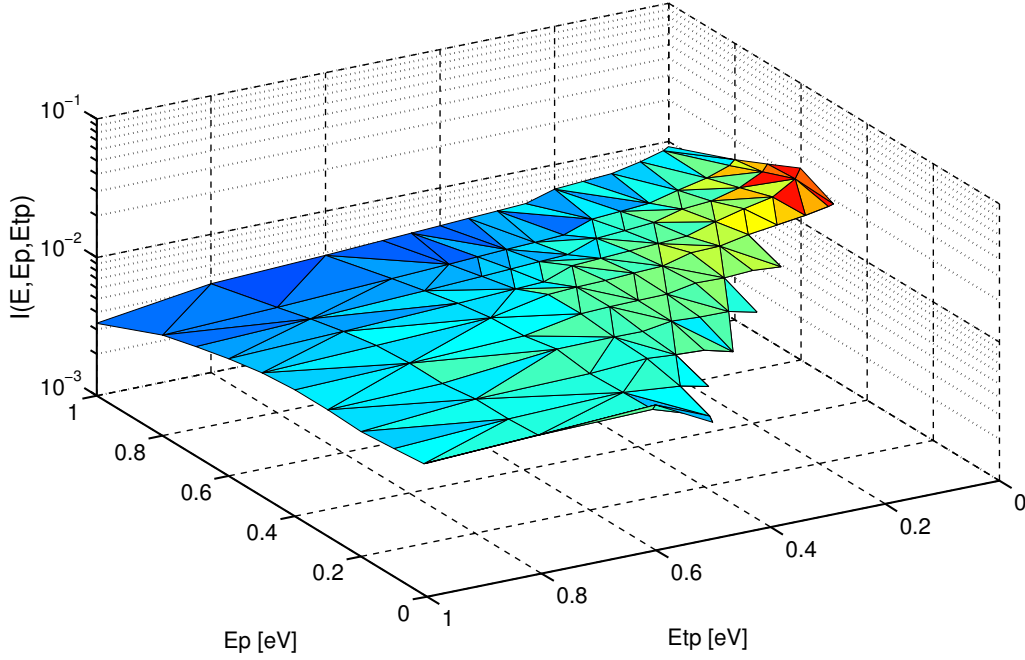


**Figure 5.21:** Plot of the integral  $I$  according to (5.4) scaled by  $1 \times 10^{11}$  for  $E = 500$  meV as a function of  $E_p \equiv E'$  and  $E_{tp} \equiv \tilde{E}'$ , for  $t_{\max} = 10$  s.

### Simplification Of The Scattering Operator

The scattering coefficient (4.47) is now simplified using a zeroth-order expansion of  $\beta^2$ , which reads

$$\begin{aligned} \beta^2 &= \mathbf{k}'^2 + \mathbf{k}^2 - 2k'k \cos \alpha \\ &\approx \mathbf{k}'^2 + \mathbf{k}^2. \end{aligned} \quad (5.8)$$

The basic idea is that the angular dependency is negligible by averaging. For the further considerations spherical, parabolic bands are assumed. The scattering coefficient follows directly as

$$c_{ee} \approx c_{ee}(\mathbf{r}, E, E') = \frac{2\pi q^4 n(\mathbf{r})}{\hbar \epsilon^2} \frac{1}{[2m^* \hbar^{-2} (E' + E) + 1/\lambda_D^2]^2}. \quad (5.9)$$

In Section 4.3.5 the SHE of the in- and out-scattering operator respectively is derived. In both cases a dirac-distribution remains, which accounts for energy conservation. In principle, this Dirac distribution can be eliminated, but the problem is very difficult due to the presence of  $E^*$ , which depends on  $E$ ,  $\theta$ ,  $\varphi$ ,  $E'$ ,  $\theta'$ ,  $\varphi'$ ,  $\tilde{E}'$ ,  $\tilde{\theta}'$ , and  $\tilde{\varphi}'$ . To simplify the expressions, the angular dependency is neglected and  $E^*$  is assumed to be constant, because otherwise an implementation would not be feasible. For the value of  $E^*$ , it is suggested to assume it to be equal to the mean kinetic energy for all the further considerations, given by

$$E^* \approx \langle E(\mathbf{r}, t) \rangle = \int_{\mathbb{R}_0^+} EZ(E) f_{0,0}(\mathbf{r}, E, t) dE. \quad (5.10)$$

Another approach could be to define  $E^*$  as model parameter. Furthermore it is assumed that

$$f(E^*, \theta^*, \varphi^*) = \sum_{l=0}^{\infty} \sum_{m=-l}^l f_{l,m} Y_{l,m}(\theta^*, \varphi^*) \approx f_{0,0}(E^*) Y_{0,0}. \quad (5.11)$$

This approximation is made because no details of the second particle are known. The low-density approximation of the scattering operator is linear in the distribution function  $f$ , cf. (1.85). This is not the case for the scattering operator for electron-electron-scattering, cf. (4.70) and (4.74), thus it is essential to normalize the distribution function:

$$\int_{\mathbb{R}_0^+} Z(E) f_{0,0}(\mathbf{r}, E, t) dE \stackrel{!}{=} 1. \quad (5.12)$$

For the linear scattering operator a normalization is not necessary, because a scaling does not change the problem. The assumptions above are now applied to the in-scattering operator (4.70), to get

$$\begin{aligned} \underline{\mathbf{Q}}_{l,m}^{\text{in}}\{f\}(\mathbf{r}, E, t) &\approx 2(2\pi)^3 \sum_{l'=0}^{\infty} \sum_{m'=-l'}^{l'} \sum_{l''=0}^{\infty} \sum_{m''=-l''}^{l''} Z(E) \\ &\times \left[ \int_{\mathbb{R}_0^+} \int_{\mathbb{R}_0^+} f_{l',m'}(E') f_{l'',m''}(\tilde{E}') Z(E') Z(\tilde{E}') c_{ee}(\mathbf{r}, E, E') \right. \\ &\times \delta(E + E^* - E' - \tilde{E}') dE' d\tilde{E}' \left. \right] \\ &\times \int_{\Omega} Y_{l,m}(\theta, \varphi) d\Omega \int_{\Omega'} Y_{l',m'}(\theta', \varphi') d\Omega' \int_{\tilde{\Omega}'} Y_{l'',m''}(\tilde{\theta}', \tilde{\varphi}') d\tilde{\Omega}' \\ &\doteq \sum_{l'=0}^{\infty} \sum_{m'=-l'}^{l'} \sum_{l''=0}^{\infty} \sum_{m''=-l''}^{l''} Z(E) \\ &\times \int_{\mathbb{R}_0^+} f_{l',m'}(E') f_{l'',m''}(E + E^* - E') Z(E') Z(E + E^* - E') c_{ee} dE' \\ &\times \delta_{0,l} \delta_{0,m} \delta_{0,l'} \delta_{0,m'} \delta_{0,l''} \delta_{0,m''}, \end{aligned} \quad (5.13)$$

where “ $\doteq$ ” denotes equality up to constant factors. This finally yields

$$\begin{aligned} \underline{\mathbf{Q}}_{l,m}^{\text{in}}\{f\} &\approx C_{\text{in}} Z(E) \left[ \int_{\mathbb{R}_0^+} c_{ee}(\mathbf{r}, E, E') f_{0,0}(E') f_{0,0}(E + E^* - E') \right. \\ &\times Z(E') Z(E + E^* - E') dE' \left. \right] \delta_{0,l} \delta_{0,m}, \end{aligned} \quad (5.14)$$

with a constant  $C_{\text{in}}$ , which is discussed later. The out-scattering operator (4.74) is simplified in a similar way, which gives

$$\begin{aligned}
\underline{\mathbf{Q}}_{l,m}^{\text{out}}\{f\}(\mathbf{r}, E, t) &\approx 2(2\pi)^3 \sum_{l'=0}^{\infty} \sum_{m'=-l'}^{l'} f_{l',m'}(E) Z(E) \\
&\times \int_{\mathbb{R}_0^+} \int_{\mathbb{R}_0^+} c_{ee}(\mathbf{r}, E, E') f_{0,0}(E^*) Y_{0,0} Z(E') Z(\tilde{E}') \delta(E + E^* - E' - \tilde{E}') dE' d\tilde{E}' \\
&\times \int_{\Omega} Y_{l,m}(\theta, \varphi) Y_{l',m'}(\theta, \varphi) d\Omega \int_{\Omega'} d\Omega' \int_{\tilde{\Omega}'} d\tilde{\Omega}' \\
&\doteq \sum_{l'=0}^{\infty} \sum_{m'=-l'}^{l'} f_{l',m'}(E) f_{0,0}(E^*) Z(E) \\
&\times \int_{\mathbb{R}_0^+} c_{ee} Z(E') Z(E + E^* - E') dE' \delta_{l,l'} \delta_{m,m'}, \tag{5.15}
\end{aligned}$$

Thus, the expansion coefficients of the out-scattering operator are obtained as

$$\boxed{\underline{\mathbf{Q}}_{l,m}^{\text{out}}\{f\} \approx C_{\text{out}} f_{l,m}(E) f_{0,0}(E^*) Z(E) \int_{\mathbb{R}_0^+} c_{ee} Z(E') Z(E + E^* - E') dE',} \tag{5.16}$$

with a constant  $C_{\text{out}}$ . For a Maxwellian distribution in thermal equilibrium, it holds that  $f_{0,0} \propto \exp(-E/(k_{\text{B}}T))$  and the total scattering operator  $\underline{\mathbf{Q}}$  becomes zero. Thus, a common pre-factor  $C = C_{\text{in}} = C_{\text{out}}$  for the coefficients of the in- and out-scattering operator is required in order to fulfill this condition. To summarize, the total scattering operator reads

$$\boxed{\underline{\mathbf{Q}}_{l,m}(\mathbf{r}, E, t) \approx CZ(E) \int_{\mathbb{R}_0^+} c_{ee}(\mathbf{r}, E, E') \\
\times [f_{0,0}(E') f_{0,0}(E + E^* - E') - f_{l,m}(E) f_{0,0}(E^*)] \\
\times Z(E') Z(E + E^* - E') dE',} \tag{5.17}$$

with two parameters  $C$  and  $E^*$ . This approximation of the scattering operator for electron-electron scattering is now compared to acoustic (ac) and optical (op) phonon scattering and ionized impurity (ii) scattering. The numerical results are obtained with `Maple` using  $C = 10$ . Two different EDF  $g(E)$  depicted in Fig. 5.25 and Fig. 5.22 respectively are used for the calculations.

In thermal equilibrium the EDF in Fig. 5.22 is obtained. In Fig. 5.23 and Fig. 5.24 the result is plotted for  $N_{\text{D}} = 1 \times 10^{16} \text{ cm}^{-3}$  and  $N_{\text{D}} = 1 \times 10^{20} \text{ cm}^{-3}$  respectively. It can be seen that the in- and out-scattering coefficient for electron-electron scattering has the same value, as expected.

For the non-equilibrium EDF in Fig. 5.25, the zeroth order expansion coefficients  $\underline{\mathbf{Q}}_{0,0}$  of the scattering operator are presented in Fig. 5.26 and Fig. 5.27 for  $N_{\text{D}} = 1 \times 10^{14} \text{ cm}^{-3}$  and  $N_{\text{D}} = 1 \times 10^{20} \text{ cm}^{-3}$  respectively. It is assumed that  $n = N_{\text{D}}$ . It is apparent that electron-electron scattering, as well as ionized impurity scattering strongly depends on the electron density  $n$ . Furthermore, it is noticeable that for  $E > 0.35 \text{ eV}$  the in-scattering rate for electron-electron scattering is significantly higher than the out-scattering rate. The curves for optical phonon scattering are plotted separately for absorption (+) and emission (-).

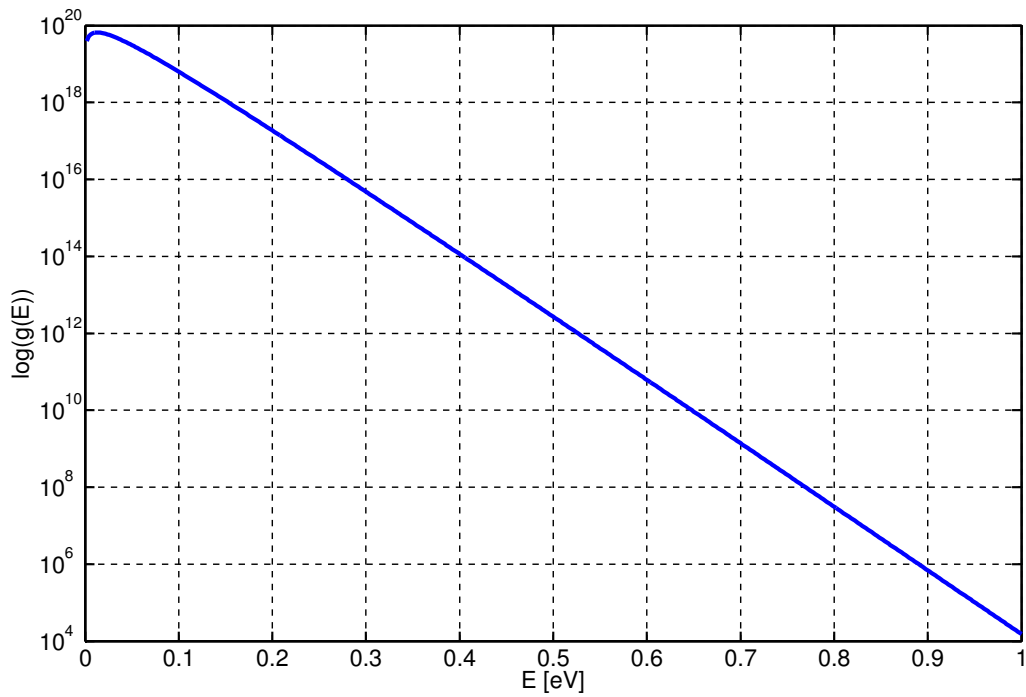


Figure 5.22: EDF used for the numerical calculations.

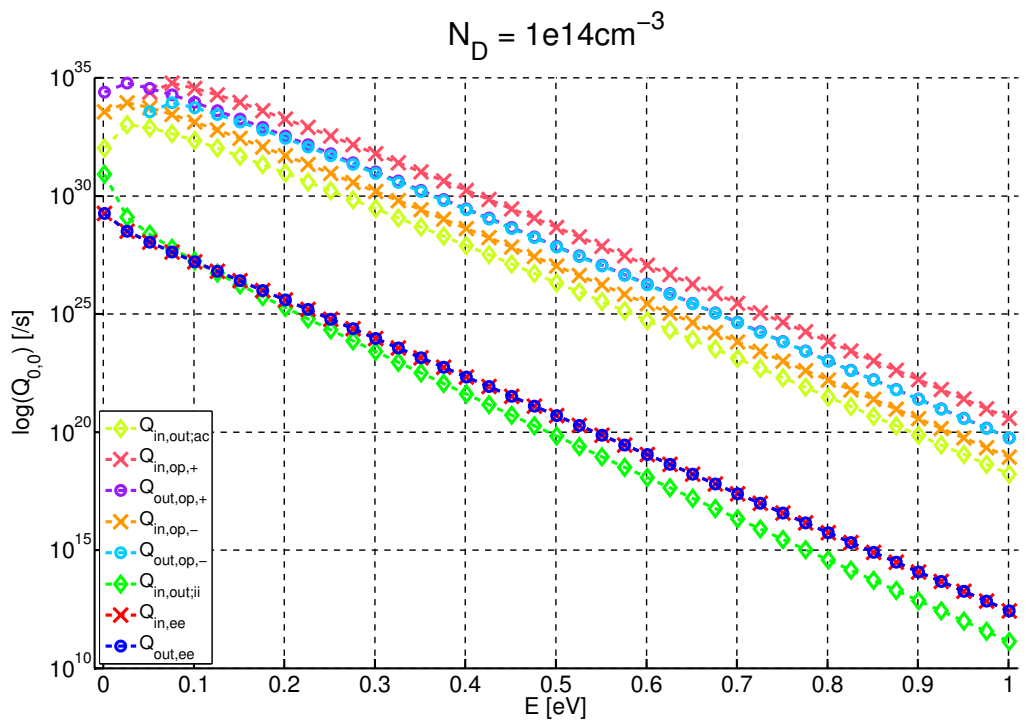
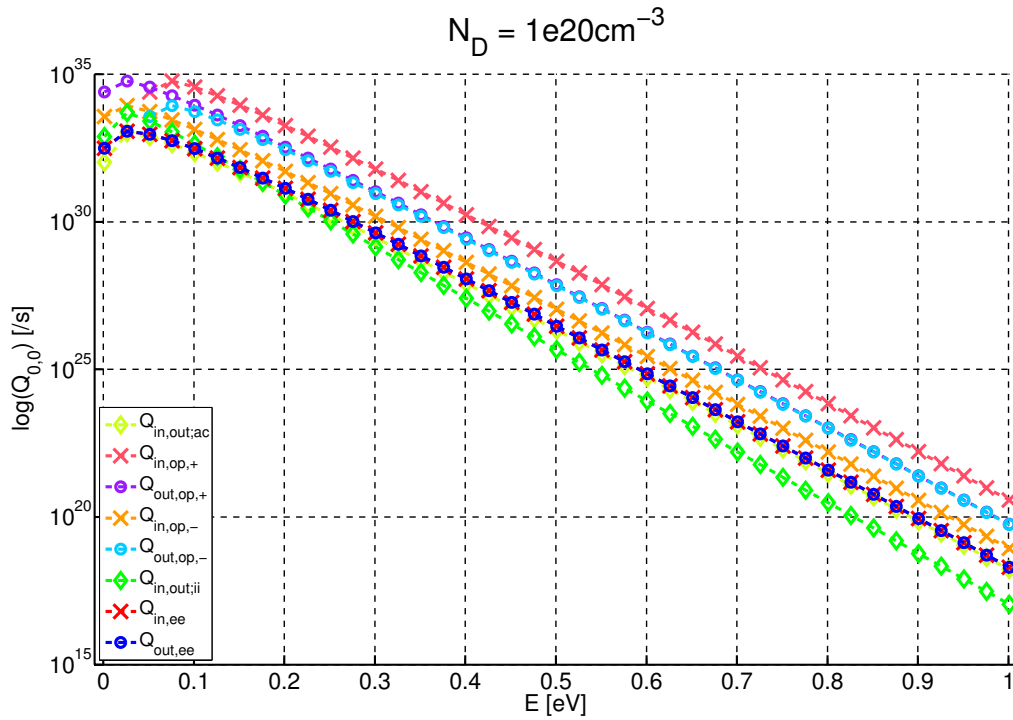
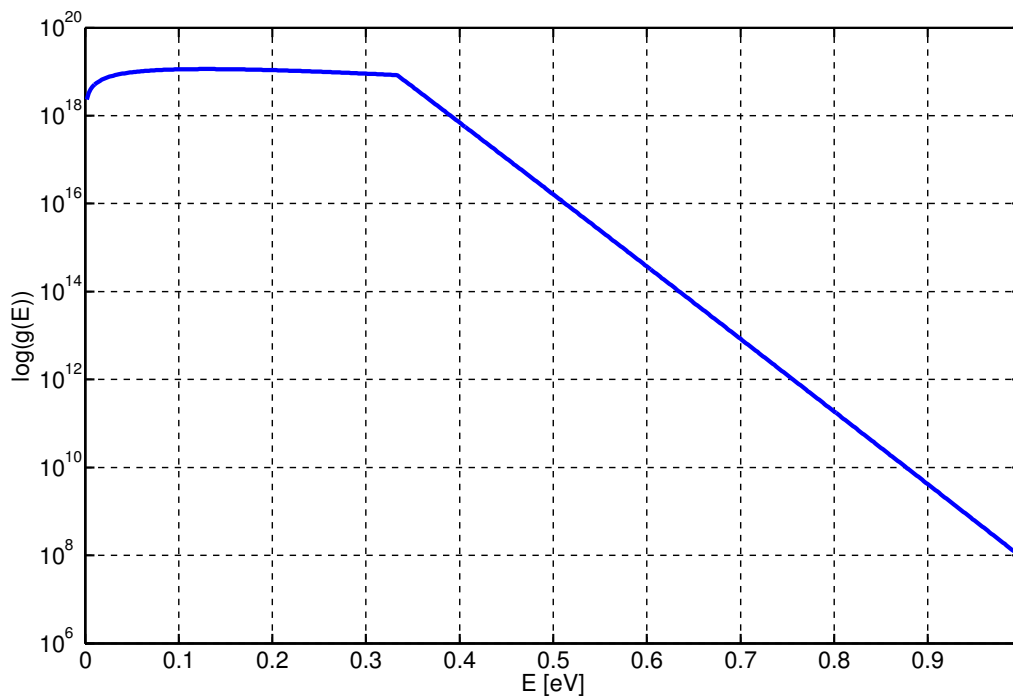


Figure 5.23: Zeroth-order expansion coefficients of the scattering operator for different scattering mechanism using the Maxwell distribution of Fig. 5.22.



**Figure 5.24:** Zeroth-order expansion coefficients of the scattering operator for different scattering mechanism using the Maxwell distribution of Fig. 5.22.



**Figure 5.25:** EDF used for the numerical calculations.

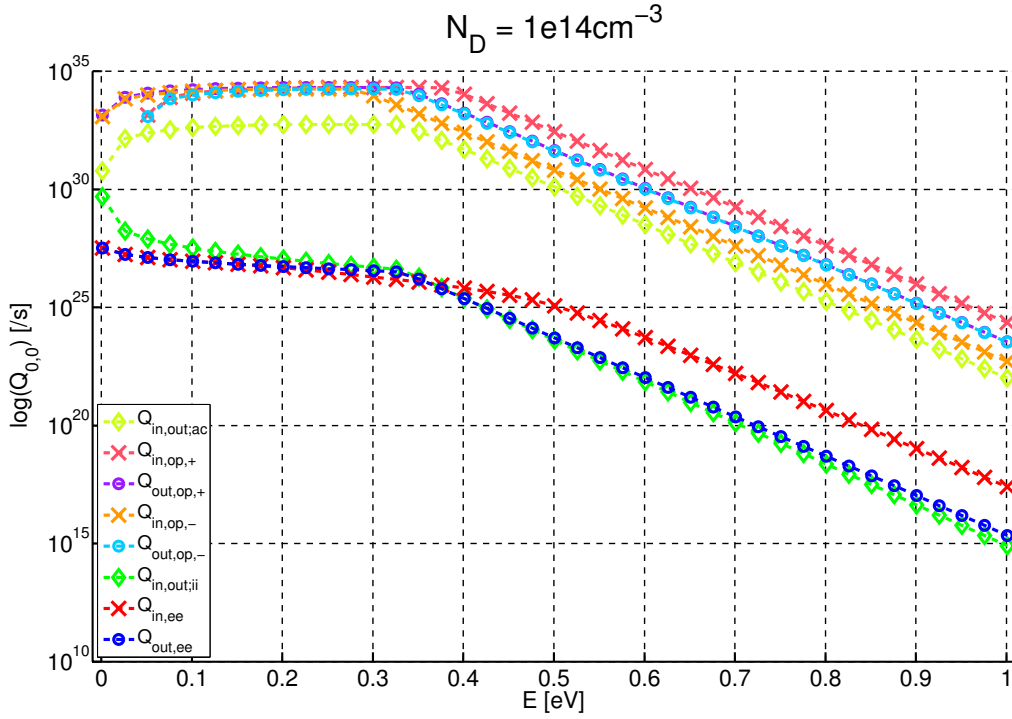


**Figure 5.26:** Zeroth-order expansion coefficients of the scattering operator for different scattering mechanism using the distribution of Fig. 5.25.

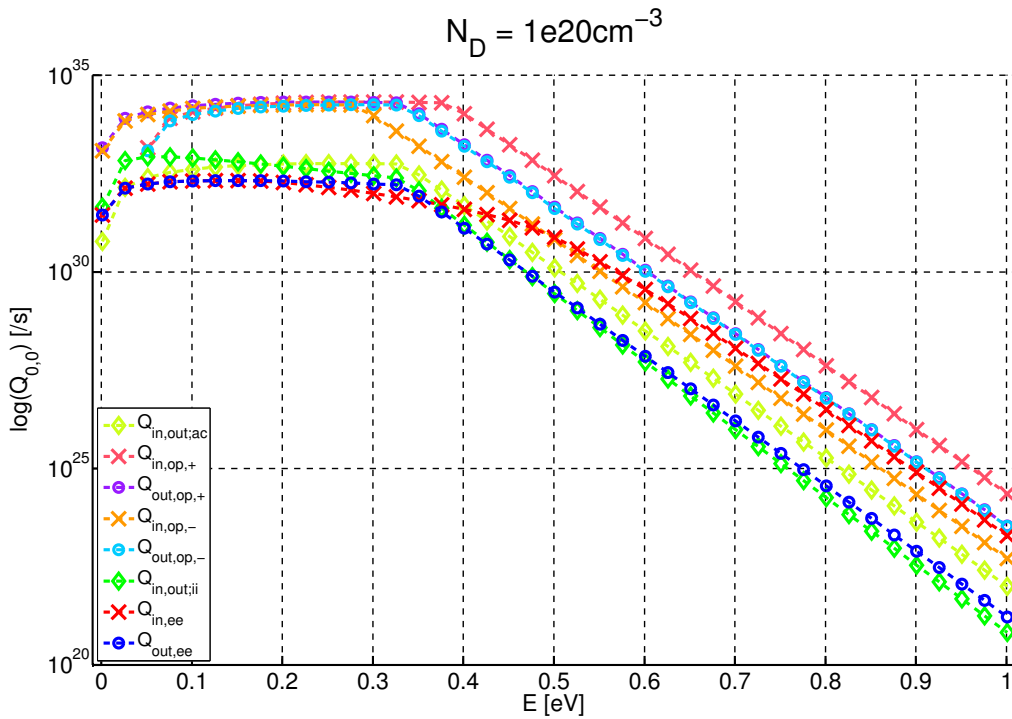


**Figure 5.27:** Zeroth-order expansion coefficients of the scattering operator for different scattering mechanism using the distribution of Fig. 5.25.

### 5.3.2 Simulation

In this section, simulation results taking electron-electron scattering into account are presented. The numerical simulations are carried out with **ViennaSHE**, where the scattering operator for electron-electron scattering is implemented according to (5.17). The parameter  $E^*$  is chosen according to (5.10). The influence of the parameter  $C$  is investigated in the following. Qualitatively the results agree with results found in literature [3,12,31]. The choice of  $C$  and  $E^*$  to match device characteristics is beyond the scope of this work. It is shown that the model is suitable to include electron-electron scattering.

At the beginning, some general considerations are made, which are valid for all the gate lengths used for the simulations. The generic device shown in Fig. 5.1 is used for the simulations. All simulations are carried out for **bias point C**, because here the effect of electron-electron scattering is readily observable. With the constant  $C$  the effect of electron-electron scattering can be tuned. It also holds that the higher the kinetic energy  $E$ , the higher is the impact of electron-electron scattering. Acoustic and optical phonon scattering as well as ionized impurity scattering are included in all calculations.

The splitting of the distribution function for high kinetic energies can be explained by the asymmetry of the scattering operator (5.17). In principle, the operator is a weighted convolution integral with a weighting factor  $c_{ee}(\mathbf{r}, E, E')$ . For in-scattering it is proportional to:

$$\underline{\mathbf{Q}}_{0,0}^{\text{in}}\{f\}(E) \propto Z(E) \int_{\mathbb{R}_0^+} c_{ee} \mathbf{g}_{0,0}(E') \mathbf{g}_{0,0}(E + E^* - E') dE', \quad (5.18)$$

where the distribution function  $f$  is combined with the generalized density of states  $Z$  to the EDF  $\mathbf{g}$ . The out-scattering part reads:

$$\begin{aligned} \underline{\mathbf{Q}}_{0,0}^{\text{out}}\{f\}(E) &\propto f_{0,0}(E) Z(E) \underbrace{f_{0,0}(E^*)}_{=C^*=\text{const.}} \underbrace{\int_{\mathbb{R}_0^+} c_{ee} Z(E') Z(E + E^* - E') dE'}_{\text{independent of } f(E)} \\ &\propto C^* \mathbf{g}_{0,0}(E) \int_{\mathbb{R}_0^+} c_{ee} Z(E') Z(E + E^* - E') dE', \end{aligned} \quad (5.19)$$

where the integral is independent of the distribution function. In thermal equilibrium both parts of the scattering operator provide the same contribution. Numerical results show that for a non-equilibrium distribution function the in-scattering operator gives higher values than the out-scattering operator for high values of the kinetic energy  $E$ , cf. Fig. 5.26 and Fig. 5.27. Thus there is a net in-scattering for high values of  $E$ , which results in the increase of the distribution function in non-equilibrium.

### 20 nm-Device

For the 20 nm-device, the constant  $C$  is chosen to be 0.1. In Fig. 5.28 the distribution function is shown for  $x = 30$  nm, which is at the middle of the gate. The distribution function at  $x = 40$  nm is very similar, cf. Fig. 5.29. It is interesting that the difference of the distribution function for high values of the kinetic energy  $E$  with and without electron-electron scattering is several orders of magnitude.

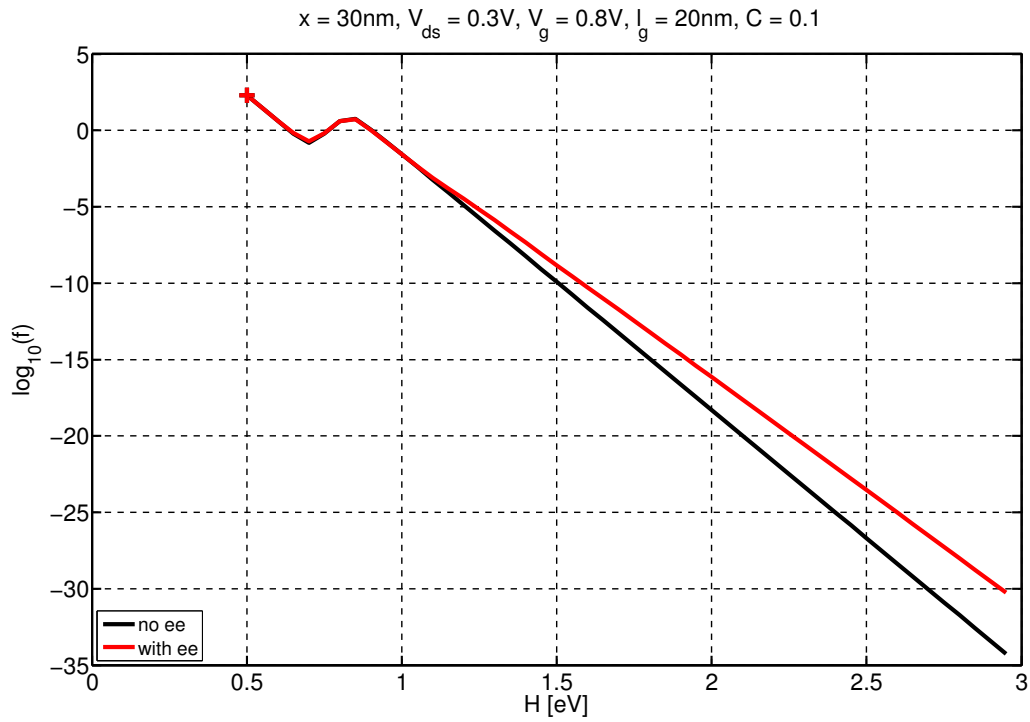


**Figure 5.28:** Comparison of the distribution function with and without electron-electron scattering.

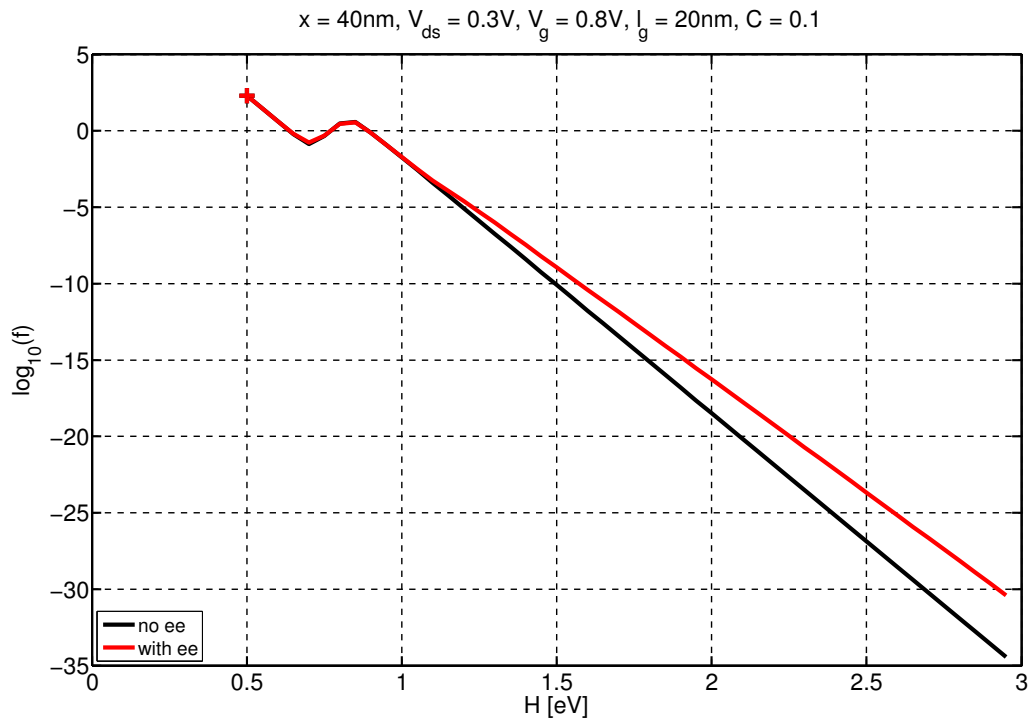


**Figure 5.29:** Comparison of the distribution function with and without electron-electron scattering.

### 100 nm-Device

In Fig. 5.30 and Fig. 5.31 the distribution function is shown at  $x = 150\text{ nm}$  for  $C = 0.1$  and  $C = 0.01$  respectively. The distribution function at  $x = 200\text{ nm}$  can be found in Fig. 5.32 and Fig. 5.33. The



simulation shows that a change of  $C$  by one order of magnitude results in a change of the distribution function by several orders of magnitude at high energies.

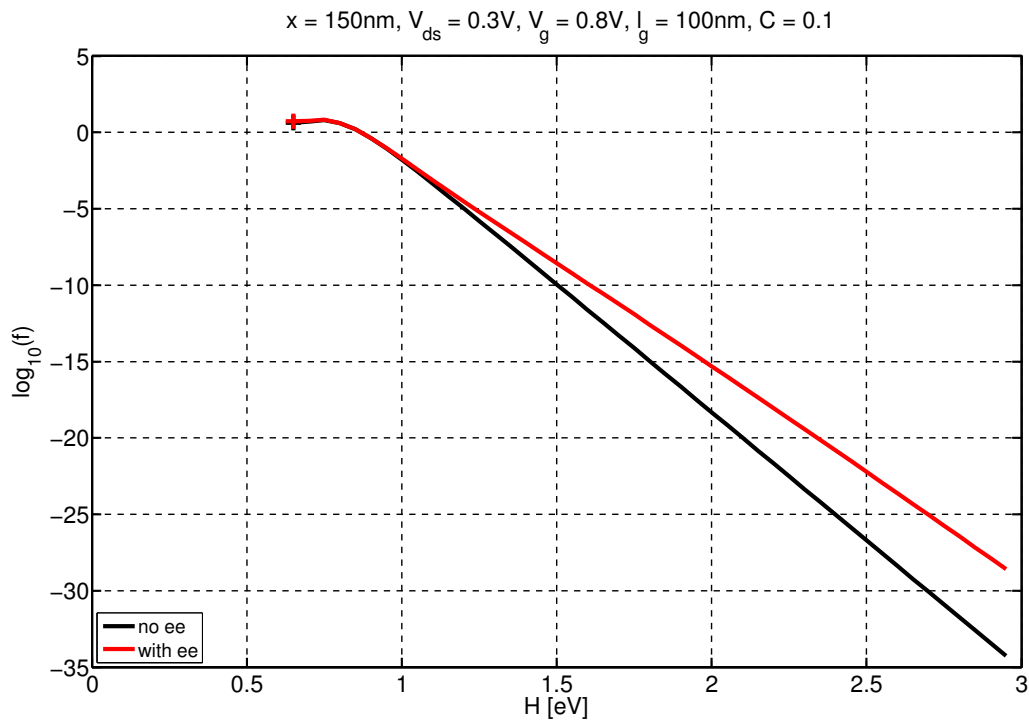


**Figure 5.30:** Comparison of the distribution function with and without electron-electron scattering.

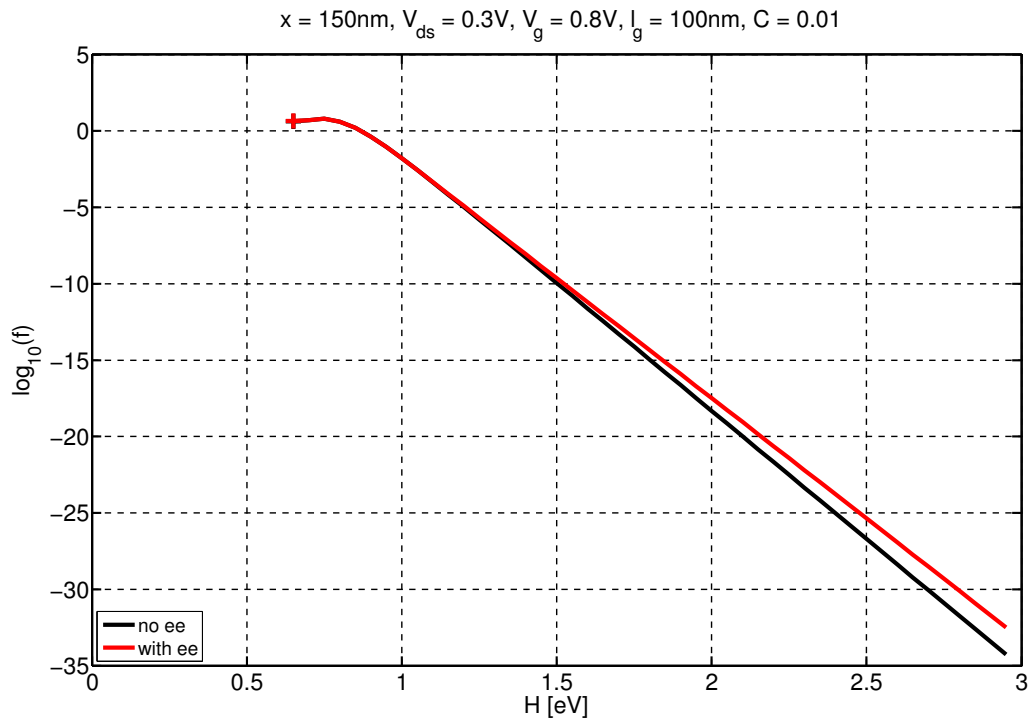


**Figure 5.31:** Comparison of the distribution function with and without electron-electron scattering.

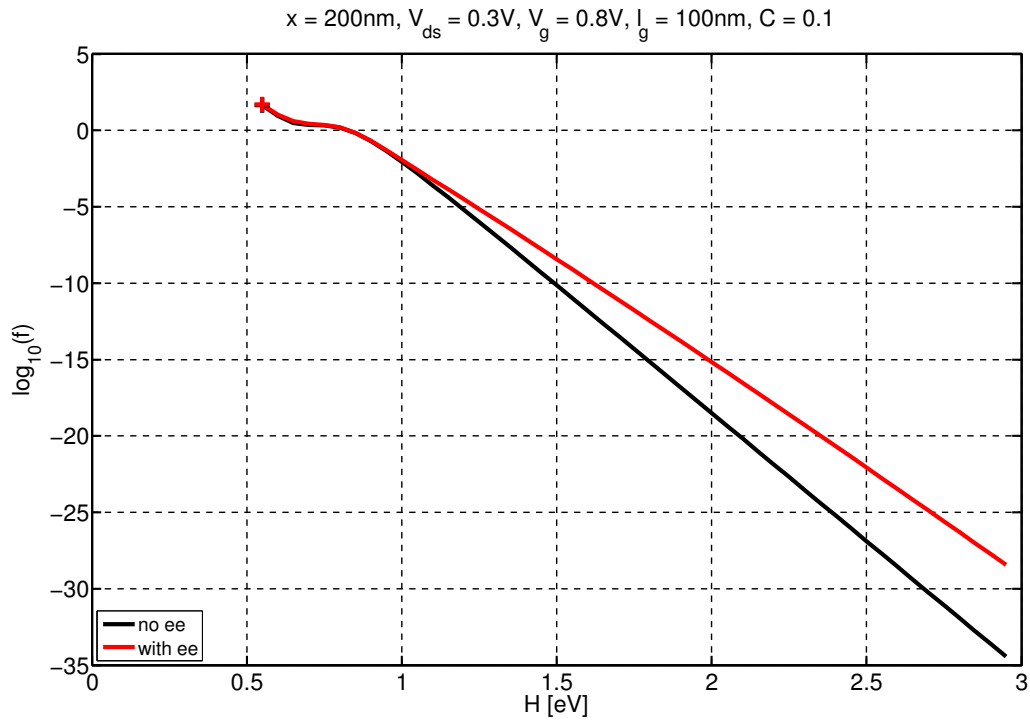


**Figure 5.32:** Comparison of the distribution function with and without electron-electron scattering.

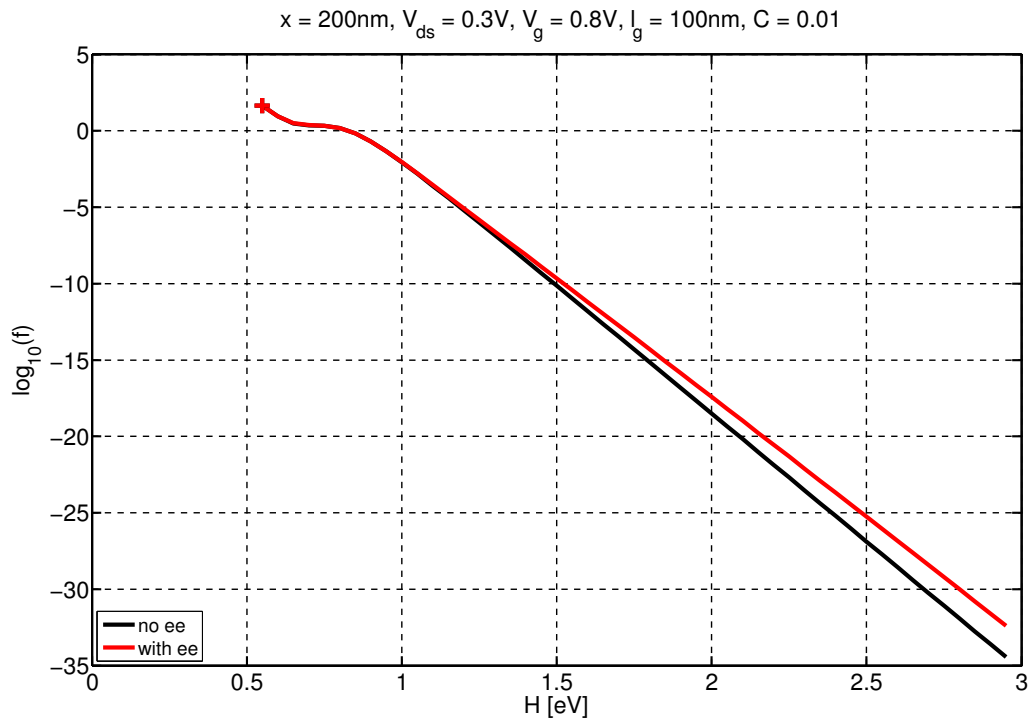


**Figure 5.33:** Comparison of the distribution function with and without electron-electron scattering.

### 300 nm-Device

The distribution function for  $x = 600\text{ nm}$  is plotted for  $C = 0.1$  and  $C = 0.01$  in Fig. 5.34 and Fig. 5.35 respectively.

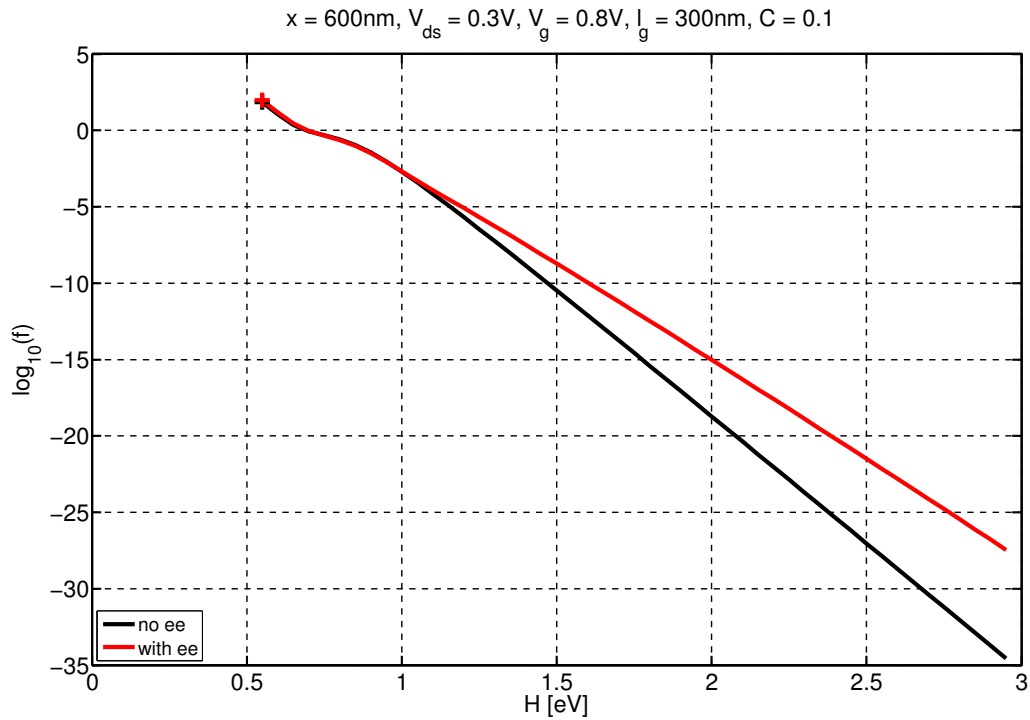


**Figure 5.34:** Comparison of the distribution function with and without electron-electron scattering.

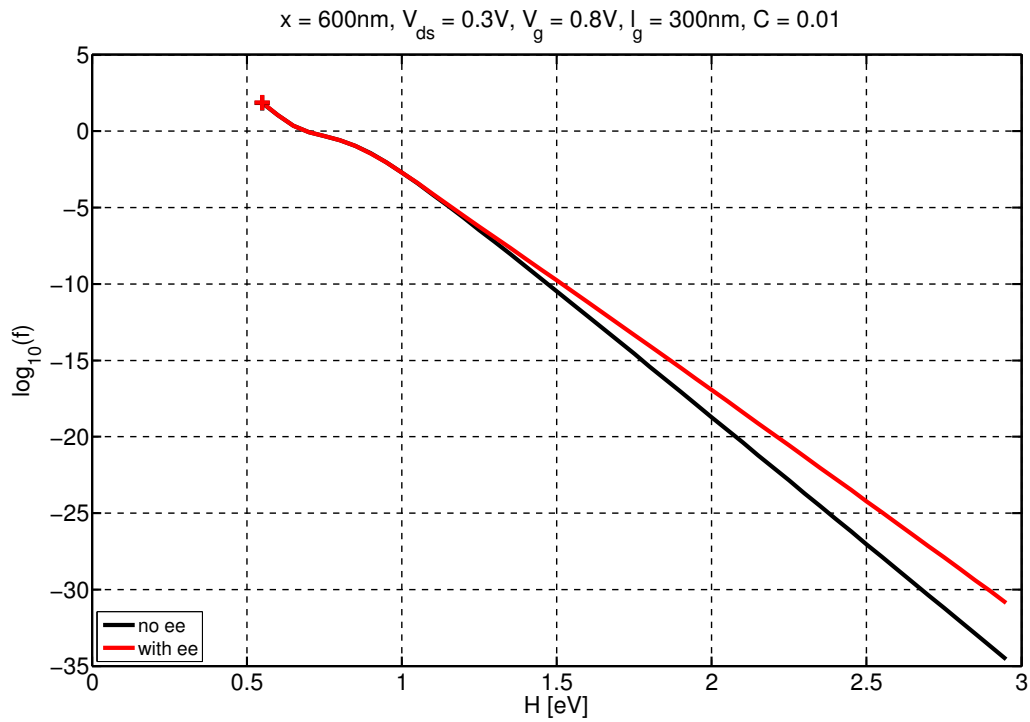


**Figure 5.35:** Comparison of the distribution function with and without electron-electron scattering.

## Chapter 6

# Conclusion and Outlook

In this diploma thesis a simplified model of the scattering operator for electron-electron scattering for arbitrary-order SHE of the BTE is developed successfully from the scratch for the first time. The work deals mainly with the physical aspects, while numerical details are only considered whenever necessary. The impact of the scattering mechanism are demonstrated by numerical simulations using ViennaSHE.

The SHE-coefficients of the scattering operator for electron-electron scattering given by (5.17) contain two parameters  $C$  and  $E^*$ . These two parameters are estimated from physical motivations but a rigorous calibration is still open. For  $E^*$  the average kinetic energy of the carriers seems to be a good estimate. The simulations show that especially the choice of  $C$  depends on the gate length and possibly on the device architecture. The challenge is to find a set of  $C$  and  $E^*$ , which reproduces the behavior of the device correctly.

Impact ionization occurs for values of the kinetic energy higher than the energy band gap. Therefore, the impact of electron-electron scattering on impact ionization processes is essential, because electron-electron scattering causes an increase of the high energy tail of the distribution function. In terms of reliability issues, a correct description of electron-electron scattering is necessary in order to obtain accurate results for the distribution function at high energies. In Fig. 6.1 this situation is depicted for the impact ionization rate  $W_{II}(E)$  and a distribution function  $f(E)$ .

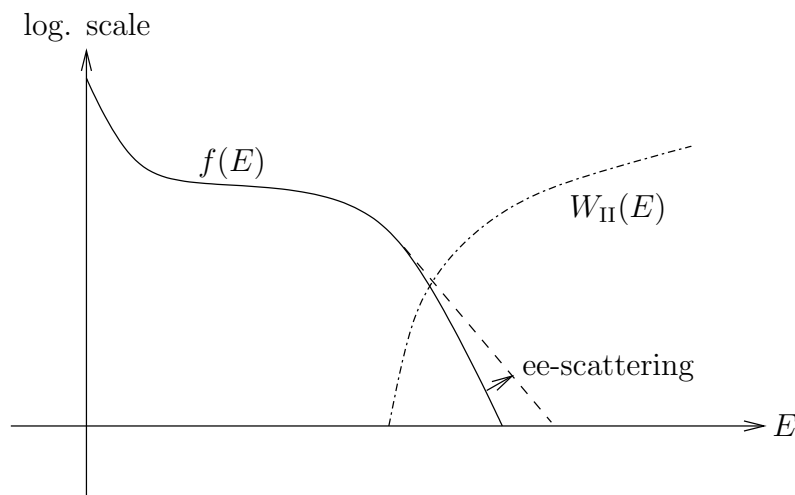


**Figure 6.1:** Influence of electron-electron scattering on impact ionization. Electron-electron scattering increases the distribution function  $f(E)$  for high values of the kinetic energy  $E$ .

One topic for future work is to fit the parameters of the suggested model to get an accurate

description of electron-electron scattering. The fit of the parameters could be done by e.g. comparison with Monte Carlo results or appropriate measurement techniques, which have yet to be developed. Together with the inclusion of impact ionization into **ViennaSHE**, this would provide a powerful tool for numerical studies in the context of device reliability.

Another possible extension of **ViennaSHE** is to implement more sophisticated models for the electronic band structure, which in part are also presented in this thesis. This in turn would require a revision of the models for scattering developed so far, because they are strongly connected to the model of the electronic band structure used for the simulations.

At present, the distribution function  $f$  is solved for a single conduction band only. As discussed in Section 1.2.4, also a distribution function for the valence band should be calculated simultaneously. This would require the inclusion of a generation-recombination operator at the right side of the BTE in addition to the scattering operator. Also multi-band models for the conduction band would require such a treatment.

An extension of the simulator to materials other than silicon would be interesting due to the rise of new material systems used in the semiconductor industry. In this context, the possibility to simulate High Electron Mobility Transistors would be of interest.

# Appendix A

## Dirac Notation

In the Dirac notation a quantum state is described by a state vector. The state vector is written as  $|\Psi\rangle$  and called *ket-vector*. The *bra-vector*  $\langle\Psi|$  is the dual vector to  $|\Psi\rangle$ . This notation is independent of the used basis system. In the spatial representation, the state of a quantum system is described by the spatial wave function  $\Psi(\mathbf{r})$ . The transition from the state vector to the spatial wave function  $|\Psi\rangle \rightarrow \Psi(\mathbf{r})$  is discussed in the following. It is important to note that  $\Psi(\mathbf{r}) \neq |\Psi\rangle$ . Special states are written as

$$|a\rangle \rightarrow \Psi_a(\mathbf{r}), \quad (6.1)$$

with an index  $a$ . The wave function

$$\Psi(\mathbf{r}) = \sum_n c_n \Psi_n(\mathbf{r}) = \int_{\mathbb{R}^3} c_\xi \Psi_\xi(\mathbf{r}) d\xi = \int_{\mathbb{R}^3} c_{\mathbf{p}} \Psi_{\mathbf{p}}(\mathbf{r}) d\mathbf{p}, \quad (6.2)$$

can e.g. be expanded in terms of energy-eigenfunctions  $\Psi_n(\mathbf{r})$ , spatial-eigenfunctions  $\Psi_\xi(\mathbf{r})$  or momentum-eigenfunctions  $\Psi_{\mathbf{p}}(\mathbf{r})$ , each in the spatial representation. The eigenfunctions form an orthonormal basis system with respect to the inner product on  $\mathbf{L}^2$ , which is the room of square-integrable functions. They can be compared to the basis vectors in finite dimensional vector spaces and the expansion coefficients  $c_n$ ,  $c_\xi$  and  $c_{\mathbf{p}}$  can be compared to the coordinates. E.g. the spatial-eigenfunctions  $\Psi_\xi(\mathbf{r})$  are the eigenfunctions of the spatial operator  $\underline{\mathbf{R}}_{\mathbf{r}}$ . In Dirac notation, they are described by the eigenvalue equation

$$\underline{\mathbf{R}}|\xi\rangle = \xi|\xi\rangle, \quad (6.3)$$

with the spatial eigenstates  $|\xi\rangle$  and the spatial eigenvalues  $\xi$ . To solve this equation, the spatial operator in the spatial representation, which reads  $\underline{\mathbf{R}}_{\mathbf{r}} = \mathbf{r}$ , is used. Therefore the eigenvalue equation in spatial representation is

$$\mathbf{r}\Psi_\xi(\mathbf{r}) = \xi\Psi_\xi(\mathbf{r}), \quad (6.4)$$

with the associated eigenfunctions  $\Psi_\xi(\mathbf{r}) = \delta(\xi - \mathbf{r})$ . From (6.2) follows that

$$\Psi(\mathbf{r}) = \int_{\mathbb{R}^3} c_\xi \delta(\xi - \mathbf{r}) d\xi = c_{\mathbf{r}}, \quad (6.5)$$

thus the wave function is equal to the expansion coefficients in a spatial-eigenfunctions expansion. The following two definitions are necessary to connect the state vector with the wave function, which is its spatial representation.

**Definition 10.** *The inner product of two complex-valued functions  $f : \mathbb{R}^3 \rightarrow \mathbb{C}$  and  $g : \mathbb{R}^3 \rightarrow \mathbb{C}$  is defined as*

$$(f, g) := \int_{\mathbb{R}^3} f^*(\mathbf{r})g(\mathbf{r})d\mathbf{r}. \quad (6.6)$$

**Definition 11.** *The product of a bra-vector  $\langle a|$  and a ket-vector  $|b\rangle$  is defined by the inner product of two complex valued functions as*

$$\langle a|b\rangle := (\Psi_a(\mathbf{r}), \Psi_b(\mathbf{r})) = \int_{\mathbb{R}^3} \Psi_a^*(\mathbf{r})\Psi_b(\mathbf{r})d\mathbf{r}. \quad (6.7)$$

With Definition 11  $\Psi(\mathbf{r})$  can be written as a projection in the Hilbert Space  $\mathbb{H}$ . Therefore the spatial eigenstate  $|\xi\rangle$  is written as  $|\mathbf{r}\rangle$  and the associated eigenfunctions are written as  $|\mathbf{r}\rangle \rightarrow \Psi_{\mathbf{r}}(\mathbf{r}') = \delta(\mathbf{r}-\mathbf{r}')$ . This yields

$$\Psi(\mathbf{r}) = \langle \mathbf{r}|\Psi\rangle = \int_{\mathbb{R}^3} \Psi_{\mathbf{r}}(\mathbf{r}')\Psi(\mathbf{r}')d\mathbf{r}' = \int_{\mathbb{R}^3} \delta(\mathbf{r}-\mathbf{r}')\Psi(\mathbf{r}')d\mathbf{r}'. \quad (6.8)$$

Alternatively the integrals in Definition 11 can be formulated in other representations, e.g. in the momentum representation, where  $\langle a|b\rangle := \int_{\mathbb{R}^3} \varphi_a^*(\mathbf{p})\varphi_b(\mathbf{p})d\mathbf{p}$ . The momentum wave function is obtained by  $\varphi(\mathbf{p}) = \langle \mathbf{p}|\Psi\rangle$ , with  $|a\rangle \rightarrow \varphi_a(\mathbf{p})$ . In the following only spatial representations and the abstract Dirac notation are used. Next, Definition 11 is used to evaluate the expectation value of an observable, which is described by  $\langle A\rangle = \langle \Psi|\underline{\mathbf{A}}|\Psi\rangle$ . With  $\underline{\mathbf{A}}|\Psi\rangle = |\Phi\rangle$ ,

$$\langle A\rangle = \langle \Psi|\Phi\rangle = (\Psi(\mathbf{r}), \Phi(\mathbf{r})) \quad (6.9)$$

is obtained. With the spatial representation of  $\underline{\mathbf{A}}$  this yields

$$\langle A\rangle = (\Psi(\mathbf{r}), \Phi(\mathbf{r})) = (\Psi(\mathbf{r}), \underline{\mathbf{A}}_{\mathbf{r}}\Psi(\mathbf{r})) = \int_{\mathbb{R}^3} \Psi^*(\mathbf{r})\underline{\mathbf{A}}_{\mathbf{r}}\Psi(\mathbf{r})d\mathbf{r}, \quad (6.10)$$

e.g. the expectation value of the location with the spatial operator  $\underline{\mathbf{R}}$  is evaluated by

$$\langle R\rangle = \int_{\mathbb{R}^3} \Psi^*(\mathbf{r})\mathbf{r}\Psi(\mathbf{r})d\mathbf{r}. \quad (6.11)$$

A general expression  $\langle a|\underline{\mathbf{A}}|b\rangle$  is called matrix element and can be evaluated by

$$\langle a|\underline{\mathbf{A}}|b\rangle = \int_{\mathbb{R}^3} \Psi_a^*(\mathbf{r})\underline{\mathbf{A}}_{\mathbf{r}}\Psi_b(\mathbf{r})d\mathbf{r}. \quad (6.12)$$

Matrix elements play an important role in the modeling of scattering, see Section 3.3.

# Bibliography

- [1] F. Bloch. Über die Quantenmechanik der Elektronen in Kristallgittern. *Zeitschrift für Physik*, 52(7-8):555–600, 1928.
- [2] R. Brunetti and C. Jacoboni. A Many-Band Silicon Model for Hot-Electron Transport at High Energies. *Solid-State Electronics*, 32(12):1663–1667, 1989.
- [3] J. D. Bude and M. Mastrapasqua. Impact Ionization and Distribution Functions in Sub-Micron nMOSFET Technologies. *IEEE Electron Device Letters*, 16(10), 1995.
- [4] S. Datta. *Quantum Transport - Atom to Transistor*. Cambridge University Press, 2005.
- [5] L. de Broglie. The Wave Nature of the Electron. *Nobel Lecture*, 1929.
- [6] G. Fasching. *Werkstoffe für die Elektrotechnik*. Springer, 4th edition, 2005.
- [7] A. Gnudi, D. Ventura, and G. Baccarani. Modeling Impact Ionization in a BJT by Means of Spherical Harmonics Expansion of the Boltzmann Transport Equation. *IEEE Transactions on Computer-Aided Design of Integrated Circuits and Systems*, 12(11), 1993.
- [8] W. A. Harrison. *Electronic Structure and the Properties of Solids*. Dover, 1989.
- [9] S.-M. Hong and C. Jungemann. A Fully Coupled Scheme for a Boltzmann-Poisson Equation Solver based on a Spherical Harmonics Expansion. *Journal of Computational Electronics*, (8):225–241, 2009.
- [10] J. D. Jackson. *Klassische Elektrodynamik*. de Gruyter, 4th edition, 2006.
- [11] C. Jacoboni and P. Lugli. *The Monte Carlo Method for Semiconductor Device Simulation*. Springer, 1989.
- [12] C. Jacoboni and L. Reggiani. The Monte Carlo Method for the Solution of Charge Transport in Semiconductors with Application to Covalent Materials. *Reviews of Modern Physics*, 55(3):645–705, July 1983.
- [13] S. Jin, S.-M. Hong, and C. Jungemann. An Efficient Approach to Include Full-Band Effects in Deterministic Boltzmann Equation Solver Based on High-Order Spherical Harmonics Expansion. *IEEE Transactions on Electron Devices*, 58(5):1287–1294, May 2011.
- [14] A. Jünger. Transport Equations for Semiconductors. Lecture Notes in Physics No. 773, 2009.
- [15] C. Jungemann, A.T. Pham, C. Ringhofer, M. Böllhofer, and B. Meinerzhagen. Stable discretization of the Boltzmann equation based on spherical harmonics, box integration, and a maximum entropy dissipation principle. *Journal of Applied Physics*, 100, 2006.
- [16] C. Kittel. *Einführung in die Festkörperphysik*. Oldenbourg, 14th edition, 2005.



- [17] H. Kosina. *Simulation des Ladungstransportes in elektronischen Bauelementen mit Hilfe der Monte-Carlo-Methode*. PhD thesis, TU Wien, May 1992.
- [18] W. Liang, N. Goldsman, I. Mayergoyz, and P. J. Oldiges. 2-D MOSFET Modeling Including Surface Effects and Impact Ionization by Self-Consistent Solution of the Boltzmann, Poisson, and Hole-Continuity Equations. *IEEE Transactions on Electron Devices*, 44(2), 1997.
- [19] C. W. Liu, S. Maikap, and C.-Y. Yu. Mobility-Enhancement Technologies. *IEEE Circuits & Devices Magazine*, pages 21–36, 2005.
- [20] M. Lundstrom. *Fundamentals of Carrier Transport*. Cambridge University Press, 2nd edition, 2000.
- [21] R. M. Martin. *Electronic Structure: Basic Theory and Practical Methods*. Cambridge University Press, 2010.
- [22] G. E. Moore. Cramming more Components onto Integrated Circuits. *Electronics*, 19(3):114–117, 1965.
- [23] A. Prechtel. *Elektrodynamik*. TU Wien, 2005.
- [24] B. K. Ridley. *Quantum Processes in Semiconductors*. Oxford University Press, 1999.
- [25] K. Rupp. Numerical Solution of the Boltzmann Transport Equation using Spherical Harmonics Expansions. Master’s thesis, Vienna University of Technology, 2009.
- [26] K. Rupp et al. Matrix Compression for Spherical Harmonics Expansions of the Boltzmann Transport Equation for Semiconductors. *Journal of Computational Physics*, 2010.
- [27] F. Schwabl. *Quantenmechanik*. Springer, 7th edition, 2007.
- [28] J. Singh. *Electronic and Optoelectronic Properties of Semiconductor Structures*. Cambridge University Press, 2003.
- [29] T. Steffen. *Repetitorium der gewöhnlichen Differentialgleichungen*. Binomi Verlag, 2005.
- [30] K. Tomizawa. *Numerical Simulation of Submicron Semiconductor Devices*. Artech House Materials Science Library. Artech House, 1993.
- [31] D. Ventura, G. Baccarani, and A. Gnudi. Inclusion of Electron-Electron Scattering in the Spherical Harmonics Expansion Treatment of the Boltzmann Transport Equation. *Proc. SISDEP*, 5, 1993.